

High-Temperature Carbon Dioxide Capture Using Metal Oxides

By

Christian Vogt

Dipl.-Ing. (Chemical Engineering), University of Dortmund, Germany

A thesis

submitted in fulfilment of the requirements for the degree of

Doctor of Philosophy

School of Chemistry

Monash University

Victoria, Australia

October 2013



MONASH University



Notice 1

Under the Copyright Act 1968, this thesis must be used only under the normal conditions of scholarly fair dealing. In particular no results or conclusions should be extracted from it, nor should it be copied or closely paraphrased in whole or in part without the written consent of the author. Proper written acknowledgement should be made for any assistance obtained from this thesis.

Notice 2

I certify that I have made all reasonable efforts to secure copyright permissions for third-party content included in this thesis and have not knowingly added copyright content to my work without the owner's permission.

Table of Contents

Abstract.....	ix
General Declaration	xiii
Acknowledgements	xv
List of Abbreviations.....	xix
List of Figures	xxi
List of Tables	xxxi
Chapter 1 Introduction.....	1
1.1 General background.....	1
1.2 Carbon dioxide capture process integration	5
1.2.1 Chemical looping combustion.....	5
1.2.2 Post-combustion capture	6
1.2.3 Oxy-fuel combustion.....	7
1.2.4 Pre-combustion capture	8
1.3 Carbon dioxide capture methods.....	10
1.3.1 Solvent absorption.....	10
1.3.2 Cryogenics.....	11
1.3.3 Membranes.....	11
1.3.4 Adsorption	13
1.3.5 Metal oxides for carbon dioxide capture	15
1.4 Project objective	22
1.5 Research hypotheses	22
Chapter 2 Screening study of prospective metal oxides.....	25
2.1 Introduction	25
2.2 Selection of metal oxides	25
2.2.1 Lanthanum oxide	25
2.2.2 Dolomite	25
2.2.3 Zinc oxide	26
2.2.4 Cadmium oxide	26

2.2.5	Mesoporous magnesium oxide.....	27
2.3	Experimental	27
2.3.1	Synthesis of sorbents.....	27
2.3.2	Nitrogen physisorption	30
2.3.3	Thermogravimetric analysis	31
2.3.4	Screening tests.....	31
2.4	Results and discussion.....	32
2.4.1	List of materials made.....	32
2.4.2	Surface area and pore size distribution of MgO-based sorbents.....	33
2.4.3	Screening of new sorbents.....	35
2.4.4	Cadmium carbonate results	37
2.4.5	Lanthanum carbonate	37
2.4.6	Zinc oxide	38
2.4.7	Magnesium oxide sorbents	39
2.5	Conclusion.....	43
2.6	References for Chapter 1 and 2.....	44
Chapter 3	Investigation of CdO-alkali halide carbon dioxide sorbents.....	53
3.1	Chapter overview	53
	Cadmium oxide/alkali metal halide mixtures - a potential high capacity sorbent for pre-combustion CO ₂ capture.....	55
3.2	Abstract.....	55
3.3	Introduction.....	56
3.4	Experimental section.....	59
3.4.1	Chemicals.....	59
3.4.2	Preparation of sorbents.....	59
3.4.3	Nitrogen physisorption	60
3.4.4	Thermogravimetric analysis of carbon dioxide sorption.....	60
3.4.5	Infrared spectrometry	63
3.4.6	Powder X-ray diffraction.....	63
3.4.7	Transmission electron microscopy.....	64
3.5	Results and discussion.....	64

3.5.1	CO ₂ sorption analysis.....	64
3.5.2	Infrared spectrometry	71
3.5.3	Sample crystallinity and morphology	73
3.6	Concluding remarks	75
3.7	Acknowledgements	77
	Supplementary Material.....	78
3.8	Nitrogen adsorption isotherm and pore size distribution.....	78
3.9	Le Bail fit of the XRD data.....	78
3.9.1	Statistics	78
3.9.2	Le Bail fit graphs.....	79
3.9.3	Results	81
3.10	EDX results and Powder Diffraction File data	81
	Cadmium oxide/alkali metal halide mixtures for pre-combustion CO ₂ capture. Part 2: Multiple sorption cycles	85
3.11	Abstract.....	85
3.12	Introduction	86
3.13	Experimental section.....	88
3.13.1	Preparation of cadmium oxide/alkali halide composite samples.....	88
3.13.2	Preparation of SBA-15 silica.....	88
3.13.3	Pelletised samples	89
3.13.4	Thermogravimetric analysis of carbon dioxide sorption.....	89
3.13.5	Elemental analysis.....	92
3.13.6	Powder X-ray diffraction.....	93
3.14	Results and discussion.....	94
3.14.1	Thermogravimetric analysis of the sample stability	94
3.14.2	Elemental analysis.....	97
3.14.3	Powder X-ray diffraction.....	99
3.14.4	Pelletised material	101
3.15	Concluding remarks	105
3.16	Acknowledgements	107
	Supplementary material.....	108
3.17	Pore size distribution of SBA-15.....	108

3.18	TGA cyclic experiments plots	109
3.19	Le Bail fit of the powder XRD data	116
3.19.1	Results	116
3.19.2	Statistics	116
3.19.3	Le Bail fit graphs.....	117
3.20	References for Chapter 3.....	119
Chapter 4	Investigation of the decay mechanism of a CdO-NaI sorbent.....	123
4.1	Chapter overview	123
	Investigation of the capacity decay of a CdO/NaI mixed sorbent for pre-combustion CO ₂ capture.....	125
4.2	Abstract	125
4.3	Introduction.....	126
4.4	Experimental	127
4.4.1	Sample preparation	127
4.4.2	Electron microscopy	127
4.4.3	In-situ powder X-ray diffraction	128
4.4.4	Fixed bed CO ₂ sorption and residual gas analysis.....	129
4.4.5	X-ray photoelectron spectroscopy.....	129
4.5	Results	130
4.5.1	Sample morphology	130
4.5.2	Exit gas analysis during a CO ₂ sorption experiment.....	135
4.5.3	X-ray photoelectron spectroscopy.....	139
4.5.4	In-situ powder X-ray diffraction	149
4.6	Conclusion.....	150
4.7	Acknowledgements.....	151
4.8	References for Chapter 4.....	153
Chapter 5	Improvement of Mg-Cs mixed sorbents	155
5.1	Chapter overview	155
	Improvements in the pre-combustion carbon dioxide sorption capacity of a magnesium oxide-caesium carbonate sorbent.....	157
5.2	Abstract.....	157

5.3	Introduction	158
5.4	Experimental	160
5.4.1	Synthesis of Mg-Cs ₂ CO ₃ via the wet mixing method	160
5.4.2	Synthesis of Mg-Cs ₂ CO ₃ via solvothermal method	160
5.4.3	Nitrogen physisorption	162
5.4.4	Thermogravimetric analysis of carbon dioxide sorption.....	162
5.4.5	Powder X-ray diffraction.....	163
5.4.6	Transmission electron microscopy	163
5.5	Results.....	164
5.5.1	CO ₂ sorption analysis.....	164
5.5.2	Morphology and crystallinity of the materials.....	168
5.6	Conclusion.....	178
5.7	Acknowledgements	180
	Supplementary material.....	181
5.8	Nitrogen physisorption isotherms and BJH pore volume distribution.....	181
5.9	Detailed TGA plots	183
5.10	Energy dispersive X-ray spectra and additional elemental maps.....	187
5.10.1	EDX spectra, dark field image and elemental maps of the nano-wet mix as synthesised sample.	188
5.10.2	EDX spectra, dark field image and elemental maps of the nano-direct as synthesised sample	191
5.10.3	EDX spectrum and dark-field image of the elemental maps of the nano-wet mix carbonated sample.....	194
5.10.4	EDX spectra, dark and bright-field images and elemental maps of the nano-direct carbonated sample.	195
5.11	References for Chapter 5	197
Chapter 6	Effect of syngas constituents on the sorbents	199
6.1	Chapter overview	199
	The effect of syngas constituents on CdO and MgO-based sorbents for pre-combustion CO ₂ capture	201
6.2	Abstract.....	201
6.3	Introduction	202

6.4	Experimental section.....	204
6.4.1	Sorbent synthesis.....	204
6.4.2	Thermogravimetric analysis (TGA).....	204
6.4.3	Analysis of samples exposed to H ₂ S.....	206
6.5	Results.....	206
6.5.1	Cadmium-based sorbent.....	206
6.5.2	Magnesium-based sorbent.....	212
6.5.3	Powder X-ray diffraction.....	217
6.6	Conclusion.....	218
6.7	Acknowledgements.....	220
6.8	References for Chapter 6.....	220
Chapter 7	Concluding remarks.....	223
7.1	Cadmium based sorbents: summary.....	223
7.2	Magnesium-based sorbents: summary.....	226
7.3	Suggestions for future work.....	227
Chapter 8	Experimental details.....	229
8.1	Introduction.....	229
8.2	Chemicals.....	229
8.3	Synthesis.....	230
8.4	Thermogravimetric analysis.....	231
8.5	Powder X-ray diffraction.....	234
8.5.1	Basic principles.....	234
8.5.2	Pattern refinement.....	237
8.6	Electron microscopy.....	238
8.6.1	TEM.....	239
8.6.2	SEM.....	241
8.7	Fourier-transform infrared spectroscopy.....	242
8.8	Inductively coupled plasma mass spectrometry.....	243
8.9	Atomic absorption spectrometry.....	243
8.10	Fixed-bed sorption study.....	244
8.11	Mass spectrometry.....	244

8.12	Nitrogen adsorption.....	245
8.13	X-ray-photoelectron spectroscopy	247
8.14	References for Chapter 8	249
Appendix 1: Additional Journal Paper.....		251
Appendix 2: About the author		261

Abstract

Carbon dioxide (CO₂) emissions to the atmosphere are considered a significant contributor to climate change due to the activity of the carbon dioxide molecule in the infrared spectrum. This causes solar radiation to be 'trapped' in the earth's atmosphere if increased CO₂ concentrations are present, leading to global warming. In order to decrease CO₂ emissions from stationary sources, like fossil fuel-fired power plants, and halt global warming, carbon capture and storage is proposed as a viable option. Here, a big fraction of the CO₂ normally being emitted to the atmosphere is to be separated from a flue gas stream of a conventional combustor facility (known as post-combustion) or from a synthesis gas (syngas) stream obtained by gasification of the fuel before its combustion (known as pre-combustion). The characteristics of the post-combustion flue gas and the pre-combustion syngas are substantially different, so that capture technologies must be developed for their respective application. The captured CO₂ can then be either used in industrial applications like enhanced oil recovery, if a market exists, or else be stored in places separate from the atmosphere, so as to not cause global warming. Underground storage, consisting of saline aquifers or depleted natural gas caverns, is among the options considered for permanent and safe CO₂ storage.

This project investigated the use of metal oxide-based sorbents for pre-combustion capture of CO₂ at 250 to 400 °C from syngas generated in the Integrated Gasification Combined Cycle (IGCC) process. At this temperature, syngas leaves the water gas shift reactor, which is the ultimate part of the gasification system within the IGCC process. Capturing the CO₂ in-situ at this temperature is considered beneficial, as it eliminates the requirement to cool or heat the gas to CO₂ sorption temperature, which would come with an energy penalty.

In the first part, various metal oxides were screened for their suitability to capture CO₂ in the temperature range of IGCC syngas. These were lanthanum oxide, magnesium oxide, zinc oxide and cadmium oxide. Based on a literature review, it was found that their carbonates decompose at temperatures considered here. A thermogravimetric screening test routine was outlined and the materials tested by exposure to carbon dioxide on a temperature ramp from 120 to 650 °C. Pure metal oxides and carbonates were considered

as well as oxides doped with alkali metal compounds. It was found that cadmium oxide doped with various alkali halides sorbs and desorbs CO₂ well in the screening test, so that more detailed studies were proposed. A magnesium oxide/cesium carbonate composite, which was analysed in detail in a previous project and synthesised using a variety of precursors here, was screened as well and found suitable. As the latter material exhibited a comparatively poor overall CO₂ sorption capacity, it was hypothesised that improvements could be made by varying the synthesis method.

In the second part, cadmium oxide/alkali halide mixtures were analysed for their optimal concentration of dopant required to give maximum CO₂ sorption capacity. A variation of alkali halide dopants showed that 17.5 wt% of sodium iodide (based on cadmium carbonate used as synthesis precursor) used in synthesis yields the best-performing sorbent. This sorbent was tested in detail via thermogravimetric analysis (TGA) for single-cycle and multiple cycle CO₂ sorption and desorption by partial pressure variation under isothermal conditions at various temperatures. The carbonation of cadmium oxide to carbonate and its decarbonation was confirmed as the reaction mechanism via powder X-ray diffraction (XRD) and Fourier-transform infrared (FTIR) spectroscopy. XRD also showed no significant change in the unit cell parameters of cadmium oxide due to sodium iodide doping. It was shown that alkali halides are necessary promoters for the carbonation reaction, as pure cadmium oxide did not exhibit any CO₂ inclusion and conversion into cadmium carbonate. For the sodium iodide-doped cadmium oxide, a stoichiometric recarbonation was achieved, resulting in a mass gain of 26 % (based on cadmium oxide and considering the presence of dopant here).

It was also shown in multicyclic sorption experiments, that a significant decay in working capacity (i. e., the amount of CO₂ both captured and released per cycle) occurred if the initial decarbonation of the cadmium carbonate precursor was performed in air. This could be improved by carbonate decomposition in inert gases like nitrogen or argon. Elemental analysis performed by inductively coupled plasma mass spectrometry (ICP-MS) and atomic absorption spectrometry (AAS) showed that iodine is lost from the sample, which might be attributed to oxidation of iodide to iodine. The loss of iodine promoter is considered to be the cause of a decay in working capacity of the sorbent. Water vapour

addition (1 vol%) to the sorption gases lead to an increase in stability in terms of the working capacities over the number of cycles, but had no noticeable effect on the iodine loss over sorption cycles. Powder samples were considered for multicyclic sorption as well as pelletised samples. It was shown that pelletisation via mechanical compression under vacuum resulted in materials with lower working capacities than powder equivalents, being attributed to the larger pellets being less accessible to the gas than small powder grains. Pellets made from carbonate lost their mechanical strength after 25 CO₂ sorption cycles, whereas pellets made in the oxide state virtually exhibited no working capacity. Introduction of SBA-15 (porous silica) as spacer made the oxide pellets more accessible to the gas so that they showed a certain working capacity. However, this again led to partial loss of mechanical strength, but to a lower extent as observed for the carbonate pellets.

In the third part of the thesis, the physico-chemical properties of the cadmium oxide/sodium iodide material were studied in detail. Transmission electron microscopy (TEM) showed morphological changes if the samples underwent multiple sorption cycles. Initially, spherical cadmium oxide nanoparticles of approx. 200 nm width were observed, which partially broke into irregular pieces after 25 sorption cycles. It was also confirmed by scanning electron microscopy (SEM) and elemental mapping that sodium iodide is interspersed into the cadmium oxide as discrete particles. In-situ powder XRD showed that sodium iodide contained in the cadmium oxide/sodium halide mixture is amorphous at room temperature after initial calcination, but becomes crystalline upon heating to CO₂ sorption temperature (in this case 325 °C). These results lead to the conclusion that the cadmium oxide/sodium halide mixed sorbent is not a mixed metal oxide, but rather a mixture of halide and an oxide particles. The initiation of the CO₂ sorption by the dopant halide must thus be due to a mechanistic contribution of the crystalline halide, rather than the formation of a cadmium-alkali-halide-oxide mixed phase under CO₂ uptake after sorption. Analysis of the exit gas from CO₂ desorption in a fixed bed by mass spectrometry confirmed the loss of iodine by showing mass-to-charge values of 126 in the mass spectrum, whereas X-ray photoelectron spectroscopy (XPS) revealed two species of iodine on the material's surface, possibly due to different oxidation states. These results support the idea that iodine might be lost during multicyclic sorption by oxidation of iodide to iodine.

In the fourth part of the thesis, improvements in the sorption capacities of magnesium oxide/cesium carbonate sorbents are shown. Using a solvothermal process involving hydration of magnesium methoxide and cesium carbonate methanolic solution mixed with toluene and subsequent treatment in an autoclave at 265 °C and flash-evaporation of the solvent, higher surface areas were obtained compared to the material made from commercial magnesium oxide as substrate. The activated solvothermally-made magnesium oxide/cesium carbonate sorbent appeared chemically similar to the one made from commercial templates as shown by XRD, but exhibited a higher working capacity (5 wt% instead of 4 wt%) than the latter. TEM and elemental mapping techniques showed that the solvothermal method leads to smaller particle sizes and also showed a mostly uniform distribution of the cesium throughout the magnesium, with occasional clustering of cesium being observed.

The fifth part of the thesis investigates the effect of syngas components on the sorbents. As syngas contains hydrogen, which is a strong reducing agent, it was deemed necessary to assess if the sorbents are stable if hydrogen is present during CO₂ sorption. It was also analysed if hydrogen sulphide, which is a trace component in syngas, has an effect on the sorbents. It was shown that hydrogen tends to lower the working capacity of the cadmium sorbents, possibly due to reduction of the cadmium oxide to cadmium metal. Lowering the sorption temperature 20 °C below the one achieving the highest multicyclic working capacity (i. e., to 285 °C), was able to significantly reduce capacity loss in a CO₂ sorption experiment containing hydrogen. The magnesium-cesium sorbent appeared stable in the presence of hydrogen. Hydrogen sulphide, however, had a significant impact on both the cadmium and magnesium-based materials by reducing their working capacities.

In summary, a cadmium oxide based CO₂ sorbent was developed and its physical and chemical properties examined. A magnesium-based mixed oxide developed in a previous study was improved in sorption capacity. The stability of both these materials under simulated syngas conditions was examined and future work is proposed to focus on the application of real syngas to these sorbents, with the goal of further improvements in their stability.

Monash University

Declaration for thesis based or partially based on conjointly published or unpublished work

General Declaration

In accordance with Monash University Doctorate Regulation 17.2 Doctor of Philosophy and Research Master's regulations the following declarations are made:

I hereby declare that this thesis contains no material which has been accepted for the award of any other degree or diploma at any university or equivalent institution and that, to the best of my knowledge and belief, this thesis contains no material previously published or written by another person, except where due reference is made in the text of the thesis.

This thesis includes two original papers published in peer reviewed journals and four unpublished publications. The core theme of the thesis is 'High temperature carbon dioxide capture using metal oxides'. The ideas, development and writing up of all the papers in the thesis were the principal responsibility of myself, the candidate, working within the School of Chemistry under the supervision Prof Alan L Chaffee and Prof Paul Webley. The thesis is less than 70000 words in length.

The inclusion of co-authors reflects the fact that the work came from active collaboration between researchers and acknowledges input into team-based research.

In the case of six subchapters, as outlined in the following table, my contribution to the work involved the following:

Thesis chapter	Publication title	Publication status*	Nature and extent of candidate's contribution
3	Cadmium oxide/alkali metal halide mixtures - a potential high capacity sorbent for pre-combustion CO ₂ capture	published in J Mater Chem A	Proposed original idea; prepared and analysed samples; identified major issues; developed interpretations; fully drafted papers and conclusions (75 %)
3	Cadmium oxide/alkali metal halide mixtures for pre-combustion CO ₂ capture. Part 2: Multiple sorption cycles	fully written, to be adjusted for submission to J Mater Chem A	Proposed original idea; prepared and analysed samples; identified major issues; developed interpretations; fully drafted papers and conclusions (80 %)

4	Investigation of the capacity decay of a CdO/NaI mixed sorbent for pre-combustion CO ₂ capture	fully written, to be adjusted for submission to J Mater Chem A	Proposed original idea; prepared and analysed samples; identified major issues; developed interpretations; fully drafted papers and conclusions (70 %)
5	Improvements in the pre-combustion carbon dioxide sorption capacity of a magnesium oxide-cesium carbonate sorbent	fully written, to be adjusted for submission to J Phys Chem C	Proposed original idea; prepared and analysed samples; identified major issues; developed interpretations; fully drafted papers and conclusions (75 %)
6	The effect of syngas constituents on CdO and MgO based sorbents for pre-combustion CO ₂ capture	fully written, to be adjusted for submission to Energy & Fuels	Proposed original idea; prepared and analysed samples; identified major issues; developed interpretations; fully drafted papers and conclusions (80 %)
Appendix	Nanoscale Structural Investigation of Cs ₂ CO ₃ -Doped MgO Sorbent for CO ₂ Capture at Moderate Temperature	published in J Phys Chem C	Performing in-situ and ex-situ powder XRD experiments, performing TGA experiments, editorial & results discussion assistance (20 %)

I have / ~~have not~~ (circle that which applies) renumbered sections of submitted or published papers in order to generate a consistent presentation within the thesis.

Signed:

Date:

Acknowledgements

I wish to extend my gratitude to my first supervisor, Prof Alan L Chaffee. His support throughout my candidature has always been welcoming and given me the opportunity to learn to develop myself as a researcher. His guidance has allowed me to independently fill my own research project with life, yet always being there to support me when things were heading into a road block. I also thank him for his patience during my initial application for the position, when things took several turns from an administrative point of view until I was finally able to start. It was a great pleasure to be part of Alan's workgroup.

Thanks are also addressed to my second supervisor, Prof Paul Webley. I appreciate his guidance from an 'out of the School of Chemistry'-perspective during our regular meetings. Some ideas definitely came from discussions with him, which have influenced this project in a positive way.

I thank Prof Stuart Batten and Dr Katya Pas for taking the role of advisors in the School of Chemistry and carefully monitoring the milestones of this project during my candidature.

My sincere thanks must be addressed to Gregory Knowles for getting me in touch with all the instruments we have in our lab, and for the many discussions we had about my research methods and results.

I would like to also thank Dr Shery Chang for her collaboration with performing TEM experiments and analysing results. I will always remember her relaxed, yet results-focussed 'can do' attitude, which has given me a serious lot of inspiration.

I have received a lot of support from various people within the vicinity of the School of Chemistry at Monash University, which I am very thankful for:

- to Dr Yi Fei and Dr Marc Marshall for help with the use of autoclaves and the sandbath;
 - to Dr Jamileh (Shah) Taghavi for providing TEM elemental maps of my samples;
 - to Christin Patzschke for performing SEM on my samples and the support during the long nightshifts at the powder XRD facility at the Australian Synchrotron.
- Thanks also to Dr Gongkui (James) Xiao for the latter;
-

- to Dr Martin Duriska and Craig Forsyth, thanks for help with operating the departmental powder XRD facility;
- to Dr Kia Wallwork, Dr Qinfen Gu and Dr Justin Kimpton (Powder Diffraction beamline staff at the Australian Synchrotron), thanks for help during my in-situ powder XRD experiments and for a deeper insight into what this great technique is capable of;
- to Dr Anthony Auxilio for help on the AutoChem instrument and mass spectrometer;
- to Dr Thomas Gengenbach (CSIRO) for performing XPS experiments and his assistance with data analysis;
- to Dr Massimo Raveggi (Monash Geosciences) for providing access to the ICP-MS facility and his help with planning the experiments;
- to Bruce Dobney for providing access to the FTIR spectrometers and a magnesium metal sample;
- to Maoyuan Liu for his contributions and discoveries about MgO-Cs sorbents during his time in the workgroup;
- to Vera Eate and Rodney Hall for providing access to AAS analysis;
- to the staff of the Science workshops, Nino Benci, David Zuidema, Alan Holland, Rod Cutts, Ben Fries, Cameron Hort and Dominic Nguyen for their assistance with the repair of instrument parts. Thanks also to Steven Morton for printing services provided for our annual CO2CRC symposium posters;
- to Anna Severin for successfully convincing me that administrative hurdles are smaller than they look like;
- to Dr Georg Beilharz and Robert Seefeld for their help in all things related to the School's infrastructure.

Financial support obtained from the Australian Government through its CRC program to support this CO2CRC research project is acknowledged. Thank you also to Prof Dianne Wiley and Prof Peter Cook for organising my postgraduate scholarship. The support through the Faculty of Science Dean's International Scholarship scheme is also gratefully acknowledged.

To Brad Wells, Anita D'Angelo, Lachlan Ciddor, Dr Priscilla Johnston, Dr Emily Perkins, Dr Emma Qi, Rini Subagyono, Dr Vidura Jayaratne, Mehrdad Parsa, Sing Yee Yeung, Mohammad Amer, Prof Roy Jackson, Dr Mohammad Chowdhury, Dr Zhijian Liang, Mamun Mollah, Dr Mee Chin Chow, Keryn Roberts, Dr Lisa Wittick, Leesun Kim, Maria Triantis, Phil Holt – thank you all for your friendship and companionship.

Only in this section as the last point, thanks to my parents, Dr Alfons and Barbara Vogt and my brother Alexander for their unconditional support in pursuing this part of my career.

List of Abbreviations

AAS	Atomic Absorption Spectrometry
ADF	Annular Dark Field
BET	Brunauer-Emmett-Teller (method for surface area determination)
BF	Bright Field
BJH	Barrett-Joyner-Halenda (method for pore size distribution calculation)
CCS	Carbon Capture and Storage
CO2CRC	Cooperative Research Centre for Greenhouse Gas Technologies
ED	Electron Diffraction
EDX	Energy-Dispersive X-ray (Spectroscopy)
FTIR	Fourier-Transform Infrared
FTM	Facilitated Transport Membrane
IGCC	Integrated Gasification Combined Cycle
LNG	Liquefied Natural Gas
MOF	Metal-Organic Framework
PSA	Pressure Swing Adsorption
SEM	Scanning Electron Microscopy
STEM	Scanning Transmission Electron Microscopy
TEM	Transmission Electron Microscopy
TGA	Thermogravimetric Analysis
TSA	Temperature (or Thermal) Swing Adsorption
VSA	Vacuum Swing Adsorption
WGS	Water-Gas Shift
XPS	X-ray Photoelectron Spectroscopy
XRD	X-ray Diffraction

List of Figures

Figure 1.1.1: Schematic illustration of the earth's greenhouse effect [8].....	2
Figure 1.1.2: a. Fraction of renewable energy of global electricity generation 2011, b. global final energy consumption, distribution 2010. Values from [12].	4
Figure 1.1.3: An artist's illustration of industrial CO ₂ sources and disposal possibilities [8]	5
Figure 1.2.1: Conceptual scheme of the chemical looping combustion process [18]. 'Me' stands generically for a metal.	6
Figure 1.2.2: Conceptual scheme of the post-combustion carbon dioxide separation [2, 20].6	
Figure 1.2.3: Conceptual scheme of the oxy-fuel process [2, 20]	7
Figure 1.2.4: Conceptual scheme of the IGCC process with carbon dioxide separation [24].9	
Figure 1.3.1: CO ₂ absorption reaction with a primary or secondary amine [29].	11
Figure 1.3.2: Synthesis of MCM-41 as an example for a high-surface area silica [43].	14
Figure 2.3.1: Temperature program for the TGA screening experiment.....	32
Figure 2.4.1: N ₂ ad-/desorption isotherms for the porous MgO and precursors. Same MgO sample data shown in a. and b. on different scales.	33
Figure 2.4.2: Pore volume distribution derived by the BJH model	35
Figure 2.4.3: TGA screening test of 10.5 wt.% NaI on CdCO ₃ , 25.1 mg raw sample: a. TG reading as per instrument output, b. TG reading normalised to 100 % of initial mass. Red arrows indicate region used for TG vs. T plot (Figure 2.4.4)	36
Figure 2.4.4: TGA screening test of 10.5 wt.% NaI on CdCO ₃ , TG relative = 100 % from the beginning of the temperature ramp.....	36
Figure 2.4.5: TGA screening test of La ₂ (CO ₃) ₂ , a. pure, b. doped with 9.5 wt.-% Cs ₂ CO ₃	38
Figure 2.4.6: TGA screening test of La ₂ (CO ₃) ₂ , temperature vs. TG	38
Figure 2.4.7: TGA screening test of zinc oxide, a. pure ZnO tested in wet CO ₂ , b. ZnO with 15 wt.-% NaI tested in dry CO ₂	39
Figure 2.4.8: TGA screening test of CsCO ₃ /MgO made from different precursors (acetate calcined at 650 and 850 °C) and pure MgO	40
Figure 2.4.9: TGA screening test of Cs/Mg from Mg(NO ₃) ₂ , a. different pre-treatment times, b. 6000 s pre-treatment time full plot.....	40

Figure 2.4.10: TGA screening test of $\text{CaCO}_3/\text{MgO}/\text{K}_2\text{CO}_3$, a. full plot, b. sorption vs. temperature	41
Figure 2.4.11: a. TGA recovery/screening of $\text{CaCO}_3/\text{MgO}/\text{K}_2\text{CO}_3$ sorbent, b. screening of sorbent made at a lower calcination temperature of $450\text{ }^\circ\text{C}$ with doping after calcination.	43
Figure 3.4.1: a. Initial screening program for TGA; b. sorption/desorption program. The dashed line on the temperature graph indicates the mass readings used for further calculation.....	62
Figure 3.5.1: TGA screening tests ($5\text{ }^\circ\text{C}/\text{min}$ ramp in CO_2 , 100 % at $125\text{ }^\circ\text{C}$) of sodium iodide/cadmium mixed oxide of different NaI content: a. full thermogram of 17.5 % NaI as synthesised material; b. after pre-calcination in muffle furnace in air at $500\text{ }^\circ\text{C}$ for 3 h; c. as synthesised material (carbonate).....	65
Figure 3.5.2: TGA screening test of 17.5 NaI sample and pure NaI with and without CO_2 addition. 17.5 % NaI sample calcined at $500\text{ }^\circ\text{C}$ in air 3 h prior to analysis.	67
Figure 3.5.3: Two-hour sorption and one-hour desorption studies of samples calcined in air $500\text{ }^\circ\text{C}$ 3 h, pre-treated in Ar. a. Sample 17.5 % NaI at various temperatures ($^\circ\text{C}$), pre-treatment $610\text{ }^\circ\text{C}$ 1 h, b. 15 % NaI sample made by dry and wet mixing, $610\text{ }^\circ\text{C}$ pre-treatment (20 min).	67
Figure 3.5.4: Working capacities derived from the difference between thermogravimetric maxima and end points in Figure 3.5.3a.	69
Figure 3.5.5: Multiple sorption. Four cycles of 17.5 % NaI at $305\text{ }^\circ\text{C}$, sample calcined in air $500\text{ }^\circ\text{C}$ before experiment. Partial pressure swing (50 % CO_2/Ar 12 min vs. pure Ar 24 min), pre-treatment and end step in Ar. 100 % mass at the start of experiment.	70
Figure 3.5.6: a. Screening TGA test of mixed Cd oxides incorporating alternative alkali halide dopants and pre-treated for 3 h at $500\text{ }^\circ\text{C}$ in air, b. 2 h adsorption, 1 h desorption at $290\text{ }^\circ\text{C}$ of samples with substituted dopants, pre-treatment in thermoanalyser at $380\text{ }^\circ\text{C}$ in Ar 1 h.....	71
Figure 3.5.7: FTIR spectra of 17.5 NaI (calcined in air $500\text{ }^\circ\text{C}$ 3 h) sample, a. oxide state, b. carbonate state	72
Figure 3.5.8: Powder XRD patterns of 17.5 % NaI sample and pure comparison materials	74

Figure 3.5.9: TEM images (a. & b.) of 17.5 % NaI, electron diffraction (c. & d., A-K denote diffraction lines as identified as CdO, refer supplementary material). Sample calcined in air, a. & c. neat, b. & d. after 4 cycles (Figure 3.5.5),	75
Figure 3.8.1: a. N ₂ adsorption-desorption isotherm (gas volume at STP adsorbed vs. p/p ₀), b. BJH pore volume of a 17.5 % NaI sample, after initial calcination at 500 °C in air 3 h	78
Figure 3.9.1: Le Bail refinement plot of 17.5 % NaI sample, as synthesised	79
Figure 3.9.2: Le Bail refinement plot of pure CdO.....	80
Figure 3.9.3: Le Bail refinement plot of pure CdCO ₃	80
Figure 3.10.1: EDX spectrum for 'edx 2' label in article.	81
Figure 3.10.2: EDX spectrum for 'edx 3' label in article.	82
Figure 3.10.3: EDX spectrum for 'edx 4' label in article.	82
Figure 3.13.1: Adsorption/desorption TGA program. The dashed line on the temperature graph indicates mass readings used in subsequent data processing.....	90
Figure 3.14.1: a. Full thermogram of a 17.5 % NaI sample, cycles at 285 °C, wet gas (285-Ar380-s-w), showing activation step, 25 cycles (12 min sorption, 24 min desorption), final desorption, b. excerpt from a. with 100 % set at the beginning of the sorption cycles, working capacity derivation shown at final cycle. c. and d. analogue a and b, calcined sample (285-a510-s-w)	95
Figure 3.14.2: Multicyclic adsorption-desorption of various alkali halide/CdO samples at different temperatures. Refer to Table 3.13.1 for sample designators. a. 17.5 % NaI samples pre-treated in Ar and in air, no water added during TGA; b. as for a but with 1 % water addition in TGA; c. 17.5 % NaI samples and different pre-treatments; d. other alkali halides. Last letter d = dry gas, w = wet gas.	96
Figure 3.14.3: Elemental analysis of as synthesised (a/s) 17.5 % NaI samples calcined in air, N ₂ and uncalcined (carbonate state), a. mass-%, b. Na and I relative to amount of Cd. Max. error 5.29 % (absolute) for Cd of a duplicate measurement of N ₂ calcined sample.....	98
Figure 3.14.4: Elemental analysis of 17.5 % NaI/CdO samples after cyclic CO ₂ sorption experiments, a. dry gas, b. wet gas, c. & d. like a, b with I and Na content relative to Cd. Samples correspond to Figure 3.14.2 a and b.	99
Figure 3.14.5: Powder XRD patterns of a 17.5 % NaI sample obtained from in-situ synchrotron experiments at the end of each cycle at 325 °C: a. decarbonated state, b.	

carbonated state. Arrow indicates two peaks assigned to NaI. Sample calcined in air at 500 °C before experiment.	100
Figure 3.14.6: Working capacities of pelletised 17.5 % NaI material. Pelletisation performed in oxide (N ₂ calcination) and carbonate state. Dry gas.	103
Figure 3.14.7: Images of 17.5 % NaI pellets. a. fresh carbonate pellet, b. segments cut off for TGA, c. & d. brittle segments after sorption cycles, e. & f. brittle carbonate pellet calcined at 500 °C in N ₂ , g. sturdy pellet pressed as oxide, h. 4.22 % SBA-15 pellet after 25 CO ₂ sorption cycles. Diameter of pellet after pressing 13 mm, width of tweezers (shown for comparison) 10 mm.	105
Figure 3.17.1: a. N ₂ adsorption isotherm, b. BJH pore volume for SBA-15.	108
Figure 3.18.1: Full thermograms (left) and normalised thermograms to 100 % active sorbent (right) of multicyclic sorption-desorption of Cd-NaI (17.5 %) sorbent at constant temperatures (275 and 295 °C) in dry and wet gas. Refer to Table 1 in the main article for sample labels. Starred (*) sample thermograms appear in full in main article as well.	111
Figure 3.18.2: Full thermograms (left) and normalised thermograms to 100 % active sorbent (right) of multicyclic sorption-desorption of Cd-NaI (17.5 %) sorbent at constant temperatures (275 and 295 °C) in dry gas, comparing different pre-treatments, as well as short and long cycles. Refer to Table 1 in the main article for sample labels.	112
Figure 3.18.3: Full thermograms (left) and normalised thermograms to 100 % active sorbent (right) of multicyclic sorption-desorption of Cd sorbent with different alkali promoters at constant temperatures (275 and 295 °C) in dry gas, comparing short and long cycles. Refer to Table 1 in the main article for sample labels.	114
Figure 3.18.4: Full thermograms (left) and normalised thermograms to 100 % active sorbent (right) of multicyclic sorption-desorption of pelletised Cd-17.5 % NaI sorbent at constant temperature (295 °C) in dry gas, comparing short and long cycles. Refer to Table 3.13.1 in the main article for sample labels.	116
Figure 3.19.1: Le Bail refinement plot of LaB ₆ standard, synchrotron	117
Figure 3.19.2: Le Bail refinement plot of 17.5 % NaI sample, decarbonated in situ in 3 rd cycle, synchrotron.....	118
Figure 3.19.3: Le Bail refinement plot of 17.5 % NaI sample, carbonated in situ in 3 rd cycle, synchrotron	118

Figure 4.4.1: AutoChem fixed-bed exit gas mass spectrometry program	129
Figure 4.5.1: TEM images and electron diffraction patterns of CdO-NaI sorbent calcined in N ₂ (a, b), pure CdO made from CdCO ₃ (c, d). Assignments A-K are made according to Powder Diffraction File entry 04-001-3770 for CdO.....	131
Figure 4.5.2: TEM images (a, c, d) and electron diffraction pattern (b) of a CdO-NaI mixed sample calcined in air, after 25 CO ₂ sorption cycles. EDX spectra refer to image c. Assignments A-K are made according to Powder Diffraction File entry 04-001-3770 for CdO.	132
Figure 4.5.3: TEM images (a, c, d) and electron diffraction pattern (b, corresponding to box 'ED' in a) of a CdO-NaI sample calcined in N ₂ , after 25 cycles of CO ₂ sorption and desorption, d. boxed area in c. enlarged, e. FFT image of d. used to calculate lattice parameters. Assignments a-h correspond Powder Diffraction File entry 00-006-0302 (NaI).	134
Figure 4.5.4: SEM image of a fresh CdO-NaI sample calcined in air.	134
Figure 4.5.5: SEM elemental maps and electron image of the mapped area of a fresh CdO-NaI sample calcined in air.....	135
Figure 4.5.6: Exit gas mass spectra for a fixed-bed blank run. a. during N ₂ purge, b. during 50 % CO ₂ in N ₂ purge. Note: Spectra were observed to be independent of temperature setting (isothermal or ramp).	137
Figure 4.5.7: Examples of gas mass spectra obtained during the first temperature ramp for a CdO-NaI sample calcined in air. a. high amounts of water released at 148 °C, b. iodine release at 304 °C.....	138
Figure 4.5.8: Exit gas mass spectrum of a calcined CdO-NaI sample during CO ₂ addition at 300 °C showing iodine release.....	138
Figure 4.5.9: XP spectra for Cd 3d of neat mixed CdO-NaI samples and pure CdO (a) and CdO-NaI after 25 CO ₂ sorption cycles (b).....	141
Figure 4.5.10: XP spectra for O 1s of neat mixed CdO-NaI samples and pure CdO (a) and CdO-NaI after 25 CO ₂ sorption cycles (b).....	143
Figure 4.5.11: XP spectra for C 1s of neat mixed CdO-NaI samples, pure CdO and NaI (a) and CdO-NaI after 25 CO ₂ sorption cycles (b).	144

Figure 4.5.12: XP spectra for I 3d of neat mixed CdO-NaI samples, pure CdO and NaI (a) and CdO-NaI after 25 CO ₂ sorption cycles (b).	146
Figure 4.5.13: XP spectra for Na 1s of neat mixed CdO-NaI samples, pure CdO and NaI (a) and CdO-NaI after 25 CO ₂ sorption cycles (b).	147
Figure 4.5.14: In-situ powder XRD patterns measured in N ₂ purge of a CdO-NaI sample calcined in air. a. Full pattern at room temperature and 325 °C in N ₂ purge, b. same dataset as a. but with CdO peaks removed. Intensities for pure NaI reference (lab instrument) multiplied with 10, other intensities to scale.	150
Figure 5.4.1: TGA program used for single-cycle (610 °C) or multi-cyclic (510 °C) sorption analysis.....	163
Figure 5.5.1: a. Full thermogram of a 2 hr sorption, 1 hr desorption run of a Mg-Cs-wetmix sample at 354 °C, b. 2 h Sorption and 1 h desorption excerpt from a. with 100 % mass set at the start of the sorption run for different temperatures, with working capacity indicated for the 313 °C experiment, c. working capacities derived from b.	165
Figure 5.5.2. a. Full thermogram of a wet mix sample in 12 min sorption, 24 min desorption cycles at 390 °C, b. working capacities for wet mix samples at different temperatures over 25 cycles, c. and d. for nano-wetmix and nano-direct samples, respectively.	166
Figure 5.5.3: Powder X-ray diffraction patterns of the solvothermally synthesised Mg-Cs composite materials and the nano-Mg substrate. Peak markers are set according to Powder Diffraction File.	169
Figure 5.5.4: TEM image (a) and electron diffraction pattern (b) for the nano-Mg sample. Diffraction pattern matches MgO.	170
Figure 5.5.5: a, b, d ,e: TEM images of nano-wet mix as synthesised sample, c: electron diffraction pattern for b.	171
Figure 5.5.6: (a, c, d, f) TEM images of nano-direct sample, as synthesised; (b) electron diffraction image for (a), (e) for 'area1' marked in (d); (f) enlarged section of 'area1' in (d).	172
Figure 5.5.7: (a-c) TEM images of nano-wet mix sample after calcination (d) electron diffraction pattern of (c).....	173
Figure 5.5.8: (a, c, d) TEM images of nano-direct sample after calcination, (b) electron diffraction for (a), (e) for (d) respectively.....	173

Figure 5.5.9: (a, b) TEM images of nano-wet mix sample after carbonation, (c) electron diffraction pattern of (b).....	174
Figure 5.5.10: (a, c) TEM images of nano-direct sample after carbonation, (b) electron diffraction pattern of (a).....	174
Figure 5.5.11: Elemental maps for carbon, cesium, magnesium and oxygen and scanning transmission electron microscopy dark field image of the nano-wet mix sample in the as-synthesised state. Refer to supplementary materials for duplicate specimens and EDX spectra.....	175
Figure 5.5.12: Elemental maps for carbon, cesium, magnesium and oxygen and scanning transmission electron microscopy dark field image of the nano-direct sample in as-synthesised state. White arrow indicates a cluster with increased Cs content, but low in Mg. Refer to supplementary materials for duplicate specimens and EDX spectra.....	176
Figure 5.5.13: Elemental maps for carbon, cesium, magnesium and oxygen and scanning transmission electron microscopy dark field (mislabelled 'BF') image of the nano-wetmix sample after carbonation. White arrow indicates a cluster with increased Cs content, but low in Mg. Refer to supplementary materials for EDX spectrum.....	177
Figure 5.5.14: Elemental maps for carbon, cesium, magnesium and oxygen and scanning transmission electron microscopy dark field (mislabelled 'BF' at the bottom) images of the nano-direct sample after carbonation. White arrow indicates a cluster with increased Cs content, but low in Mg. Refer to supplementary materials for duplicate specimens and EDX spectra.....	178
Figure 5.8.1: Nitrogen adsorption isotherms at 77 K for the wet-mix samples made from commercial MgO (a), BJH pore volume (b), isotherms for the Mg-nano template (c) and for the Mg-Cs oxide composite made via solvothermal methods (d), BJH pore volume plot for solvothermally made samples (e).....	182
Figure 5.9.1: Thermograms (cycle plots, 100 % mass at start of cycles, left) and full plots (100 % mass at start of experiment, right) for the MgO-Cs ₂ CO ₃ materials.....	187
Figure 6.4.1: a. TGA screening test procedure, b. multicyclic procedure. * Test gas denotes 50 % H ₂ in Ar or 1 % H ₂ S (Cd) or 0.2 % H ₂ S (Mg) in Ar for a.; and either 50 % Ar, 0.2 % H ₂ S, 49.8 % CO ₂ or 48.8 % H ₂ , 48.8 % CO ₂ , 2.4 % water (sorption cycles), dry Ar (desorption cycles) for b.....	205

Figure 6.5.1: Hydrogen TGA screening test of a CdCO ₃ -NaI sorbent sample. a. full thermogram, b. second temperature ramp of a. with hydrogen exposure vs. temperature.	207
Figure 6.5.2: Hydrogen sulphide TGA screening test of a CdCO ₃ -NaI sorbent sample. a. full thermogram, b. second temperature ramp of a. with hydrogen sulphide exposure plotted vs. temperature.	208
Figure 6.5.3: Isothermal multiple sorption cycles (12 min sorption in 50 % Ar/49.8 % CO ₂ /0.2 % H ₂ S, 24 minutes desorption in pure Ar) of a CdCO ₃ -NaI sample. a. 285 °C, b. 305 °C. Pre-treatment and after-treatment in pure Ar at 380 °C.....	210
Figure 6.5.4: Isothermal 25-cycles TGA experiment using Cd-NaI sorbent in 48.8 % H ₂ , 48.8 % CO ₂ and 2.4 % water (12 minutes sorption) and pure dry Ar (24 minutes desorption). a. 285 °C, b. 305 °C.	212
Figure 6.5.5: Hydrogen TGA screening test of a Mg-Cs-wetmix sorbent sample. a. full thermogram, b. second temperature ramp with hydrogen exposure vs. temperature.....	213
Figure 6.5.6: H ₂ S TGA screening test of a Mg-Cs-wetmix sorbent sample. a. full thermogram, b. second temperature ramp with hydrogen sulphide exposure vs. temperature.	213
Figure 6.5.7: Isothermal multiple sorption cycles (12 min sorption 50 % Ar/49.8 % CO ₂ /0.2 % H ₂ S, 24 minutes desorption pure Ar) of a Mg-Cs-wetmix (a, b) and a Mg-nano-direct sample (c, d). a+c. 350 °C, b+d. 370 °C. Pre-treatment and after-treatment in pure Ar at 510 °C. Experiment d. was stopped as no more cyclic capacity was observed.....	215
Figure 6.5.8: Isothermal (370 °C) 25-cycles TGA experiment using Mg-Cs sorbent in 48.8 % H ₂ , 48.8 % CO ₂ and 2.4 % water (12 minutes sorption) and pure dry Ar (24 minutes desorption). a. Mg-Cs-wetmix, b. Mg-nano-direct.	216
Figure 6.5.9: Powder XRD patterns (Cu K α radiation) of a MgO-Cs wetmix and a CdCO ₃ -NaI sample conditioned in 2 % H ₂ S at 380 °C for two hours.	217
Figure 8.3.1: a. sand bath, b. closed autoclave, c. opened autoclave.	231
Figure 8.4.1: Setaram TAG 24-16 thermoanalyser and auxiliaries.....	232
Figure 8.4.2: Schematic of the TAG 16-24 thermoanalyser. a. Top-to-bottom gas flow, b. Bottom-to-top gas flow	233

Figure 8.5.1: Illustration of an X-ray beam being reflected by two atom layers in a crystal lattice.	235
Figure 8.5.2: Bruker D8 focus powder diffractometer.....	236
Figure 8.5.3: Schematic of the diffractometer at the Powder Diffraction beamline of the Australian Synchrotron.	237
Figure 8.6.1: Location of the bright field (BF) and annular dark field (ADF) detectors in STEM [7].	240
Figure 8.6.2: JEOL 2100F transmission electron microscope.....	241
Figure 8.6.3: JEOL 7001 F scanning electron microscope.....	242
Figure 8.10.1: Left: AutoChem instrument. Right: Furnace opened with quartz sample tube.....	244
Figure 8.13.1: a. Removal of a 1s photoelectron during XPS, b. Auger electron ejection as a result of an electron vacancy in the K shell [12].....	247

List of Tables

Table 1.2.1: Flue gas composition of a typical low-sulphur east USA bituminous coal fired in 20 % excess air [21]. Balance gas is N ₂	7
Table 1.2.2: Syngas compositions in %, dry gas basis [27].....	9
Table 2.4.1: List of samples examined in this chapter	32
Table 2.4.2: BET surface areas of the magnesium oxides and their precursors.....	34
Table 2.4.3: Mass loss experiment for pure calcium carbonate.....	42
Table 3.4.1: Cadmium carbonate materials tested. Mass percentages refer to the basis of CdCO ₃	62
Table 3.9.1: Statistics of the Le Bail fits.....	79
Table 3.9.2: Results of the Le Bail refinement of the laboratory XRD data for cadmium oxide and carbonate.....	81
Table 3.10.1: Assignment of electron diffraction pattern observations corresponding to label A-K in the article, d-spacing values obtained from Powder Diffraction File entry 04-001-3770 (CdO)	83
Table 3.13.1: Samples used in multicyclic adsorption/desorption tests.	91
Table 3.14.1: Theoretically achievable mass gains by full carbonation compared with the working capacities achieved in Figure 3.14.6 in the short cycle experiments. 17.5 % NaI based on CdCO ₃ is assumed here to be inert during initial decarbonation, SBA-15 throughout the experiment.....	104
Table 3.19.1: Results of the Le Bail refinement of the synchrotron XRD data (refer Figure 6) for cadmium oxide and carbonate	116
Table 3.19.2: Statistics of the Le Bail fits.....	117
Table 4.5.1: Temperatures for release of compounds during the temperature ramp test for the CdO-NaI sample calcined in air before the experiment.....	139
Table 4.5.2: Temperatures for release of compounds during the temperature ramp test for the CdCO ₃ -NaI sample used in the carbonate state (decarbonated in fixed-bed instrument)	139
Table 4.5.3: Molar ratios of iodine to sodium as determined by XPS	140

Table 4.5.4: Literature values for Cd 3d binding energies taken from [10] (except *). Averages were taken if multiple entries in the same order of magnitude were found in the database.	141
Table 4.5.5: Literature values for O 1s binding energies taken from [10]. Averages were taken if multiple entries in the same order of magnitude were found in the database.	143
Table 4.5.6: Literature values for C 1s binding energies. Averages were taken if multiple entries in the same order of magnitude were found in the database.....	144
Table 4.5.7: Literature values for I 3d binding energies taken from [10]. Averages were taken if multiple entries in the same order of magnitude were found in the database. Cd 3p shown for comparison.	146
Table 4.5.8: Literature value for Na 1s binding energy [10].	147
Table 5.5.1: BET surface areas from N ₂ physisorption. Refer to supplementary materials for isotherms.....	168
Table 6.5.1: Working capacities (wt%) for sorbent samples in H ₂ and H ₂ S multicyclic experiments.	211
Table 6.5.2: Working capacities of a previous project in dry and wet (1.2 % water) gas cycles containing 50 % CO ₂ /Ar and pure Ar (no H ₂ S). Refer section 3.14.1 and 3.18 for Cd and Chapter 5 for Mg samples. Cd sample name of sections 3.14.1 and 3.18 given in comments.....	211
Table 6.5.3: Assessment of degradation of CdO sample due to assumed S ²⁻ retention of the experiment in Figure 6.5.3b.....	211
Table 8.2.1: Specifications of chemicals used in this thesis.....	229

Chapter 1 Introduction

1.1 General background

The term ‘global warming’, also called ‘climate change’ or ‘greenhouse effect’, refers to an increase in the earth’s surface temperature, caused by so-called greenhouse gases. These gases, of which many are natural components of the atmosphere, are mostly translucent to visible light, but have the ability to absorb radiation in the infrared spectrum. When sunlight (i. e., its fraction of the visible light spectrum) reaches the earth, it is first absorbed by the earth’s surface and then re-radiated as longer-wavelength infrared radiation. This radiation is then partially ‘trapped’ in the atmosphere, as the greenhouse gases then hinder the energy associated with the infrared light from escaping into space (Figure 1.1.1). Without the natural greenhouse gases, the earth would on average be 33 °C cooler and potentially unable to create conditions supportive for life as we know it [1].

Activities of human civilisation, however, have created technologies that strongly rely on energy conversion, which in turn is backed up by a widespread use of fossil fuels. These fuels generate carbon dioxide (CO₂) as an exhaust gas during their combustion. An increase in living standard in developing nations is predicted also to increase energy demands by 57 % from 2004 to 2030 [2], peaking no earlier than in the year 2025 in the case of China and India [3].

Carbon dioxide, being the greenhouse gas of greatest impact emitted by human activity [4], causes an undesirable intensification of the greenhouse effect, which is predicted to lead to rising sea levels, desertification and species extinction. Secondary effects, like an increase in water vapour content in the atmosphere due to a higher temperature, might further accelerate the greenhouse effect, as water vapour is also an infrared-active gas, and, thus, can be considered a greenhouse gas [5]. A more recent study has found that non-condensing greenhouse gases, particularly CO₂, are the most important factor in the control of the earth’s temperature, and that the feedback system involving condensing vapours (like water) and the earth’s albedo (this is a measure of radiation reflectivity,

influenced by the appearance of reflective/white glacial ice vs. darker rocks, among others) is very complex [6].

As the extent of the contribution of energy generation to human carbon dioxide emissions is considered to be more than 75 % and the majority of emission sources are stationary emitters like power and heat generation systems [5], reduction strategies for greenhouse gases in this sector are considered most likely to offer the greatest impact [7].

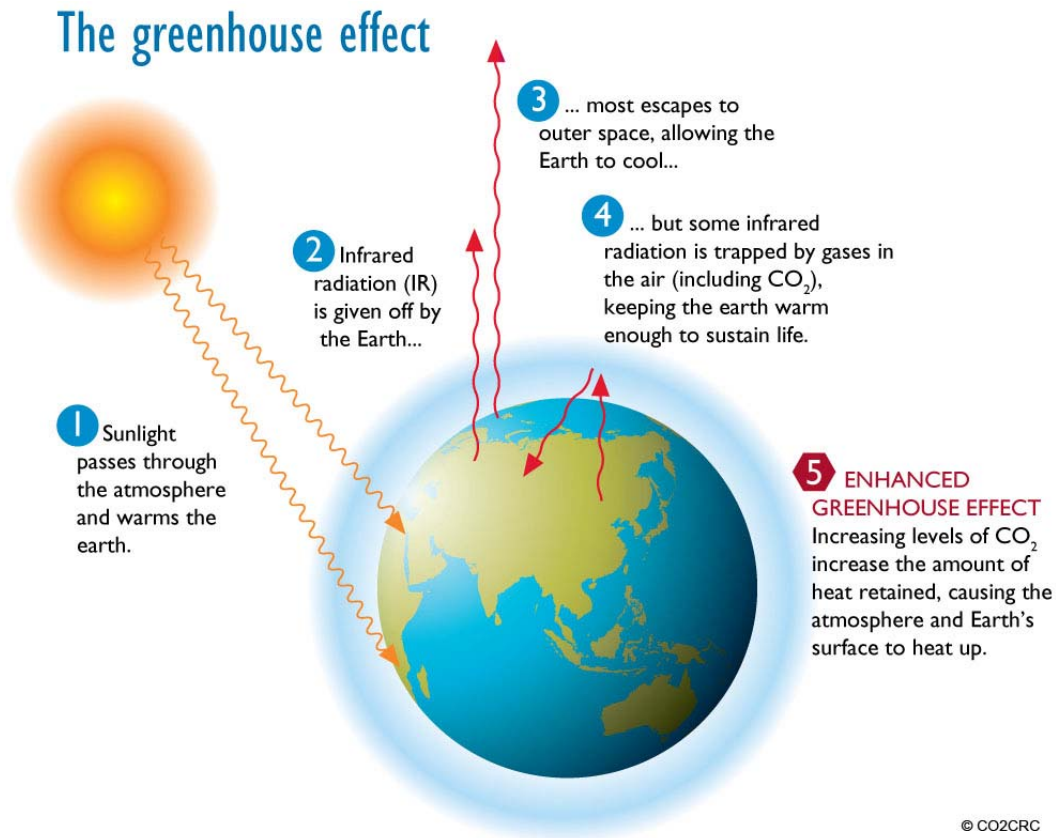


Figure 1.1.1: Schematic illustration of the earth's greenhouse effect [8]

To move away from high carbon dioxide emissions, there are three prospective strategies:

Firstly, the amount of energy used by society can be reduced. If it is assumed that society does not want to compromise its living standard, which requires technology that, in turn, consumes energy, more energy-efficient ways of energy conversion and supply need to be developed to address this first option.

Secondly, another possibility is to make the switch to fuels which have a lower specific carbon content. For example, methane (CH₄), a major component of natural gas, has a calorific value of 50 MJ/kg [9]. With combustion according to eqn. 1.1.1 and accounting for

the molar masses of CO₂ (44 g/mol) and CH₄ (16 g/mol), it can be calculated that the combustion of methane yields emissions of 2.75 g CO₂ per g of methane. Considering the calorific value stated above, this means that 0.055 g CO₂ per kJ of thermal energy will be emitted if methane is used as a fuel.



If we consider anthracite, a high rank coal, which contains 92.2 mass% of carbon [10], it can easily be shown that 3.7 g CO₂ per g carbon (molar mass 12 g/mol) are emitted according to eqn. 1.1.2. This yields 3.4 g CO₂ per g anthracite, under the assumption that carbon is the major contributor to the calorific value. As anthracite is reported to have a calorific value of 35.7 MJ/kg [10], it can be concluded that a kJ of thermal energy derived from anthracite emits 0.095 g CO₂, almost double the value for methane.



The use of natural gas would thus be of considerable benefit as a substitute for coal in order to reduce energy-specific carbon dioxide emissions. Of even greater benefit would be the use of renewable energy sources, like solar, wind and hydropower, which offer an almost carbon-free alternative. However, the low fraction of penetration of these energy sources (Figure 1.1.2) in the global energy market will need to be increased significantly. Currently this faces constraints due to the deployment times required [11, 12]. Some renewable energy sources, like wind or solar power, are not available constantly (i. e., wind can only be harvested when it is blowing, solar energy can only be used during daytime) and are thus unable to provide the base load for an electricity grid.

The third strategy of reducing carbon dioxide emissions involves carbon capture and storage (CCS, Figure 1.1.3). The high abundance and low cost of coal make it a likely key player in the energy generation industry of the near future [4, 13], so that this strategy focuses on continuing the use of fossil fuels, while avoiding the emission of carbon dioxide to the atmosphere. This is done by separating the carbon dioxide gas from exhaust gas or fuel gas streams, then subsequently storing it in a place where it can be safely contained for long periods. The introduction of the CO₂ into the chemical industry market as a

feedstock for chemical reactions will also be of consideration, if such a market can be developed.

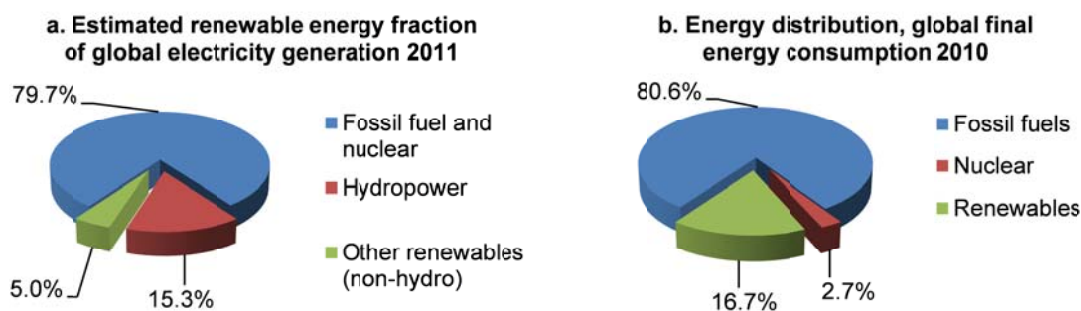


Figure 1.1.2: a. Fraction of renewable energy of global electricity generation 2011, b. global final energy consumption, distribution 2010. Values from [12].

Storage of CO₂ was proposed by injection into deep sea waters [14], but concerns have arisen that this would pose an impact on the marine ecosystem and, thus, “replace one environmental problem with another” [4]. More recent research efforts are focussed on CO₂ storage in depleted oil and gas reservoirs, rock cavities, saline aquifers, unmineable coal seams or the use of CO₂ in the recovery of coalbed methane, or oil [15]. The latter, known as ‘Enhanced Oil Recovery (EOR)’, is predicted to use significant amounts of CO₂ that can only be supplied if CO₂ is obtained through capture from industrial sources [16]. Part of the CO₂ used in EOR remains in the oil reservoir, so that this technique can be considered a CO₂ storage strategy. Another suggested manner of CO₂ disposal is mineral carbonation. Naturally occurring minerals, like magnesium or calcium silicates, are able to form non-toxic carbonated materials with CO₂, which can then easily be disposed of or used in the construction industry [17].

Before any considerations for the use or storage of CO₂ can be made, ways must be found to recover it from power plant processes. This, so-called CO₂ capture, represents the main focus of this thesis, as will be elucidated below.

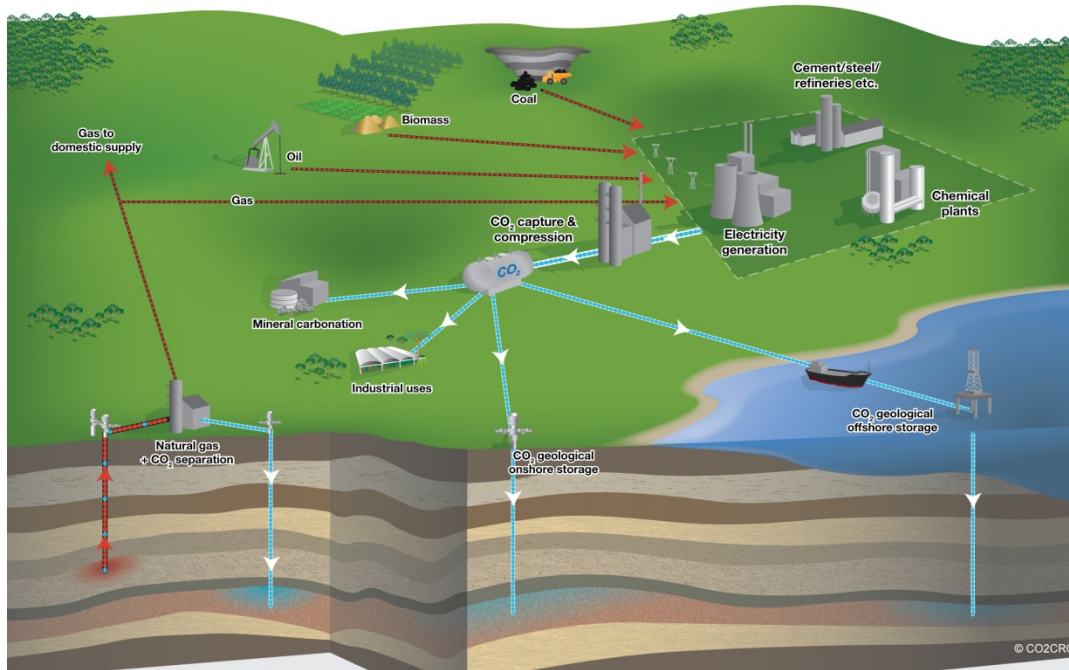


Figure 1.1.3: An artist's illustration of industrial CO₂ sources and disposal possibilities [8]

1.2 Carbon dioxide capture process integration

This sub-chapter describes the different CO₂ capture approaches. As different energy conversion technologies result in different properties of the CO₂-bearing gas streams, it is important to design CO₂ capture processes and materials to make them most suitable for the process they are intended to perform in.

1.2.1 Chemical looping combustion

A series of novel energy conversion processes have been described that involve carbon dioxide capture in their process flow sheet [4]. An example is the chemical looping combustion process, which reacts carbon-containing fuel gas with a metal oxide as oxygen carrier to generate heat. The exhausted metal oxide is then looped into a separate oxidation reactor, where it is regenerated by oxidation with air, and then recirculated into the combustion reactor (Figure 1.2.1). As the principal products of fuel combustion in the presence of a metal oxide are water and carbon dioxide, carbon dioxide capture can be achieved at low energy and cost expenditure [18]. A more recent study has proposed a modified process, where calcium oxide is used for both oxidation of the carbon and capture of the carbon dioxide to form calcium carbonate. This is then looped through a regenerator to be converted back to calcium oxide, yielding pure carbon dioxide [19].

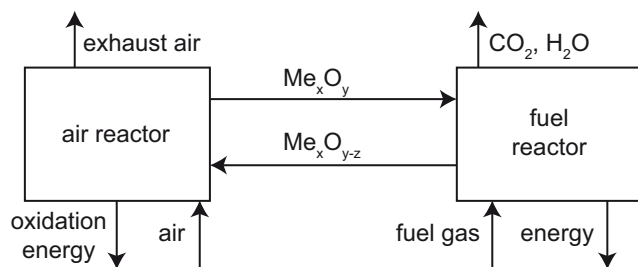


Figure 1.2.1: Conceptual scheme of the chemical looping combustion process [18]. 'Me' stands generically for a metal.

As the novel energy generation processes are very diverse, this chapter will not elaborate on them in detail. The subsequent subchapters will focus on carbon dioxide capture technologies that incorporate well-known processes – coal gasification and the conventional power plant combustion process.

1.2.2 Post-combustion capture

A possible way to remove CO₂ from exhaust gas streams is to use the flue gas of conventional power plants, extract the CO₂ into a separate stream and release a CO₂-depleted flue gas to the atmosphere (Figure 1.2.2).

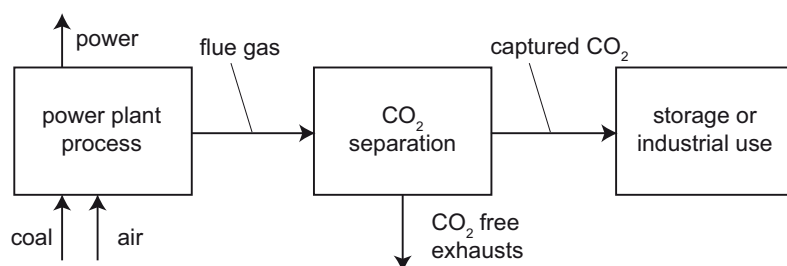


Figure 1.2.2: Conceptual scheme of the post-combustion carbon dioxide separation [2, 20].

As this approach requires the fuel to be incinerated first, it is referred to as 'post-combustion' capture. This approach has the advantage that it can be easily retrofitted into existing power plants [20]. In this case, the flue gas contains a high amount of nitrogen originating from the air used during combustion, and a CO₂ content of 13 to 16 vol% for coals [4, 21] or 3 to 4 vol% for natural gas [4] (Table 1.2.1). The conventional combustion is normally carried out around atmospheric pressure and the temperature of the end-of-tail flue gas is normally not below 130 °C due to the danger of condensation of sulphuric acids

inside the flue gas duct. More modern power plants are able to reduce the flue gas temperature to values as low as 72 °C by using the cooling tower draft as a flue stack replacement [22].

Table 1.2.1: Flue gas composition of a typical low-sulphur east USA bituminous coal fired in 20 % excess air [21]. Balance gas is N₂.

compound	CO ₂	H ₂ O	O ₂	SO ₂	NO _x	HCl	Hg
concentration	15-16 vol%	6-7 vol%	3-4 vol%	500-1000 ppm	500 ppm	100 ppm	1 ppb

1.2.3 Oxy-fuel combustion

The comparatively low CO₂ concentration obtained in post-combustion flue gas provides a challenge for CO₂ sorption systems, as due to the high amount of inert nitrogen and the low CO₂ concentration, high volume flows of gas have to be processed by a CO₂ capture system, requiring large apparatus and thus, creating high investment costs [4, 20].

A solution to this problem is oxy-fuel combustion, which is very similar to the pre-combustion approach, but uses pure oxygen as combustion gas instead of air (Figure 1.2.3). This approach requires an air separation unit that removes the nitrogen from air to provide oxygen. As combustion in pure oxygen would result in temperatures that are too high for currently available construction materials to withstand, a fraction of about 2/3 of the flue gas is recirculated into the combustion process. This way, carbon dioxide concentrations of more than 80 % can be achieved and the concentration of nitrogen oxides is also reduced, as airborne nitrogen is removed before combustion. A disadvantage of the oxy-fuel process is the requirement of an air separation unit, which is expensive both in terms of energy consumption and capital cost [4, 20].

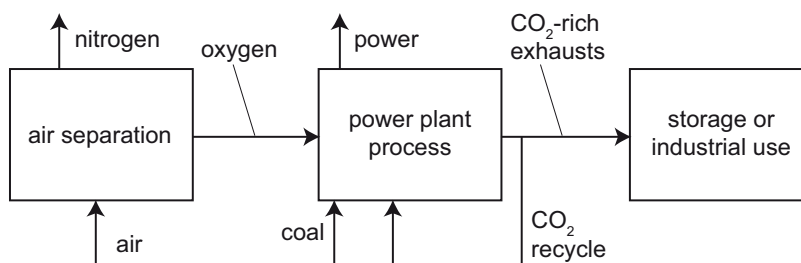
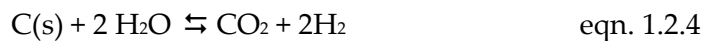


Figure 1.2.3: Conceptual scheme of the oxy-fuel process [2, 20]

1.2.4 Pre-combustion capture

The approach known as ‘pre-combustion’ carbon dioxide capture [23, 24] is achieved by the Integrated Gasification Combined Cycle (IGCC) process (Figure 1.2.4), which involves high temperature gasification of coal into an intermediate synthesis gas (syngas) mixture. This syngas is created by treating the coal with water vapour in a lean oxygen atmosphere, in this way avoiding complete combustion of the coal [24]. With this approach, the reactions in eqn. 1.2.1 to eqn. 1.2.5 occur, producing a syngas consisting mainly of carbon monoxide, carbon dioxide, water vapour and hydrogen, as well as impurities that contain sulphur and nitrogen [25].



The reactions in eqn. 1.2.1, eqn. 1.2.2 and eqn. 1.2.5 are exothermic and provide energy for the autothermal operation of the reactor, i. e., to power the endothermic reactions of the char and water (eqn. 1.2.3 and eqn. 1.2.4). In a water-gas shift (WGS) reactor, located downstream of the gasifier, the yield of carbon dioxide and hydrogen can be increased according to eqn. 1.2.6.



If the carbon dioxide could be conveniently captured from the syngas in the WGS reactor, (non-polluting) water would be the principal combustion product released from the power plant, after combustion of the hydrogen gas for power generation in a combined gas and steam turbine process. The removal of carbon dioxide in-situ in the WGS reactor would also encourage a shift in the equilibrium of the water-gas reaction (eqn. 1.2.6) towards the valuable product, hydrogen.

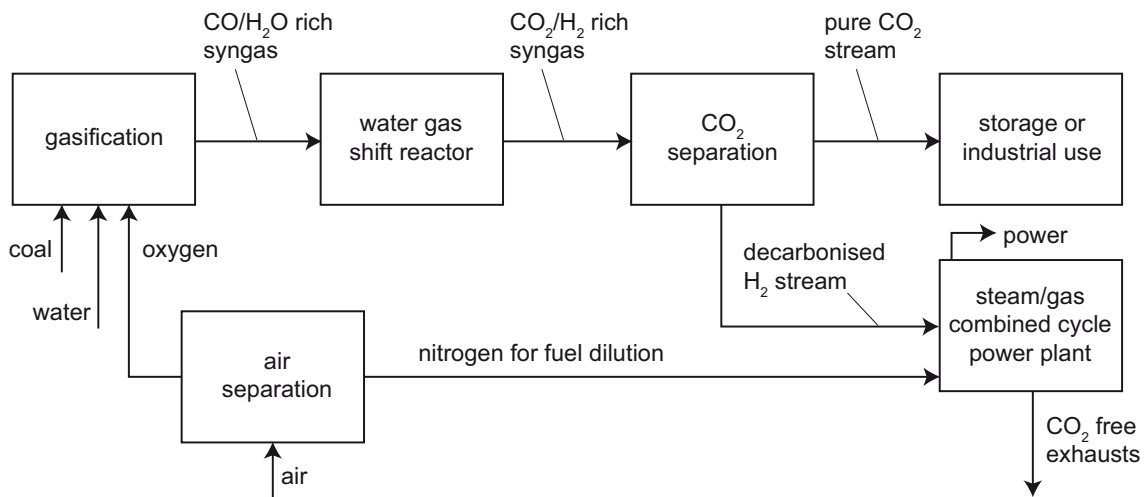


Figure 1.2.4: Conceptual scheme of the IGCC process with carbon dioxide separation [24].

In comparison to the post-combustion approach, pre-combustion syngas consists of different constituents (Table 1.2.2). The nitrogen content is low, as only fuel nitrogen is carried into the gasification chamber. Furthermore, due to the lean oxygen environment, trace contaminants resulting from sulphur and nitrogen contained in the fuel are of a different nature in pre-combustion (H_2S , NH_3 , COS) compared to post-combustion (SO_x , NO_x) gases [21, 25]. Temperatures in the gasifier usually range between 800 and 1800 °C [25], whereas pressures of atmospheric up to 50 bar are reported, depending on the type of gasifier [26].

Table 1.2.2: Syngas compositions in %, dry gas basis [27].

compound	CO	H ₂	CO ₂	N ₂
dry-coal fed gasifier	65	30	2	3
slurry-fed gasifier	44	37	16	3
after WGS reactor	4	55	38	3

As the gas leaves the water-gas shift reactor at temperatures between 250 and 400 °C [23] and at pressures of typically 20 to 30 bar [28], it would be beneficial to capture the carbon dioxide in this temperature range, without any necessities to further cooling or heating of the gas.

The pre-combustion capture process is considered to involve a high capital cost, but it is also reported that CO_2 capture is more easily achieved due to the high CO_2 content of the

syngas compared to flue gas (Table 1.2.1 and Table 1.2.2). This might lead to reduced expense in terms of the carbon capture cost, giving the pre-combustion process good prospects for future implementation [2, 4, 20]. For this reason, this project is focussed on pre-combustion capture methods capable of operating between 250 and 400 °C.

1.3 Carbon dioxide capture methods

1.3.1 Solvent absorption

Absorption processes for carbon dioxide using an aqueous amine solution, Selexol (dimethylethers of polyethylene glycol) or Rectisol (methanol) have been employed for more than 40 years [29]. In the Selexol and Rectisol process, the liquid serves as a physical solvent, whereas in aqueous amine solvents, chemically reactive absorption is performed.

Another process uses a potassium carbonate solution as chemical absorbent. Here, the overall reaction (eqn. 1.3.1) involves water and carbon dioxide to form potassium hydrogen carbonate [30].



For absorption processes, normally a gas stream is supplied through the bottom of an absorber column and the absorbent solution is supplied at the top. The laden solvent is subsequently pumped into a regeneration column, where the carbon dioxide is released by heating or flash evaporation (pressure release).

The reaction of the amine with carbon dioxide (Figure 1.3.1) is performed at a temperature around 40 °C with absorbent regeneration at 100 to 140 °C [29], whereas potassium carbonate solutions absorb at 40 °C and are regenerated at above 107 °C [30]. The Selexol process is performed at even colder temperature (-40 °C). For pre-combustion carbon dioxide capture, these temperatures would require significant cooling of the syngas associated with an energy penalty; so that these processes are not part of the scope of this study. Furthermore, amine solvents are prone to react with trace contaminants during the carbon dioxide absorption process, like oxygen, sulphur and nitrogen oxides, and corrosion products from within the reactor, causing degradation of the absorbent performance [31].

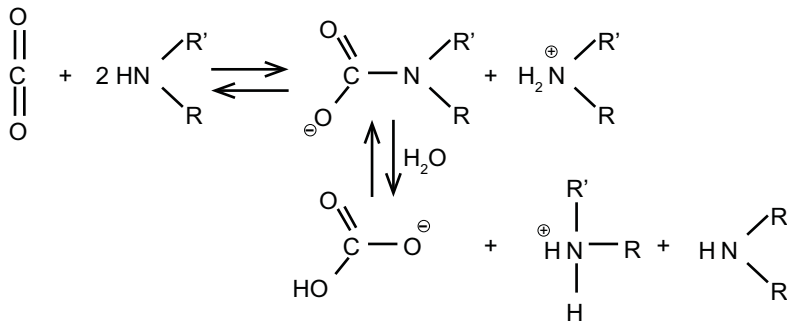


Figure 1.3.1: CO₂ absorption reaction with a primary or secondary amine [29].

1.3.2 Cryogenics

Cryogenic carbon dioxide capture methods involve cooling of the gas in order to bring carbon dioxide below its boiling or sublimation point. The advantage of this process is that liquid carbon dioxide can be generated. The process is projected to operate well for gases with a high carbon dioxide concentration, including oxyfuel exhaust gas and pre-combustion syngas [32].

The cooling process requires a lot of energy and, thus, is only viable if cryogenic carbon dioxide is required for another purpose. An additional requirement is the removal of hydrocarbons and water traces in the gas upstream of the cryogenic process, due to their tendency to freeze and block equipment [32]. The superiority of a cryogenic carbon dioxide capture process over membranes has been reported under conditions where the energy demand for cooling could be met by a nearby liquefied natural gas (LNG) evaporation unit incorporating heat integration [33]. An older study (2003), however, summarises doubts about the attractiveness of cryogenics for carbon dioxide separation [21].

As for liquid absorption processes (section 1.3.1), cryogenics are considered a means of end-of-tail carbon dioxide capture, requiring their optimal operating temperature below the one of syngas. For this reason, cryogenic processes are not considered to be prospective for an in-situ capture of carbon dioxide from hot syngas within the water-gas shift reactor.

1.3.3 Membranes

An IGCC plant that uses a metallic membrane reactor for hydrogen separation from syngas was hypothetically described and analysed by process design calculation and

simulation [24]. The benefit of this process layout is in the ability to effect in-situ separation of hydrogen and carbon dioxide at the temperature of the water-gas shifted syngas (in the study, around 450 °C). Pd-Cu alloys were reported as hydrogen-permeable membrane materials, and which also have the benefit of being tolerant to sulphur compounds. Furthermore, the presence of a catalyst to promote the water-gas shift reaction (eqn. 1.2.6) on the raffinate side, inside the membrane separator, encourages a high yield of hydrogen. This is further encouraged by constant removal of hydrogen through the membrane according to Le Châtelier's principle [34]. The authors, however, conclude that the benefits of the membrane process are only a few per centage points in terms of performance and cost. This is because of the expensive membrane materials (Pd) that are required. It is also stated that the membrane reactor would likely need to be very large due to a high required surface area (caused by low permeability) and also delicate, posing potential problems in a syngas environment that might contain aggressive chemicals and that is also subject to changing concentration of its components [35, 36]. A different study came to a similar conclusion, stating that membranes with a good compromise between high permeability combined with high selectivity and chemical stability require further research [2].

Other types of membranes permeable to carbon dioxide comprise polymers, Facilitated Transport Membranes (FTM), inorganic membranes, hybrid organic-inorganic membranes and hollow fibre gas-liquid contactors. These are reported to operate at low temperatures (-20 to 35 °C for organic membranes, -20 to 180 °C for inorganic membranes, 25 to 35 °C for hybrid membranes, 20 to 40 °C for hollow fibre contactors and 23 to 26 °C for FTM) [32]. Another study reports higher temperatures for hydrogen permeability, especially for inorganic membranes of up to 650 °C, and for a polymeric membrane of 270 °C [37]. This study also outlines future research requirements in terms of inexpensive membrane materials and manufacture, chemical and long-term stability and pilot plant scale investigations to test membrane scale-up and the effects of realistic industry conditions.

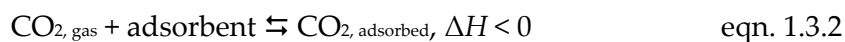
In conclusion, membranes appear prospective for use in pre-combustion capture, but at present require significant trade-offs between e.g. selectivity vs. permeability or

permeability vs. ease of synthesis [38]. Furthermore, the majority of membranes are reported for low temperature use.

1.3.4 Adsorption

1.3.4.1 Definition and application

Adsorption generally describes trapping gases on solid surfaces of an adsorbent [39], according to reaction eqn. 1.3.2 for carbon dioxide, as an example.



The reaction is in most cases exothermic on adsorption and thus, endothermic on desorption, i. e., release of the gas molecules from the adsorbent. For a process like carbon dioxide capture, where the gas is to be adsorbed and subsequently re-desorbed, different modes of process design can be employed [40]. Firstly, in thermal or temperature swing adsorption (TSA), adsorption is carried out at a lower temperature than desorption. Heating up the laden adsorbent causes the endothermic desorption reaction to be favoured, releasing the adsorbed molecules. Secondly, pressure swing adsorption (PSA) uses isothermal conditions (same temperature) for both adsorption and desorption, and the adsorption is carried out at a higher pressure than the desorption. According to eqn. 1.3.2, Le Châtelier's principle dictates the reaction will proceed to the right if the partial pressure of the gas increased. Lowering the pressure would then drive the reaction to the left-hand side, causing desorption. PSA normally refers to the use of elevated pressures (above atmospheric) being used in the process, whereas if a vacuum is involved for desorption, the term vacuum swing adsorption (VSA) is commonly used. Pressure (or vacuum) and thermal swings can also be combined.

Vacuum and pressure swing have advantages in the process design, as a pressure change can very quickly be applied to a sorbent bed, whereas uniform heating and cooling takes substantially longer times [41]. For this reason, a special focus is given to the capability of materials to perform under isothermal pressure swing conditions in the scope of this thesis.

1.3.4.2 Adsorption materials

A variety of materials have been described as carbon dioxide adsorbents. These materials generally possess high surface areas, which facilitate the physisorption of gases in its own right. In order to increase their selectivity towards carbon dioxide compared to other gases (like nitrogen in the case of post-combustion carbon dioxide capture flue gas), they can be chemically functionalised. Examples for such adsorbents are mesoporous silica-based adsorbents, carbon-based adsorbents, and metal organic frameworks (MOF).

SBA-15 mesoporous silica is synthesised using a surfactant (e. g. Pluronic P123) directing the silica precursor (tetramethoxysilane, tetraethoxysilane, tetrapropoxysilane) into a hexagonal array of micelles in an acidic medium [42]. Hydrolysis of the silica precursor and removal of the surfactant (by solvent washing or calcination) then yields a mesoporous, high surface area silica framework. MCM-41 (Figure 1.3.2), being made from sodium silicate, involves a similar synthesis technique, also using a surfactant in acidic solution [43].

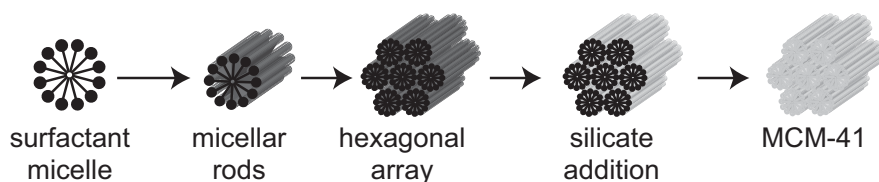


Figure 1.3.2: Synthesis of MCM-41 as an example for a high-surface area silica [43].

The silica can subsequently be functionalised using polyethylenimine [44], generating amine functions either tethered onto the surface of the support, filled into the pores, or polymerised in-situ into the support [45]. The amine functions can react with carbon dioxide according to eqn. 1.3.3. Such materials can then be considered to be chemisorbents, as the amine functional groups form a chemical bond with the carbon dioxide upon adsorption.



Metal organic frameworks consist of organic ligands, forming networks with metallic ion nodes. These networks can be porous and of high surface area (up to 5000 m²/g), so that they are prospective for gas adsorption techniques [29]. Also MOFs are considered for

amine functionalization in order to enhance their carbon dioxide sorption ability, but their water stability must be ensured if used in water-containing gas streams like flue gas or syngas [46, 47].

Activated carbons studied in this context have also been subjected to amine functionalisation using a surface grafting method [48] or a polyethyleneimine pore loading technique [49] in order to make them more efficient for carbon dioxide capture.

The aforementioned adsorbents are reported to work at temperatures from room temperature to a maximum of 200 °C, the latter for regeneration. For this reason, they are not of particular relevance for in-situ high temperature application for pre-combustion carbon dioxide capture as outlined in the previous sections.

1.3.5 Metal oxides for carbon dioxide capture

In order to design an adsorption process for carbon dioxide, metal oxides, which convert to their respective carbonates upon exposure to a carbon dioxide-containing gas stream, are considered suitable candidate materials. If such oxides can form carbonates within the range of 250 to 400 °C, they will show potential to be used in-situ for the water-gas shift reaction with carbon dioxide capture (refer section 1.2.4). As these metal oxides are considered to show a chemical reaction to form carbonates in their bulk, rather than by surface physisorption or chemisorption as outlined in section 1.3.4, it is questionable whether the term 'adsorption' is appropriate. For this reason, the more generic terms 'sorption' and 'sorbent' will be used in the context of this thesis, when referring to metal oxide carbonation reactions.

1.3.5.1 Calcium oxide containing sorbents

In the recent years, calcium oxide has been studied intensely as a prospective carbon dioxide sorbent. Natural limestone, as well as synthesised materials (with or without support) have been used as a source of calcium oxide [50-78]. The carbon dioxide capture properties of calcium oxide are given by the reversion of the lime calcination reaction, eqn. 1.3.4 (M = alkaline earth metal, in this case calcium). Regeneration then releases pure carbon dioxide, which can be used for further industrial processes or sequestration.



The temperatures required for the sorption of carbon dioxide on calcium oxide (carbonation) are between 600 and 700 °C, whereas regeneration (calcination) requires even higher temperatures of approx. 900 °C. It is reported that cyclic ad-/desorption leads to a reduction in sorption capacity. This has been the focus of a significant body of scientific work [50, 51, 57, 59-61, 63, 67, 74].

According to the change in molecular weight during the reaction in eqn. 1.3.4, a mass increase of 78 % (based on the initial amount of pure calcium oxide) is possible if all calcium oxide is converted (stoichiometric conversion). A multitude of authors have reported that up to more than 90 % of this stoichiometric conversion can be achieved in thermogravimetric analysis (TGA) and fixed bed tests [57, 58, 63, 69-71, 74, 77]. While these authors refer to the reaction in eqn. 1.3.4 as the carbon capture reaction, they have employed different precursors for the synthesis of the sorbent. Chen et al. [54], for instance, synthesised an alumina support for the calcium oxide sorbent, by mixing calcium oxide and either aluminium isopropoxide or aluminium nitrate enneahydrate in an aqueous solution. By calcination of the precipitated solids afterwards, a $\text{Ca}_{12}\text{Al}_{14}\text{O}_{33}$ compound is formed. Calcium oxide supported by this compound was shown to be slightly more stable than pure calcium oxide during several carbonation-calcination cycles in 10 % carbon dioxide gas in nitrogen. But with approx. 25 % mass increase, only less than half of the stoichiometric capacity was achieved in 10 and 60 minutes carbonation runs and there was still a decrease in capacity to be observed with multiple ad-/desorption cycles.

Feng et al [57] used calcium chloride as a precursor to impregnate calcium oxide onto γ -alumina. After calcination at 823 K, the obtained sorbent showed approx. 90 % stoichiometric conversion during a 5 minute carbonation experiment, and exhibited stable capacity over 9 cycles, using pure carbon dioxide for the sorption step.

Florin et al. [58] used commercial nano-sized calcium carbonate particles for calcination and carbonation experiments. The sorption capacity of these samples was initially high (90 %), but decreased to approx. 20 %, using 15 % carbon dioxide in nitrogen for the sorption step.

Florin et al. and Manovic et al. found that a prolonged carbonation cycle, after capacity reduction due to multiple sorption cycles, leads to an increase of the sorption capacity in following cycles, [58, 70, 71].

The causes for the decreasing capacity of calcium oxide sorbents during cycling are stated to be (a) sintering due to the high temperatures involved [54, 79] and (b) a shift from smaller mesopores to larger macropores during multicyclic carbon dioxide sorption. The latter has been clearly demonstrated by mercury porosimetry [74]. The loss-in-capacity problem can be remediated by creating nanoparticles of calcium oxide, either by dispersing the sorbent onto a support [57, 67] or by a flame-spray method that creates small particles [68]. Impregnation with potassium permanganate also has been shown to maintain a higher sorption capacity over a multitude of sorption cycles [66]. It appears that differences in the performance of various calcium oxide materials can be related to the sorbents' morphology rather than its surface/gas reaction chemistry. X-ray diffraction studies undertaken by Gupta et al. revealed peaks for calcium oxide, no matter which precursor the oxide sample was prepared from. But it was shown that different pore sizes and surface properties had different sorption behaviour [63]. Alvarez et al. quantified the formation of closed pores during cycling by calculating a theoretical density of the sorbent and comparing it with the density obtained by mercury porosimetry at maximum pressure of 225 MPa; the group observed an increase in closed pores as the number of cycles progressed [51].

Regarding calcium oxide based sorbents, it must be noted that the carbonation and calcination temperatures are comparatively high – around 650 °C for carbonation and around 900 °C for calcination. Thus, pure calcium oxide based sorbents are not ideally suited for the pre-combustion carbon dioxide capture process after the water-gas shift reactor described in section 1.2.4.

However, by changing the structural properties (see above) or introducing other metal compounds, a suitable sorbent based on calcium oxide can be synthesised. Sirivardane et al. [73] reported a solid-state mixing procedure of sodium hydroxide and calcium oxide. The so prepared sorbent had a sorption capacity of more than 13 wt% carbon dioxide at 315 °C and was regenerable at 700 °C.

Sultan et al. [80] used commercially available calcium-magnesium acetate as a precursor for a sorbent, which was able to capture 55 wt.-% of carbon dioxide from a 50 % carbon dioxide containing gas stream at 750 °C.

Reddy and Smirniotis [81] used alkali metal dopants to increase the capacity of a calcium oxide sorbent, reaching 50 % weight increase with a cesium-doped sorbent at 600 °C.

Lu et al. [68] used a flame-spray method to synthesize calcium oxide sorbents from a calcium naphthenate precursor, also with zirconium doping. Depending on the properties, some of the resultant sorbents showed 95 % molar conversion during carbonation in the first cycle and were stable for several cycles at 700 to 850 °C.

1.3.5.2 Magnesium oxide

Although the carbonation-calcination reaction of magnesium oxide is similar in principle to that of calcium oxide (eqn. 1.3.4 with M being Mg) [82], less information for magnesium oxide carbonation can be found in literature. According to a thermodynamical calculation performed by Feng et al., the calcination temperature for magnesium carbonate can be considered lower than the one for calcium oxide. Depending on the gas composition, carbon dioxide desorption is reached between approx. 230 to 370 °C [56]. This temperature range is similar to that of the water-gas shift reaction; thus, magnesium oxide may be more suitable for the pre-combustion carbon dioxide capture process.

A theoretical calculation of the molar mass increase during the carbonation of magnesium oxide reveals that the potential mass increase of magnesium oxide is 109 %; in other words this is the theoretical sorption capacity.

Yong et al. [83] have reported that magnesium oxide has a capacity of 0.5 mmol/g at atmospheric pressure and 300 °C (equal to a weight increase of 2.2 %). This is obviously far below the value that is theoretically achievable. The reason for this behaviour is reported as due to the carbon dioxide mostly being surface-bound [79].

Bhagiyalakshmi et al. [84] reported a process for producing a mesoporous support-free sorbent. Impregnating mesoporous silica with a carbohydrate solution and then calcining it under nitrogen flow delivered a mesoporous carbon. By washing with hydrofluoric acid to remove the silica and impregnating and calcining the obtained carbon with magnesium

nitrate precursor, a mesoporous support-free magnesia sorbent was prepared. This material was found to sorb 8 % of its initial weight of carbon dioxide and thus to have a higher capacity than the magnesium oxide sorbents reported by Yong et al. [83].

Hassanzadeh et al. [82] modified a dolomite containing calcium as well as magnesium carbonate by 'half-calcining' it at 350 °C, and thus, calcining the magnesium, but not the calcium carbonate. This sorbent then had a capacity of 35 % molar conversion of the magnesium oxide portion (i. e. 38 wt% based on the magnesium oxide content) after a carbonation of 30 minutes at 450 °C. As these experiments were performed in a thermogravimetric analyser under high pressure (20 atm), the results cannot be compared to the more widely performed investigations at atmospheric pressure. It is argued that high surface areas led to fast reaction, but that small pores blocked easily during carbonation, thus, making it impossible to reach the stoichiometric conversion. Sultan et al. come to a similar explanation, stating that higher surface areas and pore volumes measured by BJH are to be associated with a higher capacity [80].

Recent work at Monash University has demonstrated that cesium-doped magnesium oxide is a suitable carbon dioxide sorbent, with a mass increase of approx. 12 % [85].

Other applications of magnesium oxide can be found as a support for calcium oxide sorbents, where calcination and carbonation temperatures are adjusted beyond the calcination temperature of magnesium oxide, so that the calcium oxide fraction is to be considered the reactant [67, 80].

1.3.5.3 Alkali metal carbonates

Alkali metal carbonates are able to capture carbon dioxide according to the reaction in eqn. 1.3.5 (A = alkali metal). Water must be present for this reaction.



Lee, Zhao and Liang performed analyses on alkali metal carbonate based sorbents with and without inert support [86-90]. As these sorbents operate best at temperatures of approx 60 °C and are to be calcined at below 200 °C, their application in in-situ pre-combustion carbon dioxide capture must be considered unsuitable.

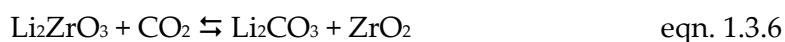
1.3.5.4 Hydrotalcites

Hydrotalcites, also called layered double hydroxides, are hydroxide compounds consisting of divalent as well as trivalent metal ions, other anions and crystal water [91]. Their carbon dioxide capture properties have been studied in a wide range of temperatures, but at 400 °C their sorption capacities are comparatively low (approx. 1 wt%) [91-94]. For a 200 °C sorption temperature, capacities of 2.9 wt% [95] were observed, whereas Yavuz et al. determined approx. 6 wt% for a potassium/gallium enhanced hydrotalcite. Here, X-ray diffraction data revealed that the gallium doping replaces aluminium ions, causing diffraction patterns to shift from 60.5 to 60 degrees 2θ with increasing gallium loading, due to a one-dimensional increase in unit cell size of the hydrotalcite [96].

The temperature range of sorption/desorption for hydrotalcite can be suitable for the pre-combustion processes, but the sorption capacities of the materials are low compared to other sorbents.

1.3.5.5 Lithium zirconate

Lithium zirconate can react reversibly with carbon dioxide according to eqn. 1.3.6.



It has been reported that this compound has a capacity of 20 wt.-% in 20 % carbon dioxide in hydrogen, after a carbonation time of 200 min at 500 °C, and can be regenerated at 680 °C [97]. Ochoa-Fernández et al. showed later, that nanocrystalline lithium zirconate, prepared by zirconyl nitrate and lithium acetate precursors, has improved kinetics and sorbs carbon dioxide to a capacity of 20 wt% after less than 10 minutes [98]. In an additional investigation, the same group of authors found that the stoichiometry of the precursors has an influence on the sorption properties, and that adding potassium leads to an improvement in kinetics at 575 °C [99]. Fauth et al. [100] also came upon a similar result using a variety of alkali and alkaline earth metal compounds as dopants. They reported that pure lithium zirconate sorbs 11.5 wt% at 500 °C after 1500 minutes, whereas doped with alkali or alkaline earth metal salts, the same value was reached after 60 minutes.

With temperatures of sorption starting only at 420 °C (found by a temperature ramp test, [97]), the reactivity of lithium zirconate may be slightly too low for direct application in pre-combustion carbon dioxide capture. The high temperatures are also required for sorption by zirconates with a lithium-/potassium carbonate/lithium hydroxide eutectic salt as a dopant, as shown by Fauth et al. [100]. Lower temperatures lead to slower kinetics, so lithium zirconates must be considered technically unsuitable for the pre-combustion capture process.

1.3.5.6 Cobalt and iron oxides

Cobalt carbonate decomposes at above 220 °C [101, 102], whereas iron carbonate does so at 459 °C [103]. This temperature range can be deemed appropriate for pre-combustion capture, but the so produced cobalt and iron intermediates are a carbon dioxide reducing catalyst in the presence of hydrogen rather than an sorbent that reversibly carbonates and are thus not suitable.

1.3.5.7 Effects of sulphur

As calcium carbonate is already used as a sulphur dioxide sorbent in the power plant industry, it of course also reacts with sulphur compounds during a carbon dioxide capture cycle. This has been described for calcium oxide [62, 65], doped calcium oxide [104], as well as for hydrotalcites [95]. In all cases, reaction with sulphur dioxide leads to the formation of sulphates, which are only decomposable at temperatures higher than the desired decarbonation temperatures. This behaviour can then be considered to represent a deactivation or poisoning of the sorbent. A carbon dioxide sorption material used in a technical application must be stable under flue gas conditions that involve impurities.

In the proposed utilisation of pre-combustion carbon dioxide capture, it must be kept in mind that a lean-oxygen gas and not an end-of-tail flue gas is present. This results in different compounds of diverse impurities, e. g. sulphur is present as hydrogen sulphide rather than sulphur dioxide in flue gas, whereas nitrogen is present as ammonia and hydrogen cyanide, rather than nitrogen oxides [105]. As up to 1.3 vol% of hydrogen sulphide can be contained in some coal-derived syngas [105], future sorbents should also be tested for their reaction with this impurity.

1.4 Project objective

The objective of this project is to develop novel carbon dioxide sorbents based on metal oxides that are high in capacity, have high selectivity to carbon dioxide and are stable through multiple sorption and desorption cycles. The primary focus hereby is the sorption-enhanced water gas shift reaction with in-situ carbon dioxide capture. Preparation methods for the sorbents of interest are developed. A particular focus of the investigation is to determine the sorbents' capabilities to operate under (simulated) isothermal pressure swing conditions between 250 and 400 °C, i. e., sorbing carbon dioxide in high partial pressures and desorbing it in low partial pressures at the same temperature. Under laboratory conditions, this is achieved by exposing the sorbent sample to carbon dioxide at atmospheric pressure (high partial pressure of carbon dioxide) and purging it with an inert gas (i. e., zero partial pressure of carbon dioxide) for desorption. Furthermore, the effect of other syngas constituents, particularly hydrogen sulphide, hydrogen and water, is assessed, as they might compete with carbon dioxide sorption, or even alter the chemistry of the materials and disrupt its carbon dioxide sorption capability. The mechanisms of sorption and desorption of carbon dioxide on the metal oxides are also investigated by studying the sorbents using a variety of ex-situ and in-situ analytical methods.

1.5 Research hypotheses

The hypotheses for this project are the following:

1. Based on a literature review (section 1.3.5), novel carbon dioxide capture sorbents based on carbonation reactions of metal oxides can be found. A simple screening test can be developed in order to determine the temperature in which the oxides form their respective carbonates.
 2. Sorbents qualifying for further investigation after this screening test are reversibly forming carbonates under pressure swing cycles and have stable working capacities over a multitude of sorption and desorption cycles.
 3. An optimal temperature can be found to achieve the highest feasible capacities in an isothermal pressure swing sorption process, probably representing a
-

compromise between achieving fast reaction rates (favoured by high temperature) and a maximum in the (thermodynamically limited) difference in capacity between high and low pressures (favoured by low temperatures).

4. The reaction mechanism and, if evident, capacity reduction/sorbent decay mechanism(s) over multiple sorption cycles can be clarified.
 5. The sorbents can be used in hydrogen-containing syngas mixtures, as the possible reduction of the metal oxide sorbent by hydrogen takes place at a different (i. e., higher) temperature than carbon dioxide sorption.
 6. Hydrogen sulphide, a syngas trace constituent, might sorb onto the samples and causes oxide to sulphide transformation, altering the sorption capacity for carbon dioxide.
-

Chapter 2 Screening study of prospective metal oxides

2.1 Introduction

This chapter presents a screening study to determine the potential of a series of metal oxides to reversibly sorb carbon dioxide in the temperature range of interest (250 to 400 °C). The test procedure is outlined and the results of the screening test are described. From the test results, conclusions are drawn for further research and the prospects of using these metal oxides for further investigation.

2.2 Selection of metal oxides

2.2.1 Lanthanum oxide

Lanthanum carbonate decomposes to oxide at 450 °C, whereas heavier lanthanides have higher decomposition temperatures [106]. Assuming that the temperature for carbonation is lower than for decarbonation, the reaction from lanthanum oxide to carbonate could be in the temperature range of interest in this project (i. e., if the reaction actually is reversible). As no information was found on the reversibility of the decomposition of lanthanum carbonate, it was decided to test this material for carbon dioxide sorption.

2.2.2 Dolomite

Hassanzadeh et al. [82] have used natural dolomite as a carbon dioxide sorbent. Dolomite is a mineral that consists both of magnesium and calcium carbonate, which was previously 'half-calcined' [82] in order to decompose magnesium carbonate to oxide, but keeping the calcium carbonate intact as a support. Doping with potassium resulted then in a suitable sorbent, which was tested at 20 atm in a pressurised thermogravimetric analyser. This group also stated that high surface area can lead to higher carbonation and decarbonation rates, but small pores can also block during carbonation, making it difficult to reach the stoichiometric capacity of the sorbent.

In this project, the idea was to synthetically make a doped 'dolomite' by impregnating potassium carbonate and magnesium nitrate on calcium carbonate and then calcining the sorbent, so that the nitrate gets converted into oxide.

2.2.3 Zinc oxide

Zinc oxide was carbonated close to ambient conditions (in a refrigerator in a water-saturated atmosphere) and decarbonated below 340 °C by Sawada et al. [107]. It was previously suggested to be unsuitable in the IGCC water gas shift temperature range [85], but as Sawada et al. carbonated it at a low temperature, it was considered worth testing it under carbon dioxide at higher temperatures. Although decarbonation occurred in air below 340 °C, it was assumed to possibly be a suitable sorbent, as it might behave differently at this temperature in an environment containing significantly more carbon dioxide than the atmosphere.

2.2.4 Cadmium oxide

Doiwa et al. reported that cadmium carbonate decomposes reversibly in the presence of sodium halides at temperatures between 250 to 300 °C, particularly favourably with sodium iodide [108]. This is a truly dynamic equilibrium, as demonstrated by ¹⁴C exchange reactions, which show ¹⁴CO₂ incorporation even into fully carbonated samples [109]. In [108], a USSR study was cited, which explained the CO₂ exchange in carbonates at room temperature through an 'ion mechanism' in the presence of water, and through an 'atom mechanism' at higher temperatures. The authors point out that the reference they cite does not explain what these terms mean. Furthermore, they conclude that a mechanism involving the formation of H₂CO₃ is unlikely, as ethanol vapour has a similar effect on promoting CdO carbonation at room temperature like water, although with lower reaction rates.

Doiwa's reports summarise the observations without giving any hint of possible industrial application for it (it is assumed that there was no community interest in carbon dioxide capture at the time (1962, 1964) of these publications). The temperature range of 250 to 300 °C was considered appropriate for the focus of this study, and so the material was included in this project.

2.2.5 Mesoporous magnesium oxide

As a literature review has shown (section 1.3.5), most sorbents do not reach their theoretical capacity. This is particularly true for calcium oxide, which is explained by a carbonate layer build-up mechanism (refer [50, 52, 53, 75]). Jahan also stated similar observations for cesium-doped magnesium oxide sorbents, which reach up to 8 wt% mass increase based on the whole sample, although this material could in theory take up to 60 % of its mass of carbon dioxide (based on the conversion of approx. 60 wt% of magnesium oxide, see section 2.3.1.4).

This led to the idea that it might be beneficial to modify the structural properties of a magnesium oxide-based sorbent. By, for example, employing a porous material that rather consists of a thin-walled honeycomb-like structure than a bulky (e. g. spherical) particle, a better penetration of the material by carbon dioxide could possibly be achieved. In this case, the build-up of carbonates in a way that they reach a critical layer thickness (if also existent for magnesium oxide/carbonate) might be avoided.

Bhagiyalakshmi et al. reported the synthesis of a mesoporous magnesium oxide [84]. For the present purpose, a mesoporous silica SBA-15 was synthesised according to a literature method [42]. The method consists of using a SBA-15 as a template to make a porous carbon, which after the removal of the silica is used as a template for impregnating magnesium nitrate. Afterwards, calcination burns off the carbon and decomposes the nitrate, resulting in a mesoporous magnesium oxide. The method is described in more detail in the experimental part, section 2.3.1.6. Bhagiyalakshmi et al. also examined the use of rice husk ash as a silica source to make SBA-15, which is not elaborated here.

2.3 Experimental

2.3.1 Synthesis of sorbents

Unless stated in the following subsections, the sorbents were prepared using a wet mixing synthesis method similar to [85]. For this purpose, the precursors of the sorbents were dispersed or dissolved (depending on their solubility) in a beaker glass in approx. 150 mL of deionised water and stirred on a magnetic hotplate stirrer while being heated in order to evaporate the liquid. As soon as all water had evaporated, the sample was removed

from the beaker glass, transferred to a Petri dish and dried in an oven at 120 °C under nitrogen flow.

Samples that require calcination in order to produce an oxide were transferred to an alumina combustion boat after evaporation and calcined in air in a muffle furnace according to the procedures outlined in the following subsections. After either calcination or drying, the samples were stored in capped and sealed vials.

2.3.1.1 Lanthanum carbonate

Lanthanum carbonate was used as a pure chemical and also wet-mixed with 9.5 wt% of cesium carbonate. As lanthanum is located in the third group of the periodic table of elements and thus close to magnesium (second group), it was thought that cesium might have a similar effect on lanthanum as it has on magnesium (refer [85]).

2.3.1.2 Zinc oxide

Zinc oxide was used as a pure chemical as well as wet-mixed with 14.8 wt% of sodium iodide.

As cadmium oxide was reported to form carbonate in the presence of sodium iodide (refer section 2.3.1.3 and [108]) and zinc and cadmium both stand in the 12th group of the periodic table, it was considered that sodium iodide might have a similar effect on zinc oxide as it has on cadmium oxide.

2.3.1.3 Cadmium carbonate

Cadmium carbonate was wet-mixed with 10.4 wt% of sodium iodide for a trial screening run (i. e., approx. 0.0013 mol alkali metal salt on 0.85 g cadmium carbonate).

2.3.1.4 Magnesium-based sorbents

Magnesium oxide was wet-mixed with 41 wt% of cesium carbonate, which equates to a molar ratio of 15 mol% Cs on the total molar amount of Cs and Mg together. This sorbent composition was found to be most suitable by Jahan [85].

An attempt to synthesise this sorbent from alternative magnesium oxide precursors was also made. For this purpose, magnesium nitrate or acetate was mixed into an aqueous solution of cesium carbonate and the water was evaporated. The acetate samples were

then calcined in air at 850 °C for eight hours, whereas for the nitrate samples, a temperature of 650 °C was used for six hours. The concentrations were adjusted to result in 15 mol% of Cs to Mg in the oxide end product, as outlined above, assuming that the nitrate or acetate converts into oxide during calcination.

2.3.1.5 Magnesium/calcium mixed carbonate

Hassanzadeh et al. [82] reported a potassium-doped natural dolomite sorbent containing 44 wt% magnesium and 54 wt% calcium carbonate. Doping this sorbent with 4 to 5 wt% potassium resulted in a sorbent that is effective at 425 °C and 20 atm. An attempt to make such a sorbent synthetically was made by wet-mixing a mixture of 1.2 wt% of potassium carbonate and 72.0 wt% magnesium nitrate hexahydrate on 26.8 wt% of calcium carbonate. The sorbent was calcined at 650 °C for 6 hours. This was considered high enough to decompose the nitrate, but low enough to avoid decomposition of the calcium carbonate. As this was later shown to be wrong and a certain amount of calcium carbonate actually did decompose (refer Table 2.4.3), the material was synthesised again by preparing a calcium carbonate/magnesium nitrate suspension first (using the same mass ratio as stated above) and evaporating the water. The remaining solids were then calcined at 450 °C for three hours in nitrogen flow and then wet-mixed with 5 wt% potassium carbonate, again in a wet mixing step, and dried in a nitrogen-purged drying oven at 120 °C.

2.3.1.6 Porous magnesium oxide

Porous magnesium oxide was synthesised using a similar method as described by Bhagiyalakshmi et al. [84]. SBA-15 was synthesised using 85 g tetraethylorthosilicate (TEOS), which was added to a solution of 40 g of surfactant (Pluronic 123) in 300 g of water and 1200 g of 2-molar hydrochloric acid, while stirring at 35 °C for 20 hours. The solution was aged at 90 °C for 24 hours without stirring. The surfactant directs the hydrolysing TEOS into forming porous silica by forming silica walls around the surfactant micelles. A subsequent filtration and calcination over 32 hours at 500 °C then burned off the surfactant, leaving a porous network. SBA-15 silica was used as kept in stock within the workgroup, which had been previously made in a large 20 g batch (lot # JB1-06a).

The second step involved making a porous carbon, using 0.6 g of sucrose dissolved in approx. 5 g of water, which was added into 1 g of SBA-15. Addition of 0.12 g of 98 %

sulphuric acid helped decomposing the sucrose to carbon. The mixture was dried in a nitrogen-purged oven at 100 °C for six hours, then heated up to 160 °C for six hours and then cooled down to room temperature in nitrogen flow. The sample turned black during this treatment. The procedure was repeated with 0.4 g sucrose and 0.06 g sulphuric acid in aqueous solution. Next, carbonation was carried out by pyrolysis at 900 °C in nitrogen flow. Then, the silica template was removed by washing twice with a hot solution (near its boiling point) of 8 g of sodium hydroxide dissolved in 200 ml of a 50 vol% water in ethanol mixture. Next, the sorbent was washed with a water/ethanol mixture while being separated from the liquid by vacuum filtration. The solid carbon was recovered and dried in nitrogen flow at 100 °C.

In the third step, the obtained carbon was mixed into a solution of 1 mol/L magnesium nitrate and stirred for 2 hours. The liquid was filtered off, the solids were recovered and calcined at 350 °C in nitrogen for two hours. These steps were repeated twice. Afterwards, the carbon was burnt off by calcining the material in air at 800 °C for 2 hours.

The obtained solid was wet-mixed with cesium carbonate solution, as explained for commercial magnesium oxide in section 2.3.1.4.

The magnesium oxide, as well as the silica and carbon precursors, were analysed by nitrogen adsorption according to section 2.3.2, in order to monitor their change in porosity.

2.3.2 Nitrogen physisorption

In order to obtain the BET surface area [110] and a pore size distribution via the BJH model [111], nitrogen physisorption at liquid nitrogen temperature (77 K) was performed using a Coulter Omnisorp 360CX gas sorption analyser. Samples of approx. 80 to 100 mg were used. All samples were pretreated under a vacuum of 10^{-5} torr at a temperature of 120 °C for a minimum of 12 hours in the degassing station of the analyser in order to desorb all impurities on the surface. Afterwards, the samples were analysed for adsorption and desorption using a 60 torr gas dosing increment. Desorption was performed until a cut-off pressure of 60 torr.

For the BET calculation, the adsorption isotherm region between relative pressures (p/p_0) of 0.05 to 0.25 was used.

2.3.3 Thermogravimetric analysis

Thermogravimetric analysis (TGA) was performed using a Setaram TAG 24 symmetrical thermoanalyser. The gases (argon and carbon dioxide) were dosed into the thermoanalyser using Bronkhorst F-201DV-RAD-11-K programmable mass flow controllers. A total gas flow of 70 mL/min was used for all experiments, consisting of either 70 mL/min argon (inert gas flow) or a mixture made up of 35 mL/min carbon dioxide and 35 mL/min argon (sorption gas flow, i. e., 50 vol% carbon dioxide). The total gas stream was divided into two streams, so that 35 mL/min were added to the sample. The other half was led over the reference side of the balance, which automatically allows for buoyancy corrections during the experiment. A sample mass of between 22 and 30 mg was used for the experiments. The temperature and gas settings are outlined in the following subsection.

2.3.4 Screening tests

Figure 2.3.1 shows the screening procedure for the test of sorbents. The aim of this TGA experiment was to examine the temperatures that the sorbent requires to sorb and desorb carbon dioxide. First, the sorbent was pre-treated under argon atmosphere at a temperature of 650 °C, which was kept for 20 minutes. This step was performed in order to remove all atmospheric surface contaminants from the sample as well as to decompose all carbonate materials to their respective oxides, which were considered the active sorbents. Next, the system was allowed to cool down to 120 °C as fast as possible (i. e., programmed at a rate of 99 K/min). From the end of the programmed ramp, an hour was allowed for the system to fully cool down and equilibrate at that temperature before the gas was switched from inert to 50 vol% carbon dioxide. After keeping the sample at 120 °C for another 30 minutes, the temperature was ramped up slowly at a rate of 5 K/min and kept at 650 °C for 15 minutes. Afterwards, the gas flow was switched back to pure argon. The temperature was held for another 15-minutes period before cooling down to 20 °C. In order to obtain a stable mass reading at the end of the experiment, the temperature was kept at this temperature for 2000 seconds (approx. 33 minutes). The sample mass was determined by an analytical balance before and after the experiment in order to ensure the thermoanalyser has given a consistent (non-drifting) mass reading over the duration of the whole experiment.

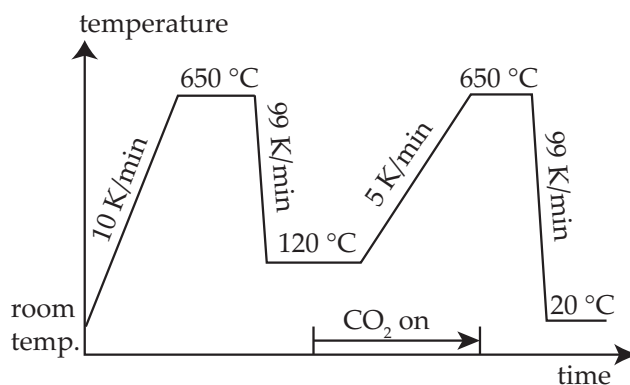


Figure 2.3.1: Temperature program for the TGA screening experiment

A humid environment was described as essential by Sawada [107] for the zinc oxide sample, due to the formation of hydrated zinc carbonates during carbonation. For this purpose, the carbon dioxide and argon supply of the thermogravimetric analyser were bubbled through a wash bottle filled with water, which was kept in a water bath at 10 °C. This resulted in a partial pressure of 0.012 bar of water vapour [112], or, in other words, 1.2 vol% of the feed gas stream at the instrument pressure of approx. 1 bar. The zinc oxide sample doped with sodium iodide was however analysed in a dry feed gas stream.

2.4 Results and discussion

2.4.1 List of materials made

Table 2.4.1 gives a brief summary of the samples produced for this chapter. The results of the analyses are given in the following subchapters; the syntheses are given in the sections indicated in the table.

Table 2.4.1: List of samples examined in this chapter

Material	Refer section	Brief summary of synthesis
$\text{La}_2(\text{CO}_3)_2$	2.3.1.1	used pure and also wet-mixed with of Cs_2CO_3
ZnO	2.3.1.2	pure (TGA in wet CO_2), as well as wet-mixed with NaI
CdCO_3	2.3.1.3	series of samples wet-mixed with sodium iodide: 0, 1, 2.5, 5, 7.5, 10, 12.5, 15, 17.5 and 20 wt.-% calcined 500 °C 3 h; screening sample 10.4 % (section 2.4.4) not calcined

Material	Refer section	Brief summary of synthesis
MgO/CaCO ₃	2.3.1.5	1. wet-mixing of CaCO ₃ , Mg ₂ (NO ₃) ₂ and K ₂ CO ₃ , calcination at 650 °C 6 h 2. wet-mixing of CaCO ₃ and Mg ₂ (NO ₃) ₂ , calcination at 450 °C, impregnation with K ₂ CO ₃
porous MgO,	2.3.1.4,	via porous silica – porous carbon – porous MgO from
MgO	2.3.1.6	Mg(NO ₃) ₂ , after calcination wet-mixing with Cs ₂ CO ₃ ; commercial MgO used directly for impregnation with Cs ₂ CO ₃
Mg ₂ (NO ₃) ₂	2.3.1.4	wet-mixed with Cs ₂ CO ₃ , calcined at 650 °C 6 h (nitrate), 650 and 850 °C (acetate) 8 h
Mg-acetate		amount of Cs ₂ CO ₃ adjusted to obtain same concentration as on MgO sample, assuming decomposition of nitrate or acetate to oxide

2.4.2 Surface area and pore size distribution of MgO-based sorbents

Adsorption isotherms for the magnesium oxide sorbents are shown in Figure 2.4.1.

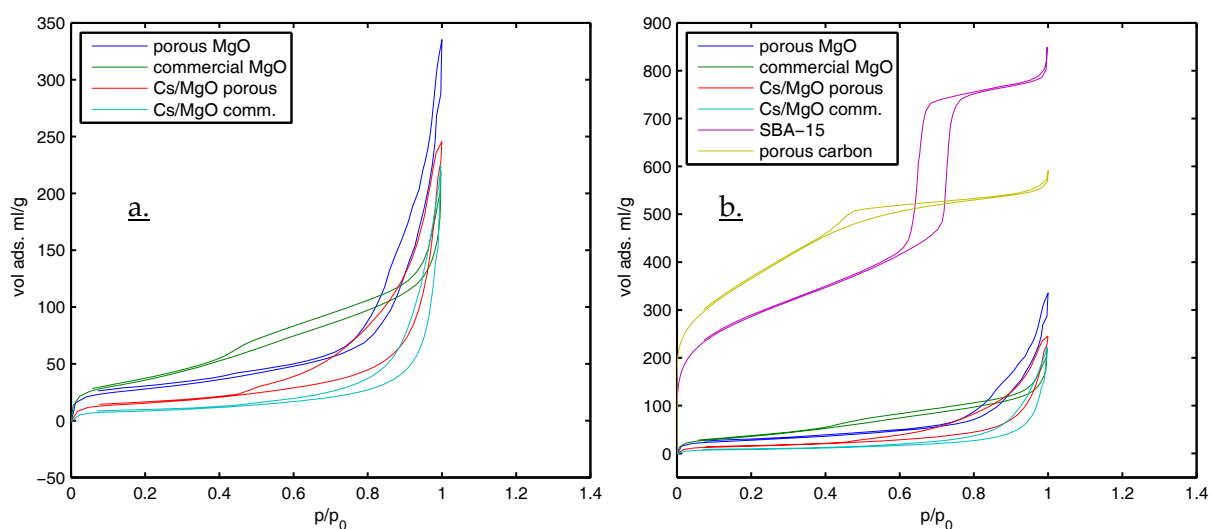


Figure 2.4.1: N₂ ad-/desorption isotherms for the porous MgO and precursors. Same MgO sample data shown in a. and b. on different scales.

SBA-15, which was employed as the template for the carbon synthesis, was porous. The BJH pore size distribution shows a peak in pore volume for a pore diameter of 6 nm (Figure 2.4.2). For the carbon that was synthesised from the silica, this most prominent pore diameter is reduced to approx. 4 nm. This may be due to the 'inversion' of the sample, i. e., what were pores in the silica became the solid material in the carbon, and vice versa. It can be argued that this leads to a smaller pore size in the carbon.

It can be observed that from the carbon template to the magnesium oxide, a lot of porosity is lost, resulting in a lower amount of nitrogen adsorbed and less hysteresis (Figure 2.4.1b). For the porous magnesium, Bhagiyalakshmi et al. [84] reported a hysteresis similar to the one observed for the SBA-15, but such a result cannot be seen in this case. A reduction in the volume of adsorbed nitrogen can also be observed after the doping procedure with cesium for the respective materials (Figure 2.4.1a), but most of the porosity in the mesopore region is lost in the step where magnesium oxide is made from the carbon material.

As the templated MgO material was close in BET surface area and pore volume to the one synthesised using MgO, it was decided that the synthesis is not viable for a substantial improvement of the magnesium-based sorbent family. Chapter 5 summarises a more successful approach in increasing the sorption capacities of magnesium-based sorbents.

Table 2.4.2: BET surface areas of the magnesium oxides and their precursors

Sample	BET surface area, m ² /g
SBA-15	1026.5
porous carbon	1303.6
porous MgO	97.8
Cs-doped porous MgO	54.7
commercial MgO	133.8
Cs-doped commercial MgO	29.7

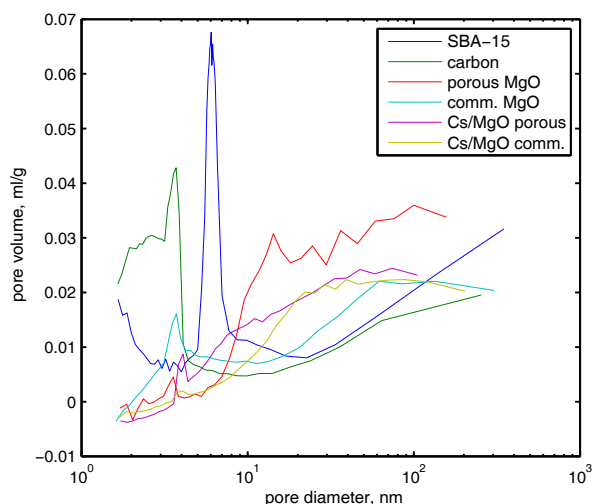


Figure 2.4.2: Pore volume distribution derived by the BJH model

2.4.3 Screening of new sorbents

2.4.3.1 Explanation of the results analysis

Figure 2.4.3 shows the TGA results of the cadmium carbonate/sodium iodide sorbent. With this example, the calculation and evaluation procedure, also employed for other samples, shall be explained. Figure 2.4.3a shows the sample temperature and absolute thermogravimetric (TG) readings given by the instrument. At the beginning of the experiment, the balance was tared, giving the reading 0 mg. From the beginning of the pre-treatment temperature ramp, the carbonate-containing sample started decomposing to oxide, which causes a mass loss. At the beginning of the second temperature ramp, carbon dioxide was introduced into the instrument. At a certain temperature, the sorption of the carbon dioxide was no longer kinetically hindered and the mass increased. Beyond a higher temperature, where desorption is thermodynamically in favour, the mass began to decrease, resulting in a peak indicating the temperature range where the sorbent is most potent.

As the sample masses used varied from experiment to experiment, it is sensible to plot the thermogravimetric (TG) reading as a relative value, according to eqn. 2.4.1. The results of this calculation are given in Figure 2.4.3b. This means, that the initial mass is taken as 100 %, or 1, and mass changes are given relative to this.

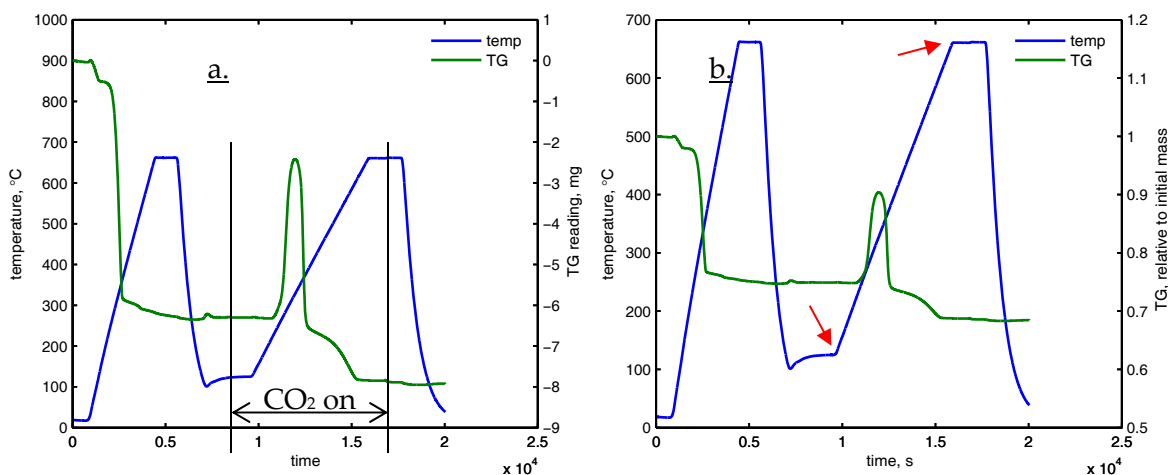


Figure 2.4.3: TGA screening test of 10.5 wt.% NaI on CdCO₃, 25.1 mg raw sample: a. TG reading as per instrument output, b. TG reading normalised to 100 % of initial mass. Red arrows indicate region used for TG vs. T plot (Figure 2.4.4)

In most cases, the pre-treatment step is irrelevant in the subsequent mass change analysis. In the specific case, the second ramp with carbon dioxide is the interesting step to look at (red arrows in Figure 2.4.3b). For this purpose, the initial mass of the sample in eqn. 2.4.1 is taken as 100 % at the beginning of the second temperature ramp (lower red arrow), and relative changes taken from thereon. The result is the plot in Figure 2.4.4.

$$TG_{\text{relative}} = \frac{TG_{\text{instrument}} + m_{\text{sample}}}{m_{\text{sample}}} \quad \text{eqn. 2.4.1}$$

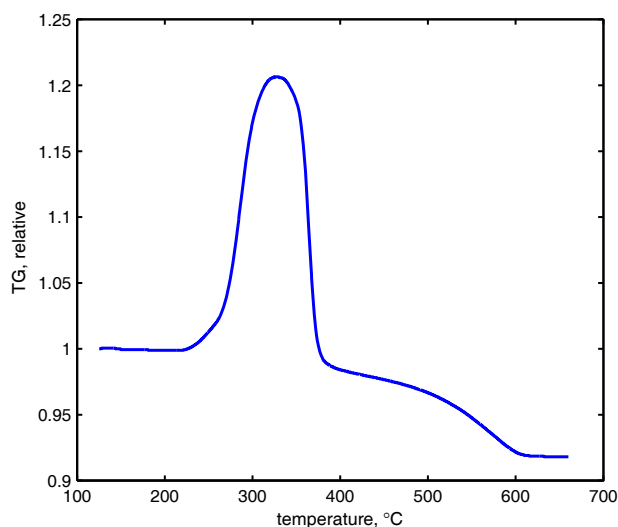


Figure 2.4.4: TGA screening test of 10.5 wt.% NaI on CdCO₃, TG relative = 100 % from the beginning of the temperature ramp

In the following sections, the plot style is the same as outlined in this section for Figure 2.4.3b and Figure 2.4.4.

2.4.4 Cadmium carbonate results

The results given in Figure 2.4.3 and Figure 2.4.4 show that cadmium carbonate in the presence of sodium iodide decomposes to oxide under heat treatment. The conversion can be considered stoichiometrically complete, as indicated in Figure 2.4.3b, where a residual mass of approx. 75 % can be observed after the first heat treatment step. This approximates the change in molar mass (82 %) from cadmium carbonate ($M = 172.4$ g/mol) to cadmium oxide ($M = 128.4$ g/mol) in a sample containing 10 % sodium iodide. The material sorbs about 20 % of its weight in the oxide state in this particular experiment (Figure 2.4.4) and can thus be considered a prospective novel carbon dioxide sorbent that is further described in Chapter 3.

2.4.5 Lanthanum carbonate

Lanthanum carbonate shows decomposition in the first high temperature treatment step. For the pure sample (Figure 2.4.5a), decomposition resulted in approx. 62 % of the mass left. The theoretical mass change from the carbonate ($\text{La}_2(\text{CO}_3)_2$, $M = 457.9$ g/mol) to the oxide (La_2O_3 , $M = 325.8$ g/mol) is 71 %. As the lanthanum carbonate comes as an unspecified hydrate from the supplier, the additional mass loss might be considered due to the dehydration.

The cesium-doped material (Figure 2.4.5b) shows only 80 % residual mass after decomposition. This is significantly less than the pure sample. It is possible that this difference is due to the doped sample being dried at 120 °C in nitrogen after the wet mixing, whereas the pure sample was taken straight from the storage container as supplied by the manufacturer. The sorption step (second temperature ramp) does not reveal much mass uptake in the plots in Figure 2.4.5.

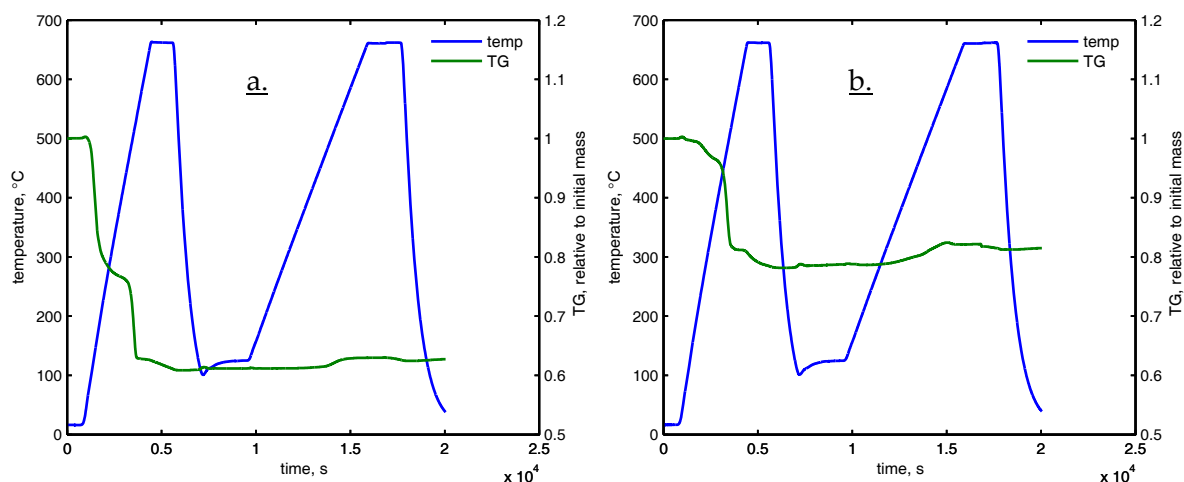


Figure 2.4.5: TGA screening test of $\text{La}_2(\text{CO}_3)_2$, a. pure, b. doped with 9.5 wt.-% Cs_2CO_3

However, if only the sorption step is considered (Figure 2.4.6), a mass uptake can be observed that is most prominent between 500 and 600 °C, whereas the cesium-doped sample sorbs about one per cent more than the pure one. In the temperature range between 250 and 400 °C, the sorption capacity is comparatively poor (approx. 1 %), so it was decided that this material not be studied further.

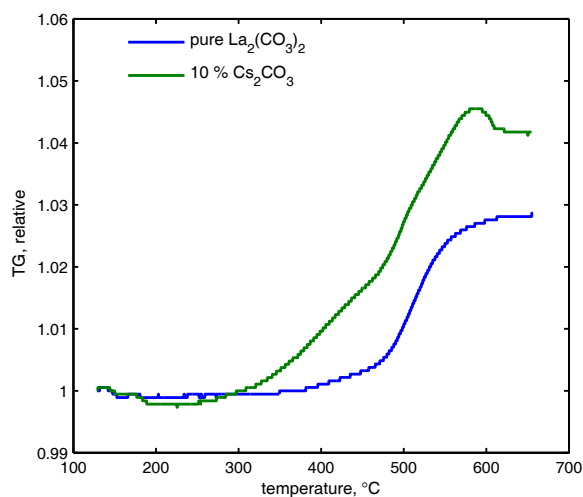


Figure 2.4.6: TGA screening test of $\text{La}_2(\text{CO}_3)_2$, temperature vs. TG

2.4.6 Zinc oxide

Zinc oxide was tested as a pure substance in wet carbon dioxide. It can be observed in Figure 2.4.7a that there is no significant mass increase during the carbon dioxide introduction into the sample. Thus, zinc oxide seems not to be a prospective sorbent. Zinc oxide doped with sodium iodide exhibited a significant mass loss (Figure 2.4.7b). A similar

mass loss observed for sodium halide enhanced cadmium oxide samples is examined in detail in Chapter 3.

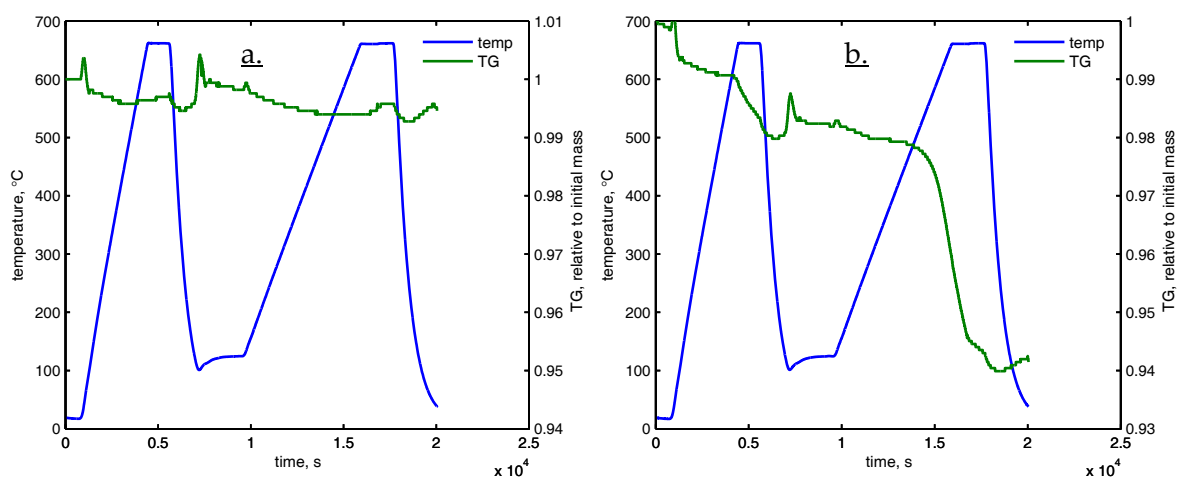


Figure 2.4.7: TGA screening test of zinc oxide, a. pure ZnO tested in wet CO₂, b. ZnO with 15 wt.-% NaI tested in dry CO₂

2.4.7 Magnesium oxide sorbents

2.4.7.1 Magnesium oxide/cesium carbonate mixed oxide

The results of the precursor study (refer section 2.3.1.4) are shown in Figure 2.4.8. It can be observed that cesium carbonate-doped magnesium oxide revealed the best carbon dioxide sorption capacity. The sorbents made from magnesium acetate or nitrate in a coprecipitation method with cesium carbonate were showing less than half the capacity in the screening experiment (refer section 2.3.4).

As all samples were treated at 650 °C in the first stage of the screening experiment, the difference in sorption capacity could be explained by the formation of a different structure of mixed oxides. In the coprecipitated samples, mixed carbonates/oxides could be more readily formed than by loading the cesium carbonate onto the magnesium oxide, which, more likely, resulted in a surface deposition of the cesium. If this was the case, this ‘doping’ would result in a more effective sorbent. The acetate sample calcined at 850 °C virtually showed no sorption. This might be due to the evaporation of cesium, resulting in the loss of the dopant activity. The melting temperature of cesium carbonate is reported as 610 °C [112], but from the analysis of coal ash it is known that alkali metal compounds tend to evaporate even below this temperature [113].

Also notable is a mass decrease at the end of the experiment, i. e. only 99 % of the starting mass is left. It appears that pre-treatment of the sample was not complete because of either (a) insufficient decomposition of the acetate or nitrate precursors, (b) a slow desorption of adsorbed gases from atmospheric exposure, or (c) the evaporation of certain components of the sample (most likely cesium) itself. So the samples were pre-treated for longer periods of time (up to 6000 s instead of 1200 s). A linear mass decrease can still be observed even after the longer pre-treatment. Its clear reason remains undetermined (Figure 2.4.9b). However, the sorption capacity showed no trend with regard to the pre-treatment time (Figure 2.4.9a).

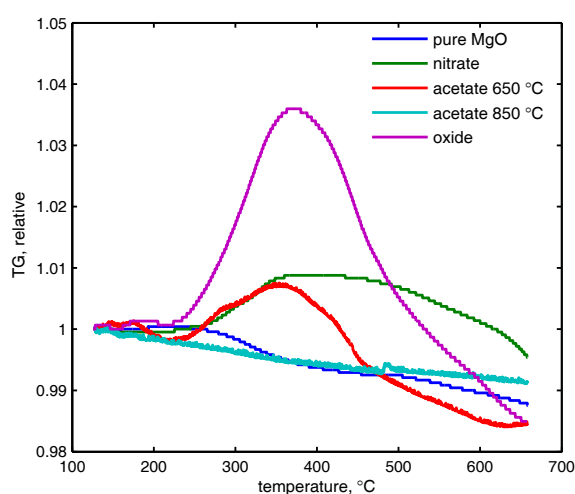


Figure 2.4.8: TGA screening test of CsCO_3/MgO made from different precursors (acetate calcined at 650 and 850 °C) and pure MgO

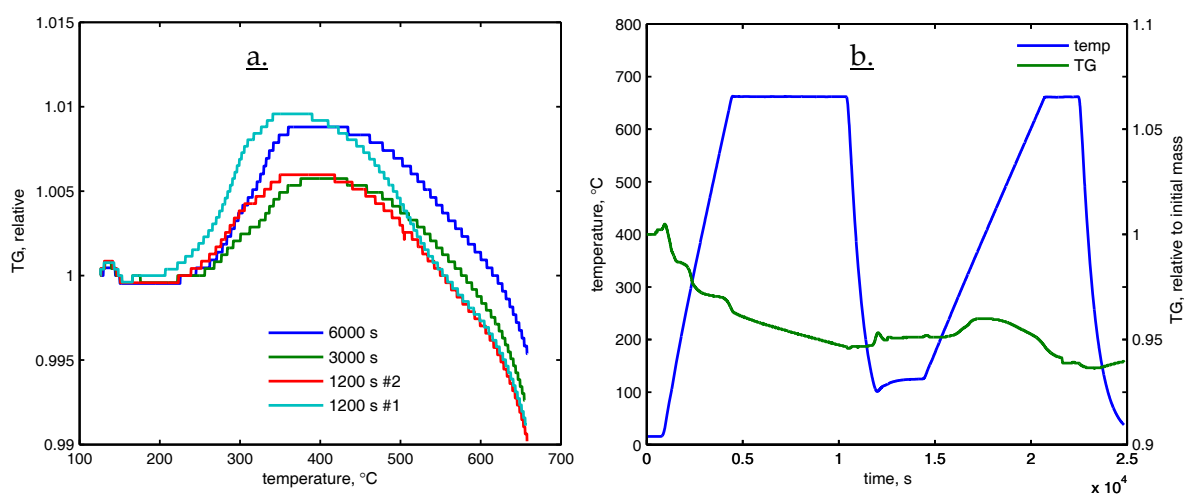


Figure 2.4.9: TGA screening test of Cs/Mg from $\text{Mg}(\text{NO}_3)_2$, a. different pre-treatment times, b. 6000 s pre-treatment time full plot

2.4.7.2 Calcium-supported magnesium sorbents

The results of the potassium carbonate/calcium carbonate/magnesium nitrate sorbents are shown in Figure 2.4.10. It is evident that the temperature of pre-treatment of 650 °C caused some of the calcium carbonate to decompose, which was unwanted. A comparison experiment with pure calcium carbonate heat-treated at the same temperature verified this (Table 2.4.3). Significant mass uptake took place at temperatures beyond 500 °C, which did not stop until the end of the carbon dioxide dosing. As magnesium oxide sorbs carbon dioxide in a lower temperature range (compare Figure 2.4.8 and Figure 2.4.9), the mass uptake can likely be associated with calcium oxide carbonation.

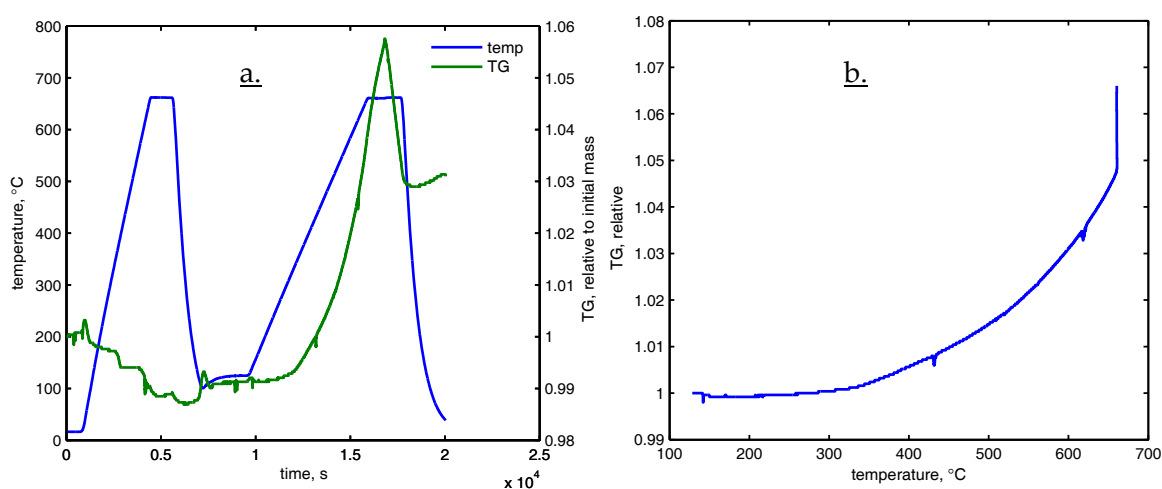


Figure 2.4.10: TGA screening test of $\text{CaCO}_3/\text{MgO}/\text{K}_2\text{CO}_3$, a. full plot, b. sorption vs. temperature

It must be noted that the material is not comparable to the natural sorbent reported by Hassanzadeh et al. [82], where the reaction of magnesium oxide was favoured by not calcining the calcium carbonate and using it as a support. However, their experiments were reported for a thermogravimetric analyser operating at a pressure of 20 atm. It might be that this higher pressure is required to promote sorption onto magnesium oxide, making their reported results not directly comparable to the ones obtained here. In their setup, sorption could be noted at a temperature of 425 °C, resulting in about 30 % of the magnesium oxide being converted.

Table 2.4.3: Mass loss experiment for pure calcium carbonate

treatment temperature, duration	residual mass
120 °C, over night	99.9 %
650 °C, 6 hours	73.9 %

In order to recover the calcium carbonate support in the material that was calcined at an obviously too high temperature, a procedure was chosen to carbonate the sorbent, before doing the screening test. The results are shown in Figure 2.4.11. Here, the sorbent was first heated up to 650 °C in a carbon dioxide atmosphere. Then, the sample was cooled down to 500 °C. Afterwards, the gas was switched to pure argon and left at that temperature for three hours. This step, it is expected, should have calcined the magnesia in the sorbent at a lower temperature whilst avoiding decomposition of the calcium carbonate. Then the sample was cooled to 120 °C in argon, followed by a ramp similar to the screening test (refer section 2.3.4), under carbon dioxide.

But neither in this experiment could a mass increase due to sorption around 400 °C be observed. Based on these results, the material should, perhaps, not be heated up to 650 °C, but rather calcined at a lower temperature, 450 °C. So the synthesis of the sorbent was attempted in a different manner, where magnesium nitrate and calcium carbonate were mixed in water first. Doping with potassium was then carried out after calcination at 450 °C. The screening test result of this material is shown in Figure 2.4.11b. As this material also did not show carbon dioxide sorption, this approach was not studied further. It is concluded that the materials prepared in this study are different from natural dolomite and thus have different sorption properties. In particular, no significant porosity or surface area could be determined for the materials synthesised here (physically impossible negative surface areas were obtained from BET calculation), whereas the dolomite used by Hassanzadeh et al. [82] had a surface area of about 5 m²/g.

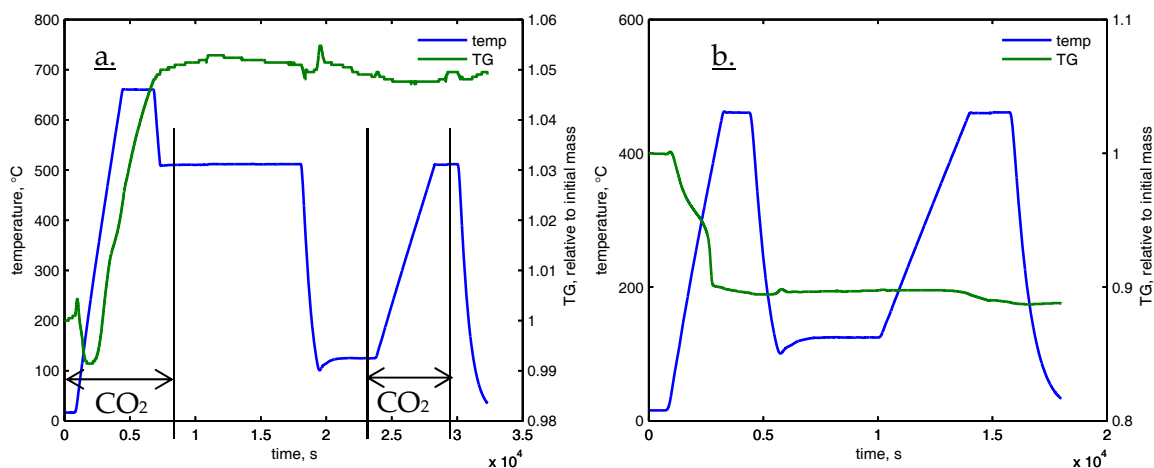


Figure 2.4.11: a. TGA recovery/screening of $\text{CaCO}_3/\text{MgO}/\text{K}_2\text{CO}_3$ sorbent, b. screening of sorbent made at a lower calcination temperature of 450°C with doping after calcination

2.5 Conclusion

A series of metal oxide systems was tested for carbon dioxide sorption in a TGA screening test. The most prospective sorbent, a cadmium carbonate/sodium iodide mixture, has shown a good response to carbon dioxide exposure on a temperature ramp of 5 K/min , exhibiting approx. 20 % mass gain between 235 and 320°C (start of mass gain and top of peak in Figure 2.4.4). This material has not previously been described as a sorbent for carbon dioxide within the scope of carbon capture from power generation processes. For this reason, it was decided to study this material in more detail. The results of these studies are described in subsequent chapters.

For a magnesium/cesium mixture, which had been described in a previous project, attempts were made to improve upon this approach, by varying the precursor (magnesium nitrate and acetate instead of oxide) and through the use of a carbon templating method. Both of these approaches were not considered successful. However, the reader is referred to Chapter 5 of this thesis, where a more successful method of improving Mg/Cs-based carbon dioxide sorbents is presented.

2.6 References for Chapter 1 and 2

- [1] "Dictionary of Energy (Expanded Edition)," C. J. Cleveland and C. Morris, Eds., ed: Elsevier, 2009.
 - [2] H. Yang, Z. Xu, M. Fan, R. Gupta, R. B. Slimane, A. E. Bland, and I. Wright, "Progress in carbon dioxide separation and capture: A review," *Journal of Environmental Sciences*, vol. 20, pp. 14-27, 2008.
 - [3] (18/09/2013). *IEA World Energy Outlook 2012, Executive Summary*. Available: <http://www.iea.org/Textbase/npsum/WEO2012SUM.pdf>
 - [4] K. S. Lackner, A. H. A. Park, and B. G. Miller, "Eliminating CO₂ Emissions from Coal-Fired Power Plants," in *Generating Electricity in a Carbon-Constrained World*, Boston: Academic Press, 2010, pp. 127-173.
 - [5] M. Mikkelsen, M. Jørgensen, and F. C. Krebs, "The teraton challenge. A review of fixation and transformation of carbon dioxide," *Energy & Environmental Science*, vol. 3, pp. 43-81, 2010.
 - [6] A. A. Lacis, G. A. Schmidt, D. Rind, and R. A. Ruedy, "Atmospheric CO₂: Principal Control Knob Governing Earth's Temperature," *Science*, vol. 330, pp. 356-359, October 15, 2010.
 - [7] K. M. K. Yu, I. Curcic, J. Gabriel, and S. C. E. Tsang, "Recent Advances in CO₂ Capture and Utilization," *ChemSusChem*, vol. 1, pp. 893-899, 2008.
 - [8] (18/09/2013). *CO₂CRC webpage, public image library*. Available: <http://co2crc.com.au/imagelibrary3/general.php>
 - [9] E.-J. Nyns, "Methane," in *Ullmann's Encyclopedia of Industrial Chemistry*: Wiley-VCH Verlag GmbH & Co. KGaA, 2000, pp. 14-23.
 - [10] J. C. Crelling, H. W. Hagemann, D. H. Sauter, R. V. Ramani, W. Vogt, D. Leininger, S. Krzack, B. Meyer, F. Orywal, R. Reimert, B. Bonn, U. Bertmann, W. Klose, and G. Dach, "Coal," in *Ullmann's Encyclopedia of Industrial Chemistry*: Wiley-VCH Verlag GmbH & Co. KGaA, 2000, pp. 259-308.
 - [11] J. M. Tour, C. Kittrell, and V. L. Colvin, "Green carbon as a bridge to renewable energy," *Nature Materials*, vol. 9, pp. 871-874, 2010.
 - [12] (18/09/2013). *Renewable Energy Policy Network for the 21st Century (REN21): Renewables Global Status Report, 2012*. Available: <http://www.map.ren21.net/GSR/GSR2012.pdf>
 - [13] H.-H. Rogner, "An assessment of world hydrocarbon resources," *Annual Review of Energy and the Environment*, vol. 22, pp. 217-262, 1997.
 - [14] C. Marchetti, "On geoengineering and the CO₂ problem," *Climatic Change*, vol. 1, pp. 59-68, 1977.
 - [15] P. Cook, A. Rigg, and J. Bradshaw, "Environmental-Putting it back where it came from: Is geological disposal of carbon dioxide an option for Australia?," *APPEA Journal-Australian Petroleum Production and Exploration Association*, vol. 40, pp. 654-666, 2000.
 - [16] M. L. Godec, V. A. Kuuskraa, and P. Dipietro, "Opportunities for Using Anthropogenic CO₂ for Enhanced Oil Recovery and CO₂ Storage," *Energy & Fuels*, vol. 27, pp. 4183-4189, 2013.
-

- [17] V. Prigiobbe, M. Hänchen, M. Werner, R. Baciocchi, and M. Mazzotti, "Mineral carbonation process for CO₂ sequestration," *Energy Procedia*, vol. 1, pp. 4885-4890, 2009.
- [18] B. Kronberger, E. Johansson, G. Löffler, T. Mattisson, A. Lyngfelt, and H. Hofbauer, "A Two-Compartment Fluidized Bed Reactor for CO₂ Capture by Chemical-Looping Combustion," *Chemical Engineering & Technology*, vol. 27, pp. 1318-1326, 2004.
- [19] D. Wang, S. Chen, C. Xu, and W. Xiang, "Energy and exergy analysis of a new hydrogen-fueled power plant based on calcium looping process," *International Journal of Hydrogen Energy*, vol. 38, pp. 5389-5400, 2013.
- [20] A. A. Olajire, "CO₂ capture and separation technologies for end-of-pipe applications - A review," *Energy*, vol. 35, pp. 2610-2628, 2010.
- [21] C. M. White, B. R. Strazisar, E. J. Granite, J. S. Hoffman, and H. W. Pennline, "Separation and capture of CO₂ from large stationary sources and sequestration in geological formations-coalbeds and deep saline aquifers," *Journal of the Air & Waste Management Association*, vol. 53, pp. 645-715, 2003.
- [22] E. Rebhan, *Energiehandbuch: Gewinnung, Wandlung und Nutzung von Energie*: Springer, 2002.
- [23] P. Chiesa, S. Consonni, T. Kreutz, and R. Williams, "Co-production of hydrogen, electricity and CO₂ from coal with commercially ready technology. Part A: Performance and emissions," *International Journal of Hydrogen Energy*, vol. 30, pp. 747-767, 2005.
- [24] P. Chiesa, T. G. Kreutz, and G. G. Lozza, "CO₂ Sequestration From IGCC Power Plants by Means of Metallic Membranes," *Journal of Engineering for Gas Turbines and Power*, vol. 129, pp. 123-134, 2007.
- [25] K. Liu, Z. Cui, and T. H. Fletcher, "Coal Gasification," in *Hydrogen and Syngas Production and Purification Technologies*, K. Liu, C. Song, and V. Subramani, Eds.: Wiley-AIChE, 2009, pp. 156-218.
- [26] B. G. Miller, "Introduction to Coal Utilization Technologies," in *Clean Coal Engineering Technology*, Boston: Butterworth-Heinemann, 2011, pp. 133-217.
- [27] S. S. Hla, D. Park, G. J. Duffy, J. H. Edwards, D. G. Roberts, A. Ilyushechkin, L. D. Morpeth, and T. Nguyen, "Kinetics of high-temperature water-gas shift reaction over two iron-based commercial catalysts using simulated coal-derived syngases," *Chemical Engineering Journal*, vol. 146, pp. 148-154, 2009.
- [28] A. Platon and Y. Wang, "Water-Gas Shift Technologies," in *Hydrogen and Syngas Production and Purification Technologies*: John Wiley & Sons, Inc., 2009, pp. 311-328.
- [29] D. M. D'Alessandro, B. Smit, and J. R. Long, "Carbon Dioxide Capture: Prospects for New Materials," *Angewandte Chemie International Edition*, vol. 49, pp. 6058-6082, 2010.
- [30] K. A. Mumford, K. H. Smith, C. J. Anderson, S. Shen, W. Tao, Y. A. Suryaputradinata, A. Qader, B. Hooper, R. A. Innocenzi, S. E. Kentish, and G. W. Stevens, "Post-combustion Capture of CO₂: Results from the Solvent Absorption Capture Plant at Hazelwood Power Station Using Potassium Carbonate Solvent," *Energy & Fuels*, vol. 26, pp. 138-146, 2011.
- [31] L. Dumée, C. Scholes, G. Stevens, and S. Kentish, "Purification of aqueous amine solvents used in post combustion CO₂ capture: A review," *International Journal of Greenhouse Gas Control*, vol. 10, pp. 443-455, 2012.
-

- [32] A. D. Ebner and J. A. Ritter, "State-of-the-art Adsorption and Membrane Separation Processes for Carbon Dioxide Production from Carbon Dioxide Emitting Industries," *Separation Science and Technology*, vol. 44, pp. 1273-1421, 2009.
- [33] M. J. Tuinier, H. P. Hamers, and M. van Sint Annaland, "Techno-economic evaluation of cryogenic CO₂ capture - A comparison with absorption and membrane technology," *International Journal of Greenhouse Gas Control*, vol. 5, pp. 1559-1565, 2011.
- [34] A. Blackman, S. Bottle, S. Schmid, M. Mocerino, and U. Wille, *Chemistry*: John Wiley & Sons, 2012.
- [35] P. Chiesa and S. Consonni, "Shift Reactors and Physical Absorption for Low-CO₂ Emission IGCCs," *Journal of Engineering for Gas Turbines and Power*, vol. 121, pp. 295-305, 1999.
- [36] C. A. Scholes, S. E. Kentish, and G. W. Stevens, "Effects of Minor Components in Carbon Dioxide Capture Using Polymeric Gas Separation Membranes," *Separation & Purification Reviews*, vol. 38, pp. 1-44, 2009/01/01 2009.
- [37] C. A. Scholes, K. H. Smith, S. E. Kentish, and G. W. Stevens, "CO₂ capture from pre-combustion processes - Strategies for membrane gas separation," *International Journal of Greenhouse Gas Control*, vol. 4, pp. 739-755, 2010.
- [38] K. Ramasubramanian, Y. Zhao, and W. S. Winston Ho, "CO₂ capture and H₂ purification: Prospects for CO₂-selective membrane processes," *AIChE Journal*, vol. 59, pp. 1033-1045, 2013.
- [39] A. F. Holleman, E. Wiberg, and N. Wiberg, *Inorganic Chemistry*. Berlin, New York: Walter de Gruyter, 1995.
- [40] R. Yang, *Gas separation by adsorption processes*: Imperial College Press, 1997.
- [41] D. M. Ruthven, S. Farooq, and K. S. Knaebel, *Pressure swing adsorption*. New York: VCH Publishers, 1994.
- [42] D. Zhao, Q. Huo, J. Feng, B. F. Chmelka, and G. D. Stucky, "Nonionic Triblock and Star Diblock Copolymer and Oligomeric Surfactant Syntheses of Highly Ordered, Hydrothermally Stable, Mesoporous Silica Structures," *Journal of the American Chemical Society*, vol. 120, pp. 6024-6036, 1998.
- [43] J. S. Beck, J. C. Vartuli, W. J. Roth, M. E. Leonowicz, C. T. Kresge, K. D. Schmitt, C. T. W. Chu, D. H. Olson, and E. W. Sheppard, "A new family of mesoporous molecular sieves prepared with liquid crystal templates," *Journal of the American Chemical Society*, vol. 114, pp. 10834-10843, 1992.
- [44] G. P. Knowles, P. A. Webley, Z. Liang, and A. L. Chaffee, "Silica/Polyethyleneimine Composite Adsorbent S-PEI for CO₂ Capture by Vacuum Swing Adsorption (VSA)," in *Recent Advances in Post-Combustion CO₂ Capture Chemistry*, M. I. Attalla, Ed., Washington, DC: American Chemical Society, 2012.
- [45] A. Samanta, A. Zhao, G. K. H. Shimizu, P. Sarkar, and R. Gupta, "Post-Combustion CO₂ Capture Using Solid Sorbents: A Review," *Industrial & Engineering Chemistry Research*, vol. 51, pp. 1438-1463, 2012/02/01 2011.
- [46] C. Montoro, E. Garcia, S. Calero, M. A. Perez-Fernandez, A. L. Lopez, E. Barea, and J. A. R. Navarro, "Functionalisation of MOF open metal sites with pendant amines for CO₂ capture," *Journal of Materials Chemistry*, vol. 22, pp. 10155-10158, 2012.
- [47] J.-R. Li, J. Sculley, and H.-C. Zhou, "Metal-Organic Frameworks for Separations," *Chemical Reviews*, vol. 112, pp. 869-932, 2011.
-

- [48] C. Zhang, W. Song, G. Sun, L. Xie, J. Wang, K. Li, C. Sun, H. Liu, C. E. Snape, and T. Drage, "CO₂ Capture with Activated Carbon Grafted by Nitrogenous Functional Groups," *Energy & Fuels*, vol. 27, pp. 4818-4823, 2013.
- [49] J. Wang, H. Chen, H. Zhou, X. Liu, W. Qiao, D. Long, and L. Ling, "Carbon dioxide capture using polyethylenimine-loaded mesoporous carbons," *Journal of Environmental Sciences*, vol. 25, pp. 124-132, 2013.
- [50] J. C. Abanades and D. Alvarez, "Conversion Limits in the Reaction of CO₂ with Lime," *Energy & Fuels*, vol. 17, pp. 308-315, 2003.
- [51] D. Alvarez and J. C. Abanades, "Pore-Size and Shape Effects on the Recarbonation Performance of Calcium Oxide Submitted to Repeated Calcination/Recarbonation Cycles," *Energy & Fuels*, vol. 19, pp. 270-278, 2005.
- [52] D. Alvarez and J. C. Abanades, "Determination of the Critical Product Layer Thickness in the Reaction of CaO with CO₂," *Industrial & Engineering Chemistry Research*, vol. 44, pp. 5608-5615, 2005.
- [53] S. K. Bhatia and D. D. Perlmutter, "Effect of the product layer on the kinetics of the CO₂-lime reaction," *AIChE Journal*, vol. 29, pp. 79-86, 1983.
- [54] Y.-T. Chen, M. Karthik, and H. Bai, "Modification of CaO by Organic Alumina Precursor for Enhancing Cyclic Capture of CO₂ Greenhouse Gas," *Journal of Environmental Engineering*, vol. 135, pp. 459-464, 2009.
- [55] F. Fang, Z.-s. Li, and N.-s. Cai, "Continuous CO₂ Capture from Flue Gases Using a Dual Fluidized Bed Reactor with Calcium-Based Sorbent," *Industrial & Engineering Chemistry Research*, vol. 48, pp. 11140-11147, 2009.
- [56] B. Feng, H. An, and E. Tan, "Screening of CO₂ Adsorbing Materials for Zero Emission Power Generation Systems," *Energy & Fuels*, vol. 21, pp. 426-434, 2007.
- [57] B. Feng, W. Liu, X. Li, and H. An, "Overcoming the Problem of Loss-in-Capacity of Calcium Oxide in CO₂ Capture," *Energy & Fuels*, vol. 20, pp. 2417-2420, 2006.
- [58] N. H. Florin and A. T. Harris, "Reactivity of CaO derived from nano-sized CaCO₃ particles through multiple CO₂ capture-and-release cycles," *Chemical Engineering Science*, vol. 64, pp. 187-191, 2009.
- [59] B. González, G. S. Grasa, M. Alonso, and J. C. Abanades, "Modeling of the Deactivation of CaO in a Carbonate Loop at High Temperatures of Calcination," *Industrial & Engineering Chemistry Research*, vol. 47, pp. 9256-9262, 2008.
- [60] G. Grasa, J. C. Abanades, and E. J. Anthony, "Effect of Partial Carbonation on the Cyclic CaO Carbonation Reaction," *Industrial & Engineering Chemistry Research*, vol. 48, pp. 9090-9096, 2009.
- [61] G. S. Grasa, J. C. Abanades, M. Alonso, and B. González, "Reactivity of highly cycled particles of CaO in a carbonation/calcination loop," *Chemical Engineering Journal*, vol. 137, pp. 561-567, 2008.
- [62] G. S. Grasa, M. Alonso, and J. C. Abanades, "Sulfation of CaO Particles in a Carbonation/Calcination Loop to Capture CO₂," *Industrial & Engineering Chemistry Research*, vol. 47, pp. 1630-1635, 2008.
- [63] H. Gupta and L.-S. Fan, "Carbonation-Calcination Cycle Using High Reactivity Calcium Oxide for Carbon Dioxide Separation from Flue Gas," *Industrial & Engineering Chemistry Research*, vol. 41, pp. 4035-4042, 2002.
- [64] M. Ives, R. C. Mundy, P. S. Fennell, J. F. Davidson, J. S. Dennis, and A. N. Hayhurst, "Comparison of Different Natural Sorbents for Removing CO₂ from
-

- Combustion Gases, as Studied in a Bench-Scale Fluidized Bed," *Energy & Fuels*, vol. 22, pp. 3852-3857, 2008.
- [65] M. V. Iyer, H. Gupta, B. B. Sakadjian, and L.-S. Fan, "Multicyclic Study on the Simultaneous Carbonation and Sulfation of High-Reactivity CaO," *Industrial & Engineering Chemistry Research*, vol. 43, pp. 3939-3947, 2004.
- [66] Y. Li, C. Zhao, H. Chen, L. Duan, and X. Chen, "Cyclic CO₂ capture behavior of KMnO₄-doped CaO-based sorbent," *Fuel*, vol. 89, pp. 642-649, 2010.
- [67] W. Liu, B. Feng, Y. Wu, G. Wang, J. Barry, and J. C. Diniz da Costa, "Synthesis of Sintering-Resistant Sorbents for CO₂ Capture," *Environmental Science & Technology*, vol. 44, pp. 3093-3097, 2010.
- [68] H. Lu, A. Khan, S. E. Pratsinis, and P. G. Smirniotis, "Flame-Made Durable Doped-CaO Nanosorbents for CO₂ Capture," *Energy & Fuels*, vol. 23, pp. 1093-1100, 2008.
- [69] H. Lu, A. Khan, and P. G. Smirniotis, "Relationship between Structural Properties and CO₂ Capture Performance of CaO-Based Sorbents Obtained from Different Organometallic Precursors," *Industrial & Engineering Chemistry Research*, vol. 47, pp. 6216-6220, 2008.
- [70] V. Manovic and E. J. Anthony, "CO₂ Carrying Behavior of Calcium Aluminate Pellets under High-Temperature/High-CO₂ Concentration Calcination Conditions," *Industrial & Engineering Chemistry Research*, 2010.
- [71] V. Manovic and E. J. Anthony, "Long-Term Behavior of CaO-Based Pellets Supported by Calcium Aluminate Cements in a Long Series of CO₂ Capture Cycles," *Industrial & Engineering Chemistry Research*, vol. 48, pp. 8906-8912, 2009.
- [72] N. Rodríguez, M. Alonso, and J. C. Abanades, "Average activity of CaO particles in a calcium looping system," *Chemical Engineering Journal*, vol. 156, pp. 388-394, 2010.
- [73] R. V. Siriwardane, C. Robinson, M. Shen, and T. Simonyi, "Novel Regenerable Sodium-Based Sorbents for CO₂ Capture at Warm Gas Temperatures," *Energy & Fuels*, vol. 21, pp. 2088-2097, 2007.
- [74] P. Sun, J. R. Grace, C. J. Lim, and E. J. Anthony, "The effect of CaO sintering on cyclic CO₂ capture in energy systems," *AIChE Journal*, vol. 53, pp. 2432-2442, 2007.
- [75] B. Wang, Y. Zheng, R. Yan, C. Zheng, J. Shao, and J. Qiu, "A new indicator for determining the fast chemical reaction stage of CaO carbonation with CO₂," *Asia-Pacific Journal of Chemical Engineering*, vol. 2, pp. 197-202, 2007.
- [76] W. Wang, S. Ramkumar, S. Li, D. Wong, M. Iyer, B. B. Sakadjian, R. M. Statnick, and L. S. Fan, "Subpilot Demonstration of the Carbonation-Calcination Reaction (CCR) Process: High-Temperature CO₂ and Sulfur Capture from Coal-Fired Power Plants," *Industrial & Engineering Chemistry Research*, vol. 49, pp. 5094-5101, 2010.
- [77] Z. Yang, M. Zhao, N. H. Florin, and A. T. Harris, "Synthesis and Characterization of CaO Nanopods for High Temperature CO₂ Capture," *Industrial & Engineering Chemistry Research*, vol. 48, pp. 10765-10770, 2009.
- [78] D. Alvarez, M. Peña, and A. G. Borrego, "Behavior of Different Calcium-Based Sorbents in a Calcination/Carbonation Cycle for CO₂ Capture," *Energy & Fuels*, vol. 21, pp. 1534-1542, 2007.
- [79] S. Choi, Jeffrey H. Drese, and Christopher W. Jones, "Adsorbent Materials for Carbon Dioxide Capture from Large Anthropogenic Point Sources," *ChemSusChem*, vol. 2, pp. 796-854, 2009.
- [80] D. S. Sultan, C. R. Müller, and J. S. Dennis, "Capture of CO₂ Using Sorbents of Calcium Magnesium Acetate (CMA)," *Energy & Fuels*, 2010.
-

- [81] E. P. Reddy and P. G. Smirniotis, "High-Temperature Sorbents for CO₂ Made of Alkali Metals Doped on CaO Supports," *Journal of Physical Chemistry B*, vol. 108, pp. 7794-7800, 2004.
- [82] A. Hassanzadeh and J. Abbasian, "Regenerable MgO-based sorbents for high-temperature CO₂ removal from syngas: 1. Sorbent development, evaluation, and reaction modeling," *Fuel*, vol. 89, pp. 1287-1297, 2010.
- [83] Z. Yong, V. Mata, and A. E. Rodrigues, "Adsorption of carbon dioxide at high temperature - a review," *Separation and Purification Technology*, vol. 26, pp. 195-205, 2002.
- [84] M. Bhagiyalakshmi, J. Y. Lee, and H. T. Jang, "Synthesis of mesoporous magnesium oxide: Its application to CO₂ chemisorption," *International Journal of Greenhouse Gas Control*, vol. 4, pp. 51-56, 2010.
- [85] M. Jahan, "Removal of Carbon Dioxide from Gas Streams with Metal Oxides at High Temperature," PhD thesis, School of Chemistry, Monash University, Victoria, Australia, 2011.
- [86] J. B. Lee, C. K. Ryu, J.-I. Baek, J. H. Lee, T. H. Eom, and S. H. Kim, "Sodium-Based Dry Regenerable Sorbent for Carbon Dioxide Capture from Power Plant Flue Gas," *Industrial & Engineering Chemistry Research*, vol. 47, pp. 4465-4472, 2008.
- [87] S. Lee and J. Kim, "Dry Potassium-Based Sorbents for CO₂ Capture," *Catalysis Surveys from Asia*, vol. 11, pp. 171-185, 2007.
- [88] S. C. Lee, B. Y. Choi, T. J. Lee, C. K. Ryu, Y. S. Ahn, and J. C. Kim, "CO₂ absorption and regeneration of alkali metal-based solid sorbents," *Catalysis Today*, vol. 111, pp. 385-390, 2006.
- [89] Y. Liang, D. P. Harrison, R. P. Gupta, D. A. Green, and W. J. McMichael, "Carbon Dioxide Capture Using Dry Sodium-Based Sorbents," *Energy & Fuels*, vol. 18, pp. 569-575, 2004.
- [90] C. Zhao, X. Chen, and C. Zhao, "Study on CO₂ capture using dry potassium-based sorbents through orthogonal test method," *International Journal of Greenhouse Gas Control*, vol. doi:10.1016/j.ijggc.2009.12.010, 2010.
- [91] H. T. J. Reijers, S. E. A. Valster-Schiermeier, P. D. Cobden, and R. W. van den Brink, "Hydrotalcite as CO₂ Sorbent for Sorption-Enhanced Steam Reforming of Methane," *Industrial & Engineering Chemistry Research*, vol. 45, pp. 2522-2530, 2005.
- [92] P. D. Cobden, P. van Beurden, H. T. J. Reijers, G. D. Elzinga, S. C. A. Kluiters, J. W. Dijkstra, D. Jansen, and R. W. van den Brink, "Sorption-enhanced hydrogen production for pre-combustion CO₂ capture: Thermodynamic analysis and experimental results," *International Journal of Greenhouse Gas Control*, vol. 1, pp. 170-179, 2007.
- [93] Y. Lwin and F. Abdullah, "High temperature adsorption of carbon dioxide on Cu-Al hydrotalcite-derived mixed oxides: kinetics and equilibria by thermogravimetry," *Journal of Thermal Analysis and Calorimetry*, vol. 97, pp. 885-889, 2009.
- [94] M. K. Ram Reddy, Z. P. Xu, G. Q. Lu, and J. C. Diniz da Costa, "Layered Double Hydroxides for CO₂ Capture: Structure Evolution and Regeneration," *Industrial & Engineering Chemistry Research*, vol. 45, pp. 7504-7509, 2006.
- [95] M. K. R. Reddy, Z. P. Xu, G. Q. Lu, and J. C. Diniz da Costa, "Effect of SO_x Adsorption on Layered Double Hydroxides for CO₂ Capture," *Industrial & Engineering Chemistry Research*, vol. 47, pp. 7357-7360, 2008.
-

- [96] C. T. Yavuz, B. D. Shinall, A. V. Iretskii, M. G. White, T. Golden, M. Atilhan, P. C. Ford, and G. D. Stucky, "Markedly Improved CO₂ Capture Efficiency and Stability of Gallium Substituted Hydrotalcites at Elevated Temperatures," *Chemistry of Materials*, vol. 21, pp. 3473-3475, 2009.
- [97] K. Nakagawa and T. Ohashi, "A Novel Method of CO₂ Capture from High Temperature Gases," *Journal of The Electrochemical Society*, vol. 145, pp. 1344-1346, 1998.
- [98] E. Ochoa-Fernández, M. Rønning, T. Grande, and D. Chen, "Synthesis and CO₂ Capture Properties of Nanocrystalline Lithium Zirconate," *Chemistry of Materials*, vol. 18, pp. 6037-6046, 2006.
- [99] E. Ochoa-Fernández, M. Rønning, X. Yu, T. Grande, and D. Chen, "Compositional Effects of Nanocrystalline Lithium Zirconate on Its CO₂ Capture Properties," *Industrial & Engineering Chemistry Research*, vol. 47, pp. 434-442, 2007.
- [100] D. J. Fauth, E. A. Frommell, J. S. Hoffman, R. P. Reasbeck, and H. W. Pennline, "Eutectic salt promoted lithium zirconate: Novel high temperature sorbent for CO₂ capture," *Fuel Processing Technology*, vol. 86, pp. 1503-1521, 2005.
- [101] K. G. Andrew and E. B. Michael, "Chapter 12 Decomposition of carbonates," in *Studies in Physical and Theoretical Chemistry*. vol. Volume 86: Elsevier, 1999, pp. 345-364.
- [102] L. K. Avramov and I. M. Janatchkova, "Kinetic Study of the Thermal Decomposition of Cobaltous Carbonate at Atmospheric Pressure," *Zeitschrift für physikalische Chemie*, vol. 241, pp. 244-247, 1969.
- [103] H. E. Kissinger, H. F. McMurdie, and B. S. Simpson, "Thermal Decomposition of Manganous and Ferrous Carbonates," *Journal of the American Ceramic Society*, vol. 39, pp. 168-172, 1956.
- [104] H. Lu and P. G. Smirniotis, "Calcium Oxide Doped Sorbents for CO₂ Uptake in the Presence of SO₂ at High Temperatures," *Industrial & Engineering Chemistry Research*, vol. 48, pp. 5454-5459, 2009.
- [105] F. N. Cayan, M. Zhi, S. R. Pakalapati, I. Celik, N. Wu, and R. Gemmen, "Effects of coal syngas impurities on anodes of solid oxide fuel cells," *Journal of Power Sources*, vol. 185, pp. 595-602, 2008.
- [106] V. A. Sharov and G. V. Bezdenezhnykh, "Thermal Decomposition of Lanthanide, Yttrium, and Scandium Oxalates and Carbonates," *Russian Chemical Reviews*, vol. 50, pp. 630-636, 1981.
- [107] Y. Sawada, M. Murakami, and T. Nishide, "Thermal analysis of basic zinc carbonate. Part 1. Carbonation process of zinc oxide powders at 8 and 13°C," *Thermochimica Acta*, vol. 273, pp. 95-102, 1996.
- [108] A. Doiwa and A. Tomanek, "Die Bildung von Cadmiumcarbonat und Cadmiumsulfid aus Cadmiumoxid," *Zeitschrift für anorganische und allgemeine Chemie*, vol. 334, pp. 12-14, 1964.
- [109] A. Doiwa and H. Lommel, "¹⁴CO₂-Austausch an Cadmiumcarbonat," *Angewandte Chemie*, vol. 76, pp. 578-578, 1964.
- [110] S. Brunauer, P. H. Emmett, and E. Teller, "Adsorption of Gases in Multimolecular Layers," *Journal of the American Chemical Society*, vol. 60, pp. 309-319, 1938.
-

-
- [111] E. P. Barrett, L. G. Joyner, and P. P. Halenda, "The Determination of Pore Volume and Area Distributions in Porous Substances. I. Computations from Nitrogen Isotherms," *Journal of the American Chemical Society*, vol. 73, pp. 373-380, 1951.
- [112] R. C. Weast, *CRC Handbook of Chemistry and Physics*. Cleveland, Ohio: CRC Press, 1975.
- [113] A. Lissner, "Über die Mineralstoffe in Braunkohlen," *Sitzungsberichte der Deutschen Akademie der Wissenschaften zu Berlin, Klasse für Chemie, Geologie und Biologie*, vol. 1, 1956.
-

Chapter 3 Investigation of CdO-alkali halide carbon dioxide sorbents

3.1 Chapter overview

This chapter describes a detailed investigation on carbon dioxide sorbents based on cadmium oxide. As outlined in Chapter 2, a mixture of cadmium carbonate and sodium iodide, calcined to oxide within the TGA experiment, showed a high carbon dioxide uptake in a TGA screening test.

This chapter contains two papers (each with supplementary information):

The first paper investigates different loadings of sodium iodide and identifies the optimum concentration using the screening test mentioned before. The substitution of sodium iodide by potassium iodide, lithium iodide and bromide, and sodium bromide was also investigated. The reversible carbonate formation of the cadmium oxide in the presence of sodium iodide, being the best performing promoter, was confirmed using infrared spectroscopy and powder X-ray diffraction.

The second paper details the sorbent behaviour under up to 25 cycles of carbon dioxide sorption and desorption and shows the reversibility of the reaction, which performed best if the samples were not exposed to air during initial decarbonation to cadmium oxide. For the sorbents containing sodium iodide, it was shown that multicyclic capacity loss is associated with iodine loss from the sample. Pellets made in oxide and carbonate state from the sample containing sodium iodide were also investigated.

Page 55-83: Reproduced by permission of The Royal Society of Chemistry, 2013.

Full citation: <http://dx.doi.org/10.1039/C3TA12087B>

C. Vogt, G. P. Knowles, S. L. Y. Chang, and A. L. Chaffee, "Cadmium oxide/alkali metal halide mixtures - a potential high capacity sorbent for pre-combustion CO₂ capture," *Journal of Materials Chemistry A*, vol. 1, pp. 10962-10971, 2013.

Declaration for Thesis Chapter

Cadmium oxide/alkali metal halide mixtures - a potential high capacity sorbent for pre-combustion CO₂ capture

Monash University

Declaration for Thesis Chapter 3.1-3.10

Declaration by candidate

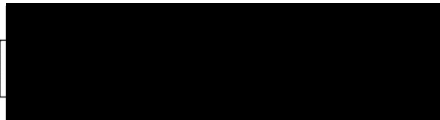
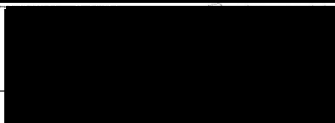
In the case of Chapter 3.1-3.10, the nature and extent of my contribution to the work was the following:

Nature of contribution	Extent of contribution (%)
Proposed original idea; prepared and analysed samples; identified major issues; developed interpretations; fully drafted papers and conclusions	75 %

The following co-authors contributed to the work. If co-authors are students at Monash University, the extent of their contribution in percentage terms must be stated:

Name	Nature of contribution	Extent of contribution (%) for student co-authors only
Gregory P Knowles	Aided method development (TGA), input to results analysis, input to manuscript revision	N/A
Alan L Chaffee	Supervision, assisted interpretation of results, editorial assistance	N/A
Shery L Y Chang	Operation of electron microscope, input to microscopy results discussion	N/A

The undersigned hereby certify that the above declaration correctly reflects the nature and extent of the candidate's and co-authors' contributions to this work*.

Candidate's Signature		Date	26/9/13
Main Supervisor's Signature		Date	27/9/13

*Note: Where the responsible author is not the candidate's main supervisor, the main supervisor should consult with the responsible author to agree on the respective contributions of the authors.

Cadmium oxide/alkali metal halide mixtures - a potential high capacity sorbent for pre-combustion CO₂ capture

Christian Vogt[#], Gregory P Knowles[#], Shery LY Chang⁺ and Alan L Chaffee^{#*}

[#] Cooperative Research Centre for Greenhouse Gas Technologies (CO₂CRC), School of Chemistry, Monash University, VIC 3800

⁺ Monash Centre for Electron Microscopy, Monash University, VIC 3800

⁺ Current Address: Ernst Ruska-Centrum, Forschungszentrum Jülich GmbH, 52425 Jülich, Germany

* corresponding author: [REDACTED]

Phone: + [REDACTED] Fax: + [REDACTED]

3.2 Abstract

A series of cadmium oxide based materials were prepared by mixing cadmium carbonate with alkali metal halides. Subsequent heat treatment then transformed the cadmium carbonate into oxide to yield the active carbon dioxide sorbent. It was observed from thermogravimetric analysis that neat cadmium oxide does not sorb significant amounts of carbon dioxide, whereas doping the material with alkali halides facilitates conversion to cadmium carbonate. The cadmium oxide/sodium iodide mixture, in particular, was found to reversibly bind up to 24 wt % carbon dioxide in the temperature range of 250 to 300 °C, which is consistent with an almost stoichiometric conversion of the cadmium oxide to cadmium carbonate. The carbon dioxide could subsequently be released, in the same temperature range, when the gas supply was switched from carbon dioxide to an inert gas flow. The formation of the carbonate was separately verified by both infrared spectrometry and powder X-ray diffraction (XRD). In addition, XRD provided simultaneous detection of both the oxide and carbonate phases thus demonstrating their inter-dependency and is consistent with the absence of other cadmium phases. Le Bail refinement of the unit cell parameters did not reveal a significant change in the unit cell

size of the cadmium oxide or carbonate due to mixing with alkali metal halides. Transmission electron microscopy on a 17.5%NaI sample indicated that the material consists of spherical particles of ~250 nm diameter. Nitrogen physisorption experiments showed that the sodium iodide-enhanced material is non-porous and of a low surface area.

Keywords: Pre-combustion, carbon dioxide capture, cadmium oxide, high-temperature sorption, partial pressure swing

3.3 Introduction

Efforts are underway to reduce greenhouse gas emissions that are associated with anthropogenically induced climate change. Nevertheless, carbon dioxide emitting fossil fuels, like coal, are likely to play a key role in the power generation sector of the near future [1-3]. In order to reduce carbon dioxide emissions while generating power from fossil fuels, new power generation processes are under development that can incorporate carbon dioxide capture into their process flow sheet and so avoid its release to the atmosphere.

The proposed Integrated Gasification Combined Cycle (IGCC) process involves high temperature gasification of coal into an intermediate synthesis gas (syngas) mixture. This syngas is created by gasifying the coal to hydrogen, carbon monoxide and carbon dioxide using water vapour in a lean oxygen atmosphere that avoids complete combustion of the coal [4]. Impurities that evolve from the sulphur and nitrogen compounds contained in the coal can be present in the syngas as well [5]. A water gas shift (WGS) reactor is employed downstream of the gasifier to increase the yield of hydrogen via the oxidation of the carbon monoxide product gas with water, yielding hydrogen and carbon dioxide.

Subsequent selective removal of the carbon dioxide component (pre-combustion capture) would leave an enriched hydrogen product suitable for power generation using a gas/steam turbine combined cycle for which the only significant exhaust stream would be environmentally friendly water [4, 6]. The in-situ removal of carbon dioxide from within the WGS reactor would also support a shift in the equilibrium of the water-gas reaction towards the valuable hydrogen, according to Le Châtelier's principle [7].

As the gas leaves the water-gas shift reactor at temperatures between 250 and 400 °C [6], it would be beneficial to capture the carbon dioxide in this temperature range, without any necessity to further cool or heat the gas. In order to be useful as an industrial sorbent, the material should also reversibly sorb and desorb carbon dioxide, have a high CO₂ selectivity and sorption capacity, deliver fast sorption/desorption kinetics and exhibit long-term capacity stability. The process configuration for reversible sorption could involve either a thermal swing, where sorption is carried out at lower temperatures, and heating encourages the sorbent to release the CO₂, or a pressure (or vacuum) swing, where sorption takes place at higher and desorption at lower partial pressures. Pressure or vacuum swing is likely to be favoured from a process design point of view, because pressure changes can be more quickly achieved than temperature changes [8, 9].

For this purpose, a range of materials have been considered, including layered double hydroxides [10-12], lithium zirconates [13], magnesium/potassium double salts [12, 14] and calcium carbonate.

Layered double hydroxides have been studied in the temperature range of the IGCC process, but at temperatures around 200 to 400 °C, their sorption capacities are reported to be fairly low, around 1 to 2.9 wt % [10, 12].

Calcium carbonate, which under heat calcines to calcium oxide according to eqn. 3.3.1, has been studied by a number of research groups. This includes studies of the kinetics of sorption/desorption and the stability of the sorbents during carbonation-calcination cycling at lab scale [15-19], modelling of the capacity decay due to sintering at high temperatures [20] as well as pilot plant scale studies on a carbonator-calciner system [21, 22]. The uptake of sulphur oxides by calcium oxide has also been studied and occurs in competition with carbonation [23, 24].



This reaction requires a comparatively high temperature (typically 800 °C and beyond for calcination, above 600 °C for carbonation), so that the sorbent is not active in the temperature range of interest in the IGCC process.

Lithium zirconates, which sorb carbon dioxide according to eqn. 3.3.2, also require higher temperatures for sorption (500 °C) and desorption (680 °C) than the WGS reactor, with sorption kinetics becoming slow below this temperature window [25]. They can be considered high capacity sorbents, as they sorb up to 20 wt % of carbon dioxide [13], but additional heating of the syngas to reach the necessary sorption/desorption temperature range would result in an energy penalty in the IGCC process with carbon dioxide capture.



Magnesium/potassium carbonate double salts have been studied and found to be promising materials for pre-combustion carbon dioxide capture. Their utilisation involves the formation of potassium carbonate and magnesium oxide phases during desorption, and a mixed potassium/magnesium oxide and carbonate phase during carbonation. Cyclic working capacities of about 8 wt % have been achieved [14]. However, a further increase in capacity is always desirable, as it would help decrease the size of a sorption reactor and thus, cut the costs of carbon dioxide capture.

Doiwa et al. [26, 27] have described the carbonation of cadmium oxide. Pure cadmium oxide itself does not sorb any carbon dioxide to form cadmium carbonate, but does so if mixed with sodium halides in a temperature range between 250 and 300 °C, which is suited to WGS reactor conditions. To the best of our knowledge, cadmium compounds have so far not been considered as carbon dioxide sorbents. We have thus hypothesised that a cadmium oxide/alkali halide might be suitable for pre-combustion carbon dioxide capture.

In this study, cadmium oxide/alkali halide mixtures were synthesised by using simple wet or dry mixing approaches, followed by heat treatment. The product materials were examined for carbon dioxide sorption capacity via thermogravimetric analysis (TGA), having in mind the application of these materials in a pre-combustion carbon dioxide capture system. One of the materials was subsequently analysed by Fourier-transform infrared spectrometry (FTIR) to verify carbonate formation during sorption. Powder X-ray diffraction (XRD) was used to determine the crystal phases prevalent during the sorption

and desorption of carbon dioxide and to examine their unit cell parameters. Nitrogen physisorption was used to determine the surface area of the material.

3.4 Experimental section

3.4.1 Chemicals

Cadmium carbonate (99+ % metals basis, Alfa Aesar, containing 0.003 % of nitrate), sodium iodide (99 %, Alfa Aesar), sodium bromide (> 99.0 % Sigma-Aldrich), potassium iodide (99.5 %, BDH), potassium bromide (98.5 %, Univar for synthesis, and IR grade, Sigma-Aldrich for FTIR sample preparation), lithium iodide (98 % for synthesis, Merck), lithium bromide (> 99 %, Alfa Aesar) and sodium carbonate (> 99 %, BDH) were used as supplied. Carbon dioxide (food grade, BOC), argon (high purity, BOC) were used after purification by a Hydropurge II water trap in the TGA experiments. Liquid nitrogen (BOC); gaseous nitrogen was obtained from the headspace above the liquid.

3.4.2 Preparation of sorbents

Cadmium carbonate (~ 1 g) was mixed with sodium iodide (0, 7.5, 10.0, 12.5, 15.0, 17.5 & 20.0 wt %), sodium bromide (12.9, 13.8 and 20.6 wt %) potassium iodide (20.1, 23.5 and 24.3 wt %), potassium bromide (15.4 wt %), lithium iodide (16.4 wt %), lithium bromide (12.4 wt %) and sodium carbonate (18.5 wt %) via either dry or wet mixing.

For the wet mix, suspensions of cadmium carbonate dispersed in alkali metal halide aqueous solution of approx. 100 mL were dehydrated by evaporation of the water using an electric hotplate stirrer. After almost complete evaporation of the water, the slurry samples were moved to a nitrogen purged oven at 120 °C and left overnight, resulting in completely dry powder samples. Except where specifically indicated, all samples described in this study were prepared using the wet mixing technique.

For comparison, one sample was prepared using a dry mixing approach. Here, cadmium carbonate and sodium iodide were mixed with mortar and pestle, without the addition of any liquid.

Some of the samples were subsequently calcined in an alumina crucible in air within a CM Inc. brand rapid temperature furnace at a rate of 10 °C/min to 500 °C and then kept at this temperature for three hours before cooling down at 30 °C/min.

The sample designations indicate the mass % of the alkali metal halide as a fraction of the cadmium carbonate as calculated from the mass amount of reagents used. A pure cadmium oxide sorbent was prepared directly via calcination of the cadmium carbonate in air. The formerly white solid turned dark red during this treatment, indicating the decomposition of cadmium carbonate to cadmium oxide. After synthesis or calcination, samples were stored in sealed vials for further use.

3.4.3 Nitrogen physisorption

Nitrogen sorption/desorption was conducted at 77 K via a Coulter Omnisorp 360 CX gas sorption analyser. A sample of 2 g was degassed at 120 °C under a vacuum of $2 \cdot 10^{-5}$ torr (2.66 mPa) for 24 hours prior to analysis. The BET surface area was calculated between relative pressures of 0.05 and 0.35 on the sorption isotherm.

3.4.4 Thermogravimetric analysis of carbon dioxide sorption

Carbon dioxide sorption screening tests (Figure 3.4.1a) and single-cycle isothermal sorption studies (Figure 3.4.1b) were performed using a Setaram TAG 24-16 symmetrical thermoanalyser. Argon and carbon dioxide were dosed into the thermoanalyser via Bronkhorst model F-201DV-RAD-11-K programmable mass flow controllers. A total gas flow of 70 mL/min (i. e., 35 mL/min sample gas and 35 mL/min on the reference side of the balance) was used for all experiments, consisting of either 70 mL/min argon (inert gas flow) or a mixture made up of 35 mL/min carbon dioxide and 35 mL/min argon (sorption gas flow, i.e., 50 vol % carbon dioxide, close to the value of 38 % as reported for a water gas shift reactor outlet gas stream [28]). A sample mass of approximately 20 mg of an oxide material or 30 mg of a carbonate material was used for the experiments. Temperatures given in the text are the sample temperatures measured; fluctuations of temperature over time at isothermal setting of the thermoanalyser led to errors of no more than ± 3 °C.

A screening test procedure, as shown in Figure 3.4.1a, was used for an initial characterisation of the materials. The experiment consisted of a pre-treatment step (660 °C, 20 min, 610 °C for pre-calcined samples) in argon atmosphere. After cooling down to 125 °C, the gas supply was changed to 50 % carbon dioxide in argon, and the temperature ramped up to 660 °C. At the beginning of this second temperature ramp, the mass was set to 100 % and mass readings considered relative to that, along the ramp shown as a dashed line in Figure 3.4.1a. Samples used in this test were either used directly as synthesised (i.e., containing cadmium carbonate), or else after calcination in air (500 °C, 3 h). The samples that were tested according to this procedure are given in Table 3.4.1.

A second set of experiments consisted of choosing several temperatures to set up a sorption and desorption run as illustrated in Figure 3.4.1b and Table 3.4.1. Here, samples were pre-treated at either 610 °C for 20 minutes (as indicated in Figure 3.4.1b) or 380 °C for 1 h in argon and then cooled down to the sorption temperature, which was then kept constant. After one hour of equilibration time, the mass reading was set to 100 % and the gas flow was switched to CO₂ sorption and maintained for two hours. Afterwards, the gas flow was switched back to argon and the mass changes measured over another hour. The change from argon to carbon dioxide and back at a constant temperature was intended to mimic a pressure swing sorption by changing the partial pressure of carbon dioxide from 0 (= argon purge) to 0.5 (CO₂ mixture). A final increase in temperature (to between 380 and 450 °C) brought the samples fully back to the oxide state for further analysis.

Multicyclic sorption was tested for the 17.5 % NaI sample using a method similar to that of Figure 3.4.1b. In this experiment, however, the isothermal step for sorption and desorption was set to be long enough to accommodate four cycles (12 minutes sorption, 24 minutes desorption each), which were achieved by switching the gas between 50 % CO₂ and pure argon repeatedly.

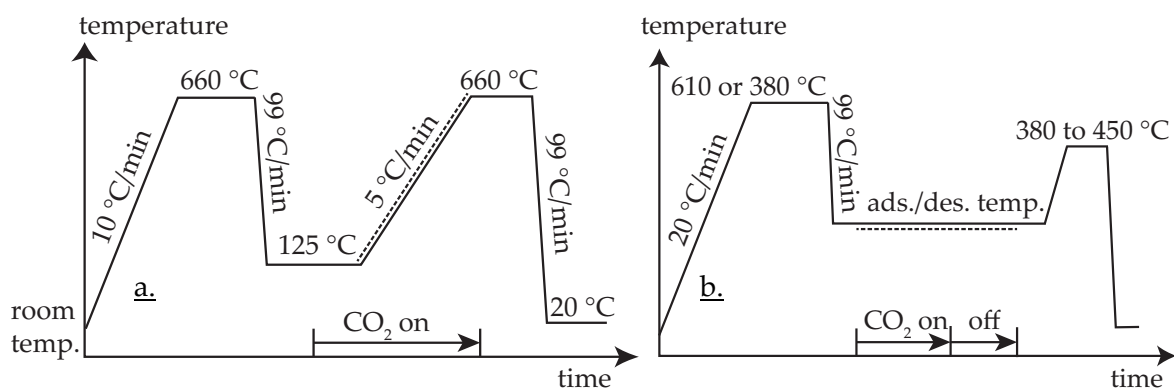


Figure 3.4.1: a. Initial screening program for TGA; b. sorption/desorption program. The dashed line on the temperature graph indicates the mass readings used for further calculation.

Table 3.4.1: Cadmium carbonate materials tested. Mass percentages refer to the basis of CdCO_3 .

screening test (Figure 3.4.1a)	one cycle sorption pre-treatment: 610 °C (Figure 3.4.1b):	one cycle sorption pre-treatment: 380 °C (Figure 3.4.1b):
pure CdO ‡	17.5 % NaI (sorption temp °C):	non-calcined samples at 290 °C:
7.5 % NaI *	247 ‡	NaI 17.5 % ~
10 % NaI *	267 ‡	LiI 16.4 %
12.5 % NaI *	277 ‡	NaBr 12.9 %
15 % NaI *	298 ‡	LiBr 12.4 %
17.5 % NaI *	308 ‡	KI 23.5 %
20 % NaI *	318 ‡	
pure NaI #	328 ‡	
13.8 % NaBr (dry mix) ‡	293 (dry & wet mix) ‡	
20.6 % NaBr ‡	* both calcined in air and in carbonate state	
24.3 % KI ‡	# also in pure Ar (no CO ₂)	
20.1 % KI (dry mix) ‡	‡ calcined in air	
15.4 % KBr (dry mix) ‡	~ also four-cycle experiment	
18.5 Na ₂ CO ₃ ‡		

3.4.5 Infrared spectrometry

Infrared spectra were obtained on a Perkin-Elmer Spectrum RXI Fourier-transform infrared spectrometer. For analysis, single grains of the prepared sorbents (< 1 mg) dried in nitrogen flow (minimum 24 hours at 120 °C) were dispersed into 0.3 g of oven-dried IR-grade potassium bromide and then pressed at 8 tons force for 10 minutes into 13 mm diameter pellets using a Specac brand press and pellet die. A pure potassium bromide pellet was used as a background correction sample; background correction was performed automatically by the instrument control software. The pellets were dried in nitrogen flow at 120 °C for at least three hours immediately before the analysis to ensure they are as dry as possible. A resolution of 0.25 cm⁻¹ was chosen and spectra were taken as an average of 16 scans between wavenumbers of 4000 to 400 cm⁻¹.

3.4.6 Powder X-ray diffraction

Laboratory powder X-ray diffraction experiments were performed on a Bruker D8 focus powder diffractometer using Cu K α radiation (1.5418 Å). The 17.5 % NaI sample (calcined in air at 500 °C for 3 h) and pure comparison samples were used as approximately 0.5 g subsamples, whereas 20 mg was used of the carbonated sample. Samples were mounted on a flat plastic sample holder for analysis and data was acquired at 0.2 ° 2 θ per minute speed at a resolution of 0.005 °.

The unit cell parameters of cadmium oxide and cadmium carbonate were refined using the Le Bail method and the software package GSAS-EXPGUI [29, 30]. Powder Diffraction File (version 4+, 2011) entries 04-001-3770 (cadmium oxide) and 04-014-4823 (cadmium carbonate) were used as starting values for the unit cell parameters. XRD patterns were converted from 2 θ with the respective wavelength to the wavelength-independent values of Q using the software CMPR [31]. The definition of Q is given in eqn. 3.4.1, wherein λ is the wavelength of the X-rays used to acquire the pattern. The value of Q has a unit of reciprocal length, as evident by eqn. 3.4.1.

$$Q = \frac{4\pi \sin \frac{2\theta}{2}}{\lambda} \quad \text{eqn. 3.4.1}$$

3.4.7 Transmission electron microscopy

Transmission electron microscopy (TEM) and energy-dispersive X-ray spectroscopy (EDX) of a 17.5 % NaI sample was performed on a JEOL 2100F model instrument. Bright-field TEM imaging was used to investigate the morphology of the sample and electron diffraction was used to examine the crystallinity of the material. d-spacings from Powder Diffraction File entry 04-001-3770 (CdO) were used to match the electron diffraction patterns. Camera length was calibrated using a silicon calibration TEM sample.

3.5 Results and discussion

3.5.1 CO₂ sorption analysis

The full thermogram of the 17.5 % NaI as synthesised sample (included in Figure 3.5.1c) is shown in Figure 3.5.1a. Figure 3.5.1b and c present the portions of the thermogram between 10000 and 16000 s (i. e., spanning the second temperature ramp) plotted as a function of temperature and normalised to 100 % mass at the beginning of the ramp. Several samples are shown with different sodium iodide loadings, along with a pure cadmium oxide sample, as they were heated at 5 °C/min in carbon dioxide. For Figure 3.5.1b, the samples had previously been calcined in air (500 °C, 3h), whereas for Figure 3.5.1c, the samples were used directly as synthesised. In the latter case, the decomposition of carbonate to oxide occurred in the thermoanalyser during the pre-treatment step (see Section 3.4.4).

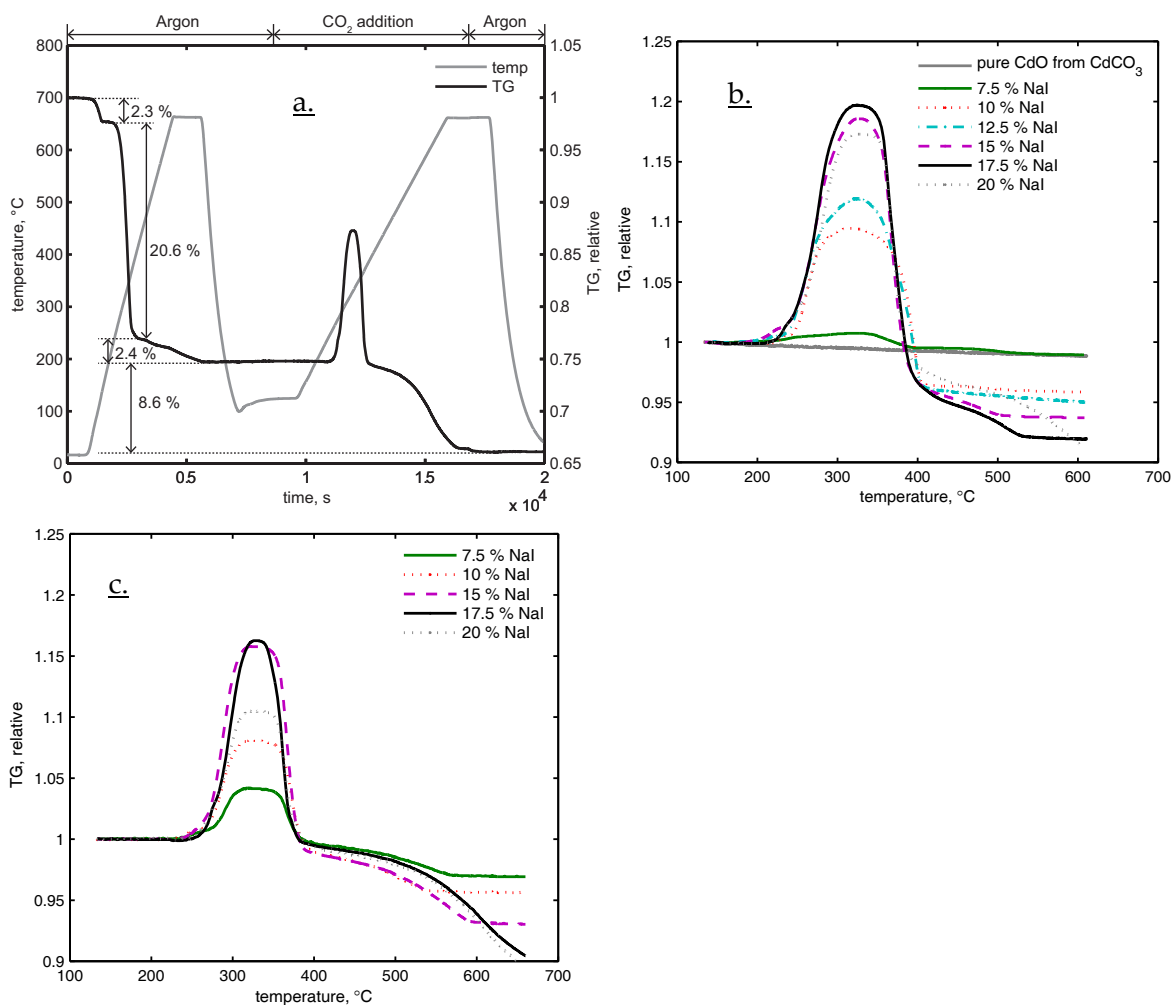


Figure 3.5.1: TGA screening tests (5 °C/min ramp in CO₂, 100 % at 125 °C) of sodium iodide/cadmium mixed oxide of different NaI content: a. full thermogram of 17.5 % NaI as synthesised material; b. after pre-calcination in muffle furnace in air at 500 °C for 3 h; c. as synthesised material (carbonate).

The results show that the pure cadmium carbonate that was calcined to oxide does not sorb any carbon dioxide under these conditions. An amount of 10 wt % of sodium iodide (calcined sample) or 7.5 % (uncalcined sample) is required to trigger any significant sorption. The results also show that a sample made with 17.5 % sodium iodide gives the highest-capacity sorption. At the higher 20 % sodium iodide loading, the capacity is reduced. Thus, sodium iodide behaves as a promoter at lower levels of addition, but when present in excess is detrimental for carbon dioxide sorption.

In each case, the mass uptake and subsequent loss occur over the same temperature range, (i. e., the peak is always at the same position). This result seems to indicate that the sodium

iodide is acting as a promoter for the actual reaction (cadmium oxide to cadmium carbonate), which always occurs at the same temperature.

The significant mass losses at the end of the TGA experiments (temperatures beyond 400 °C) are notable in the samples containing 10 % and more sodium iodide (Figure 3.5.1). A clear explanation for this phenomenon is still being sought (refer to section 3.11 and following for results). In theory, a 17.5 % sodium iodide/cadmium carbonate mixture would contain 28.7 mass % carbonate and 14.8 mass % iodide. Decarbonation of the mixture would result in a mass loss of 21 %, which is consistent with the value of 20.6 % shown in Figure 3.5.1a. The first 2.3 % weight loss is assumed to be due to desorption of atmospheric contaminants and water, as this occurs at comparatively low temperature. Noteworthy are gradual mass losses at higher temperatures during the pre-treatment step (2.4 %) and a further one at the end of the run, together totalling 11 %.

Both of these latter mass losses might be attributable to two causes. Firstly, the evaporation of some sodium iodide is possible. Its melting point is reported as 661 °C [32], which might correlate with sufficient vapour pressure for evaporation to occur at the temperatures used here. Secondly, the mass losses (especially the one after 1.3×10^4 s) are hypothesised to be due to the loss of iodine. The amount of iodide used to synthesise the fresh sample (14.8 %) is sufficient to account for these mass losses. However, for this to occur would require some of the iodide to be oxidised by an as yet undetermined mechanism. Evidently, carbon dioxide plays a vital role in this mechanism, as the mass loss after its injection is substantially higher than during the initial pre-treatment step under inert conditions.

Another TGA screening experiment was performed to test this influence of evaporation and/or reaction. Pure sodium iodide as well as the 17.5 % NaI sample were exposed to carbon dioxide as well as pure argon in the screening test (Figure 3.4.1a). The results of this test show no mass decrease for pure sodium iodide up to temperatures of about 550 °C both in carbon dioxide and in pure argon. Furthermore, the 17.5 % NaI sample did not exhibit a mass loss below 660 °C when heated in an inert argon environment. Mass losses were observed at 550 °C and higher for sodium iodide, both in carbon dioxide and argon. It can be speculated that a significant vapour pressure of sodium iodide is built up

around 550 °C, causing evaporation of the solid. Altogether, the results indicate that a reaction of cadmium, iodide and carbon dioxide must take place to account for the mass loss that occurs above 400 °C. It can be speculated that the reaction might even occur at lower temperature, if it is masked in this experiment by simultaneous carbon dioxide sorption occurring in this same temperature range.

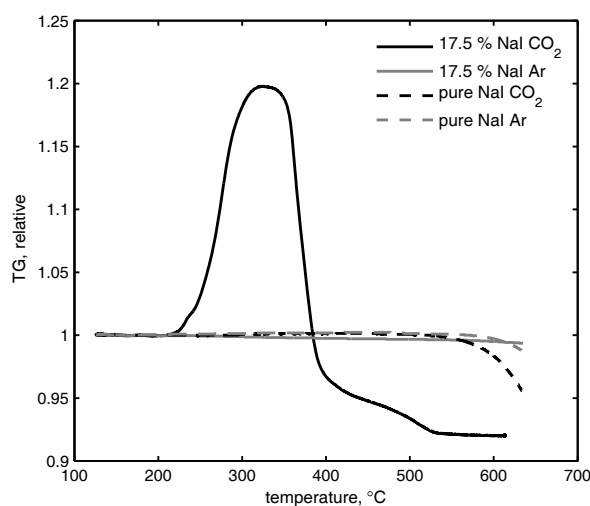


Figure 3.5.2: TGA screening test of 17.5 NaI sample and pure NaI with and without CO₂ addition. 17.5 % NaI sample calcined at 500 °C in air 3 h prior to analysis.

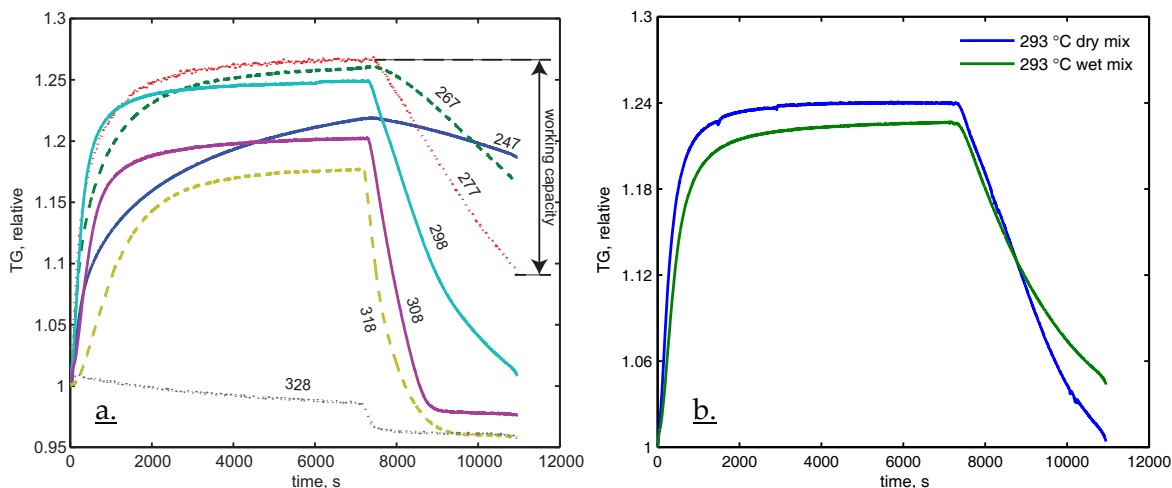


Figure 3.5.3: Two-hour sorption and one-hour desorption studies of samples calcined in air 500 °C 3 h, pre-treated in Ar. **a.** Sample 17.5 % NaI at various temperatures (°C), pre-treatment 610 °C 1 h, **b.** 15 % NaI sample made by dry and wet mixing, 610 °C pre-treatment (20 min).

The results of the screening test in Figure 3.5.1 show that sorption of carbon dioxide is in favour between 235 °C (left bottom of the peak) and 315 °C (top of the peak). Therefore, a

series of temperatures between these two limits were chosen to perform sorption and desorption experiments according to the procedure given in section 3.4.4 and Figure 3.4.1b. A 17.5 % NaI sample was chosen for this and further tests. The results, given in Figure 3.5.3a, show that the temperature of 247 °C is too low to achieve the maximum sorption capacity of 26 %. When the sorption mode was ended after two hours and the sorbents purged with inert gas for another hour, it can be observed that the mass also did not decrease very much. At higher temperatures, maximum sorption is reached (i.e., 267 to 298 °C). These results can be logically explained. At lower temperatures, conversion of oxide to carbonate is kinetically hindered and the decomposition of carbonate to oxide is not thermodynamically favoured. Higher temperatures improve the kinetics, but shift the equilibrium so that sorption is less strongly favoured. At a temperature of 328 °C, the oxide is thermodynamically preferred, but a small amount of cadmium carbonate can be assumed to be present. In Figure 3.5.3a, it becomes evident that the mass gain due to carbon dioxide uptake is masked by a mass loss during carbon dioxide addition. Switching back to inert gas then causes a further mass loss.

It was confirmed that the method of synthesis (dry mixing vs. wet impregnation, refer section 3.4.2) has no significant effect on the sorption properties of the material (Figure 3.5.3b). The dry-mixed sample, however, sorbed and desorbed carbon dioxide a bit faster than the wet mixed one; this might be attributable to a smaller particle size achieved by thorough grinding of the sample with mortar and pestle prior to calcination.

Around 298 °C, both sorption and desorption were effectively achieved in an isothermal partial pressure swing, as the capacity is still comparatively high and the decarbonation occurs readily when the CO₂ partial pressure is zero. This can be seen in the plot of the working capacity versus temperature in Figure 3.5.4; this gives the differences between the highest relative thermogravimetric mass reading (in 50% CO₂, 50% Ar) and the lowest relative mass reading at the end of the one-hour desorption run (in argon). These values give an indication of how much carbon dioxide can be both captured and then released at the same temperature.

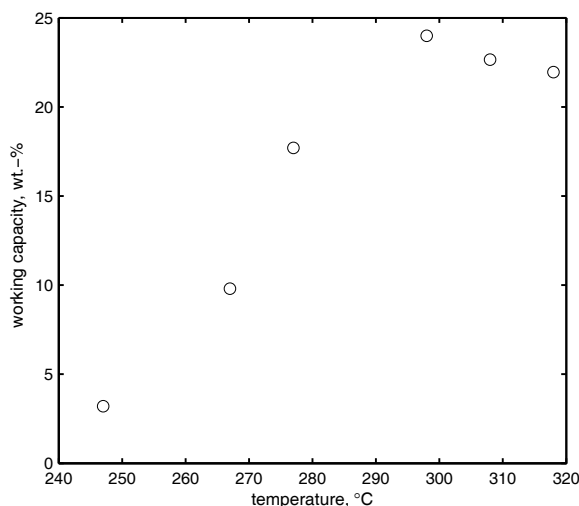


Figure 3.5.4: Working capacities derived from the difference between thermogravimetric maxima and end points in Figure 3.5.3a.

The initial high capacities of the sorbent are noteworthy. During sorption, a 26.6 % mass gain is observed at the optimal sorption temperature of 277 °C. Acknowledging that there is 17.5 % sodium iodide in the sample (considered to be inert in this estimation), the total conversion of cadmium oxide (molar mass 128.4 g/mol) to cadmium carbonate (172.42 g/mol) would correspond to a mass gain of 28 %. So it is clear that near stoichiometric conversion is occurring. Given the fact that the material is of low BET surface area (2.4 m²/g), this also indicates that carbon dioxide penetrates the particles without the constraint of any intense diffusion limitation through a product layer, as has been described for carbonation of calcium oxide [33].

The data show that the temperature corresponding to the highest sorption uptake (277 °C) is not the one corresponding to the highest working capacity (298 °C, Figure 3.5.4). This is because of the balance between low temperatures favouring high-capacity sorption and high temperatures favouring facile desorption, when an isothermal (partial) pressure swing is employed. However, the highest working capacities achieved in this study are 24 % at 298 °C and 23 % at 308 °C.

Another experiment examined the cyclic sorption capability of the 17.5 % NaI sorbent calcined in air, with the results shown in Figure 3.5.5. The thermogram shows that the sorbent repeatedly takes up mass within a short timeframe of 12 minutes and releases it under isothermal conditions upon switching to inert/argon purge for 24 minutes. A

gradual mass decrease over time is evident in this experiment during the addition of CO₂, which is assumed due to the same mechanism as described earlier.

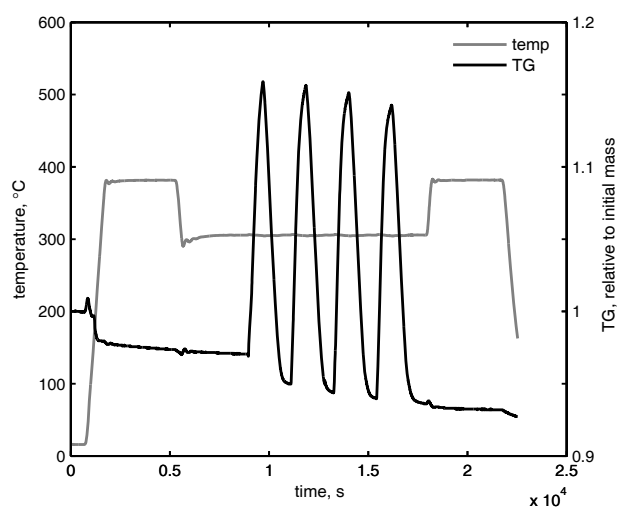


Figure 3.5.5: Multiple sorption. Four cycles of 17.5 % NaI at 305 °C, sample calcined in air 500 °C before experiment. Partial pressure swing (50 % CO₂/Ar 12 min vs. pure Ar 24 min), pre-treatment and end step in Ar. 100 % mass at the start of experiment.

Interestingly, cadmium oxide mixtures prepared with sodium bromide, potassium bromide or sodium carbonate, using both wet and dry mixing methods, show no significant sorption in the screening test if they are calcined in air before the test (Figure 3.5.6a). This is further supported by a sorption and desorption test similar to those in Figure 3.5.3, but with a sodium bromide containing cadmium carbonate sample that was calcined in air (not illustrated). The sample calcined in air showed no sorption at 308 °C, which is in general agreement with the screening test result (Figure 3.5.6a).

Another set of sorption-desorption tests were performed using lithium bromide and iodide. These solids were used without calcination in the muffle furnace and pre-treated in the thermoanalyser in argon before analysis at 380 °C for one hour. This lower pre-treatment temperature was chosen because cadmium carbonate decomposes at this temperature easily within the set pre-treatment time [34], and the temperature is well below the melting point of the lithium compounds [32]. Sorption-desorption results of these materials, given in Figure 3.5.6b, show that lithium iodide leads to similar behaviour as sodium iodide (Figure 3.5.3), promoting the carbonation reaction of cadmium oxide. It can also be seen that use of iodine compounds leads to faster kinetics in the carbonation

relative to their bromine analogues, whereas potassium iodide facilitates only weak sorption of approx. 5 %. Given the fact that a lithium bromide containing sample sorbs a fair amount of carbon dioxide in this experiment, which contrasts the result in Figure 3.5.6a for a different (i. e., sodium) bromide, it seems likely that the different modes of pre-treatment (calcination in air at 500 °C, Figure 3.5.6a, vs. pre-treatment in argon, Figure 3.5.6b) have had an influence on the sorption capabilities of the materials. Based on this conclusion, a sodium bromide-containing cadmium carbonate sample was tested again in the sorption-desorption test, this time without any pre-treatment in air. The result, which is also shown in Figure 3.5.6b, confirms that the pre-treatment step does have an influence on the material's capability to sorb carbon dioxide.

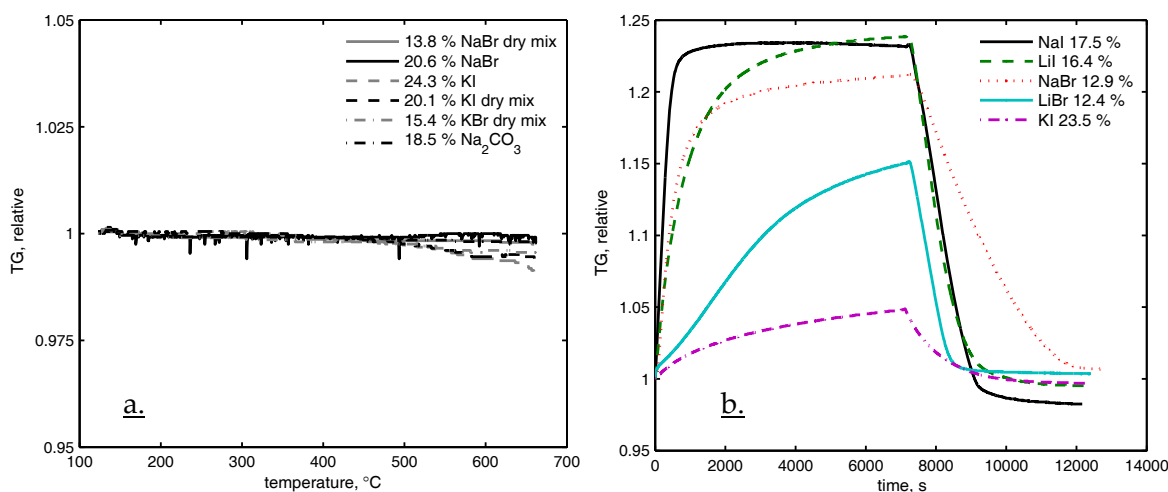


Figure 3.5.6: a. Screening TGA test of mixed Cd oxides incorporating alternative alkali halide dopants and pre-treated for 3 h at 500 °C in air, b. 2 h adsorption, 1 h desorption at 290 °C of samples with substituted dopants, pre-treatment in thermoanalyser at 380 °C in Ar 1 h.

3.5.2 Infrared spectrometry

Infrared spectrometry results performed on a 17.5 % NaI sample are given in Figure 3.5.7. Pure cadmium carbonate and pure oxide made by heat-treating cadmium carbonate was examined for comparison.

Figure 3.5.7a shows the sorbent in its oxide state. The fresh (calcined) sorbent is compared with a sample that had been carbonated and afterwards decarbonated in the thermogravimetric analyser, as well as with a cadmium oxide sample not containing any sodium iodide. A sine-shaped background absorption curve can be observed for all oxide samples, which similarly has been reported by Rieder et al. [35] for cadmium oxide. Also

notable are the peaks at wavenumbers around 3657 and 1384 cm^{-1} . These have been reported as associated with trace amounts of nitrate (1384 cm^{-1} , [36]), and with hydroxyl groups (3800 to 3200 cm^{-1} , [37]).

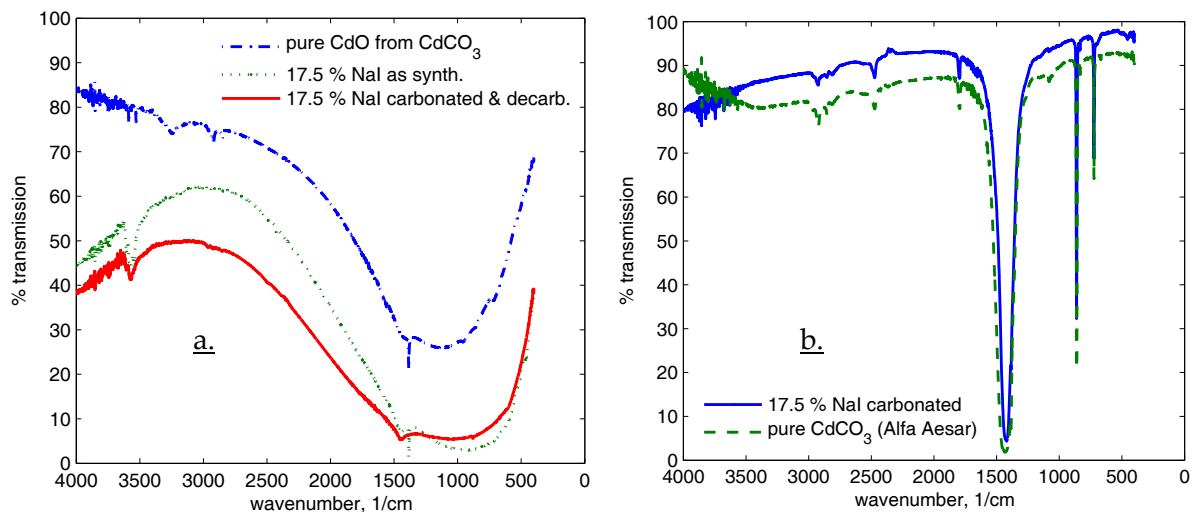


Figure 3.5.7: FTIR spectra of 17.5 NaI (calcined in air 500 °C 3 h) sample, a. oxide state, b. carbonate state

The hydroxyl peak is most prominent in the samples that contain sodium iodide and is probably a result of the affinity for water of the sodium iodide. The nitrate peak is most prominent in the untreated and pure oxide sample. It probably originates from nitrate impurities in the cadmium carbonate (see section 3.4.1). After decarbonating the sample once, as done for the calcined and pure oxide sample, these impurities have apparently not decomposed fully. However, as soon as the sample has undergone a carbonation/decarbonation cycle, and so was exposed to high temperatures for a significant time, the nitrate peak disappears.

A sample that was carbonated in the thermoanalyser for three hours in a 50 % carbon dioxide in argon mixture at 285 °C and subsequently cooled down in the same gas mixture is shown in Figure 3.5.7b, along with a pure cadmium carbonate. It can be observed that the two spectra resemble each other. This gives an indication that the oxide sorbent transforms into the carbonate during carbon dioxide sorption. The shape of the spectrum has also been reported by Stuart as a typical carbonate spectrum between wavenumbers of 2000 and 500 cm^{-1} [37].

The infrared spectrometry results clearly suggest that a metal carbonate forms during carbonation, which is then decomposed during decarbonation. The sodium iodide does not provide any peaks in the wavenumber area studied here.

3.5.3 Sample crystallinity and morphology

The results of the powder diffraction studies are given in Figure 3.5.8. In this figure, a comparison between the 17.5 % NaI sample (calcined in air at 500 °C for 3 h) and pure cadmium oxide, cadmium carbonate and sodium iodide is possible. It can be observed that the cadmium carbonate phase is prevalent in the fully carbonated 17.5 % NaI sample, whereas it reverts to cadmium oxide as soon as it is decarbonated. It can also be observed that there is no distinct crystalline sodium iodide phase present in the 17.5 % NaI sample. This suggests that sodium iodide is present in an amorphous phase, or else somehow incorporated or substituted into the cadmium oxide or carbonate lattice. If the latter, it might be expected that there could be a change in the unit cell parameters of the cadmium oxide or carbonate and this motivated a detailed investigation of the data using a Le Bail refinement.

Detailed results of the Le Bail refinement are given in the supplementary materials. It was found that the cadmium oxide unit cell of the mixed material is 4.6994 Å in size, whereas pure cadmium oxide was found to have 4.6949 Å. The latter value is close to the Powder Diffraction File (version 4+ 2011) entry for cadmium oxide 04-001-3770 (4.6951 Å). As a refinement of pure cadmium carbonate compared to the database entry (refer to supplementary materials) resulted in a difference of 0.013 Å in one dimension, the difference of the cadmium oxide unit cell was considered to be due to uncertainties in the refinement, rather than an actual change in its size upon sodium iodide doping. This favours the former suggestion that sodium iodide is present as an amorphous phase.

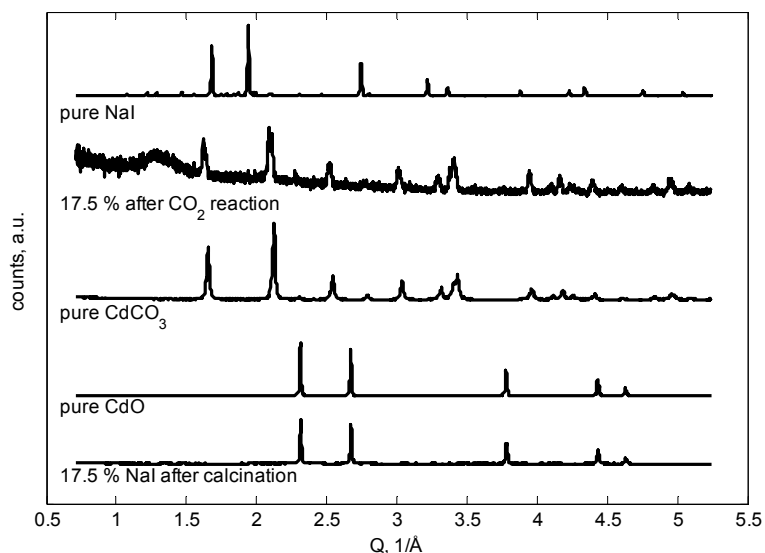


Figure 3.5.8: Powder XRD patterns of 17.5 % NaI sample and pure comparison materials

TEM images (Figure 3.5.9a and b) show that the sorbent consists of beads of approx. 250 nm diameter and that its morphology is hardly changed after four cycles of CO₂ exposure (Figure 3.5.9b). Electron diffraction patterns show a spot pattern rather than ring-shaped appearance in both instances (c and d). This indicates that the particles are polycrystalline and the crystal size is comparatively large. This observation is consistent with the powder XRD pattern of the oxide state (Figure 3.5.8), as the pattern shows narrow peaks. The electron diffraction patterns match the d-spacings for CdO obtained from Powder Diffraction File, which is indicated in Figure 3.5.9 c and d (refer to supplementary materials for d-spacings and indices). Sodium iodide was not found in the electron diffraction pattern of the neat and used samples, however a weak iodine signal was found in the EDX spectrum from areas marked in Figure 3.5.9b (refer to supplementary materials; the presence of the weak Na signal was not conclusive in this case as it overlaps with Cu signals from the TEM grid bars). The TEM results are in agreement with the XRD patterns (Figure 3.5.8), as they indicate large and highly crystalline CdO particles, as well as the presence of amorphous phase sodium iodide, being relatively well-distributed throughout the sample.

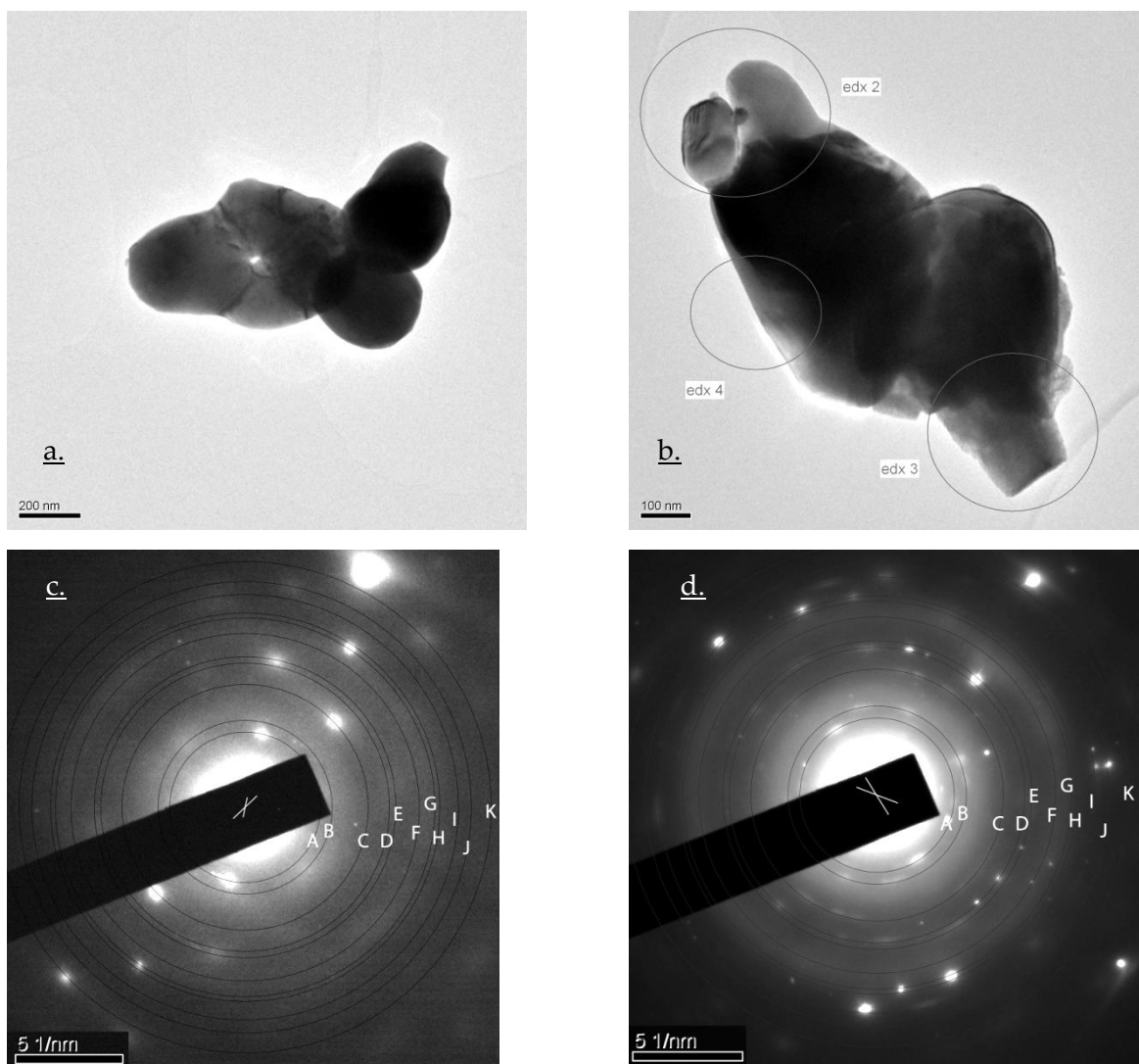
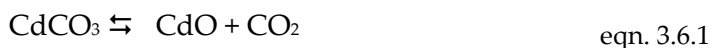


Figure 3.5.9: TEM images (a. & b.) of 17.5 % NaI, electron diffraction (c. & d., A-K denote diffraction lines as identified as CdO, refer supplementary material). Sample calcined in air, a. & c. neat, b. & d. after 4 cycles (Figure 3.5.5),

3.6 Concluding remarks

In this study, a cadmium/alkali halide mixture was synthesised and characterised for pre-combustion carbon dioxide capture. Synthesis can easily be achieved by dry mixing of cadmium carbonate and alkali halide or by wet mixing of alkali halide solution onto cadmium carbonate. Heat treatment of the material, preferably performed in an inert gas such as argon, results in the active sorbent. A composition with 17.5 % sodium iodide based on cadmium carbonate gives the best carbon dioxide sorption properties as determined in TGA. A trial to substitute sodium iodide with a range of other sodium and potassium salts resulted in materials with no significant carbon dioxide sorption if the heat

treatment is performed in air. If pre-treated in inert gas, dopants alternative to sodium iodide show CO₂ sorption, but with less favourable kinetics. TGA results show that the material with the optimum level of promoter carbonates almost stoichiometrically in an atmosphere containing 50 % carbon dioxide at temperatures between 247 and 318 °C. A subsequent purge with inert gas releases carbon dioxide easily at a temperature around 308 °C, suggesting that the material has good pressure swing sorption capabilities. Noteworthy are the comparatively high sorption capacities in the context of the material having a low BET surface area. The samples are assumed to be air-sensitive at high temperatures, as samples containing alternative dopants to sodium iodide show no sorption if they are pre-treated in air at elevated temperatures after synthesis. If pre-treated in inert atmosphere, substitution of sodium iodide dopant is possible. Characterisation of the material by FTIR spectrometry and powder XRD shows that cadmium carbonate is formed and decomposed during sorption-desorption runs, according to eqn. 3.6.1.



XRD analysis revealed that cadmium oxide and carbonate phases are visible in the mixed sample, but a discrete sodium iodide phase could not be observed. It appears that the sodium iodide dopant is distributed amorphously within the cadmium oxide since Le Bail refinement did not reveal any change of the XRD unit cell parameters. TEM images indicate a spherical morphology of the samples, with CdO particles of 250 nm diameter and a polycrystalline appearance. In addition, the combination of electron diffraction and EDX results suggest that sodium iodide is present in the sorbent in an amorphous form.

The results of this study suggest that CO₂ sorbents based on cadmium may be viable for use in a pressure swing sorption process due to their ability to reversibly carbonate and decarbonate at the same temperature. In order to be industrially interesting, research must now be focussed on maintaining a high sorption capacity over a multitude of carbonation-decarbonation cycles and analysing the effect of other syngas constituents (hydrogen, water and trace compounds like hydrogen sulphide) on the sorbent.

Cadmium oxide is known to be toxic when ingested, so this is a concern that would need to be fully assessed if it were to be used industrially. Since the sorbent would probably be fully contained as a fixed bed it seems likely that this risk would be manageable.

Further research that sheds light on the exact sorption mechanism of the materials presented here may also lead to the development of less toxic analogues.

3.7 Acknowledgements

We thank Dr Martin Duriska (laboratory powder XRD, Monash Chemistry) and Bruce Dobney (FTIR, Monash Chemistry) for help with data acquisition and analysis. Monash Centre for Electron Microscopy is acknowledged for the use of the TEM facility. The authors acknowledge funding provided by the Australian Government through its Cooperative Research Centre (CRC) program to support this CO2CRC research project. Financial support from the Faculty of Science, Monash University, is also gratefully acknowledged.

Supplementary Material

Cadmium oxide/alkali metal halide mixtures - a potential high capacity sorbent for pre-combustion CO₂ capture

Christian Vogt[#], Gregory P Knowles[#], Shery LY Chang⁺ and Alan L Chaffee^{#*}

[#] Cooperative Research Centre for Greenhouse Gas Technologies (CO₂CRC), School of Chemistry, Monash University, VIC 3800

⁺ Monash Centre for Electron Microscopy, Monash University, VIC 3800

^{*} Current Address: Forschungszentrum Jülich GmbH, 52425 Jülich, Germany

* corresponding author: [REDACTED]

Phone: + [REDACTED] Fax: + [REDACTED]

3.8 Nitrogen adsorption isotherm and pore size distribution

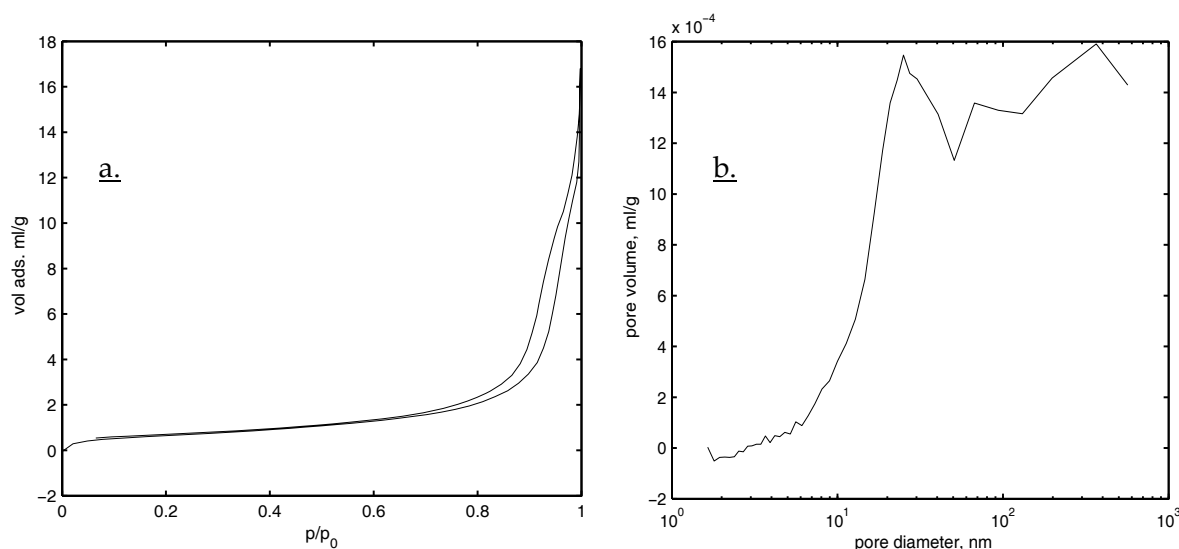


Figure 3.8.1: a. N₂ adsorption-desorption isotherm (gas volume at STP adsorbed vs. p/p_0), b. BJH pore volume of a 17.5 % NaI sample, after initial calcination at 500 °C in air 3 h

3.9 Le Bail fit of the XRD data

3.9.1 Statistics

The statistical values of the Le Bail fits performed in the paper are given in Table 3.9.1.

Table 3.9.1: Statistics of the Le Bail fits

sample	reference in supplement	wRp	Rp	χ^2
17.5 % NaI, calcined 500 °C air	Figure 3.9.1	0.1663	0.1109	5.891
pure CdO	Figure 3.9.2	0.1145	0.0740	2.930
pure CdCO ₃	Figure 3.9.3	0.1245	0.0875	1.529

3.9.2 Le Bail fit graphs

The graphs of the Le Bail refinements of the powder XRD data are given in the figures below. The black crosses denote the observed, the red line the refined data. The background is plotted green; blue denotes the difference between calculated and observed. The difference graph is offset below the other graphs.

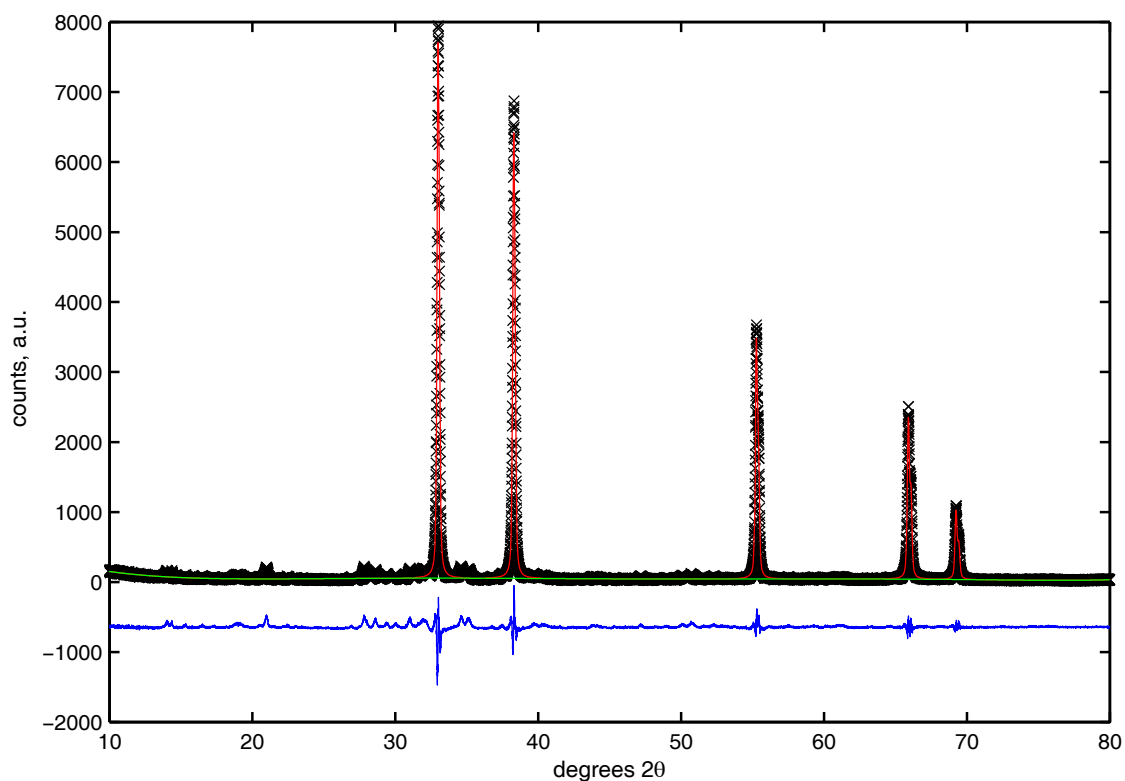


Figure 3.9.1: Le Bail refinement plot of 17.5 % NaI sample, as synthesised

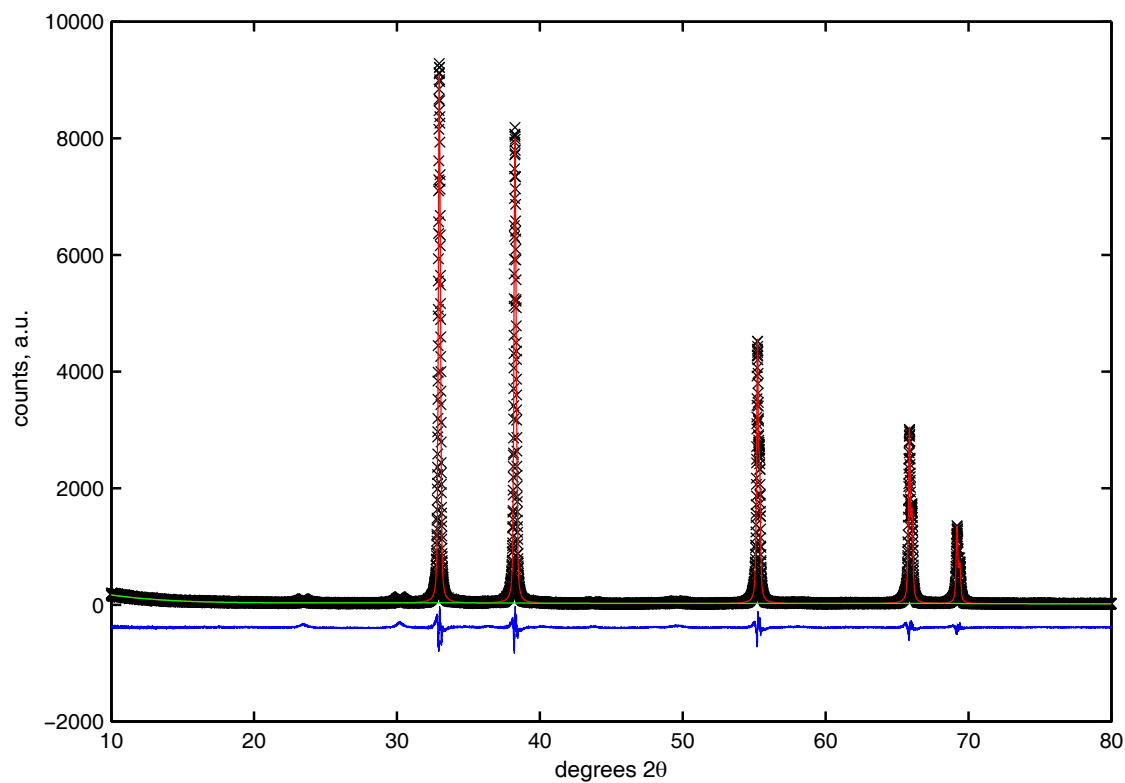
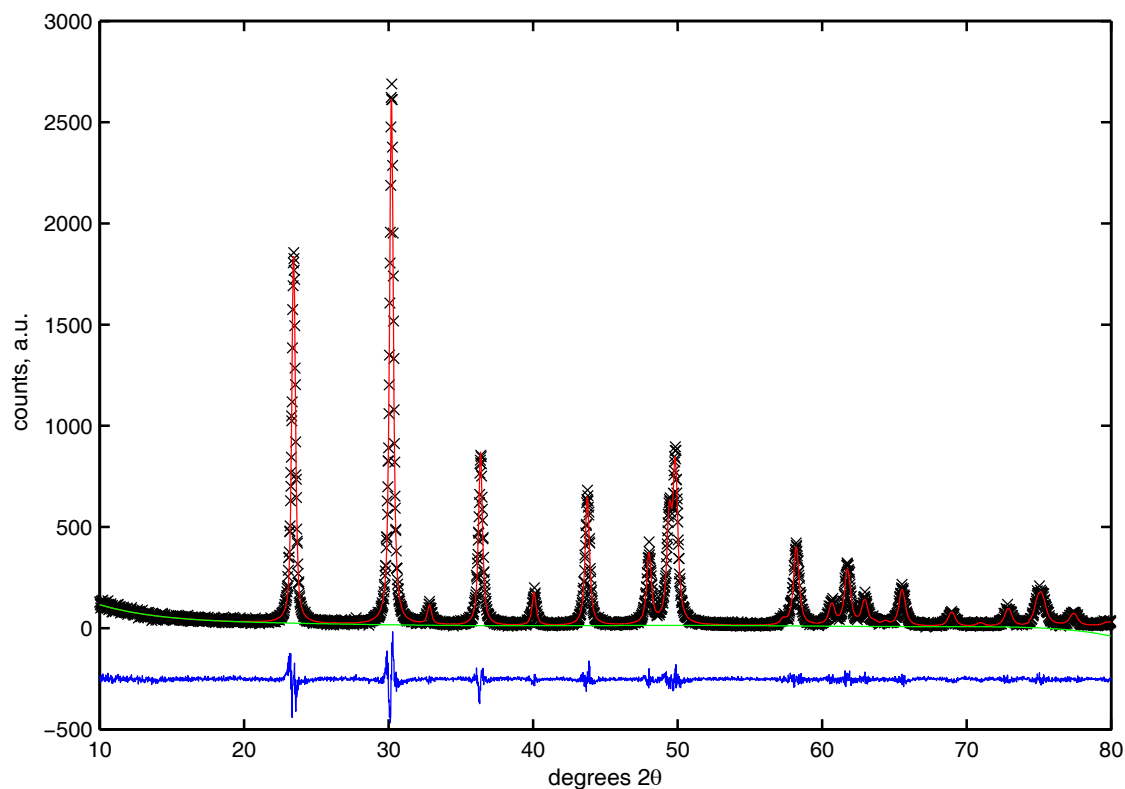


Figure 3.9.2: Le Bail refinement plot of pure CdO

Figure 3.9.3: Le Bail refinement plot of pure CdCO₃

3.9.3 Results

Table 3.9.2: Results of the Le Bail refinement of the laboratory XRD data for cadmium oxide and carbonate

sample	phase	unit cell lengths a = b	unit cell length c	space group
17.5 % NaI calcined 500 °C air 3 h	CdO	4.6994 Å	= a	Fm-3m
pure CdO	CdO	4.6949 Å	= a	Fm-3m
PDF 4+ 2011 entry 04-001-3770	CdO	4.6951 Å	= a	Fm-3m
pure CdCO ₃	CdCO ₃	4.9330 Å	16.3448 Å	R-3c
PDF 4+ 2011 entry 04-014-4823	CdCO ₃	4.9207 Å	16.2968 Å	R-3c

3.10 EDX results and Powder Diffraction File data

EDX results are given in Figure 3.10.1 to Figure 3.10.3. The increased iodine content relative to cadmium is evident in Figure 3.10.2. Table 3.10.1 shows the d-spacings and reciprocal distances for cadmium oxide, Powder Diffraction File entry 04-001-3770.

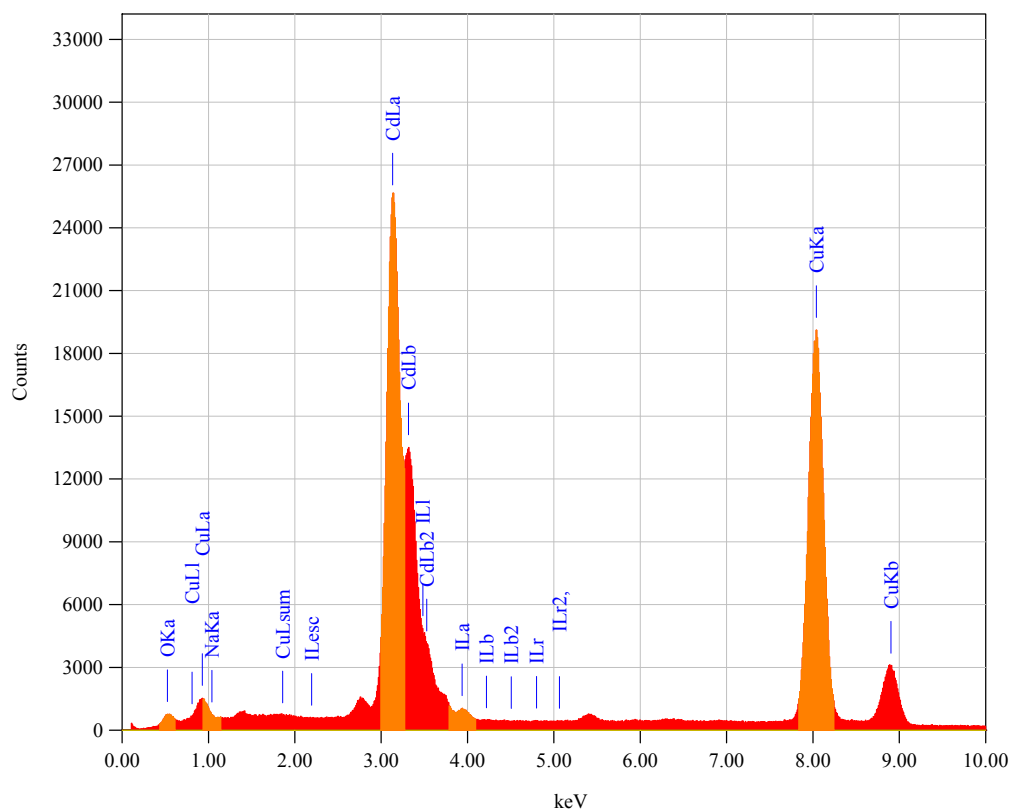


Figure 3.10.1: EDX spectrum for 'edx 2' label in article.

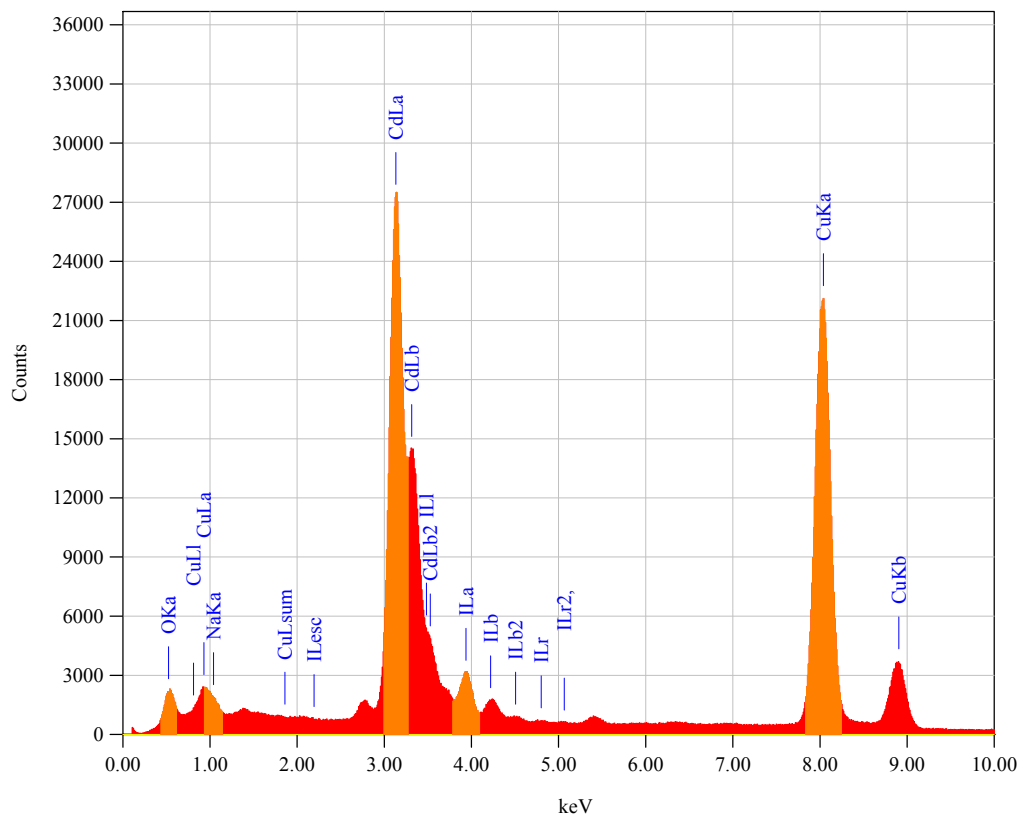


Figure 3.10.2: EDX spectrum for 'edx 3' label in article.

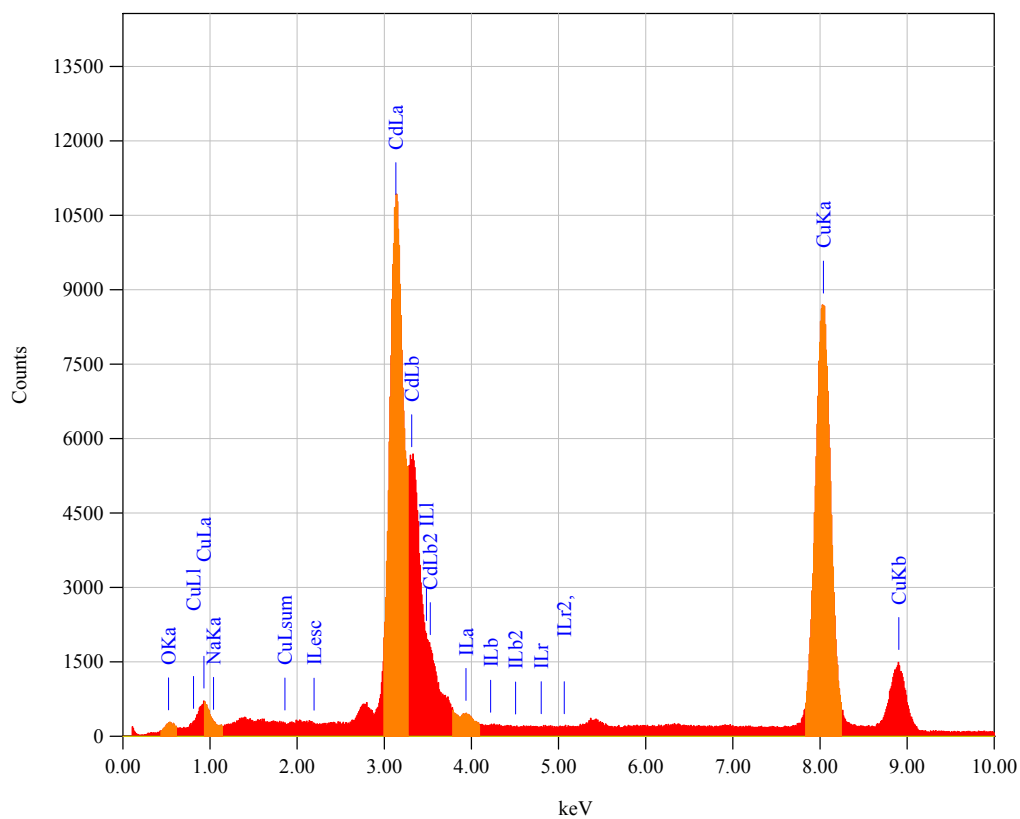


Figure 3.10.3: EDX spectrum for 'edx 4' label in article.

Table 3.10.1: Assignment of electron diffraction pattern observations corresponding to label A-K in the article, d-spacing values obtained from Powder Diffraction File entry 04-001-3770 (CdO)

Label	A	B	C	D	E	F	G	H	I	J	K
d-spacing (Å)	2.71	2.35	1.66	1.42	1.36	1.17	1.08	1.05	0.96	0.9	0.83
Reciprocal distance (1/nm)	3.69	4.26	6.02	7.06	7.38	8.52	9.28	9.53	10.43	11.07	12.05
Q (1/Å)	2.32	2.68	3.78	4.44	4.64	5.35	5.83	5.99	6.55	6.96	7.57
h	1	2	2	3	2	4	3	4	4	5	4
k	1	0	2	1	2	0	3	2	2	1	4
l	1	0	0	1	2	0	1	0	2	1	0

Declaration for Thesis Chapter

Cadmium oxide/alkali metal halide mixtures for pre-combustion CO₂ capture. Part 2: Multiple sorption cycles

Monash University

Declaration for Thesis Chapter 3.11-3.20

Declaration by candidate

In the case of Chapter 3.11-3.20, the nature and extent of my contribution to the work was the following:

Nature of contribution	Extent of contribution (%)
Proposed original idea; prepared and analysed samples; identified major issues; developed interpretations; fully drafted papers and conclusions	80 %

The following co-authors contributed to the work. If co-authors are students at Monash University, the extent of their contribution in percentage terms must be stated:

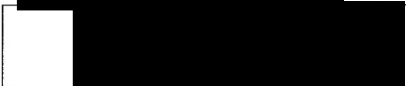
Name	Nature of contribution	Extent of contribution (%) for student co-authors only
Gregory P Knowles	Aided method development (TGA), input to results analysis, input to manuscript revision	N/A
Alan L Chaffee	Supervision, assisted interpretation of results, editorial assistance	N/A

The undersigned hereby certify that the above declaration correctly reflects the nature and extent of the candidate's and co-authors' contributions to this work*.

Candidate's
Signature

 Date 26/9/13

Main
Supervisor's
Signature

 Date 27/9/13

*Note: Where the responsible author is not the candidate's main supervisor, the main supervisor should consult with the responsible author to agree on the respective contributions of the authors.

Cadmium oxide/alkali metal halide mixtures for pre-combustion CO₂ capture. Part 2: Multiple sorption cycles

Christian Vogt, Gregory P Knowles and Alan L Chaffee *

Cooperative Research Centre for Greenhouse Gas Technologies (CO₂CRC), School of Chemistry, Monash University, VIC 3800, Australia

* corresponding author [REDACTED]

Phone: + [REDACTED] Fax: + [REDACTED]

3.11 Abstract

Cadmium oxide/alkali metal halide mixtures for pre-combustion CO₂ capture were made using a wet mixing approach. Some of the samples were pelletised, also using SBA-15 mesoporous silica as an additive. In a multiple CO₂ sorption cycle test via thermogravimetric analysis, the best performing powder material by capacity and kinetics (a cadmium oxide made from carbonate doped with 17.5 wt% sodium iodide) exhibited a sorption capacity loss from 17 wt% to 2 % after 25 cycles of partial pressure swing sorption (50 vol% CO₂ in Ar vs. pure Ar) at atmospheric absolute pressure and temperatures of 285 and 305 °C. When the initial decomposition of the carbonate took place in inert gas (Ar or N₂ instead of air), the cyclic stability was improved. Water addition (1 vol%) to the sorption gas further improved the cyclic CO₂ sorption stability and capacity. Elemental analysis of the samples after cyclic exposure to CO₂ revealed that the capacity loss is associated with loss of iodine from the sample, whereas the sodium is kept within the samples. Water addition, however, had no significant effect on this iodine loss. Pellets made from carbonate performed with a working capacity of 10 wt%, but lost their mechanical integrity during multicyclic sorption. If made in the oxide state, pellets remained sturdy, but showed almost no working capacity. The addition of 13.7 wt% SBA-15 improved the working capacity of the oxide pellet to a stable value of 5.2 wt% over 25 cycles. In-situ powder X-ray diffraction showed the reversible isothermal phase transformation of CdO to CdCO₃ during three cycles of sorption and also revealed the

presence of a crystalline sodium iodide phase, which appeared to be lost with increasing number of sorption cycles.

3.12 Introduction

The Integrated Gasification Combined Cycle (IGCC) process with water-gas shift reaction (WGS) and carbon dioxide capture has been proposed as a promising new power generation technology, which could help reduce anthropogenic greenhouse gas emissions and thereby halt global warming and climate change [1, 38]. The process consists of the gasification of coal to synthesis gas (syngas) mostly consisting of water, hydrogen, carbon monoxide and carbon dioxide. A WGS reactor is employed downstream of the gasifier to enrich the gas by converting the carbon monoxide to carbon dioxide and hydrogen by reaction with water. Subsequent carbon dioxide capture from the shifted syngas would then result in a hydrogen-rich fuel gas, the combustion of which can power a gas and steam turbine combined power plant process, leaving water vapour as the only major exhaust gas [1, 6].

Separating the carbon dioxide in-situ at the temperature of the WGS reactor would be beneficial, as it would reduce the energy penalty arising from cooling or heating the syngas to the required carbon dioxide capture/separation temperatures. Syngas typically exits the final stage of the WGS reactor at a temperature between 250 and 400 °C [6]. A range of metal oxide based sorbents have been proposed to operate in this temperature window, including layered double hydroxides [10-12], lithium zirconates [13], magnesium/potassium double salts [12, 14] and a magnesium-cesium mixed metal oxide [39]. These materials accommodate the CO₂ by reacting with it to form carbonated products. However, most working capacities are reported to be lower than 10 weight-% in the temperature range studied here, whereas the lithium zirconates require higher temperatures to perform with acceptable reaction kinetics and capacity. A high working capacity is always desirable as it would help to keep carbon capture costs to a minimum.

Calcium oxide based materials, which have been considered for carbon dioxide capture at higher temperatures (typically 600 to 900 °C) by a number of research groups, show a decay in capacity during several carbonation-decarbonation cycles. In the case of calcium

carbonate, this decay is considered to be due to sintering at high temperature and due to the filling of inter-micrograin void spaces due to carbonation [16]. A successful attempt to solve the decay in capacity was performed by calcium carbonate sorbent synthesis via CO₂ introduction into a calcium hydroxide aqueous slurry [40].

The carbonation of cadmium oxide was first studied by Doiwa et al. [26, 27], who showed that the presence of a sodium halide was essential. We have more recently reported that cadmium oxide/sodium iodide mixtures can sorb up to 24 wt% CO₂ in the temperature range of 250 to 310 °C [41]. This study showed that mixtures of various sodium and lithium halides with cadmium carbonate were able to sorb and then desorb carbon dioxide after decomposition to cadmium oxide by heating. This reversible sorption is due to the formation and decomposition of cadmium carbonate as confirmed by Fourier-transform infrared spectroscopy and powder X-ray diffraction (XRD). The best-performing material, made from 17.5 wt% sodium iodide (based on cadmium carbonate), showed a maximum weight increase of 26 wt% as CO₂ was sorbed at 265 °C. The sorption was reversible and the carbon dioxide was recovered at the same temperature by reducing the partial pressure of CO₂. Due to its high sorption capacity, this material appears prospective for carbon dioxide capture from syngas and worthy of more detailed study. It is important to determine whether any capacity loss occurs under cyclic conditions as has been reported for calcium oxide.

In the present study, cadmium oxide/alkali halide mixtures were examined under cyclic sorption conditions via thermogravimetric analysis (TGA) to investigate the stability of their working capacities. Samples were examined both as powders and pellets since the latter are more likely to be used in industrial applications. SBA-15 silica was added to the sample prior to the pelletisation process in an attempt to improve gas diffusion into the pellet. An assessment of the mechanical stability of the pellets was also performed before and after cyclic CO₂ sorption in TGA.

CdO-NaI powder samples were separately investigated by inductively coupled plasma mass spectrometry (ICP-MS) and atomic absorption spectrometry (AAS) to determine their cadmium, iodine and sodium content before and after cyclic exposure to CO₂. In-situ

powder XRD experiments at 325 °C were performed to more directly observe the reversible transformation of cadmium oxide to carbonate.

3.13 Experimental section

3.13.1 Preparation of cadmium oxide/alkali halide composite samples

Cadmium oxide/alkali metal halide composites were prepared via a wet mixing method as previously described [41] and as summarised in Table 3.13.1. Cadmium carbonate was mixed with either sodium iodide (17.5 wt%), sodium bromide (12.9 wt%), lithium iodide (15 wt%) or lithium bromide (10 wt%). Water was removed from suspensions of cadmium carbonate dispersed in the respective alkali metal halide aqueous solution by heating and evaporation during continuous stirring. The precipitated samples were then dried overnight in a nitrogen-purged oven at 120 °C, resulting in completely dry powder samples.

Some of the dried powder samples were subsequently calcined in a muffle furnace (CM Inc., model Rapid Temperature 840940) in atmospheric air at either 370 °C or 500 °C. Other samples were also separately calcined under nitrogen (Carbolite ORF-810 furnace with internal gas-purged steel tube assembly). Samples were either calcined for 3 or 24 hours. After synthesis or calcination, samples were stored in sealed vials for further use.

The sample designations indicate the mass % of the alkali metal halide as a fraction of the cadmium carbonate as calculated from the mass of reagents used. Samples with no percentage indicator comprise samples made with 17.5 wt% NaI.

3.13.2 Preparation of SBA-15 silica

SBA-15 type mesoporous silica was prepared by a method similar to that reported by Zhao [42] and adapted by Knowles et al. [43] using poly(ethylene glycol)-block-poly(propylene glycol)-block-poly(ethylene glycol) (Sigma Aldrich), tetraethylorthosilicate (Sigma Aldrich), ethanol absolute (Merck) and hydrochloric acid (Merck). The synthesis mixture was initially stirred overnight, then aged three days at 105 °C in a polypropylene jar contained within a Hawkins 'Big Boy' 22 L pressure cooker. The product was subsequently filtered, air dried and then calcined at 575 °C for two days. A pore size

distribution and nitrogen physisorption isotherm of the SBA-15 used in this study is given in the supplementary material.

3.13.3 Pelletised samples

For pelletisation, the as-synthesised and oven-dried (i. e., carbonate form) powder samples as well as a sample calcined in nitrogen in a muffle furnace (500 °C, 3 hours) were used. Mixtures of the calcined sample with SBA-15 silica were also prepared and fed to the pellet press. Mass percentages of SBA-15 are reported with respect to the mass of calcined CdO/NaI mixed sample.

Pellets of a nominally 17.5 % NaI sample were made using a Specac brand hydraulic press and 13 mm diameter circular pellet die. 0.5 g of sample was placed into the pellet die, evacuated for ten minutes and then compressed by up to 10 tons force for another ten minutes. The force was continuously brought back to 10 tons as it decreased over time. Afterwards, the pellet was removed from the die and segments cut off using a sharp blade. Up to three such segments of approx. 1 mm width were used in a TGA experiment, so as to have sample masses of approx. 20 mg (oxide state) and 30 mg (carbonated state). The physical integrity of the pellets was documented photographically and the pellets were examined manually by trying to break them using a spatula or rubbing between two gloved fingers.

3.13.4 Thermogravimetric analysis of carbon dioxide sorption

A Setaram TAG 24-16 thermoanalyser, equipped with Bronkhorst model F-201DV-RAD-11-K programmable mass flow controllers for the supply of argon and CO₂, was used in this study. TGA of multiple isothermal CO₂ sorption and desorption cycles (up to 25 cycles) was achieved by varying the CO₂ partial pressure (0 vs. 50 vol%) over samples within the instrument. A sample mass of approx. 20 mg of an oxide material or 30 mg of a carbonate material was used for the experiments.

Samples were pre-treated in-situ at 380 or 510 °C in argon purge for one hour as noted in Figure 3.13.1 and Table 3.13.1. Tests were performed in both long (one hour each for sorption and desorption) and short cycles (12 minutes adsorption, 24 minutes desorption) at temperatures of 285 and 305 °C. A final step at 380 °C in argon flow ensured that

samples were brought back to fully decarbonised state, i. e., cadmium oxide. This was necessary to provide a standardised basis for subsequent sample analysis by dissolution and elemental analysis (ICP-MS, AAS) of some of these samples.

A gas flow of 70 mL/min was always maintained, consisting of either 70 mL/min argon (inert gas flow) or a mixture made up of 35 mL/min carbon dioxide and 35 mL/min argon (sorption gas flow, i. e., 50 vol % carbon dioxide, close to the value of 38 % as reported for a water gas shift reactor outlet gas stream [28]). As per the instrument design, the gas flow was split into sample and reference gas flow, so that only half of the total flow (35 mL/min) was diverted to the sample.

Wet gas experiments were performed with argon and carbon dioxide bubbled through separate wash bottles filled with distilled water, which were maintained at 10 °C in a cooling bath. The wetted gas was mixed with a stream of dry argon originating from the balance device purge, resulting in 1 vol-% water concentration at the sorbent sample. Wet CO₂ and wet argon were used as sorption/desorption gases, whereas pre-treatment and after-treatment were performed in dry argon.

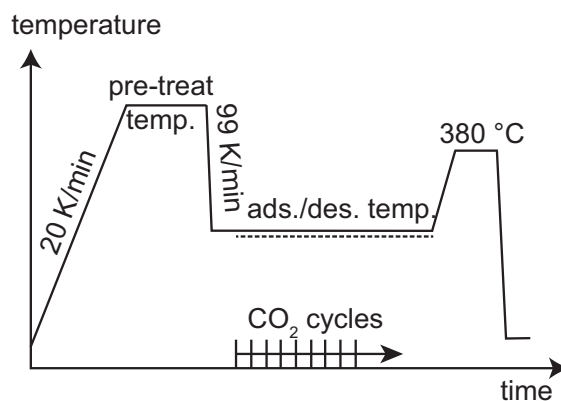


Figure 3.13.1: Adsorption/desorption TGA program. The dashed line on the temperature graph indicates mass readings used in subsequent data processing.

Table 3.13.1: Samples used in multicyclic sorption/desorption tests.

sample name	composition CdCO ₃ + ... (wt%)	pre-treatment in muffle furnace	pre-treatment in TG analyser, in Ar	sorption/desorption cycle mode
285-a510-s *	17.5 % NaI	500 °C in air 3 h	510 °C	short, 285 °C
285-Ar380-s *	17.5 % NaI	- none -	380 °C	short, 285 °C
305-a510-s *	17.5 % NaI	500 °C in air 3 h	510 °C	short, 305 °C
305-Ar380-s *	17.5 % NaI	- none -	380 °C	short, 305 °C
285-Ar380-l	17.5 % NaI	- none -	380 °C	long, 285 °C
305-a380-s	17.5 % NaI	370 °C in air 3h	380 °C	short, 305 °C
305-N500-s	17.5 % NaI	500 °C in N ₂ 24 h	510 °C	short, 305 °C
LiBr-305-Ar380-l	10 % LiBr	- none -	380 °C	long, 305 °C
LiI-305-Ar380-s	15 % LiI	- none -	380 °C	short, 305 °C
NaBr-305-Ar380-s	12.9 % NaBr	- none -	380 °C	short, 305 °C
LiI-285-Ar380-s	15 % LiI	- none -	380 °C	short, 285 °C
NaBr-285-Ar380-s	12.9 % NaBr	- none -	380 °C	short, 285 °C
carbonate pellet Ar380 305-s	17.5 % NaI	- none -	380 °C	short, 305 °C
carbonate pellet Ar380 305-l	17.5 % NaI	- none -	380 °C	long, 305 °C
oxide pellet Ar380 305-l	17.5 % NaI	500 °C in N ₂ , 3h	380 °C	long, 305 °C
oxide pellet Ar380 305-s-d	17.5 % NaI	500 °C in N ₂ , 3h	380 °C	short, 305 °C
oxide pellet	17.5 % NaI,	500 °C in N ₂ , 3h	380 °C	short, 305 °C
SBA15 4.22 %	4.22 % SBA-15			
oxide pellet	17.5 % NaI,	500 °C in N ₂ , 3h	380 °C	short, 305 °C
SBA15 13.7 %	13.7 % SBA-15			

'short' = 12 min sorption, 24 min desorption, 'long' = 1 h sorption, 1 h desorption

* wet and dry gas experiments

17.5 wt% NaI based on CdCO₃, SBA-15 amount (wt%) based on mixed CdO/NaI sample after calcination

3.13.5 Elemental analysis

All mass determinations for the elemental analysis of a 17.5 % NaI sample were performed using a Mettler H54 balance with an accuracy of 0.00001 g. Samples of 20 mg were dissolved in 40 g of 1 wt % hydrochloric acid. For cadmium and iodine analysis, the samples were further diluted down to expected values of 20 to 30 $\mu\text{g}/\text{kg}$ of cadmium and iodine using 1 % hydrochloric acid. For the determination of sodium, dilutions were performed using deionised water, giving an expected value of 1.5 mg per kg solution of sodium.

Cadmium carbonate and sodium iodide standard solutions for instrument calibration were prepared in a similar manner using the same batch of pure chemicals as used for synthesis (refer section 3.4.2 and [41]). For cadmium and iodine standards, 20 mg of sodium iodide and cadmium carbonate were dissolved separately and the samples subsequently diluted down to values of 10, 20, 40 and 60 μg cadmium or iodine per kg solution using 1 % hydrochloric acid. Dilutions were obtained using the same batch of 1 % HCl as used for dissolution. For a sodium standard, the primary dissolved sodium iodide sample mentioned above was diluted in the range of 0.5, 1, 1.7 and 2.5 mg sodium per kg solution using deionised water.

Elemental analysis for cadmium and iodine was performed by inductively coupled plasma time of flight mass spectrometry (ICP-MS) on a GBC Optimass 9500 model instrument. For sodium determination, atomic absorption spectrometry (AAS) was employed and a GBC XplorAA model instrument was used. The hydrochloric acid sample itself was used as a blank (zero concentration) calibrator in ICP-MS, deionised water was used as the blank in AAS.

The results of ICP-MS and AAS, measured in μg or mg of element per kg of solution, were calculated into weight percentage amounts of cadmium, iodine and sodium using the dilution factors and the amount of solid sample used, i. e., based on the powder mass in the decarbonated/cadmium oxide state before dilution (except for samples analysed in the cadmium carbonate state, as indicated in the text/caption). Theoretical amounts were calculated assuming 17.5 % NaI in cadmium carbonate, the decomposition of carbonate to oxide during calcination, and that Na and I are inert and non-volatile.

3.13.6 Powder X-ray diffraction

In-situ powder X-ray diffraction studies were undertaken at the Australian Synchrotron. A fresh 17.5 % NaI sample (calcined at 500 °C, 3 h) was transferred into a quartz capillary, mounted into the diffractometer and purged with either nitrogen or pure carbon dioxide during data acquisition. Heating of the sample was performed using a hot air blower, which was mounted underneath the capillary. The temperature of the hot air was set to 325 °C. Experiments were performed by interchanging the purge gas between pure nitrogen and carbon dioxide for three cycles, starting with the calcined sample. After each gas change, XRD patterns were observed until no more change was apparent (between 40 and 90 minutes).

The wavelength, zero offset and unit cell parameters of cadmium oxide and cadmium carbonate were refined via the software package GSAS-EXPGUI [29, 30] using the Le Bail method. Powder Diffraction File 4+ 2011 entries 04-001-3770 (cadmium oxide) and 04-014-4823 (cadmium carbonate) were used as starting values for the unit cell parameters. For ease of comparison of the lab data with the synchrotron data, XRD patterns were converted from 2θ with the respective wavelength to the wavelength-independent values of Q using the software CMPR [31]. The definition of Q is given in eqn. 3.13.1, wherein λ is the wavelength of the X-rays used to acquire the pattern.

$$Q = \frac{4\pi \sin \frac{2\theta}{2}}{\lambda} \quad \text{eqn. 3.13.1}$$

A lanthanum hexaboride standard (NIST 660b) was also measured as a reference without gas purge or heating in order to refine the wavelength and zero offset. The wavelength was found to be 0.8267593 Å and the zero offset -0.0206908 degrees 2θ , as determined by a Le Bail refinement (refer supplementary materials for detailed results).

Powder XRD patterns of pure comparison materials (CdO and CdCO₃) were acquired on a Bruker D8 focus diffractometer using Cu-K α radiation (1.5418 Å wavelength). Intensities were multiplied with a factor (as indicated) to make them comparable to the higher-intensity synchrotron patterns on the same intensity scale.

3.14 Results and discussion

3.14.1 Thermogravimetric analysis of the sample stability

Figure 3.14.1 shows two examples of full thermograms of 25 cycle sorption/desorption experiments (a and c) as well as excerpts with the mass at the start of the cycles set to 100 % (b and d). The derivation of the working capacities is indicated for the last cycle as the difference in relative mass for each cycle, as shown in Figure 3.14.1b. The full multicyclic plots for all materials reported can be found in the supplementary material (sample designators are listed in Table 3.13.1). In general, the results show that the working capacity decays for samples calcined in air (Figure 3.14.1c and d). Apart from the working capacity, there is a mass loss before and after cyclic exposure evident in most of the full thermogravimetric plots (refer dashed arrows in Figure 3.14.1 a, also evident in Figure 3.14.1 c and supplementary material). This can be observed in the baseline of the mass signal in the full thermograms showing higher values before than after the cyclic exposure. This suggests that some part of the sample mass must be lost by reaction and/or evaporation during the experiment and this motivated a detailed analysis of the samples for their elemental composition (section 3.14.2).

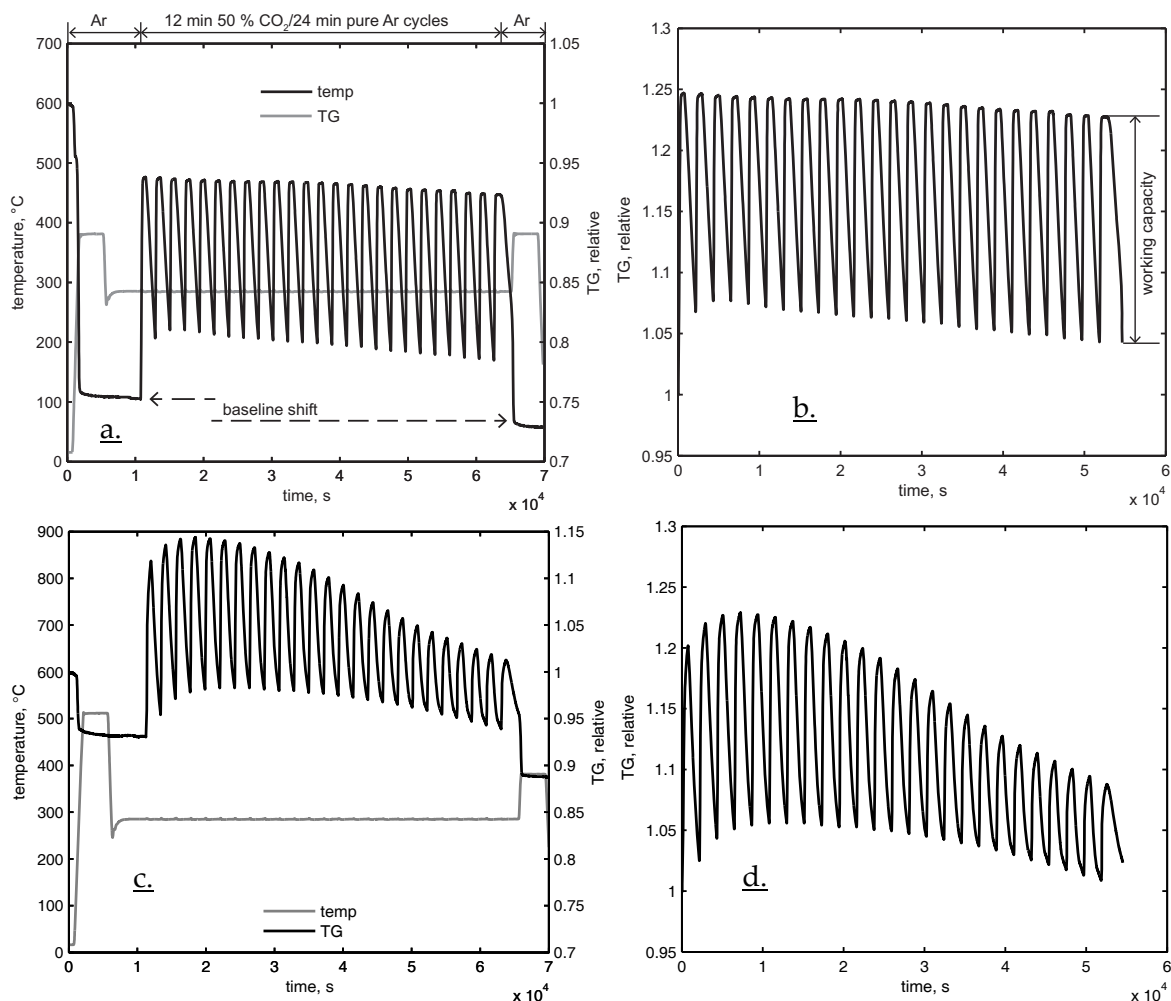


Figure 3.14.1: a. Full thermogram of a 17.5 % NaI sample, cycles at 285 °C, wet gas (285-Ar380-s-w), showing activation step, 25 cycles (12 min sorption, 24 min desorption), final desorption, b. excerpt from a. with 100 % set at the beginning of the sorption cycles, working capacity derivation shown at final cycle. c. and d. analogue a and b, calcined sample (285-a510-s-w)

Plots of the working capacities versus cycle number for all materials studied here are given in Figure 3.14.2. These results show that the sorption capacities of some materials were reduced over several adsorption-desorption cycles. Generally, it can be observed that the samples pre-treated in air at any temperature showed a fast decay during multicycle sorption and the effect was more pronounced at a temperature of 305 °C than at 285 °C (Figure 3.14.2a). Sodium iodide containing samples that had not been in contact with air, i. e., the samples calcined in an inert (nitrogen or argon) atmosphere, maintained their capacity to a much more significant extent. 1 % water addition increased both the stability and the capacity (Figure 3.14.2b), whereas higher temperatures resulted in a capacity reduction. The time of pre-treatment did not seem to play a significant role in the long-

term performance of the materials (Figure 3.14.2c); rather it seems to be a matter of exposure to air at high temperatures (380 or 510 °C) that determines the capacity stability. Non-calcined samples containing lithium iodide, however, exhibit capacity decay similar to the sodium iodide samples calcined in air (Figure 3.14.2d). The rates of CO₂ uptake (evident in the full thermograms, refer to supplementary material) of the lithium bromide sample were relatively slow, so that this experiment was only performed using long (1 hour) cycles. Alternative dopants to NaI, in general, show an overall lower capacity than NaI (Figure 3.14.2d).

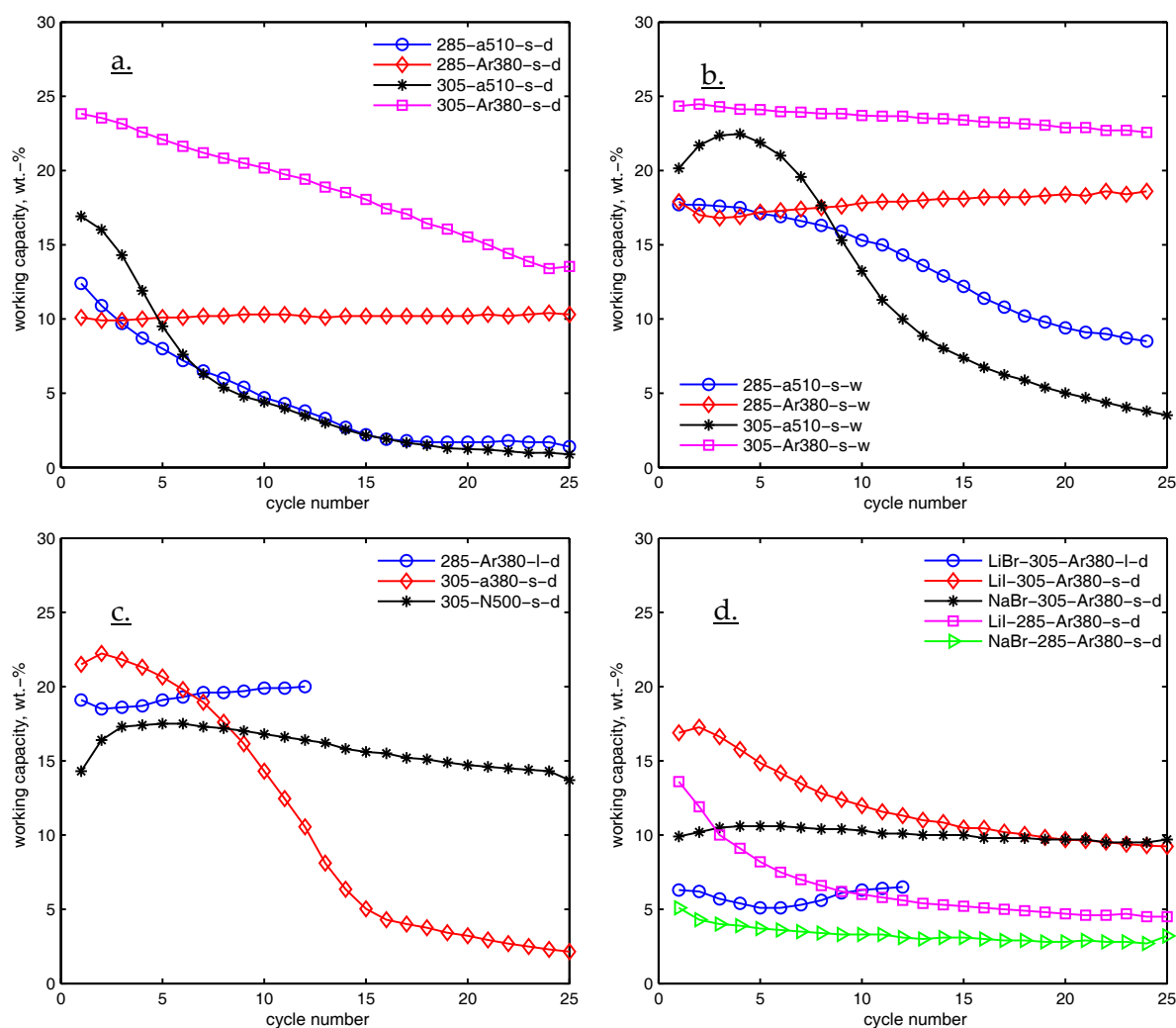


Figure 3.14.2: Multicyclic adsorption-desorption of various alkali halide/CdO samples at different temperatures. Refer to Table 3.13.1 for sample designators. a. 17.5 % NaI samples pre-treated in Ar and in air, no water added during TGA; b. as for a but with 1 % water addition in TGA; c. 17.5 % NaI samples and different pre-treatments; d. other alkali halides. Last letter d = dry gas, w = wet gas.

3.14.2 Elemental analysis

Figure 3.14.3 shows the composition of as-synthesised and calcined samples as well as theoretically expected values. The expected values are based on the mass ratios of cadmium carbonate and sodium iodide used during synthesis. It was assumed that cadmium carbonate decomposed to oxide upon calcination, and that sodium iodide was inert. The absolute cadmium content of the sample was assumed to be unchanged throughout synthesis, calcination and testing runs, since it is not volatile at the temperatures used in this study (its sublimation point is reported at 1559 °C [44]). The results for the calcined and non-calcined 17.5 % NaI samples investigated in dry and wet gas TGA cycles at 285 and 305 °C (refer to Figure 3.14.2a and b) are shown in Figure 3.14.4. The results given in Figure 3.14.3 and Figure 3.14.4 are both showing wt% and also the mass ratios relative to Cd content.

It can be noted in Figure 3.14.3 that the elemental composition of cadmium, iodine and sodium of the as-synthesised sample in the carbonated state was found to be lower than the expected theoretical values. This may be due to inaccuracies in weighing the amount of powder sample used for the dissolution. A dry sample was assumed, but the sample might have adsorbed water during handling before the dissolution. Furthermore, it is evident that the iodine to cadmium ratio (Figure 3.14.3b) is lower than the value that was expected. It is speculated that a certain amount of iodine may have been lost during wet synthesis.

Figure 3.14.3b shows that the unused/as-synthesised sample after calcination had a lower iodine content than expected if it is assumed that only cadmium carbonate decomposes to oxide and that sodium iodide remained inert during calcination. Calcination in air led to an even lower iodine content compared to calcination in nitrogen. Slightly increased Na/Cd levels that accompany lowered I/Cd ratios were attributed to a heavy element (iodine) leaving the sample. Consequently, the sodium ratio, on a mass basis, had to rise, if it is assumed that the iodine is replaced by a lighter element.

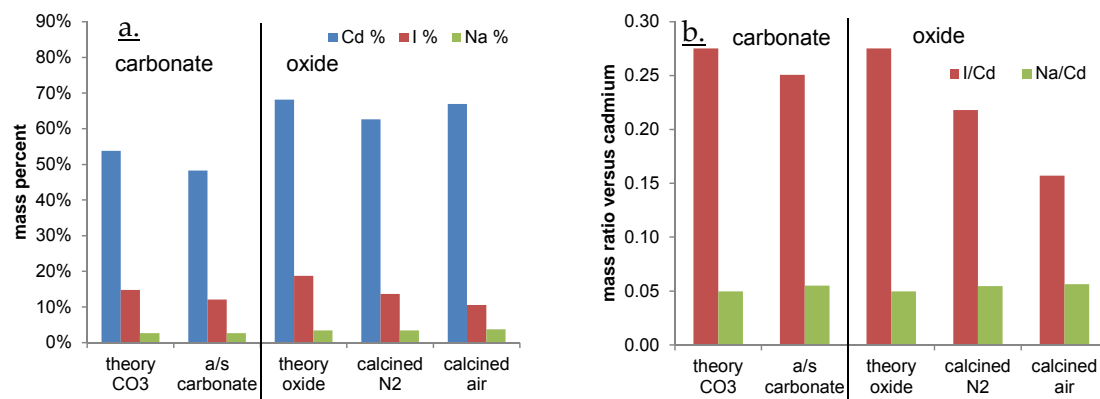


Figure 3.14.3: Elemental analysis of as synthesised (a/s) 17.5 % NaI samples calcined in air, N₂ and uncalcined (carbonate state), a. mass-%, b. Na and I relative to amount of Cd. Max. error 5.29 % (absolute) for Cd of a duplicate measurement of N₂ calcined sample.

The elemental compositions of the samples after multicyclic exposure are presented in Figure 3.14.4. It can be observed that the iodine content was lowered significantly during the TGA experiment, while the amounts of the other elements remained at similar magnitudes. Figure 3.14.4c and d also shows that the concentrations of iodine decreased relative to cadmium. It can be concluded from this observation, together with the loss of capacity after multiple carbonation-decarbonation cycles (Figure 3.14.2), that halide is an important promoter of the carbonation reaction. The maintenance of higher CO₂ sorption capacities appears to be associated with the maintenance of higher iodide content within the sample. Interestingly, sodium appeared to remain incorporated within the sample during the carbonation-decarbonation experiments, while the halide was removed from the sample. Water addition during cycling has no significant influence on the elemental composition of the samples.

Given the loss of iodine occurring in some samples, the question must be asked how the composition of the sample changes with respect to stoichiometry. As sodium iodide was added to the sample initially and sodium levels do not change significantly, sodium iodide must be somehow changing into a different form upon the removal of iodine from the sample. Furthermore, calcination in air leads to a more substantial loss of iodine than calcination in an inert environment (N₂), both after initial calcination and multicyclic CO₂ sorption. It is hypothesised that oxidation of iodide to iodine in air is involved in this mechanism. However, as iodine loss over sorption cycles (compared to initial samples) is

also observed for samples calcined in inert conditions, CO_2 seems to play a role in the decay mechanism as well. The investigation of the iodine loss mechanism is the subject of ongoing studies (presented in Chapter 4).

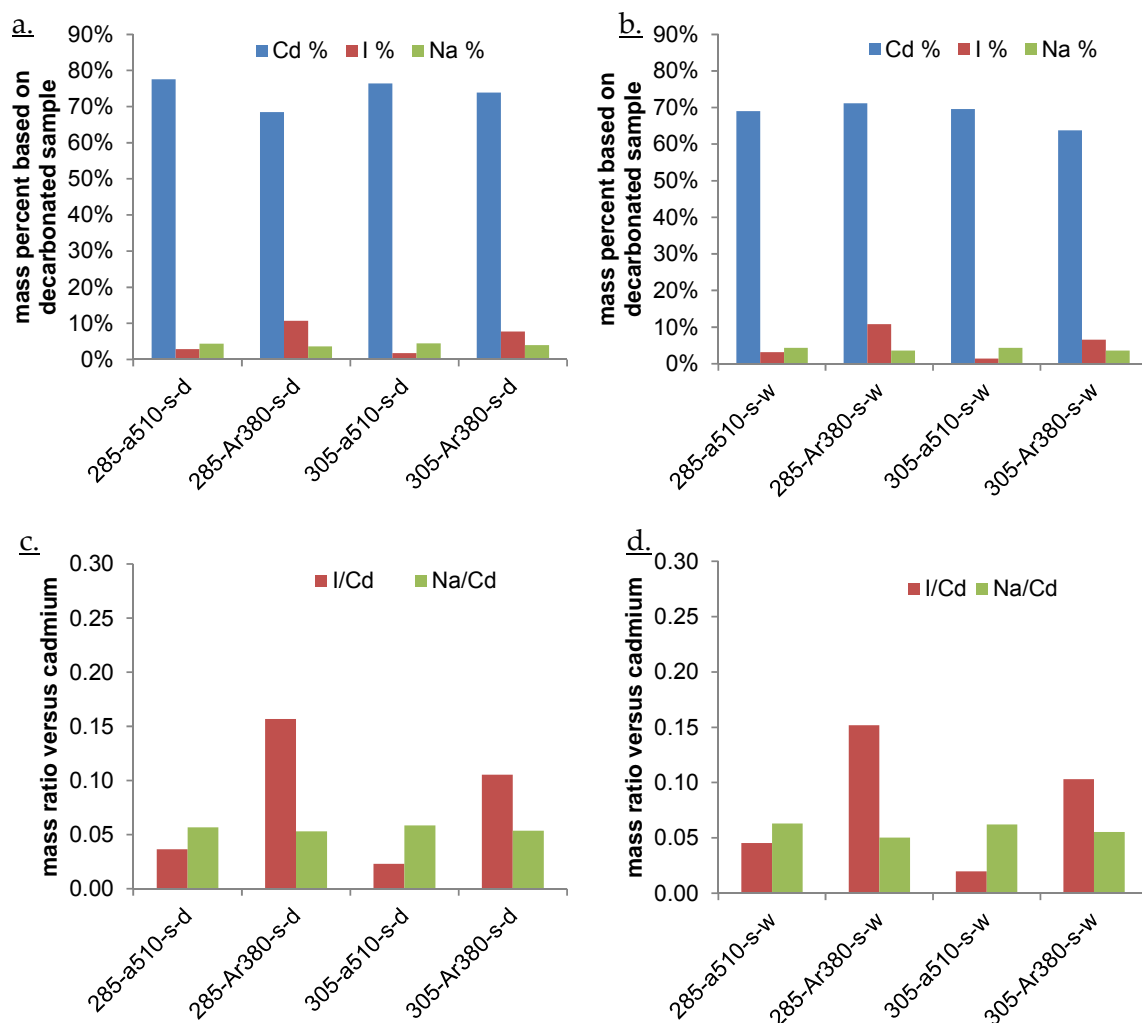


Figure 3.14.4: Elemental analysis of 17.5 % NaI/CdO samples after cyclic CO_2 sorption experiments, a. dry gas, b. wet gas, c. & d. like a, b with I and Na content relative to Cd. Samples correspond to Figure 3.14.2 a and b.

3.14.3 Powder X-ray diffraction

The results of the in-situ powder XRD studies performed at the Australian Synchrotron are given in Figure 3.14.5. A 17.5 % NaI sample (calcined in air at $500\text{ }^\circ\text{C}$) was used in this experiment. Upon heating to $325\text{ }^\circ\text{C}$ in nitrogen purge, the first scan (labelled 'start') was obtained (Figure 3.14.5a). Afterwards, the gas flow was switched to CO_2 and the pattern changed (Figure 3.14.5b). Three cycles of nitrogen and CO_2 purge resulted in carbonation

and decarbonation of the material as indicated by the diffraction patterns changing from cadmium oxide to carbonate and vice versa. Cadmium carbonate and oxide patterns are given for comparison.

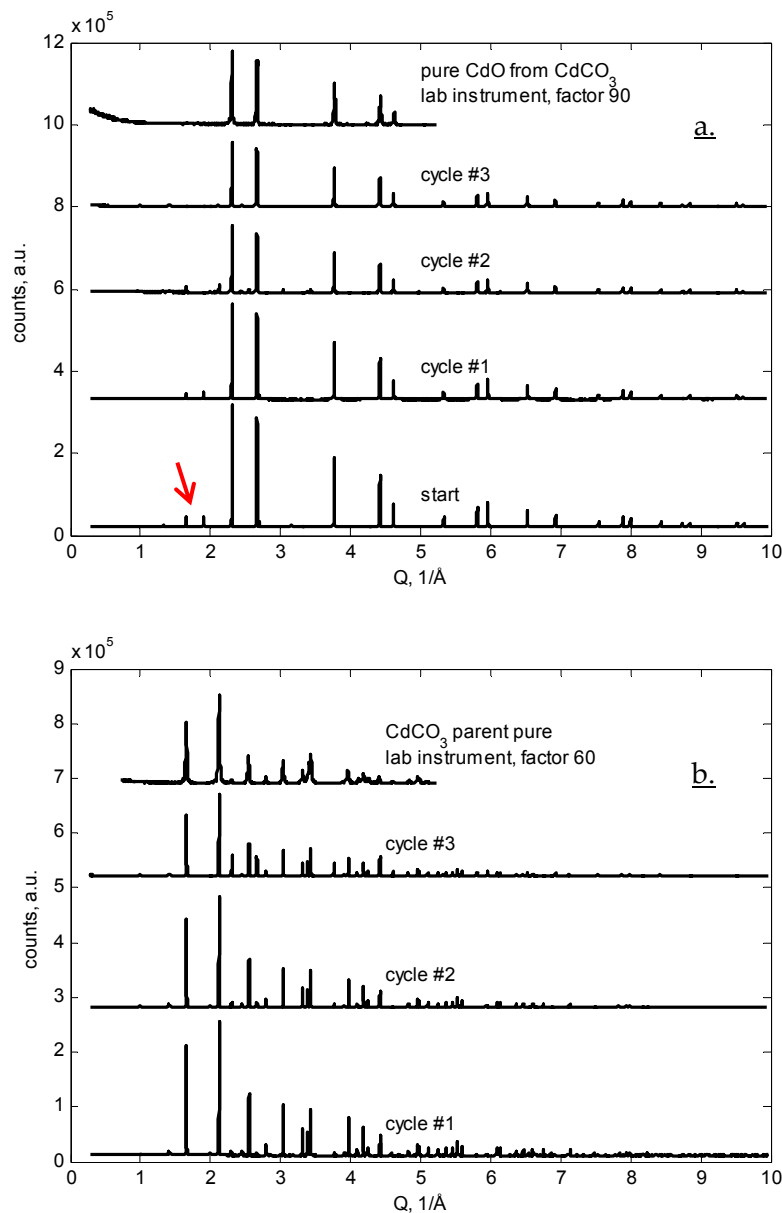


Figure 3.14.5: Powder XRD patterns of a 17.5 % NaI sample obtained from in-situ synchrotron experiments at the end of each cycle at 325 °C: a. decarbonated state, b. carbonated state. Arrow indicates two peaks assigned to NaI. Sample calcined in air at 500 °C before experiment.

Initially, a cadmium oxide phase was observed when purged with nitrogen. After exposure to pure carbon dioxide, a cadmium carbonate phase evolved. Noteworthy is the temperature of 325 °C, at which this experiment was performed. This conflicts with the

results of TGA experiments reported in the previous study in this series [41], which showed that a temperature beyond 318 °C is too high for CO₂ sorption. This discrepancy is probably because the temperature measurement for the in-situ XRD system was not located within the sample cavity but, rather, adjacent to the hot air outlet that blows on the sample capillary. The XRD capillary was also purged with cool gas, which may have contributed to the actual sample temperature being below the setpoint. The true sample temperature was almost certainly lower than the measured one, though by how much is unknown. By contrast, the temperature sensor of the thermoanalyser was located immediately underneath the sample crucible and was thus probably a more realistic representation of the true sample temperature.

Le Bail refinements of the unit cell parameters of the cadmium carbonate and oxide phase observed in the in-situ XRD experiments have also been performed on the raw synchrotron data (i. e., at a wavelength of 0.8267593 Å). The results are given in the supplementary material. It can be noted that the unit cell lengths are marginally larger (4.71 Å) than the ones given in the Powder Diffraction File database (4.69 Å) and the ones reported in [41]. This can be explained by thermal expansion at the elevated temperatures used in these experiments. There is no new structure or unit cell modification due to the carbonation reactions and/or the doping with sodium iodide apparent here.

However, another noteworthy observation was the decrease of a sodium iodide phase at 325 °C in the in-situ synchrotron experiment. An XRD scan of the fresh/calcined 17.5 % NaI sample at the synchrotron at 325 °C showed a sodium iodide phase at very low intensity (see arrow in Figure 3.14.5a, two peaks between 1.5 to 2 Å⁻¹). During multicyclic sorption at 325 °C, the intensity of the sodium iodide peak decreased significantly with the progressing number of cycles. This suggests a loss of iodine, which is consistent with the elemental analysis results in section 3.14.2. However, despite the use of high-resolution diffraction analysis employing synchrotron radiation, a new sodium-containing phase was not identified.

3.14.4 Pelletised material

The working capacities for the pelletised sorbents are presented in Figure 3.14.6. Multiple short (12 min sorption, 24 min desorption) and long cycles (one hour each) for the material

pressed in the carbonated state, as well as long cycles for the pellet made in the oxide state (with and without SBA-15 addition) were performed and the working capacities determined.

It is evident that the pelletised materials provided lower working capacities than their powder counterparts in equal short cycles (compare Figure 3.14.2). This is presumed to be due to the formation of a significant diffusion barrier within the fused pellet, which limited the access of the carbon dioxide. It can be observed that the carbonate pellets showed a capacity decrease for the long cycles. This also occurred, but was much less significant for the short cycles.

The reversible CO₂ capacity of the oxide pellets was observed to improve with cycle number during long cycles. This might be due to expansion of the oxide as soon as it transformed into carbonate, thus creating fine voids within the pellet. These, in turn, could lead to better permeation of the gas through the pellet, resulting in higher working capacities in the subsequent cycles. A similar explanation might be used for an initial increase in working capacity observed for a powder sample calcined in air (Figure 3.14.2b), as nanoparticles might fracture upon multicyclic CO₂ sorption, improving access of the gas into the core of the nanoparticle in subsequent cycles. In short cycles, the oxide pellet did not give any significant working capacity (< 0.5 %, Figure 3.14.6).

Pellets pressed using a mixture of the calcined CdO/NaI sample and SBA-15 silica initially exhibited a higher working capacity than the oxide pellet. The incorporation of 13.7 wt% SBA-15 led to a working capacity of 5.2 wt%. However, the adsorption rate is slow and CO₂ saturation was not achieved for this material, as can be seen in the full thermogram (refer to supplementary materials). The mass showed an overall increasing trend over the 25 cycles for this material, which might be attributed to the sorption rate being slightly less diffusion-limited than the desorption rate, or an expansion of the structure over multiple sorption/desorption cycles. Decreasing the amount of SBA-15 to 4.22 % led to more stable cycling (i.e., the baseline is more horizontal); perhaps there was a better balance between sorption and desorption rates in this case. However, the working capacity reduced further to 2.8 wt%.

The fact that adding SBA-15 improved the CO₂ uptake of the pellet during short cycles supports the view that CO₂ is less able to diffuse into the inner reaches of the pellet, relative to the powder samples. If a porous material is interspersed into the sorbent pellet, it can be imagined that the gas can penetrate into the core of the pellet more easily by diffusing through the void volume provided by the porous material particles. This is indeed evident in Table 3.14.1, showing that the fraction of the potential (stoichiometric) mass uptake achieved was higher for the pellets containing SBA-15. Adding a lower amount (4.22 instead of 13.7 wt%) of SBA-15 led to a lower working capacity, as accessibility was reduced by the reduced amount of empty volume. It appears that the higher amount of SBA-15 benefitted the reversible CO₂ sorption working capacity, but came with limitations in the mechanical strength of the pellets, as discussed next.

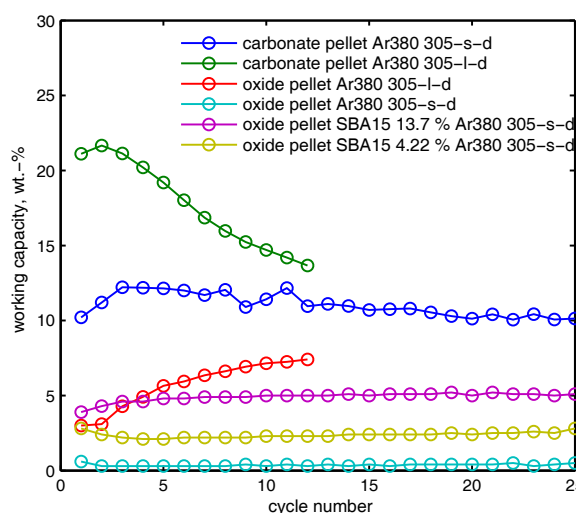


Figure 3.14.6: Working capacities of pelletised 17.5 % NaI material. Pelletisation performed in oxide (N₂ calcination) and carbonate state. Dry gas.

Table 3.14.1: Theoretically achievable mass gains by full carbonation compared with the working capacities achieved in Figure 3.14.6 in the short cycle experiments. 17.5 % NaI based on CdCO₃ is assumed here to be inert during initial decarbonation, SBA-15 throughout the experiment.

sample	CdO (wt%) in activated state	max. weight gain (wt%) by full carbonation of CdO to CdCO ₃	average working capacity (wt%) achieved	fraction of max. working capacity achieved
pure CdO, theory	100	34.3	n/a	n/a
carbonate pellet	77.84	26.7	12.2	45.7 %
oxide pellet	77.84	26.7	0.6	2.2 %
4.22 % SBA-15	74.63	25.6	2.8	10.9 %
13.7 % SBA-15	67.17	23.0	5.2	22.6 %

Figure 3.14.7 shows photographs of the pellets. The pressing of the carbonate sample gave a sturdy pellet (Figure 3.14.7a). The segments used in the TGA experiments are shown in Figure 3.14.7b. After the multicyclic exposure, the pellet fragments maintained their shape (Figure 3.14.7c), but only slight manipulations with a spatula caused them to fall apart (Figure 3.14.7d). For comparison, two whole carbonate pellets were calcined in nitrogen at 500 °C (Figure 3.14.7e). These also were very brittle and easily crushed between the fingers (Figure 3.14.7f). It might be concluded that the weakening of a carbonate pellet already occurred during the initial activation of the pellet rather than during the cyclic sorption tests. By contrast, the pellet made in the oxide state (Figure 3.14.7g) maintained its integrity well throughout a multiple cycle TGA experiment. After the TGA experiment, the pellet fragments maintained their original shape (similar to Figure 3.14.7c) and did not easily crumble when crushed or rubbed between the fingers (though some minimal amount of material did rub onto the gloves in a similar manner to a hard pencil writing on paper). The two pellets with SBA-15 added behaved in an intermediate way. After 25 CO₂ sorption cycles, the inner portion of the pellet remained sturdy, but was covered by a powdered layer, which was easily removed by rubbing the pellet between two fingers. The remainder of the pellet core and the removed powder after cyclic CO₂ exposure is shown in Figure 3.14.7h.

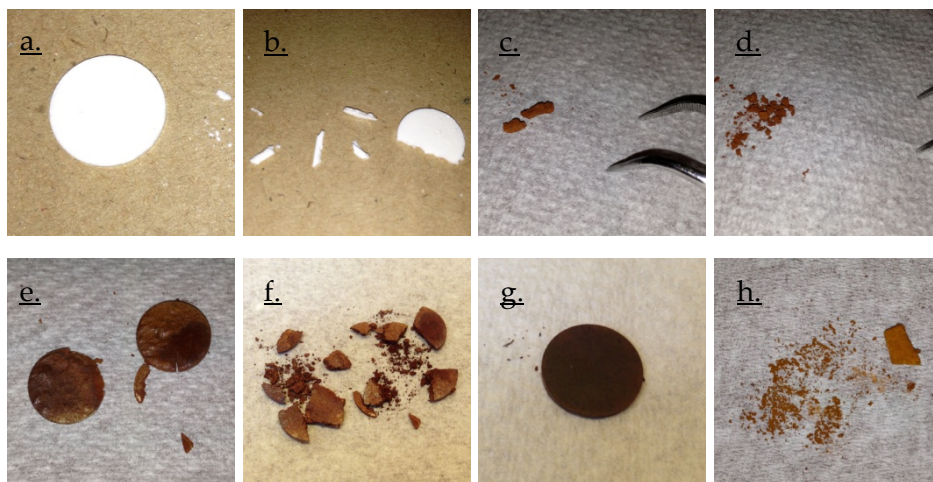


Figure 3.14.7: Images of 17.5 % NaI pellets. a. fresh carbonate pellet, b. segments cut off for TGA, c. & d. brittle segments after sorption cycles, e. & f. brittle carbonate pellet calcined at 500 °C in N₂, g. sturdy pellet pressed as oxide, h. 4.22 % SBA-15 pellet after 25 CO₂ sorption cycles. Diameter of pellet after pressing 13 mm, width of tweezers (shown for comparison) 10 mm.

The results show that the material can be pelletised and that pelletisation is best performed in the oxide state so as to maintain the mechanical integrity of the pellet during sorption cycles. However, the working capacity of the pellets was relatively low, and the addition of a porous filler material caused the pellets to partially crumble to powder during CO₂ sorption cycles. In order to overcome this problem, future studies might also consider the use of suitable binding agents.

3.15 Concluding remarks

In this study, cadmium oxide/alkali halide mixtures made from both lithium and sodium bromide and iodide were characterised in multiple sorption-desorption cycles. All materials exhibited reversible mass gains and losses under CO₂ partial pressure swing processing via TGA. The best-performing material, a sample made from 17.5 wt% NaI and CdCO₃, was analysed in detail, as samples with other alkali halides than NaI exhibited lower working capacities, slower carbon dioxide sorption or weak multicyclic CO₂ sorption stability. It was shown by TGA that a cyclic exposure to carbon dioxide in argon and pure argon induces a cyclic sorption and desorption of carbon dioxide at constant temperature, which was confirmed to be due to the reversible formation of cadmium carbonate and oxide by powder XRD. From the TGA results, it became evident that the working capacity of the material is severely reduced over 25 cycles if the initial material

activation (decomposition of the carbonate) is performed in air. Pre-treatment in an inert gas (argon or nitrogen) significantly improves the multicycle sorption stability. 1 % water addition to the feed gas stream also has a beneficial effect on the overall capacity and cyclability. In a TGA experiment in wet gas with 12 minutes sorption and 24 minutes desorption, at 285 °C, a comparably stable working capacity of approx. 18 weight-% per cycle was achieved.

The severe capacity loss of samples pre-treated in air is associated with a loss of iodine, whereas the sodium content was unaltered during the capacity loss, relative to the cadmium content and, so, appeared to be completely retained within the sample. This was confirmed by elemental analysis using AAS and ICP-MS. This must mean that sodium takes on a new form, but its exact nature so far remains unidentified. It can be speculated that the loss of iodine is related to the oxidation of iodide to iodine, which then evaporates. This is consistent with the result that samples calcined in air exhibit a greater iodine loss than if they are calcined in inert conditions (i. e., where no oxygen is available as oxidiser). Mass losses during the multicycle experiments, determined by the baseline shift, also confirm alteration and loss of sample constituents over multiple sorption cycles. Water addition during cyclic experiments apparently had no noticeable effect on the loss of iodine.

Pelletisation of the samples and subsequent multiple cycle sorption of the pelletised material resulted in lower working capacities than their powder counterparts. Pellets pressed after pre-treatment (as oxides) had better mechanical stability, but only achieved a relatively low CO₂ sorption working capacity. The reduction of the working capacity caused by pelletisation is assumed due to fusion of powder particles, resulting in diffusion limitations due to greater material thickness. For a pellet prepared from the oxide form of the sorbent with the addition of SBA-15, an improved cyclic sorption capability is presumed to be due to the porous material enabling better gas diffusion into the core of the pellet. In comparison to an oxide pellet without additive, the pellets containing silica were found to be less robust and partially crumbled into powder after 25 CO₂ sorption cycles.

The cadmium oxide/alkali halide sorbent was found to exhibit promising potential as a sorbent to reversibly capture from CO₂ from syngas associated with power generation via IGCC. The cyclic capacity of a sorbent in powder form was successfully maintained over 25 cycles without deterioration under appropriate operating conditions. Future research must now be directed at maintaining the physical integrity of pelletised samples and improving chemical stability over multiple sorption cycles.

3.16 Acknowledgements

The in-situ powder XRD work was undertaken at the Australian Synchrotron, Victoria, Australia. The Powder Diffraction beamline team (Kia Wallwork, Qinfen Gu, Justin Kimpton) is gratefully acknowledged for help with of X-ray diffraction data acquisition and refinement. The authors also thank Vera Eate, Rodney Hall (AAS, Monash Chemistry) and Massimo Raveggi (ICP-MS, Monash Geosciences) for help with data acquisition and analysis. James Bahn is acknowledged for help with synthetic work to make SBA-15. Funding provided by the Faculty of Science, Monash University, and by the Australian Government through its Cooperative Research Centre (CRC) program to support this CO2CRC research project, is gratefully acknowledged.

Supplementary material

Cadmium oxide/alkali metal halide mixtures for pre-combustion CO₂ capture. Part 2: Multiple sorption cycles

Christian Vogt, Gregory P Knowles and Alan L Chaffee

Cooperative Research Centre for Greenhouse Gas Technologies (CO2CRC), School of Chemistry, Monash University, Box 23, VIC 3800, Australia

3.17 Pore size distribution of SBA-15

The nitrogen physisorption experiment at 77 K on the SBA-15 sample used in this study was performed on a Coulter Omnisorp 360CX gas sorption analyser. The isotherm and the pore size distribution calculated by the BJH method are given in Figure 3.17.1. The BET surface area, determined between 0.05 and 0.35 relative pressures, was determined to be 974.8 m²/g.

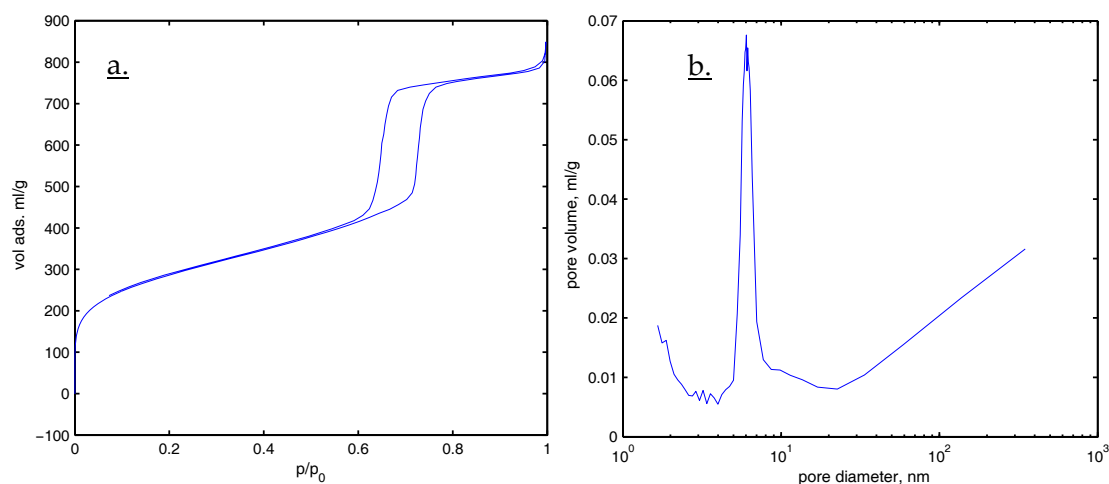
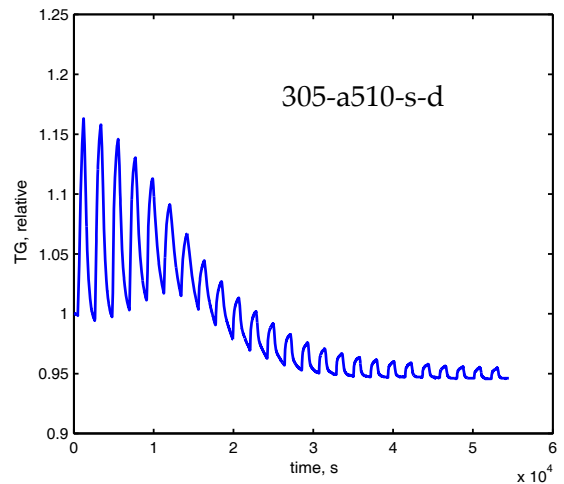
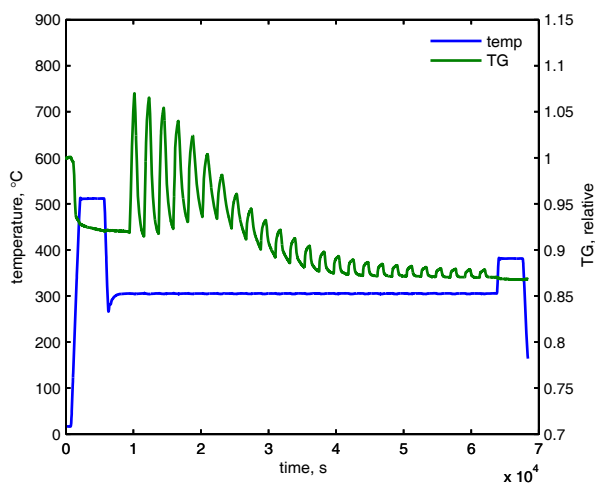
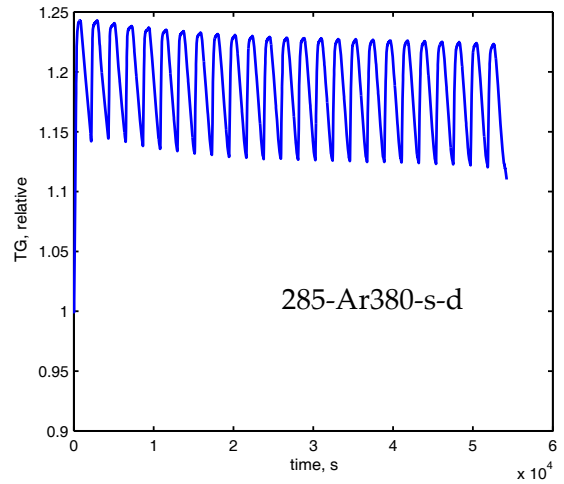
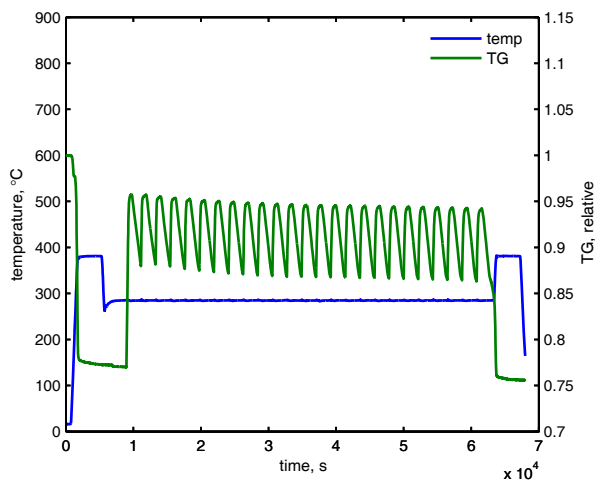
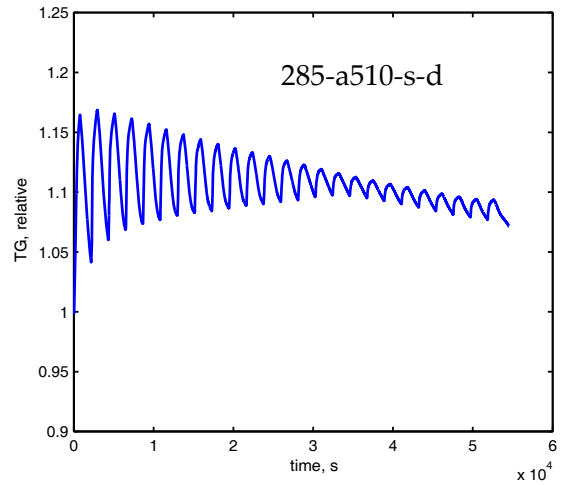
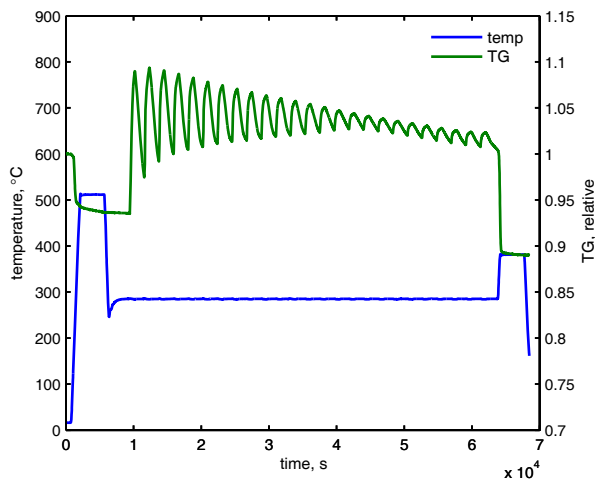
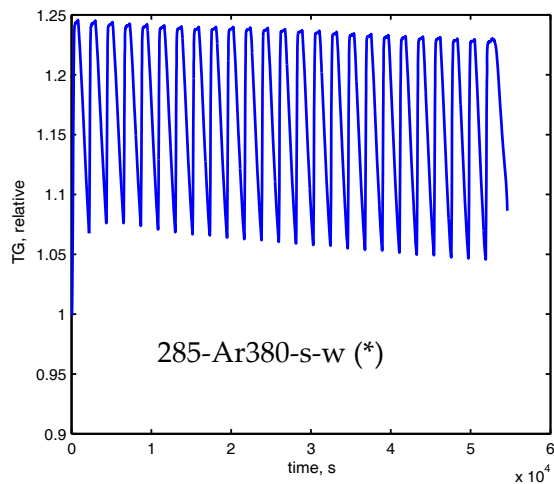
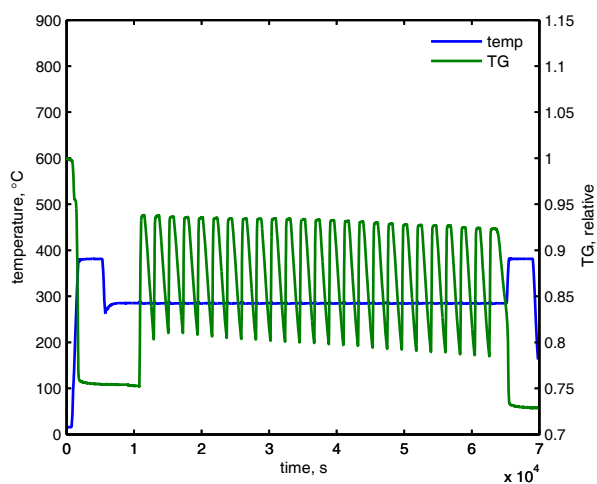
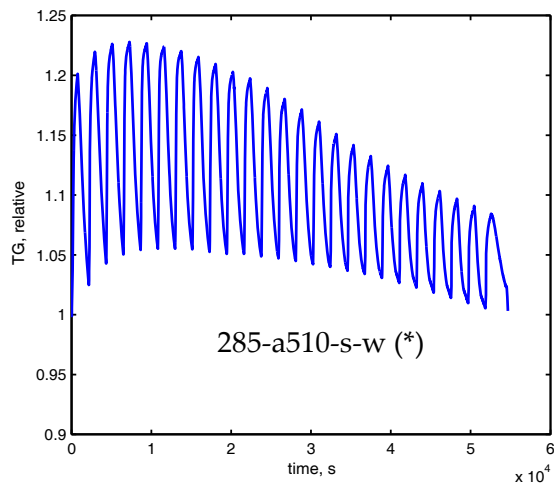
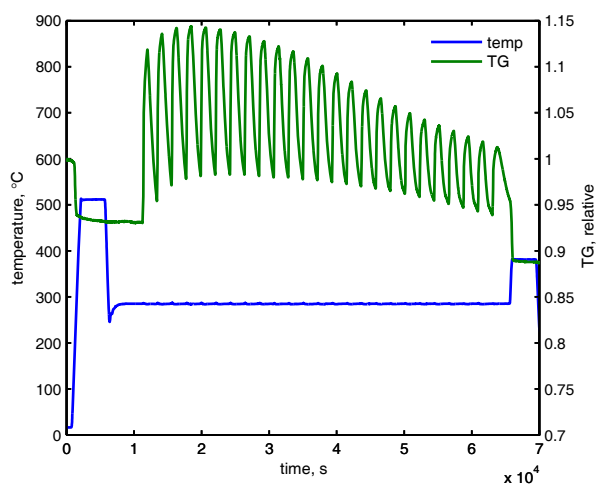
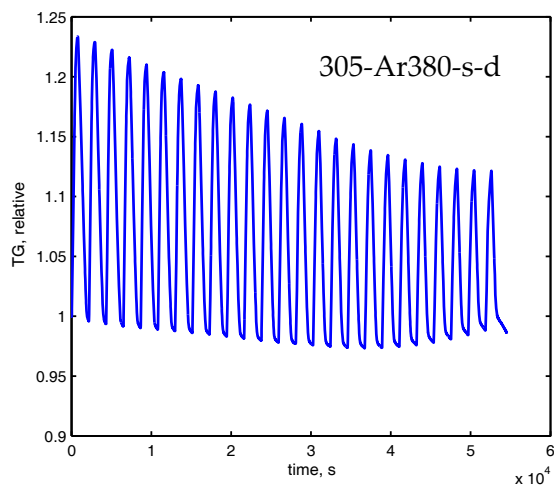
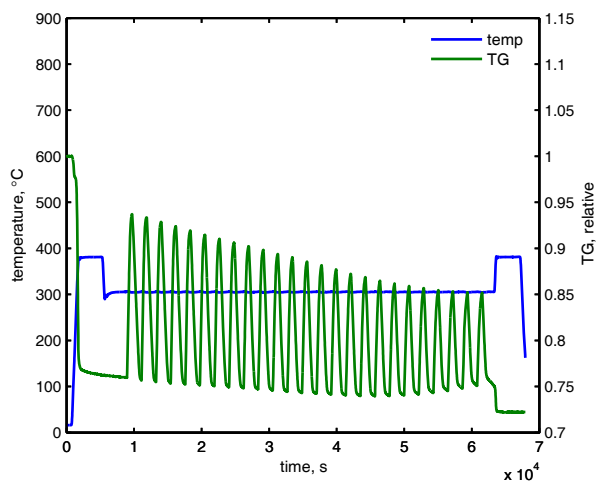


Figure 3.17.1: a. N₂ adsorption isotherm, b. BJH pore volume for SBA-15.

3.18 TGA cyclic experiments plots





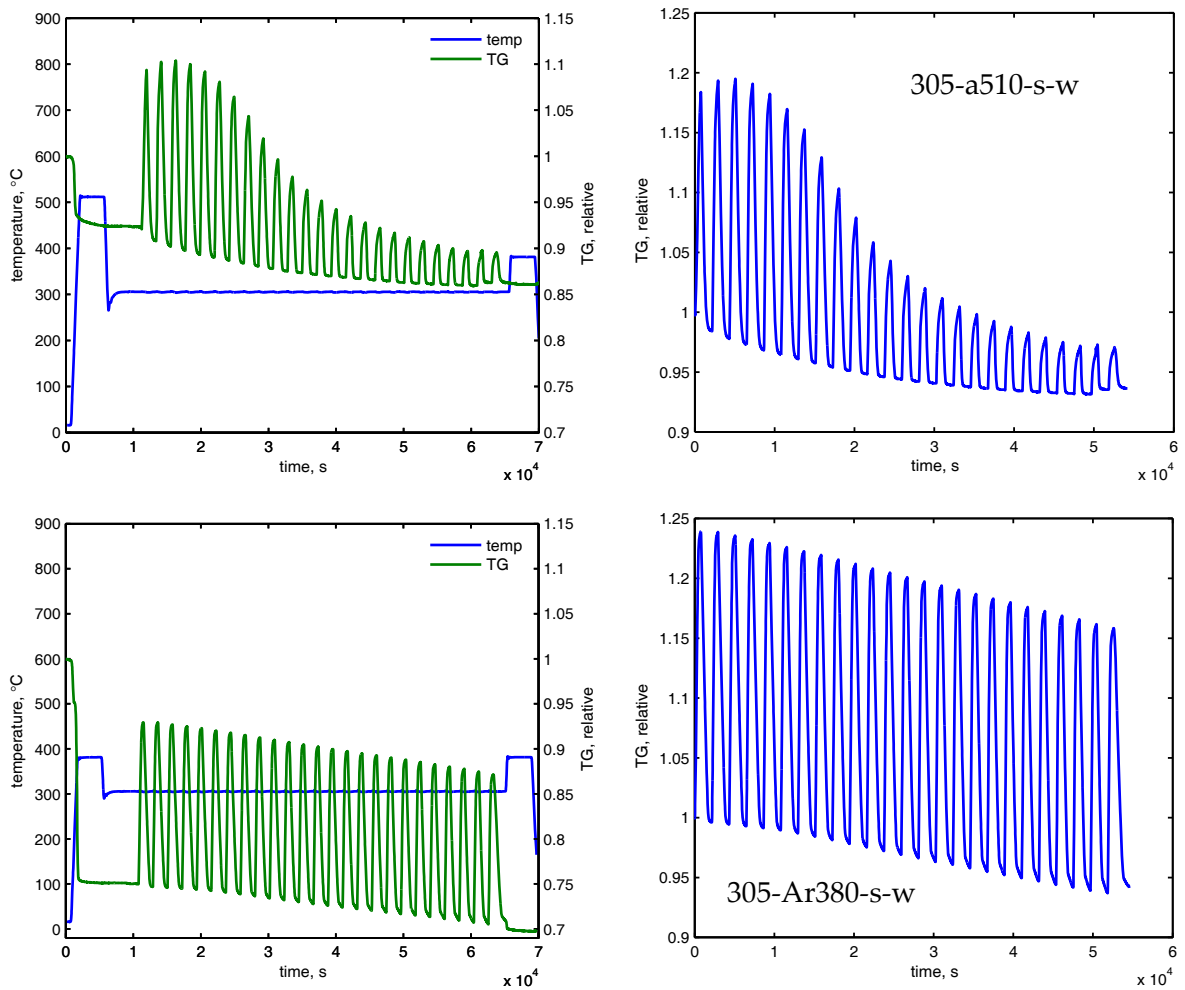
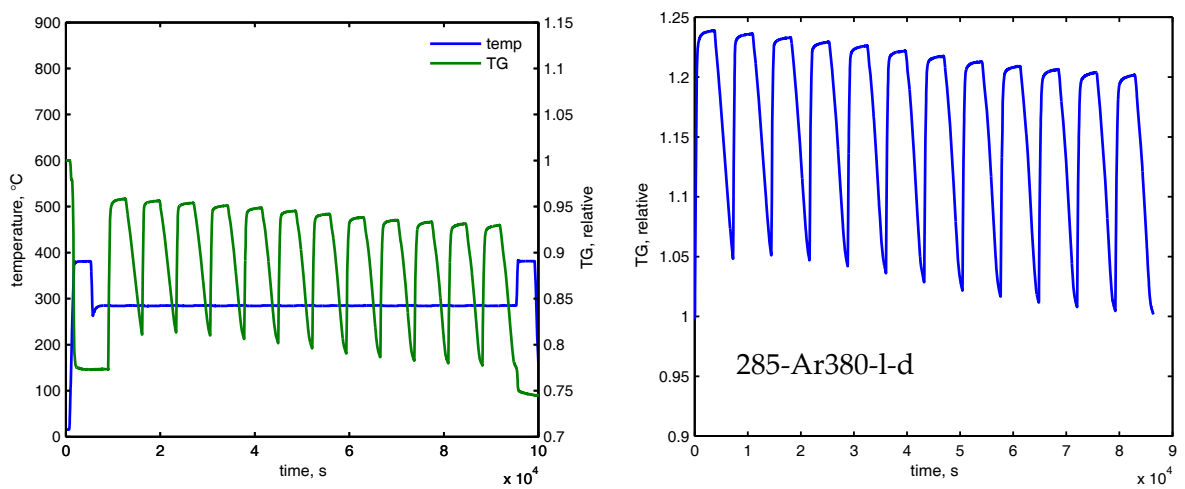


Figure 3.18.1: Full thermograms (left) and normalised thermograms to 100 % active sorbent (right) of multicyclic sorption-desorption of Cd-NaI (17.5 %) sorbent at constant temperatures (275 and 295 °C) in dry and wet gas. Refer to Table 1 in the main article for sample labels. Starred (*) sample thermograms appear in full in main article as well.



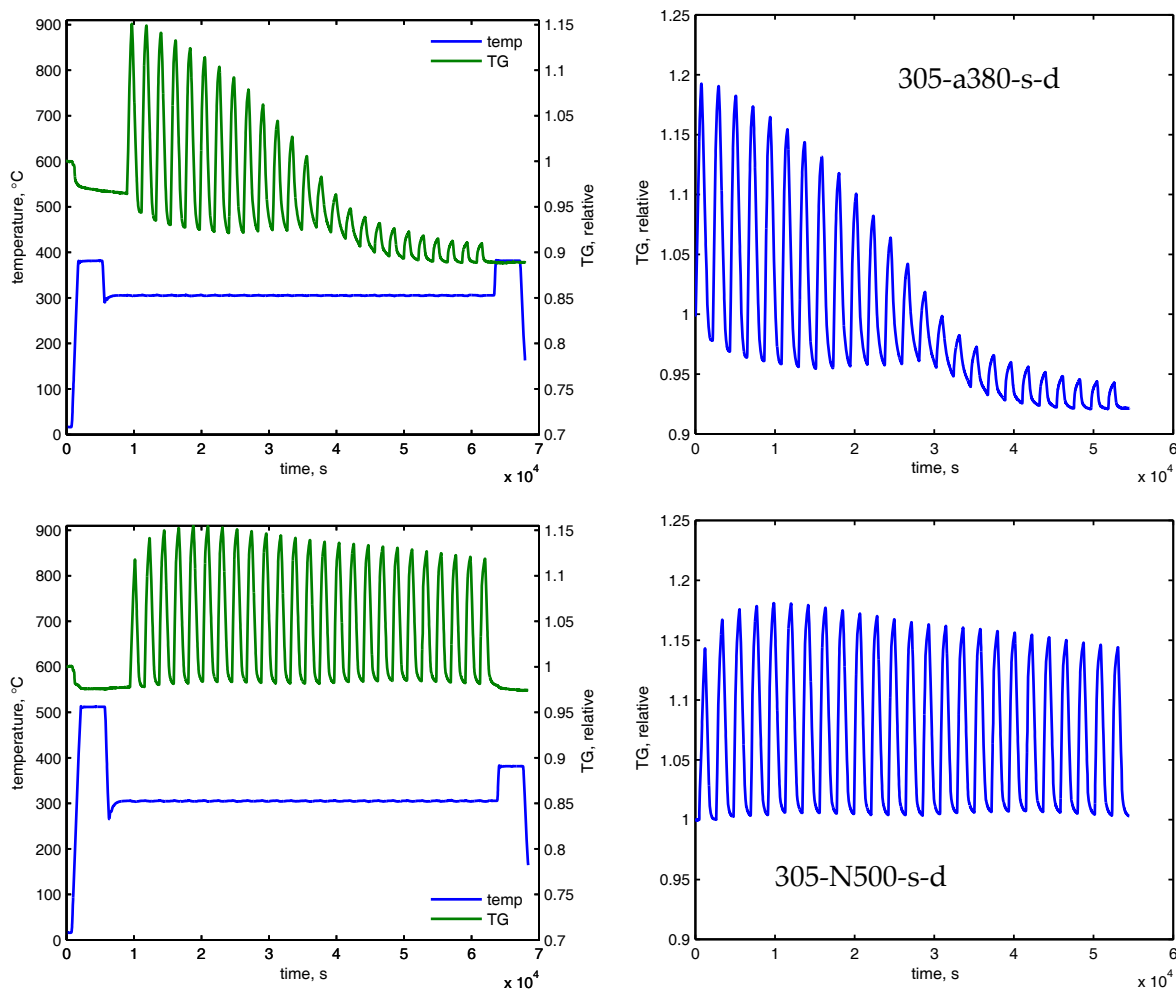
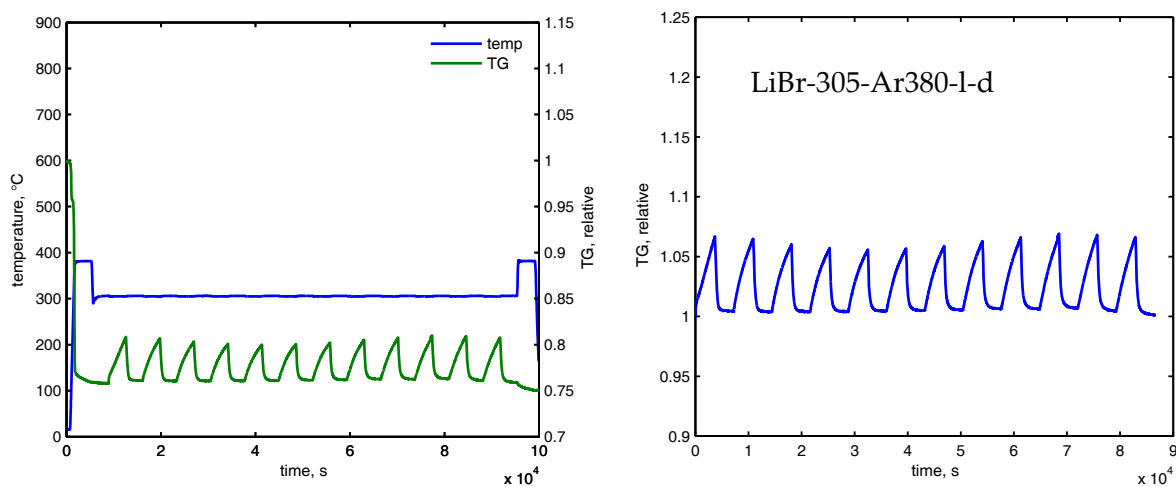
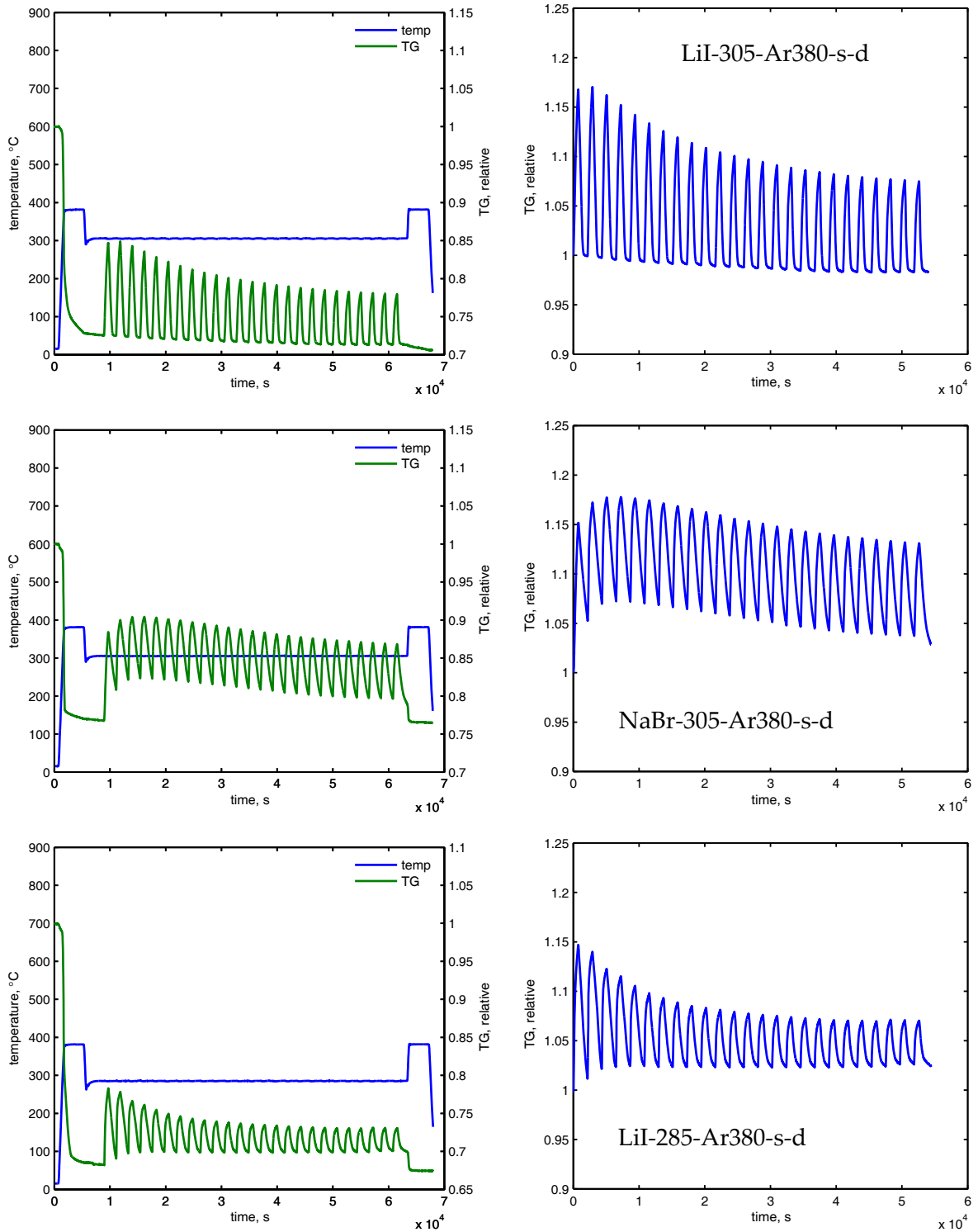


Figure 3.18.2: Full thermograms (left) and normalised thermograms to 100 % active sorbent (right) of multicyclic sorption-desorption of Cd-NaI (17.5 %) sorbent at constant temperatures (275 and 295 °C) in dry gas, comparing different pre-treatments, as well as short and long cycles. Refer to Table 1 in the main article for sample labels.





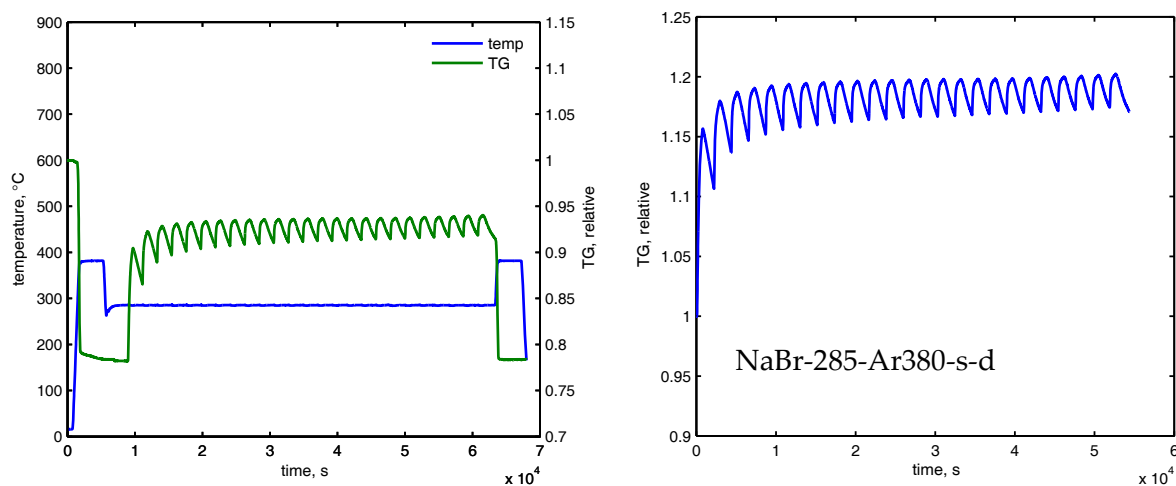
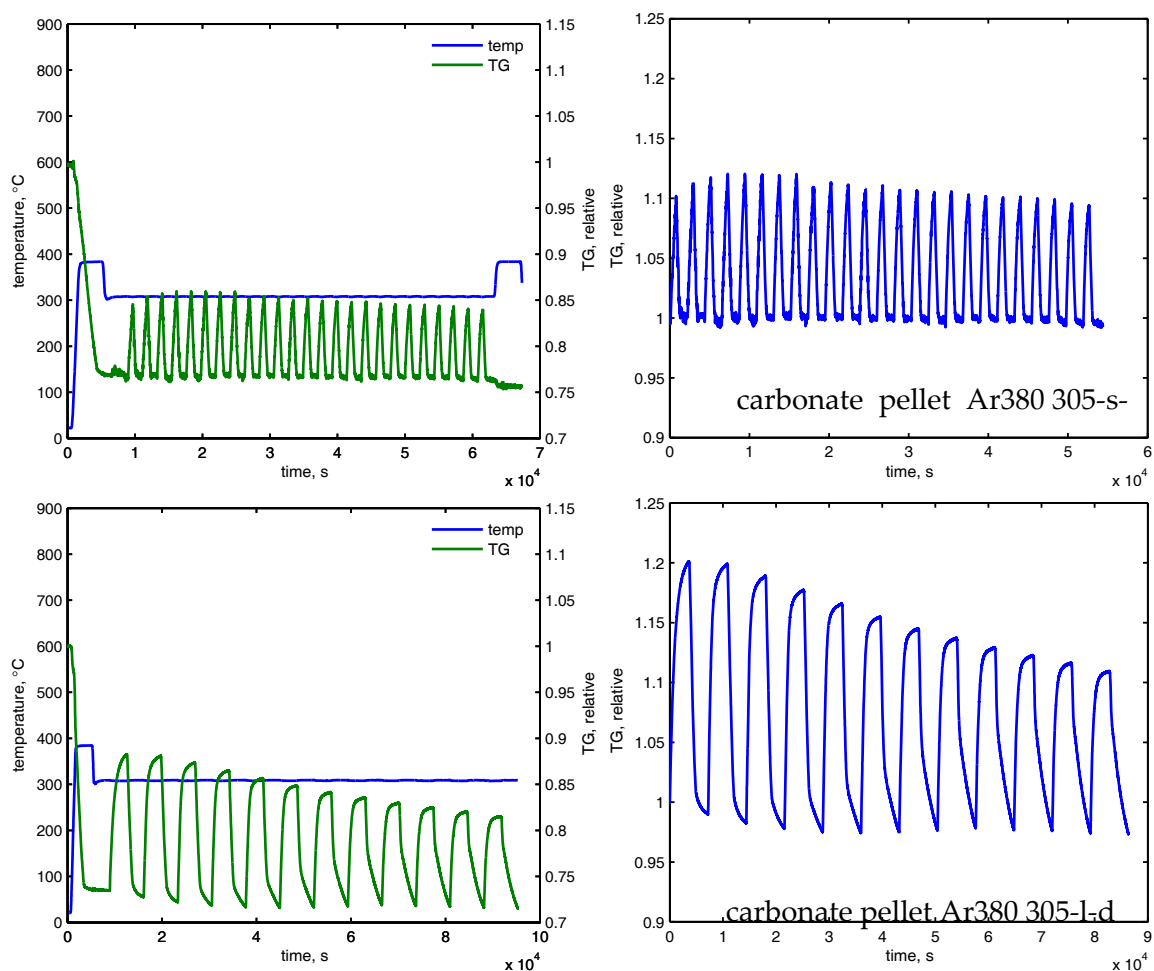
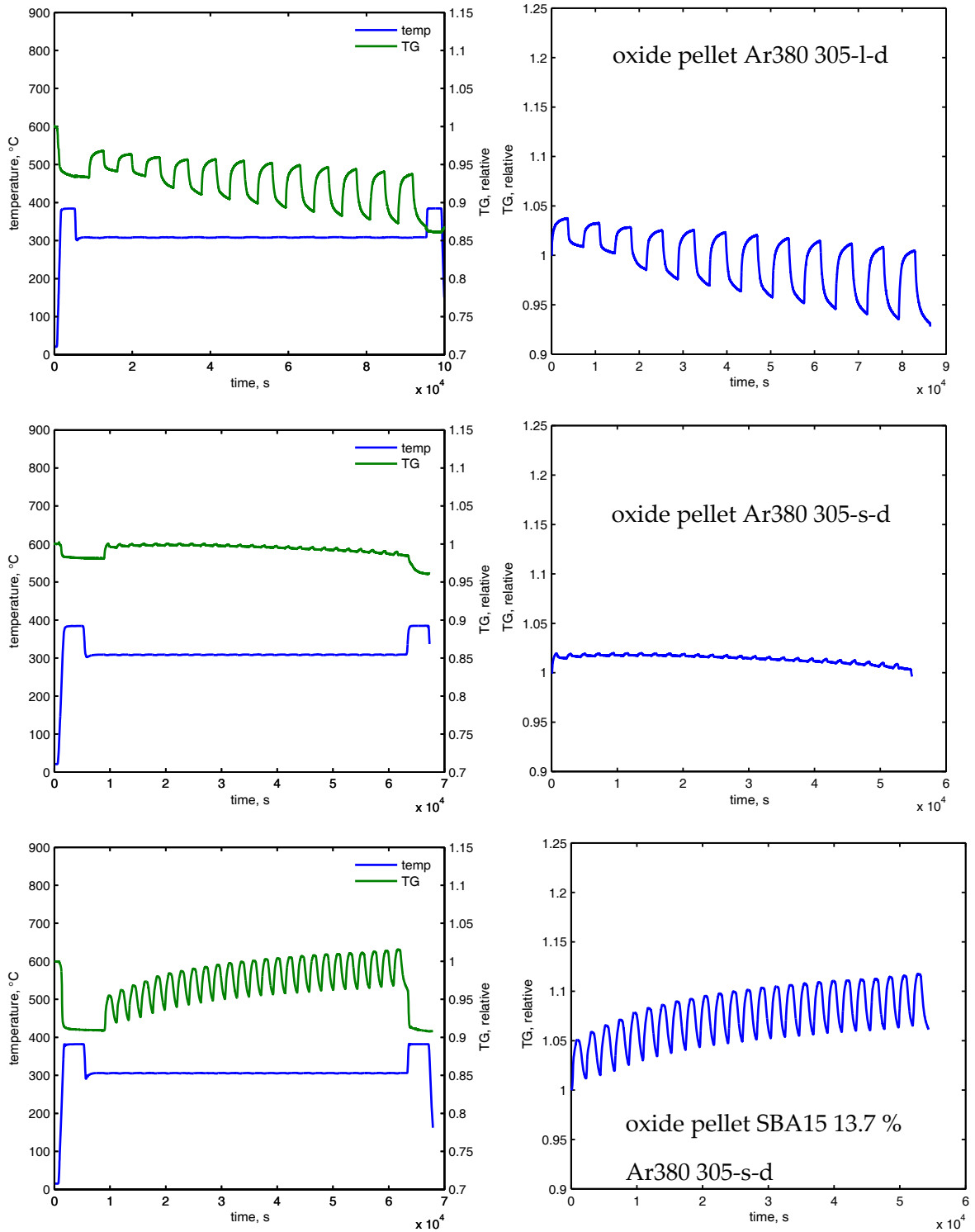


Figure 3.18.3: Full thermograms (left) and normalised thermograms to 100 % active sorbent (right) of multicyclic sorption-desorption of Cd sorbent with different alkali promoters at constant temperatures (275 and 295 °C) in dry gas, comparing short and long cycles. Refer to Table 1 in the main article for sample labels.





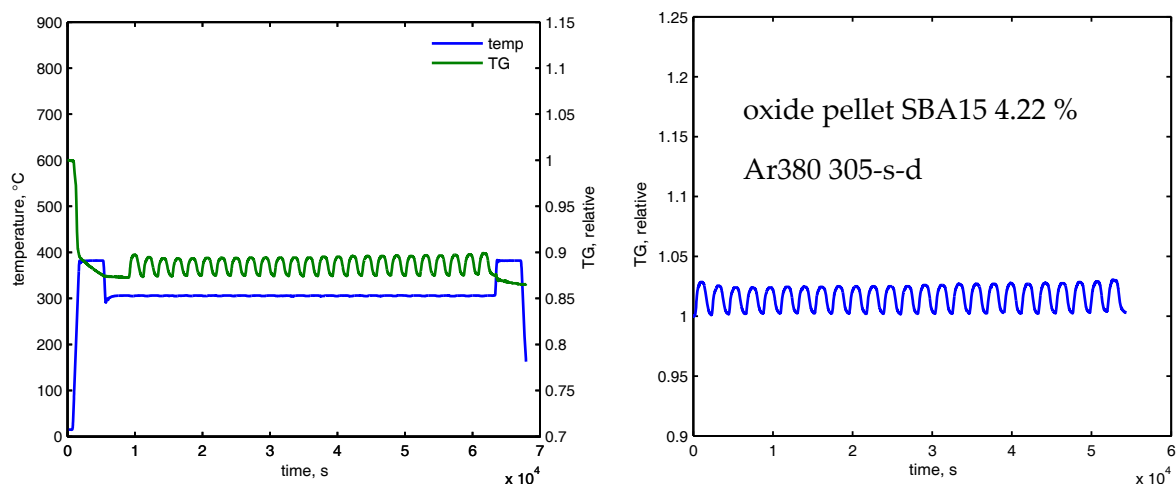


Figure 3.18.4: Full thermograms (left) and normalised thermograms to 100 % active sorbent (right) of multicyclic sorption-desorption of pelletised Cd-17.5 % NaI sorbent at constant temperature (295 °C) in dry gas, comparing short and long cycles. Refer to Table 3.13.1 in the main article for sample labels.

3.19 Le Bail fit of the powder XRD data

3.19.1 Results

The unit cell sized obtained by Le Bail refinement are given in Table 3.19.1.

Table 3.19.1: Results of the Le Bail refinement of the synchrotron XRD data (refer Figure 6) for cadmium oxide and carbonate

sample	phase	unit cell lengths a = b	unit cell length c	space group
decarbonated cycle #3	CdO	4.7121 Å	= a	Fm-3m
carbonated cycle #3	CdO	4.7125 Å	= a	Fm-3m
PDF 4+ 2011 entry 04-001-3770	CdO	4.6951 Å	= a	Fm-3m
carbonated cycle #3	CdCO ₃	4.9207 Å	16.4269 Å	R-3c
PDF 4+ 2011 entry 04-014-4823	CdCO ₃	4.9207 Å	16.2968 Å	R-3c

3.19.2 Statistics

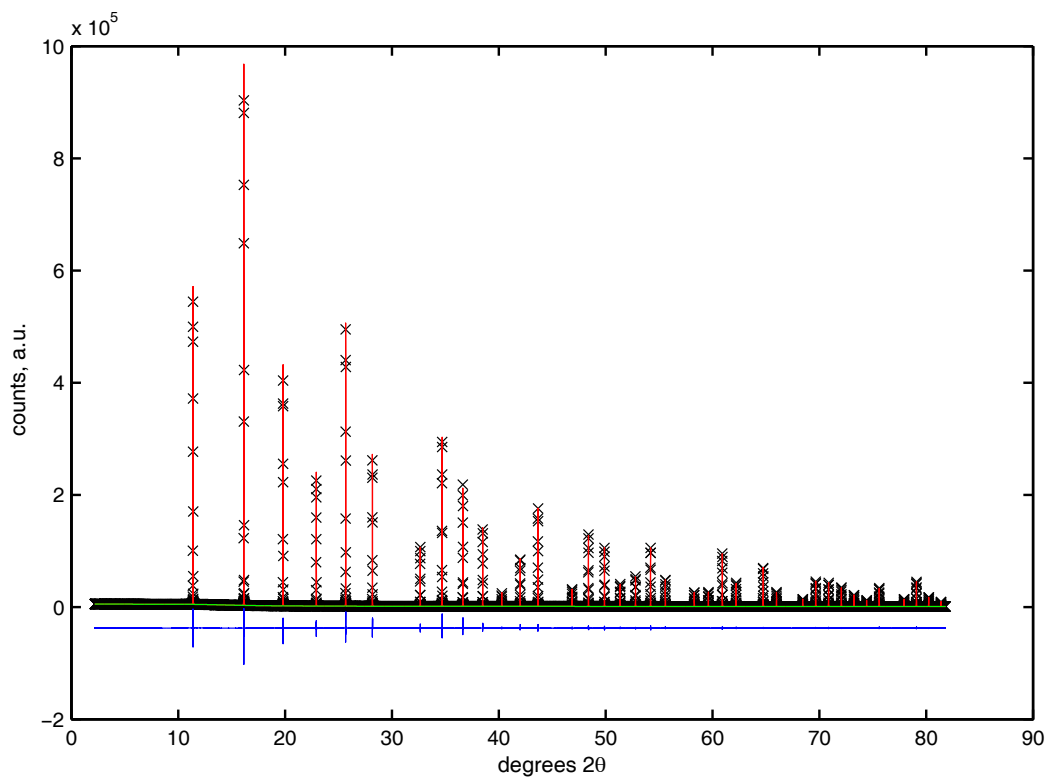
The statistical values of the Le Bail fits performed in the paper are given in Table 3.9.1.

Table 3.19.2: Statistics of the Le Bail fits

sample	reference	reference in supplement	wRp	Rp	χ^2
LaB ₆ standard	text/paper	Figure 3.19.1	0.0396	0.0332	3.337
17.5 % NaI decarb.	Table 3.19.1	Figure 3.19.2	0.0882	0.0544	13.80
carbonated cycle #3	Table 3.19.1	Figure 3.19.3	0.1042	0.0608	21.14

3.19.3 Le Bail fit graphs

The graphs of the Le Bail refinements of the powder XRD data are given in the figures below. The black crosses denote the observed, the red line the refined data. The background is plotted green; blue denotes the difference between calculated and observed. The difference graph is offset below the other graphs.

Figure 3.19.1: Le Bail refinement plot of LaB₆ standard, synchrotron

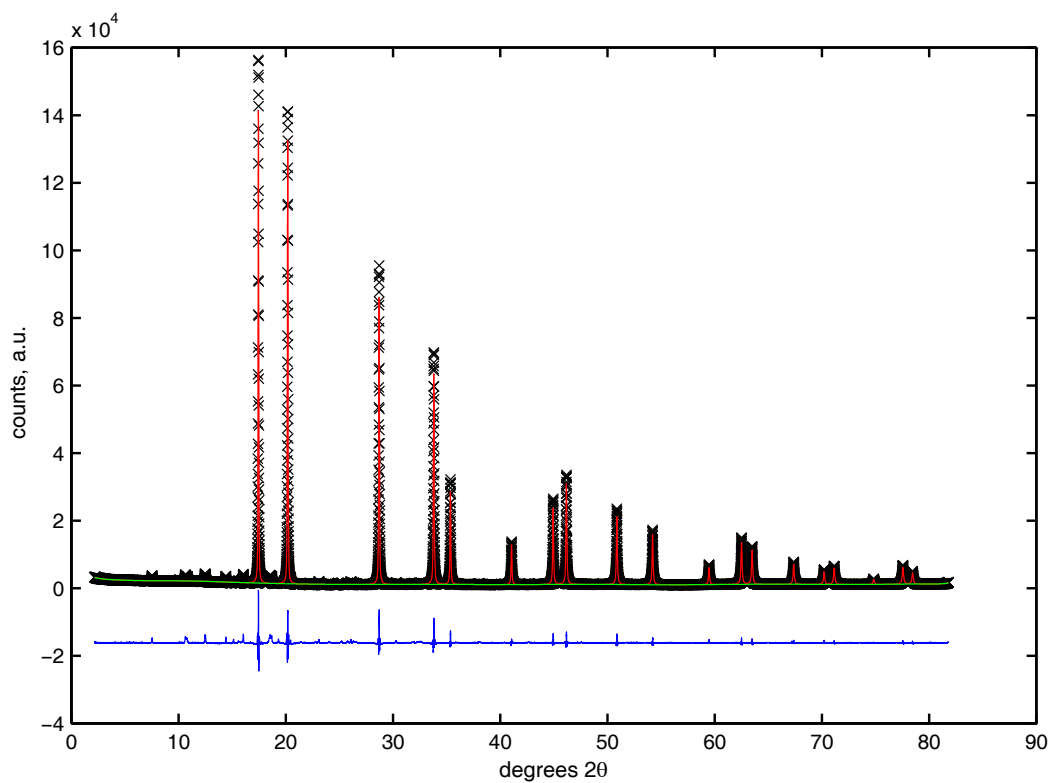


Figure 3.19.2: Le Bail refinement plot of 17.5 % NaI sample, decarbonated in situ in 3rd cycle, synchrotron

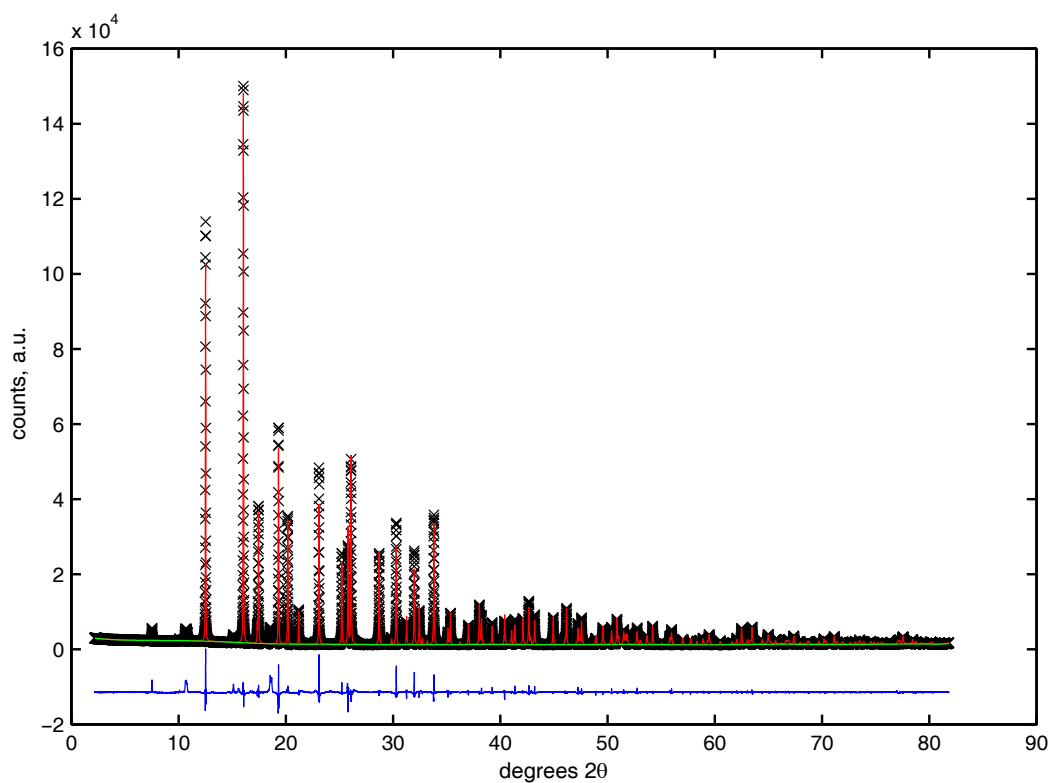


Figure 3.19.3: Le Bail refinement plot of 17.5 % NaI sample, carbonated in situ in 3rd cycle, synchrotron

3.20 References for Chapter 3

- [1] K. S. Lackner, A. H. A. Park, and B. G. Miller, "Eliminating CO₂ Emissions from Coal-Fired Power Plants," in *Generating Electricity in a Carbon-Constrained World*, Boston: Academic Press, 2010, pp. 127-173.
 - [2] M. Mikkelsen, M. Jørgensen, and F. C. Krebs, "The teraton challenge. A review of fixation and transformation of carbon dioxide," *Energy & Environmental Science*, vol. 3, pp. 43-81, 2010.
 - [3] H. Yang, Z. Xu, M. Fan, R. Gupta, R. B. Slimane, A. E. Bland, and I. Wright, "Progress in carbon dioxide separation and capture: A review," *Journal of Environmental Sciences*, vol. 20, pp. 14-27, 2008.
 - [4] P. Chiesa, T. G. Kreutz, and G. G. Lozza, "CO₂ Sequestration From IGCC Power Plants by Means of Metallic Membranes," *Journal of Engineering for Gas Turbines and Power*, vol. 129, pp. 123-134, 2007.
 - [5] K. Liu, Z. Cui, and T. H. Fletcher, "Coal Gasification," in *Hydrogen and Syngas Production and Purification Technologies*, K. Liu, C. Song, and V. Subramani, Eds.: Wiley-AIChE, 2009, pp. 156-218.
 - [6] P. Chiesa, S. Consonni, T. Kreutz, and R. Williams, "Co-production of hydrogen, electricity and CO₂ from coal with commercially ready technology. Part A: Performance and emissions," *International Journal of Hydrogen Energy*, vol. 30, pp. 747-767, 2005.
 - [7] A. Blackman, S. Bottle, S. Schmid, M. Mocerino, and U. Wille, *Chemistry*: John Wiley & Sons, 2012.
 - [8] D. M. Ruthven, S. Farooq, and K. S. Knaebel, *Pressure swing adsorption*. New York: VCH Publishers, 1994.
 - [9] R. Yang, *Gas separation by adsorption processes*: Imperial College Press, 1997.
 - [10] M. K. R. Reddy, Z. P. Xu, G. Q. Lu, and J. C. Diniz da Costa, "Effect of SO_x Adsorption on Layered Double Hydroxides for CO₂ Capture," *Industrial & Engineering Chemistry Research*, vol. 47, pp. 7357-7360, 2008.
 - [11] H. T. J. Reijers, S. E. A. Valster-Schiermeier, P. D. Cobden, and R. W. van den Brink, "Hydrotalcite as CO₂ Sorbent for Sorption-Enhanced Steam Reforming of Methane," *Industrial & Engineering Chemistry Research*, vol. 45, pp. 2522-2530, 2005.
 - [12] R. Singh, M. K. Ram Reddy, S. Wilson, K. Joshi, J. C. Diniz da Costa, and P. Webley, "High temperature materials for CO₂ capture," *Energy Procedia*, vol. 1, pp. 623-630, 2009.
 - [13] K. Nakagawa and T. Ohashi, "A Novel Method of CO₂ Capture from High Temperature Gases," *Journal of The Electrochemical Society*, vol. 145, pp. 1344-1346, 1998.
 - [14] G. Xiao, R. Singh, A. Chaffee, and P. Webley, "Advanced adsorbents based on MgO and K₂CO₃ for capture of CO₂ at elevated temperatures," *International Journal of Greenhouse Gas Control*, vol. 5, pp. 634-639, 2011.
 - [15] G. S. Grasa, J. C. Abanades, M. Alonso, and B. González, "Reactivity of highly cycled particles of CaO in a carbonation/calcination loop," *Chemical Engineering Journal*, vol. 137, pp. 561-567, 2008.
 - [16] J. C. Abanades and D. Alvarez, "Conversion Limits in the Reaction of CO₂ with Lime," *Energy & Fuels*, vol. 17, pp. 308-315, 2003.
-

- [17] D. Alvarez and J. C. Abanades, "Determination of the Critical Product Layer Thickness in the Reaction of CaO with CO₂," *Industrial & Engineering Chemistry Research*, vol. 44, pp. 5608-5615, 2005.
- [18] B. Feng, W. Liu, X. Li, and H. An, "Overcoming the Problem of Loss-in-Capacity of Calcium Oxide in CO₂ Capture," *Energy & Fuels*, vol. 20, pp. 2417-2420, 2006.
- [19] P. Sun, J. R. Grace, C. J. Lim, and E. J. Anthony, "The effect of CaO sintering on cyclic CO₂ capture in energy systems," *AIChE Journal*, vol. 53, pp. 2432-2442, 2007.
- [20] B. González, G. S. Grasa, M. Alonso, and J. C. Abanades, "Modeling of the Deactivation of CaO in a Carbonate Loop at High Temperatures of Calcination," *Industrial & Engineering Chemistry Research*, vol. 47, pp. 9256-9262, 2008.
- [21] F. Fang, Z.-s. Li, and N.-s. Cai, "Continuous CO₂ Capture from Flue Gases Using a Dual Fluidized Bed Reactor with Calcium-Based Sorbent," *Industrial & Engineering Chemistry Research*, vol. 48, pp. 11140-11147, 2009.
- [22] W. Wang, S. Ramkumar, S. Li, D. Wong, M. Iyer, B. B. Sakadjian, R. M. Statnick, and L. S. Fan, "Subpilot Demonstration of the Carbonation-Calcination Reaction (CCR) Process: High-Temperature CO₂ and Sulfur Capture from Coal-Fired Power Plants," *Industrial & Engineering Chemistry Research*, vol. 49, pp. 5094-5101, 2010.
- [23] H. Lu and P. G. Smirniotis, "Calcium Oxide Doped Sorbents for CO₂ Uptake in the Presence of SO₂ at High Temperatures," *Industrial & Engineering Chemistry Research*, vol. 48, pp. 5454-5459, 2009.
- [24] G. S. Grasa, M. Alonso, and J. C. Abanades, "Sulfation of CaO Particles in a Carbonation/Calcination Loop to Capture CO₂," *Industrial & Engineering Chemistry Research*, vol. 47, pp. 1630-1635, 2008.
- [25] D. J. Fauth, E. A. Frommell, J. S. Hoffman, R. P. Reasbeck, and H. W. Pennline, "Eutectic salt promoted lithium zirconate: Novel high temperature sorbent for CO₂ capture," *Fuel Processing Technology*, vol. 86, pp. 1503-1521, 2005.
- [26] A. Doiwa and A. Tomanek, "Die Bildung von Cadmiumcarbonat und Cadmiumsulfid aus Cadmiumoxid," *Zeitschrift für anorganische und allgemeine Chemie*, vol. 334, pp. 12-14, 1964.
- [27] A. Doiwa and H. Lommel, "¹⁴CO₂-Austausch an Cadmiumcarbonat," *Angewandte Chemie*, vol. 76, pp. 578-578, 1964.
- [28] S. S. Hla, D. Park, G. J. Duffy, J. H. Edwards, D. G. Roberts, A. Ilyushechkin, L. D. Morpeth, and T. Nguyen, "Kinetics of high-temperature water-gas shift reaction over two iron-based commercial catalysts using simulated coal-derived syngases," *Chemical Engineering Journal*, vol. 146, pp. 148-154, 2009.
- [29] B. H. Toby, "EXPGUI, a graphical user interface for GSAS," *Journal of Applied Crystallography*, pp. 210-213, 2001.
- [30] A. C. Larson and R. B. V. Dreele, "General Structure Analysis System (GSAS)," *Los Alamos National Laboratory Report* vol. LAUR 86-748, 1994.
- [31] B. H. Toby, "CMPR - a powder diffraction toolkit," *Journal of Applied Crystallography*, vol. 38, pp. 1040-1041, 2005.
- [32] R. C. Weast, *CRC Handbook of Chemistry and Physics*. Cleveland, Ohio: CRC Press, 1975.
- [33] S. K. Bhatia and D. D. Perlmutter, "Effect of the product layer on the kinetics of the CO₂-lime reaction," *AIChE Journal*, vol. 29, pp. 79-86, 1983.
- [34] B. J. Asirvatham and Z. A. Munir, "The decomposition of cadmium carbonate in air and in vacuum," *Journal of Materials Science*, vol. 21, pp. 1997-2001, 1986.
-

- [35] K. H. Rieder, M. Ishigame, and L. Genzel, "Infrared Absorption by Coupled Surface-Phonon-Surface-Plasmon Modes in Microcrystals of CdO," *Physical Review B: Condensed Matter and Materials Physics*, vol. 6, p. 3804, 1972.
- [36] S. Weiner, *Microarchaeology: Beyond the visible archaeological record*: Cambridge University Press, 2010.
- [37] B. H. Stuart, *Infrared Spectroscopy: Fundamentals and Applications*: John Wiley & Sons, Ltd, 2005.
- [38] P. Markewitz, W. Kuckshinrichs, W. Leitner, J. Linssen, P. Zapp, R. Bongartz, A. Schreiber, and T. E. Müller, "Worldwide innovations in the development of carbon capture technologies and the utilization of CO₂," *Energy & Environmental Science*, vol. 5, pp. 7281-7305, 2012.
- [39] M. Jahan, "Removal of Carbon Dioxide from Gas Streams with Metal Oxides at High Temperature," PhD thesis, School of Chemistry, Monash University, Victoria, Australia, 2011.
- [40] H. Gupta and L.-S. Fan, "Carbonation-Calcination Cycle Using High Reactivity Calcium Oxide for Carbon Dioxide Separation from Flue Gas," *Industrial & Engineering Chemistry Research*, vol. 41, pp. 4035-4042, 2002.
- [41] C. Vogt, G. P. Knowles, S. L. Y. Chang, and A. L. Chaffee, "Cadmium oxide/alkali metal halide mixtures - a potential high capacity sorbent for pre-combustion CO₂ capture," *Journal of Materials Chemistry A*, vol. 1, pp. 10962-10971, 2013.
- [42] D. Zhao, Q. Huo, J. Feng, B. F. Chmelka, and G. D. Stucky, "Nonionic Triblock and Star Diblock Copolymer and Oligomeric Surfactant Syntheses of Highly Ordered, Hydrothermally Stable, Mesoporous Silica Structures," *Journal of the American Chemical Society*, vol. 120, pp. 6024-6036, 1998.
- [43] G. P. Knowles, P. A. Webley, Z. Liang, and A. L. Chaffee, "Silica/Polyethyleneimine Composite Adsorbent S-PEI for CO₂ Capture by Vacuum Swing Adsorption (VSA)," in *Recent Advances in Post-Combustion CO₂ Capture Chemistry*, M. I. Attalla, Ed., Washington, DC: American Chemical Society, 2012.
- [44] *CRC Handbook of Chemistry and Physics*. Cleveland, Ohio: CRC Press, 2012-2013.
-

Chapter 4 Investigation of the decay mechanism of a CdO-NaI sorbent

4.1 Chapter overview

In Chapter 3, cadmium oxide/alkali halide mixed sorbent powders were presented. It was shown that a sodium iodide-loaded cadmium oxide performs best for multicyclic carbon dioxide sorption in terms of the reaction rate and the ability to reach stoichiometric carbonation in a reasonable amount of time. It was, however, discovered that a significant reduction in working capacity is observed as the sorbents progress through multiple carbon dioxide sorption cycles. This working capacity reduction was associated with the loss of iodide promoter.

This chapter contains one paper, which details this decay observation. Using a mass spectrometer to analyse the exit gas of a fixed-bed sorption experiment, the removal of iodine in its elemental form was confirmed. XPS showed a highly oxidised species of iodine on the surface of the sample in its initially activated state. Surface carbonation was also evident on the samples.

The morphology and crystallinity of the sorbent was analysed via electron microscopy and powder XRD. It was shown via TEM that the previously spherical sorbent nanoparticles formed cracks/voids after multicyclic exposure to carbon dioxide. A rise in crystallinity (higher intensities in XRD patterns) of the cadmium oxide phase as well as the formation of crystalline sodium iodide was observed upon heating the sorbent from room temperature to the carbon dioxide sorption temperature. It is speculated that this increase in crystallinity has a positive impact on the carbon dioxide sorption capability.

Declaration for Thesis ChapterInvestigation of the capacity decay of a CdO/NaI mixed sorbent for pre-combustion CO₂ capture

Monash University

Declaration for Thesis Chapter 4.2-4.8**Declaration by candidate**

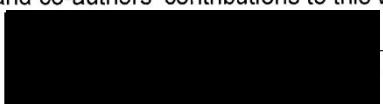
In the case of Chapter 4.2-4.8, the nature and extent of my contribution to the work was the following:

Nature of contribution	Extent of contribution (%)
Proposed original idea; prepared and analysed samples; identified major issues; developed interpretations; fully drafted papers and conclusions	70 %

The following co-authors contributed to the work. If co-authors are students at Monash University, the extent of their contribution in percentage terms must be stated:

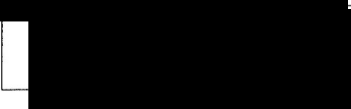
Name	Nature of contribution	Extent of contribution (%) for student co-authors only
Gregory P Knowles	Aided method development (TGA), input to results analysis, input to manuscript revision	N/A
Alan L Chaffee	Supervision, assisted interpretation of results, editorial assistance	N/A
Thomas Gengenbach	Performing XPS analysis, compiling XPS results, input to XPS data discussion	N/A
Shery L Y Chang	Operating electron microscope, input to microscopy results discussion	N/A

The undersigned hereby certify that the above declaration correctly reflects the nature and extent of the candidate's and co-authors' contributions to this work*.

Candidate's
Signature

Date

26/9/13

Main
Supervisor's
Signature

Date

27/9/13

*Note: Where the responsible author is not the candidate's main supervisor, the main supervisor should consult with the responsible author to agree on the respective contributions of the authors.

Investigation of the capacity decay of a CdO/NaI mixed sorbent for pre-combustion CO₂ capture

Christian Vogt[#], Thomas Gengenbach^x, , Shery LY Chang⁺, Gregory P Knowles[#] and Alan L Chaffee^{#*}

[#] Cooperative Research Centre for Greenhouse Gas Technologies (CO₂CRC), School of Chemistry, Monash University, VIC 3800, Australia

^x CSIRO Materials Science and Engineering, Bayview Avenue, Clayton VIC 3168, Australia

⁺ Monash Centre for Electron Microscopy, Monash University, VIC 3800, Australia

⁺ Current Address: Ernst Ruska-Centrum, Forschungszentrum Jülich GmbH, 52425 Jülich, Germany

* corresponding author: [REDACTED]

Phone: [REDACTED] Fax: + [REDACTED]

4.2 Abstract

The mechanisms for the loss of both CO₂ working capacity and mass from a CdO/NaI composite were investigated to better assess the potential use of the material to facilitate the pre-combustion capture of CO₂ from syngas. Fresh activated material was used to analyse sorption and desorption using a CO₂/N₂ mixture. Mass spectrometric analysis of the exit gas revealed the loss of elemental iodine from the system over the period, attributed to the oxidation of iodide. X-ray photoelectron spectroscopy revealed the formation of a highly-oxidised iodine species on the surface of the sorbent during initial calcination in both air and N₂, but this compound vanished after the use of the sorbent in 25 CO₂ sorption cycles. Elemental mapping showed that iodine was dislocated from the sodium, which it was considered to be originally associated to, supporting the theory of oxidation and evaporation (and possible re-deposition). Transmission electron microscopy revealed that the sorbent consisted of regular, spherical nanoparticles of approx. 250 nm diameter, which became more irregularly-shaped after CO₂ sorption cycles, considered due to void/crack formation caused by density changes upon calcination and carbonation.

In-situ powder X-ray diffraction revealed an increase in crystallinity of both CdO and NaI upon heating to CO₂ sorption temperature of 325 °C in N₂ atmosphere, compared to room temperature. It is assumed that inhibiting the oxidation of iodide promoter would potentially be the most significant contribution to improved multicyclic CO₂ sorption stability of the material.

4.3 Introduction

Carbon dioxide capture and storage is considered to be one suitable pathway supporting the mitigation of anthropogenic climate change [1]. Pre-combustion capture, i. e., the removal of CO₂ from a synthesis gas (syngas) derived from coal gasification, is considered to have certain advantages over post-combustion capture (i. e., the capture of CO₂ from a conventional power plant exhaust gas) in the terms of economic viability [2]. A series of sorbents have been considered for use in pre-combustion environments [3], wherein metal oxides are promising candidates.

Cadmium oxide/sodium halide mixtures were previously found to sorb CO₂ to form cadmium carbonate [4, 5]. We have considered these materials as potential candidates for pre-combustion CO₂ capture at temperatures around 300 °C. In a previous study, it was shown that lithium bromide and iodide, sodium bromide and iodide and potassium iodide promote the carbonation reaction of cadmium oxide, whereas a sample made from 17.5 wt% sodium iodide (based on cadmium carbonate precursor) showed the best results in terms of reaction speed and stoichiometric CO₂ uptake [6]. This sample was studied in further detail. An uptake of 26 wt% CO₂ was achieved in a single-cycle sorption experiment at 277 °C, indicating the complete reaction of the cadmium oxide contained in the sample to carbonate. Carbonate formation was confirmed by powder X-ray diffraction (XRD) and Fourier-transform infrared spectrometry (FTIR). A second study showed the reversible transformation of cadmium oxide to carbonate over 25 short (12 minutes sorption, 24 minutes desorption) CO₂ sorption and desorption cycles (Chapter 3, section 3.14). A stable cyclic working capacity of 10 wt% in dry gas and 18 wt% in wet gas (1.2 vol% water) was achieved during these experiments. The 17.5 wt% (nominal) NaI/CdO material, however, showed a significant overall mass loss and samples exposed to air at high temperatures exhibited a severe capacity reduction over 25 CO₂ sorption

cycles. Elemental analysis by dissolution of the solid samples and measurement of iodine via inductively coupled plasma mass spectrometry revealed a significant loss of iodine associated with CO₂ sorption capacity decay. These observations motivated a detailed study of the iodine loss and the surface properties of the sample, in order to obtain more information on the chemical changes occurring during calcination and CO₂ sorption and that may be associated with this capacity reduction.

In this study, the exit gas of a fixed bed sorption experiment containing a 17.5 wt% (nominal) NaI-CdO sample was analysed for iodine species via a residual gas analyser/mass spectrometer. The surface properties of the samples before and after 25 CO₂ sorption cycles were analysed by X-ray photoelectron spectroscopy (XPS) to gain information on the different species of elements present in the sample. Scanning and transmission electron microscopy (SEM, TEM) were used to examine the appearance and crystallinity of the material on a micro/nanoscale before and after CO₂ sorption cycles. In-situ powder X-ray diffraction (XRD) upon heating under a nitrogen purge was used to study the crystallinity of the sample at CO₂ sorption temperature.

4.4 Experimental

4.4.1 Sample preparation

The mixed cadmium oxide/sodium iodide CO₂ sorbent (17.5 wt% NaI based on CdCO₃) used in this study was previously reported (refer [6] and Chapter 3). Briefly, CdCO₃ (Alfa Aesar, 99+ %) was dispersed into an aqueous solution of NaI (Alfa Aesar, 99 %) using a magnetic hotplate stirrer and the water evaporated by heating. The resultant powder was dried in a nitrogen flow at 120 °C overnight. Subsequently, two subsamples of the resultant powder were calcined in nitrogen flow and in air, respectively. Calcination was performed at 500 °C for 3 hours causing the cadmium carbonate to decompose to oxide, turning the formerly white powder dark-red. A pure CdO comparison sample was made by calcining pure CdCO₃ in the same manner.

4.4.2 Electron microscopy

For the transmission electron microscopy experiments, virgin calcined samples were used as well as ones which had been used in thermogravimetric experiments that are fully

described in Chapter 3, section 3.13.4. Samples were pre-treated in the thermoanalyser in argon flow at 500 °C and subsequently exposed to 25 isothermal cycles of sorption using 50 % CO₂ in argon (12 minutes) and desorption in pure argon purge (24 minutes) at 305 °C. The last cycle involved argon purge to fully decarbonate the samples for analysis at a temperature of 380 °C.

Transmission electron microscopy (TEM) was performed on a JEOL 2100F transmission electron microscope. Electron diffraction was calibrated in the instrument using a silicon reference sample to give accurate measurement of crystal lattice d-spacings. Lattice parameters were determined from electron diffraction images using Powder Diffraction File 4+ (PDF) entries 04-001-3770 (cadmium oxide) and 00-006-0302 (sodium iodide). Lattice parameters were directly measured using the Fast Fourier transformed TEM images at high magnification, where lattices were visible. For data processing using Fast Fourier transformation (FFT), Gatan Digital Micrograph software was used.

Scanning electron microscopy (SEM) and elemental mapping of a neat CdO-NaI sample (calcined in air) was performed on a JEOL JSM-7001F instrument. Samples were coated with platinum before the analysis.

4.4.3 In-situ powder X-ray diffraction

Powder X-ray diffraction (XRD) was performed at the Powder Diffraction beamline at the Australian Synchrotron. A lanthanum hexaboride standard (NIST 660b) was used to perform a calibration run at room temperature. The wavelength and zero offset were then refined using the software package GSAS-EXPGUI [7, 8] via the Rietveld method. The wavelength and zero offset were determined to be 0.7930492 Å and -0.0029907 ° 2θ, respectively. A CdO-NaI sample (calcined in air) was analysed in a quartz capillary while being purged with nitrogen and the capillary heated using a hot air blower. XRD patterns were re-calculated from degrees 2θ at their respective wavelength into the wavelength-independent scale of Q using the software package CMPR [9].

A pure sodium iodide reference sample was measured at ambient conditions on a Bruker D8 focus powder diffractometer using Cu Kα radiation.

4.4.4 Fixed bed CO₂ sorption and residual gas analysis

Analysis of the exit gas during the sorption and desorption of CO₂ in a fixed bed was performed on a Micromeritics AutoChem II 2950 instrument equipped with a MKS Cirrus 2 mass spectrometer (MS). This system allows a gas to be purged through a heated fixed-bed sample while analysing the outlet gas using the mass spectrometer. A non-calcined/oven dried (carbonate) sample and a sample calcined in air were analysed and sample masses of between 0.26 g (calcined in air) and 0.87 g (oven-dried) were used. A blank run with no sample was used to observe background readings given by the mass spectrometer.

The measurement program is shown in Figure 4.4.1. In two sets, mass spectra (mass to charge, $m/z = 1 - 200$) were obtained continuously. First, this measurement was performed over the initial temperature ramp in nitrogen purge. A second set of mass spectra was acquired under isothermal conditions at 300 °C after the switch to 50 % CO₂ in N₂ for 30 minutes, and subsequent N₂ purge for another 30 minutes. Over the temperature ramp, mass spectra were assigned to the appropriate temperature by estimating the position on the 5 °C/min ramp using the elapsed time of the experiment, as temperature records were kept separate to the mass spectra over time (due to software limitations).

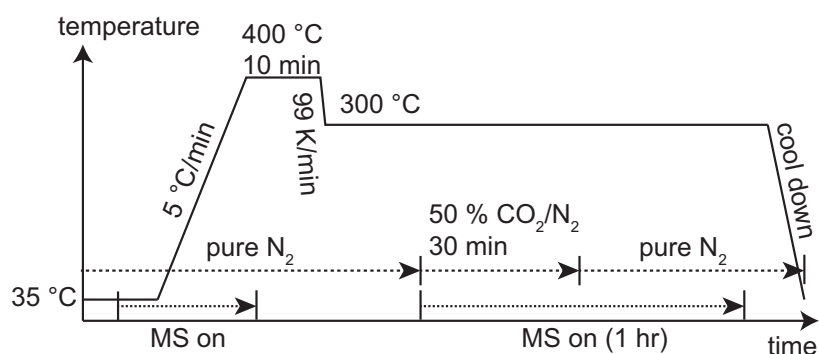


Figure 4.4.1: AutoChem fixed-bed exit gas mass spectrometry program

4.4.5 X-ray photoelectron spectroscopy

X-ray photoelectron spectroscopy (XPS) analysis was performed at CSIRO Materials Science and Engineering using an AXIS Ultra DLD spectrometer (Kratos Analytical Inc., Manchester, UK) with a monochromated Al K α source at a power of 140 W (14 kV \times 10 mA), a hemispherical analyser operating in the fixed analyser transmission mode and the standard aperture (analysis area: 0.3 mm \times 0.7 mm). The total pressure in the

main vacuum chamber during analysis was typically 10^{-8} mbar. Survey spectra were acquired at a pass energy of 160 eV. To obtain more detailed information about chemical structure, oxidation states etc., high resolution spectra were recorded from individual peaks at 20 eV pass energy (yielding a typical peak width for polymers of 1.0 eV).

Samples were filled into shallow wells of custom-built sample holders. One lot of each sample was prepared and 2 different locations were analysed on each sample at a nominal photoelectron emission angle of 0° w.r.t. the surface normal. Since the actual emission angle is ill-defined in the case of particles (ranging from 0° to 90°) the sampling depth may range from 0 nm to approx. 10 nm.

Data processing was performed using CasaXPS processing software version 2.3.15 (Casa Software Ltd., Teignmouth, UK). All elements present were identified from survey spectra. The atomic concentrations of the detected elements were calculated using integral peak intensities and the sensitivity factors supplied by the manufacturer. Binding energies were referenced to the aliphatic hydrocarbon peak at 285.0 eV and peaks identified using the NIST XPS database [10].

The accuracy associated with quantitative XPS is approx. 10 % to 15 %. Precision (i. e., reproducibility) depends on the signal/noise ratio but is usually much better than 5 %.

4.5 Results

4.5.1 Sample morphology

TEM images of the as-synthesised sample calcined in nitrogen, as well as of pure CdO made from CdCO_3 , are shown in Figure 4.5.1 along with their respective selected area electron diffraction patterns. It can be observed that both the neat mixed sorbent and the neat CdO sample consist of spherical nanoparticles of approx. 250 nm diameter (Figure 4.5.1a and c). The samples appear highly crystalline, as indicated by a spot electron diffraction pattern (Figure 4.5.1b and d), and the pattern was matched with cadmium oxide using Powder Diffraction File entry 04-001-3770. A similar observation has been made for a sample calcined in air [6]. It appears that the two calcined samples and the CdO reference sample are similar in morphology; in other words the morphology is

independent of the mode of calcination (in air or nitrogen) or the sodium iodide addition. Sodium iodide was not observed in the CdO-NaI sample and so it is assumed to be present as either discrete nanoparticles that were not sampled by the TEM experiments, or else amorphously distributed over the cadmium oxide (i. e., in non-crystalline form).

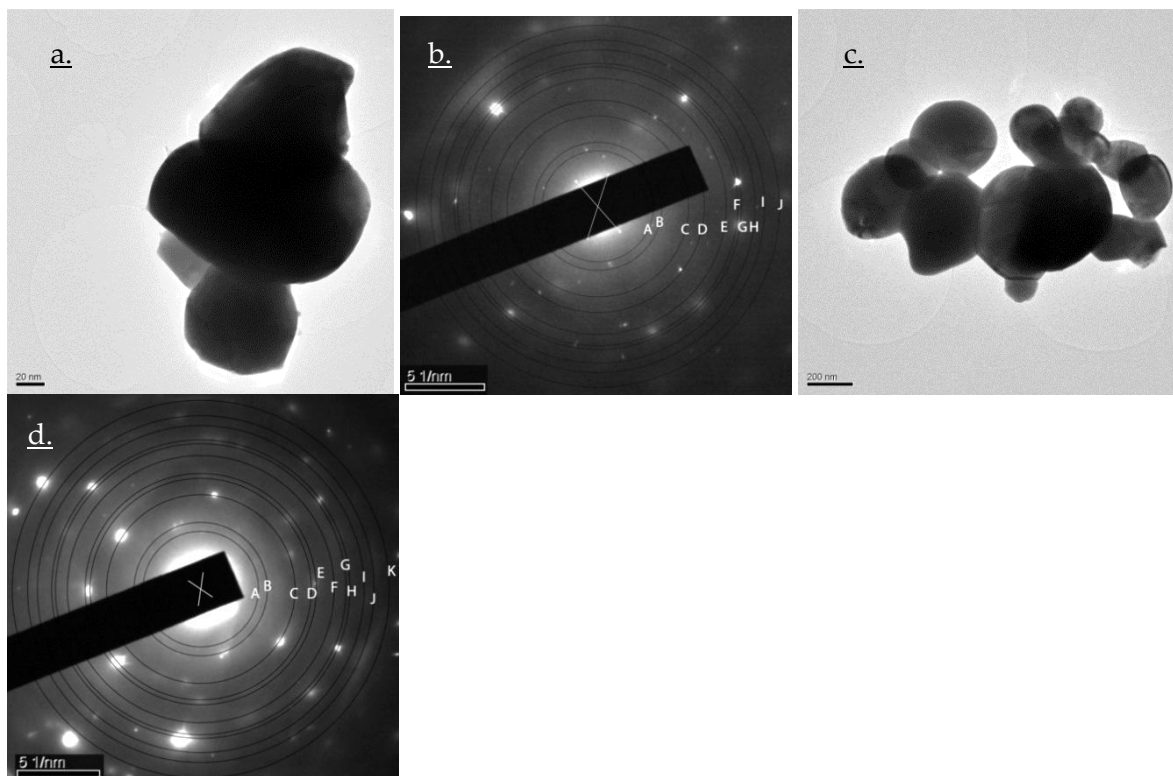


Figure 4.5.1: TEM images and electron diffraction patterns of CdO-NaI sorbent calcined in N_2 (a, b), pure CdO made from $CdCO_3$ (c, d). Assignments A-K are made according to Powder Diffraction File entry 04-001-3770 for CdO.

Figure 4.5.2 shows TEM images and diffraction obtained for a CdO-NaI sample calcined in air after exposure to 25 cycles of isothermal CO_2 sorption at 305 °C. The sorption cycling had effects on the morphology of the sample. It can be observed that formerly spherical particles (Figure 4.5.1a) became slightly fractured on their edges (Figure 4.5.2a). In this specimen, sodium iodide was also identified, as evident in the EDX spectrum (Figure 4.5.2, EDX-1c). In Figure 3c, it can be seen that discrete sodium iodide grains are present. It appears these are located adjacent to areas of high cadmium concentration, which indicates the presence of cadmium oxide and sodium iodide in separate nanoparticles.

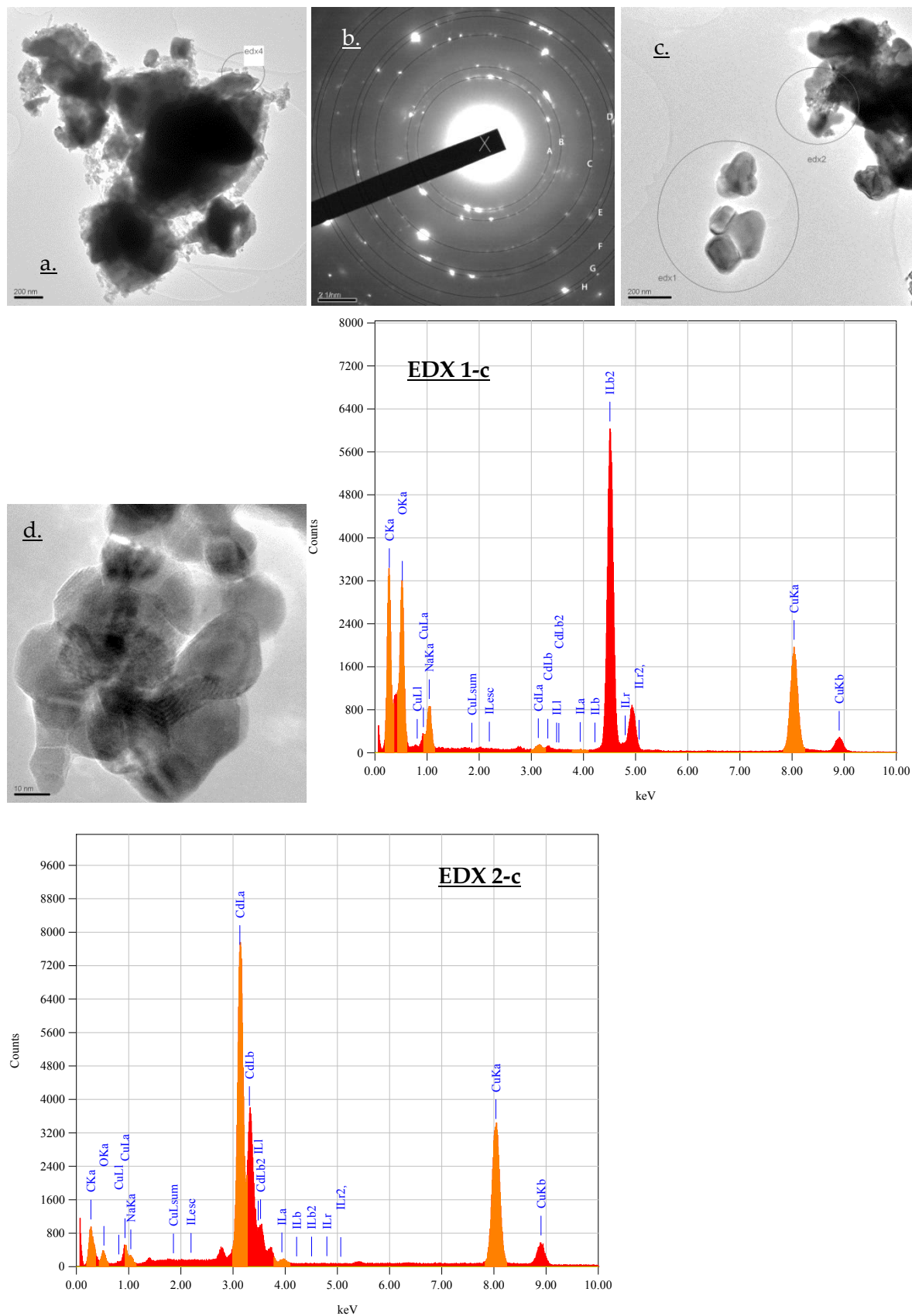


Figure 4.5.2: TEM images (a, c, d) and electron diffraction pattern (b) of a CdO-NaI mixed sample calcined in air, after 25 CO₂ sorption cycles. EDX spectra refer to image c. Assignments A-K are made according to Powder Diffraction File entry 04-001-3770 for CdO.

A more drastic morphology change is evident for the sample calcined in nitrogen after exposure to 25 CO₂ sorption cycles (Figure 4.5.3). The more severe fracturing of the particle calcined in nitrogen might be due to the more stoichiometrically complete CO₂ sorption and desorption reactions that have occurred over this sample. As the sample calcined in air lost capacity very rapidly (refer Chapter 3, section 3.14.1), the last of the 25 sorption cycles did not affect the stoichiometric conversion of CdO to CdCO₃. This might, in turn, have caused less expansion and contraction of the material during formation and decomposition of carbonate. It is likely that the mass density change when cycling between the carbonate and the oxide might be the fundamental cause of this fracturing. It can be noted that the density of cadmium oxide is reported to be between 6.95 g/mL (amorphous) to 8.15 g/mL (crystalline), whereas the density for cadmium carbonate is 5.3 g/mL [11]. Once carbon dioxide enters the oxide and carbonates are formed almost stoichiometrically, the density reduces, i.e., the material expands due to carbonate formation. This might create mechanical stress that eventually leads to cracks in the material nanoparticles. Upon the next carbon dioxide sorption cycle, this is repeated, leading to fractured material as shown by the TEM images (like shown in Figure 4.5.3).

For the upper section of the particle (labelled 'ED' in Figure 4.5.3a), the electron diffraction pattern (Figure 4.5.3b) shows discrete crystalline sodium iodide. High-resolution images show lattice fringes, which were measured by Fast Fourier transformation and were identified as both cadmium oxide and sodium iodide (Figure 4.5.3d and e and PDF entries NaI 00-006-0302 $d = 3.74 \text{ \AA}$ (111), CdO 04-001-3770 $d = 2.35 \text{ \AA}$ (111)). Thus, in this sample it appears that sodium iodide is presumably distributed over the sample as small crystallites in an uneven manner.

In order to further investigate the distribution of sodium iodide and cadmium oxide throughout the sample, a neat mixed CdO-NaI sample calcined in air was analysed via scanning electron microscopy (SEM), with elemental mapping at a lower magnification than is possible in TEM. The SEM image is shown in Figure 4.5.4. It shows that particles of more than a micrometre size are also present in the sample, which could not be seen in TEM.

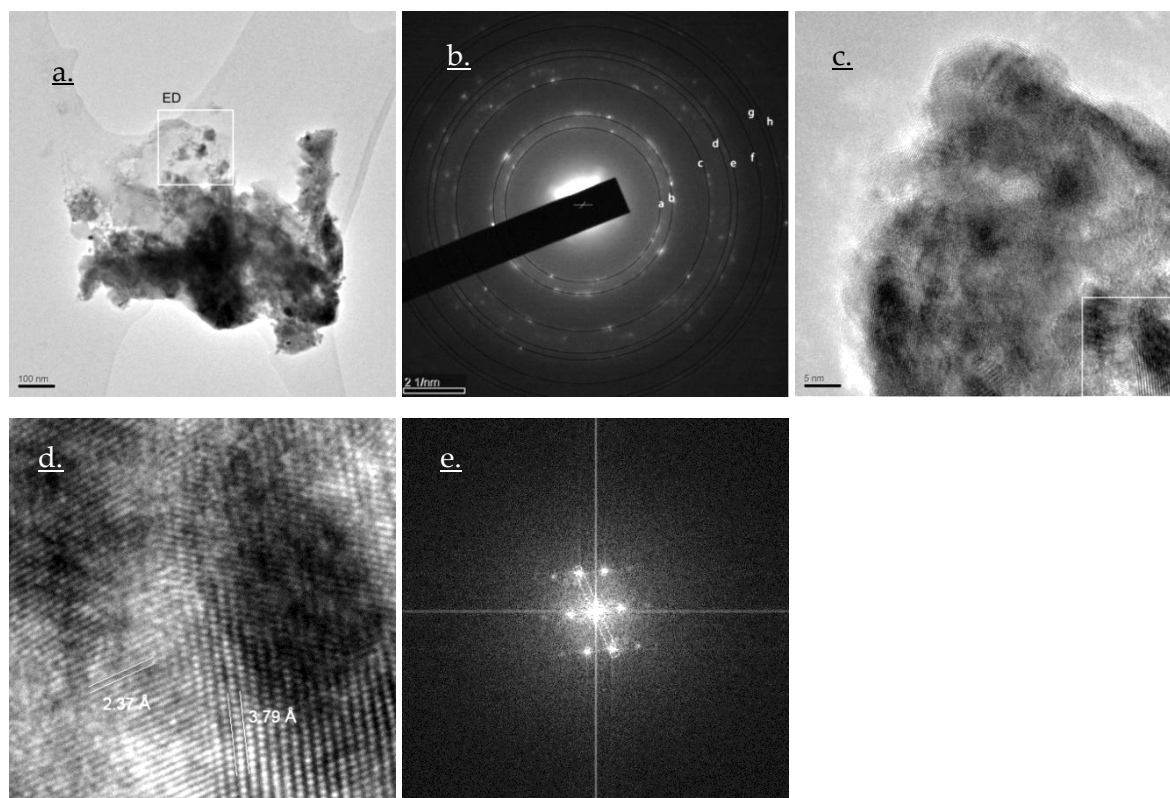


Figure 4.5.3: TEM images (a, c, d) and electron diffraction pattern (b, corresponding to box 'ED' in a) of a CdO-NaI sample calcined in N_2 , after 25 cycles of CO_2 sorption and desorption, d. boxed area in c. enlarged, e. FFT image of d. used to calculate lattice parameters. Assignments a-h correspond Powder Diffraction File entry 00-006-0302 (NaI).

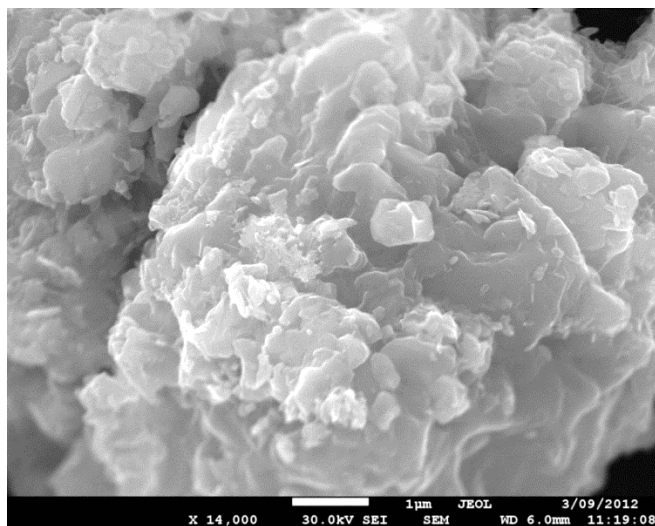


Figure 4.5.4: SEM image of a fresh CdO-NaI sample calcined in air.

The elemental maps (Figure 4.5.5) confirm the aforementioned uneven distribution of sodium and iodine throughout the sample. It can be observed that each of the elements is dispersed throughout the sample in a different fashion. Given the method of sample

preparation, one might expect cadmium and oxygen would be at relatively similar positions, as would sodium and iodine. However this is not the case. Spots where iodine but no sodium is present (white arrow) were found in the elemental maps. The segregation of iodine and sodium could be due to oxidation of iodide to iodine, which might evaporate and re-deposit on the surface of the sample.

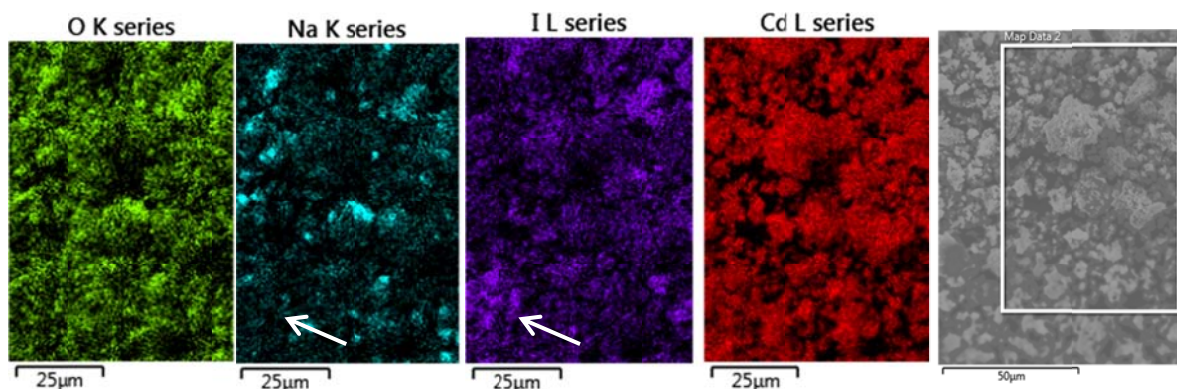


Figure 4.5.5: SEM elemental maps and electron image of the mapped area of a fresh CdO-NaI sample calcined in air.

4.5.2 Exit gas analysis during a CO₂ sorption experiment

In order to further investigate the role of the sodium iodide during the capacity decay during CO₂ sorption cycles (as reported in Chapter 3, section 3.14.2, where it was shown that iodine is lost from the samples), a study of the exit gas composition during CO₂ sorption and desorption was undertaken.

Examples of mass spectra from the fixed-bed exit gas analysis are given in Figure 4.5.6 (blank runs with nitrogen and with nitrogen/CO₂), Figure 4.5.7 (calcined CdO-NaI sample, ramp test in nitrogen) and Figure 4.5.8 (calcined CdO-NaI, sampling during CO₂ addition). The blank run (Figure 4.5.6) showed nitrogen at $m/z = 28$ and 14 , together with other distinct background spectra (all other m/z). Carbon dioxide addition to a blank run gave additional peaks at $m/z = 44$, 16 and 12 (Figure 4.5.6b). The spectra observed for nitrogen and CO₂ are in clear agreement with reference spectra obtained from the NIST library [12]. A mass-to-charge $m/z = 17$ was used to identify water. This is because $m/z = 18$ was conflicted, as it gave a strong background peak in the blank run (Figure 4.5.6).

For the CdO-NaI sample pre-calcined in air, water was released during the initial ramp (refer Figure 4.4.1) between 117 and 167 °C (refer Table 4.5.1 and Figure 4.5.7b). Increasing the temperature further led to a release of ions at $m/z = 127$, which can be assigned as I⁺

(Figure 4.5.7b). The evolution of this peak eventually ceased at a higher temperature of 341 °C, but was once again observed as soon as CO₂ was added to the process (Figure 4.5.8), then stopped as soon as CO₂ addition was terminated.

The position of the iodine peak, at $m/z = 127$, indicates that the species of iodine in the mass spectrometer must be either I⁺ or I₂²⁺, suggesting that the species evolving from the sample is iodine in its elemental form. If this is the case, the oxidation of the iodide species contained within the NaI initially added to the sample during preparation must have occurred, as the ionic form contained in NaI is considered non-volatile in this temperature range (as confirmed in a TGA experiment shown in [6]).

A similar behaviour was observed for the non-calcined sample (Table 2). The sample lost water during the ramp test, then CO₂ (due to in-situ decarbonation) and an iodine species. Under CO₂ addition, at the isothermal setting, iodine release was also observed in a similar manner to the sample calcined in air, as illustrated in Figure 4.5.7 and Figure 4.5.8. It must be noted that the temperatures were different (Table 4.5.2). Water release started at a much lower temperature and took higher temperatures to complete; this is attributable to the lack of an ex-situ pre-treatment that would have otherwise driven off a substantial amount of water already. The higher temperatures required for iodine release for the non-calcined samples (compare Table 4.5.1 and Table 4.5.2) indicate the possibility that different species of iodine are present in the two samples. It is speculated that the sample pre-calcined in air already contained a relatively volatile species of iodine (potentially I₂) prior to the exit gas analysis, and that this had completely evaporated prior to the end of the temperature ramp; whereas, for the non-calcined sample, an iodine species was still being released at the end of the ramp. In the latter, the iodine evolution ($m/z = 127$) stopped as soon as the temperature was lowered to 300 °C, and prior to the addition of CO₂.

As this iodine species was also released from the sample during CO₂ addition, it can be concluded that CO₂ itself has an effect on a reaction that transforms the iodide into a volatile species, possibly due to oxidation. This might also explain why iodine is dislocated from sodium, as evident in the element maps; i.e. because a volatile form of iodine might partially re-deposit elsewhere throughout the sample (Figure 4.5.5).

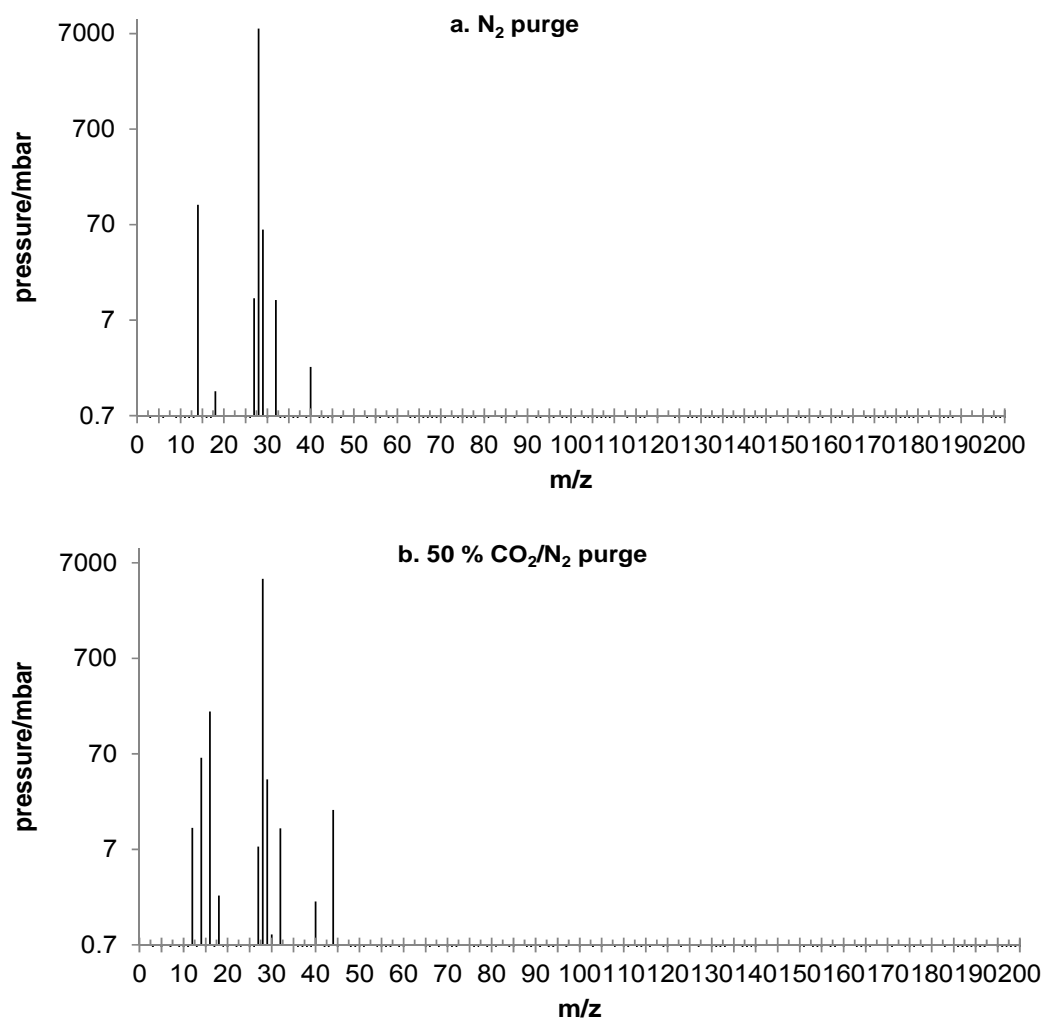


Figure 4.5.6: Exit gas mass spectra for a fixed-bed blank run. a. during N₂ purge, b. during 50 % CO₂ in N₂ purge. Note: Spectra were observed to be independent of temperature setting (isothermal or ramp).

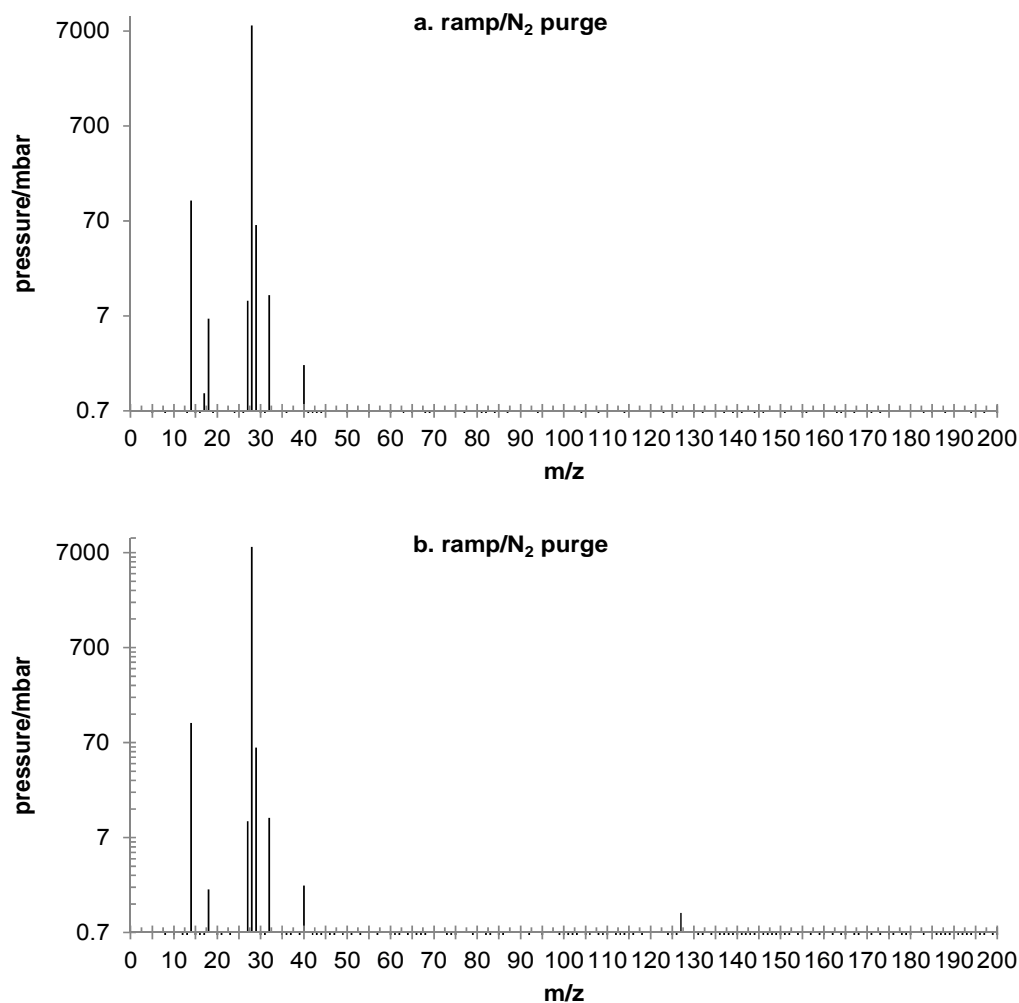


Figure 4.5.7: Examples of gas mass spectra obtained during the first temperature ramp for a CdO-NaI sample calcined in air. a. high amounts of water released at 148 °C, b. iodine release at 304 °C.

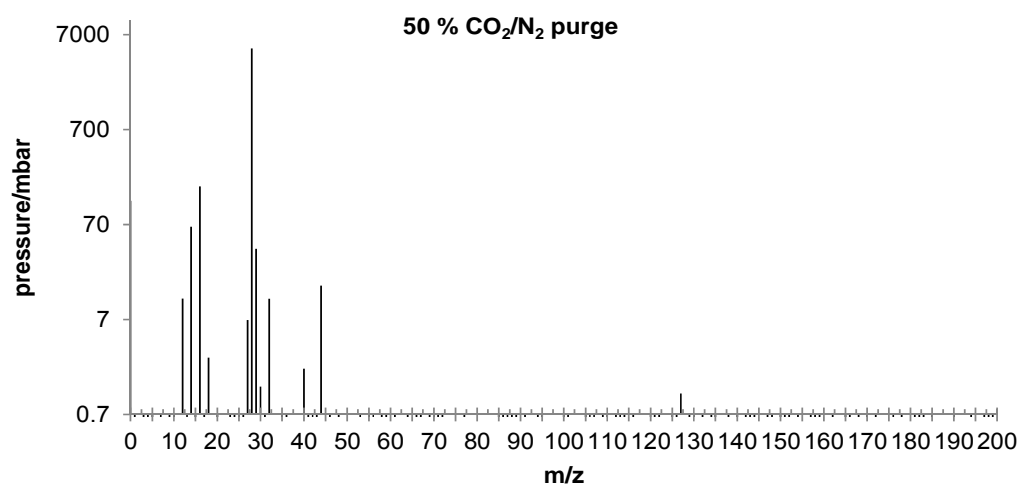


Figure 4.5.8: Exit gas mass spectrum of a calcined CdO-NaI sample during CO₂ addition at 300 °C showing iodine release.

Table 4.5.1: Temperatures for release of compounds during the temperature ramp test for the CdO-NaI sample calcined in air before the experiment

compound, m/z	start, °C	end, °C
water, 17	117	167
iodine, 127	272	341

Table 4.5.2: Temperatures for release of compounds during the temperature ramp test for the CdCO₃-NaI sample used in the carbonate state (decarbonated in fixed-bed instrument)

compound, m/z	start, °C	end, °C
water, 17	47	end of ramp
iodine, 127	391	end of ramp
CO ₂ , 44	249	end of ramp

4.5.3 X-ray photoelectron spectroscopy

4.5.3.1 Surface concentration of iodine

Table 4.5.3 shows the surface elemental ratio of iodine to sodium (mol/mol) for a calcined CdO-NaI sample before and after cyclic CO₂ exposure as well as for a pure NaI reference sample. It can be observed that the initial iodine content was reduced by calcination in both air and nitrogen. A further loss in iodine was observed after subjecting the samples to 25 CO₂ sorption/desorption cycles. The trends seen within these results are in general agreement with elemental analysis results given in Chapter 3, section 3.14.2. The higher iodine content in the fresh sample calcined in air compared to the one calcined in N₂ are an exception to this. It must however be noted that the surface analysis performed by XPS (which typically penetrates between two to five nanometres, [13]) is not necessarily representative of the bulk material; so that it appears that the general agreement between the bulk elemental analysis and XPS analysis is reasonable.

Table 4.5.3: Molar ratios of iodine to sodium as determined by XPS

	pure NaI	CdO-NaI calcined in air	CdO-NaI calcined in N ₂	CdO-NaI calc. air after 25 cycles	CdO-NaI calc. N ₂ after 25 cycles
I/Na (mol/mol)	0.97	0.85	0.67	0.16	0.32

4.5.3.2 Cadmium 3d

The plots of the high-resolution X-ray photoelectron (XP) spectra for cadmium 3d in a pure cadmium oxide sample as well as the fresh/calcined and used CdO-NaI samples are shown in Figure 4.5.9. Graphs are shown on binding energy scale and positions were corrected to the aliphatic hydrocarbon C 1s peak. For the reference CdO sample made from CdCO₃ by calcination in air (500 °C, 3 hours), the Cd 3d 5/2 peak is evident at 405 eV (Figure 4.5.9a). In comparison, the XP spectra of the fresh/calcined CdO-NaI samples show the 3d 5/2 peak at 404.5 eV, being at slightly lower binding energies than the reference CdO sample.

In the XPS database, it is reported that CdO has a distinctly lower Cd 3d 5/2 binding energy than Cd(OH)₂ and CdCO₃ (Table 4.5.4). The peak for the reference CdO sample has a binding energy that is higher than Cd in pure CdO, indicating that the surface of this sample is substantially in the form of CdCO₃ or Cd(OH)₂. A different study [14] also reported surface hydroxide and carbonate formation on a single crystal of CdO, which resulted in higher binding energies for the carbonate species (in [14], 405.9 eV) than for the oxide (404.2 eV).

In the current study, the higher Cd binding energy of the reference CdO sample may, on the one hand, be due to incomplete calcination. It has been described in the literature that the decomposition of cadmium carbonate to oxide is aided by the presence of sodium halides [15]. This 16 lines long communication entry hypothesises that the migration of alkali metal ions onto Cd²⁺ positions and a following anion vacancy mechanism ('Anionenleerstellenmechanismus') promotes diffusion and collective crystallisation ('Sammelkristallisation') of CdO. This would be consistent with reduced surface decarbonation for the reference CdO sample. On the other hand, hydroxylation or re-carbonation of the reference CdO sample surface may have occurred more extensively, as

the reference sample had been stored in a desiccator for a week before the XPS analysis, whereas the neat mixed CdO-NaI samples were only stored for two days. The slightly lower binding energy of the neat CdO-NaI samples corresponds to CdO.

The 3d 3/2 peak at ~ 411 eV shows a similar behaviour (i. e., shifting) for the different cadmium compounds studied here, as expected.

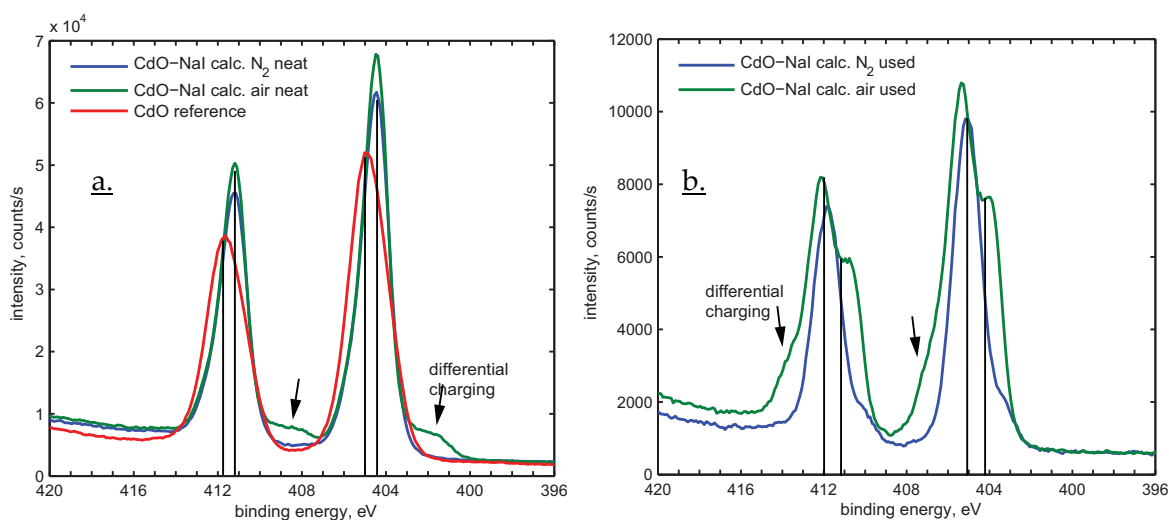


Figure 4.5.9: XP spectra for Cd 3d of neat mixed CdO-NaI samples and pure CdO (a) and CdO-NaI after 25 CO₂ sorption cycles (b).

Table 4.5.4: Literature values for Cd 3d binding energies taken from [10] (except *). Averages were taken if multiple entries in the same order of magnitude were found in the database.

compound	binding energy (eV)	remarks
CdCO ₃	405.1	3d 5/2, one entry
CdO	404.2	3d 5/2, average
Cd(OH) ₂	404.9	3d 5/2, average
CdO	411 *	3d 3/2, graph in [14]

The satellite peaks for the neat sample calcined in air (401 and 408 eV, arrow in Figure 4.5.9a) are also noteworthy. These are considered to be caused by sub-optimal compensation of differential sample charging by the charge neutraliser during analysis. This would indicate regions of varying levels of charging across the sample surface which could not be uniformly compensated, despite efforts being made to optimise charge neutraliser settings for each sample separately. It must be noted that charge neutralisation proved difficult for all samples analysed in this study.

The samples that were subjected to 25 CO₂ sorption cycles show a distinct Cd 3d 5/2 peak at 405 eV, indicating carbonation of the surface (Figure 4.5.9b). For the air-calcined sample, a distinct shoulder (arrow) is apparent at 404 eV, indicating a substantial amount of CdO on the surface. This shoulder is less evident for the sample calcined in nitrogen. This can be associated with the loss of iodine, which acts as a promoter for carbonation. A more substantial iodine loss was observed for the air-calcined sample than for the nitrogen-calcined sample (refer Chapter 3, section 3.14.2). The loss of iodine apparently causes the air-calcined sorbent to take up carbon dioxide less readily. It must be noted that these samples were left in sealed vials inside a desiccator for a week before XPS analysis. It was possible that the samples were exposed to atmospheric CO₂ left within the vials during this time, enabling slow carbonation on the surface.

Also noteworthy is a slight shift of the peak at 405 eV to higher binding energy for the sample calcined in air. This is considered to be an artefact caused by sub-optimal charge compensation (see above).

4.5.3.3 Oxygen 1s

Plots of XP spectra for the oxygen 1s line are shown in Figure 4.5.10. It is evident that the CdO reference sample has a distinct peak at 531.4 eV, which matches with the database entry for oxygen in CdCO₃ (Table 4.5.5). The peak is also evident for the neat CdO-NaI mixed samples calcined in air and N₂, but less prominent than another one observed at 529 eV for these samples (more aligned with 529.6 eV reported for CdO (Table 4.5.5)). Pure NaI gives two peaks in this region, at 531.5 and at 535 eV, which are also assumed to overlap the CdO-NaI spectra, giving a broad shoulder (arrow in Figure 4.5.10a, small peak in Figure 4.5.10b at 536 eV). These peaks are Na KLL Auger peaks [16]. At around 535 eV, oxygen in water also gives a peak, which might be observed here due to the hygroscopic nature of the sodium iodide.

Samples exposed to 25 CO₂ sorption cycles showed the peak at 531.4 eV (CdCO₃), whereas the sample calcined in air also showed a small peak at 529 eV (CdO), indicating the latter sample is less prone to carbonation due to the missing iodide promoter.

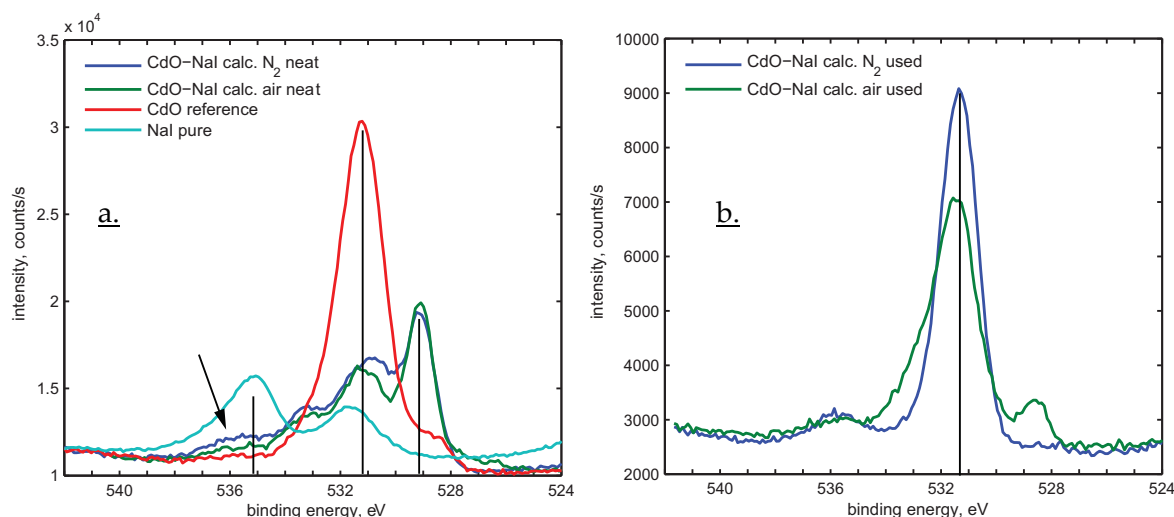


Figure 4.5.10: XP spectra for O 1s of neat mixed CdO-NaI samples and pure CdO (a) and CdO-NaI after 25 CO_2 sorption cycles (b).

Table 4.5.5: Literature values for O 1s binding energies taken from [10]. Averages were taken if multiple entries in the same order of magnitude were found in the database.

compound	binding energy (eV)	remarks
CdO	529.6	average
$CdCO_3$	531.4	one entry
$Cd(OH)_2$	530.9 and 532.5	two different entries
H_2O	534.95	average

These results support the observations made for the Cd 3d XP spectra as described in section 4.5.3.2 and are in general agreement. It is, however, hard to determine from the O 1s spectra if surface cadmium hydroxide is present, as the database gives two very different entries for oxygen in $Cd(OH)_2$ at 530.9 and 532.5 eV (Table 4.5.5).

4.5.3.4 Carbon 1s

Figure 4.5.11 shows the XP spectra for carbon. The aliphatic hydrocarbon peak is evident in all samples at 285 eV (to which it was aligned for normalisation). The samples, especially the reference CdO sample, have another distinct peak between 289.0 and 289.5 eV. This peak position is indicative of carbon in cadmium carbonate (Table 4.5.6).

The high intensity of the cadmium carbonate peak for the reference CdO sample indicates the presence of the cadmium carbonate on the surface, as had been described for the

cadmium spectra in section 4.5.3.2. This may be due to re-carbonation of the surface due to atmospheric exposure or incomplete calcination.

The low binding energy shoulder for the neat CdO-NaI sample calcined in air (~ 282.5 eV) was considered to be due to sub-optimal charge compensation as described in section 4.5.3.2.

An adventitious carbon peak is also clearly evident for pure sodium iodide. In this case, a second chemically shifted peak also appears at higher binding energy, but slightly lower (< 289 eV) than the carbonate peak; it is attributed to adventitious carbon subspecies, such as carboxylic acids, present on the surface of this sample.

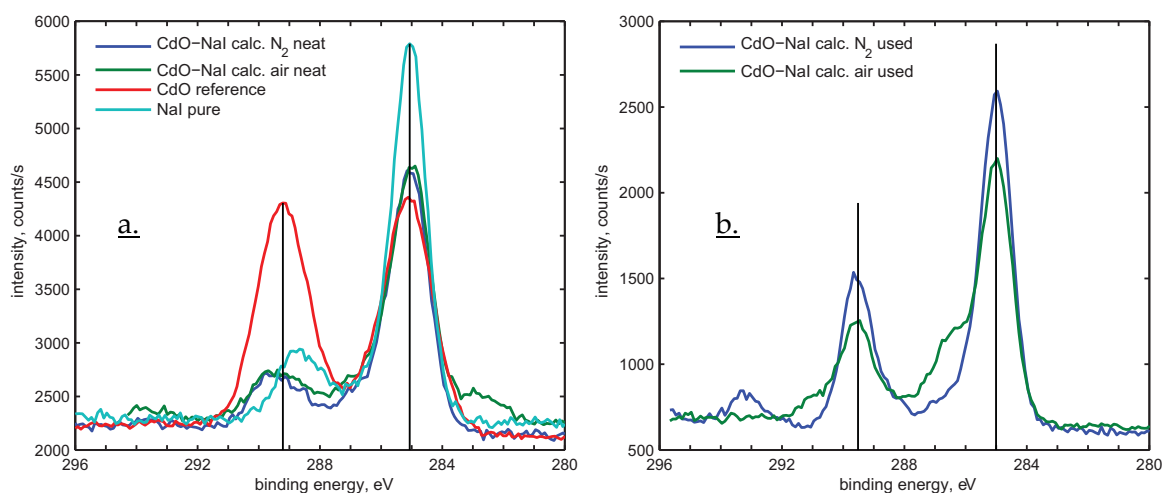


Figure 4.5.11: XP spectra for C 1s of neat mixed CdO-NaI samples, pure CdO and NaI (a) and CdO-NaI after 25 CO₂ sorption cycles (b).

Table 4.5.6: Literature values for C 1s binding energies. Averages were taken if multiple entries in the same order of magnitude were found in the database.

compound	binding energy (eV)	remarks
adventitious carbon	285	used for alignment
CdCO ₃	289.4	average, [10]

4.5.3.5 Iodine 3d

XP spectra for the iodine 3d line are given in Figure 4.5.12. It can be observed that pure sodium iodide gives a doublet peak of 619.5 (I 3d 5/2) and 631 eV (I 3d 3/2). This is in

agreement with the iodine observed within the calcined mixed CdO-NaI samples, indicating sodium iodide still being present in both the neat and used samples.

A peak of low intensity at 631 eV (Figure 4.5.12b) for the air-calcined sample after CO₂ cycles indicates a lowered iodine content on the surface, as discussed before (section 4.5.3.2). It must be noted that cadmium has a peak at 618.4 eV (Cd 3p 3/2) that overlaps with the iodine spectra (this can be seen for the reference CdO sample shown in Figure 4.5.12a), so a distinct peak is observed at this position also for the used/air-calcined sample, as cadmium was still present in the sample after the sorption cycles.

Another doublet peak is evident at 636 and 624.5 eV. The XPS database gives the entries shown in Table 4.5.7, indicating that iodates (IO₃⁻ and IO₄⁻) can likely be assigned to these peaks. Thus, it appears that iodide was oxidised upon calcination. The additional shoulder at lower binding energy for the neat CdO-NaI sample calcined in air (628 eV, arrow in Figure 4.5.12a) is assumed to be due to sub-optimal charge compensation, as discussed already for cadmium and carbon (sections 4.5.3.2 and 4.5.3.4).

Iodine (I₂) is assumed not to be observable on the surface of any sample. As it is a volatile compound under the calcination and CO₂ sorption conditions studied here, it was considered to evaporate immediately during the process, if it was formed. Its melting point is reported at 113.5 °C, its boiling point at 184.35 °C [17], and, thus, lower than CO₂ sorption temperatures around 300 °C or calcination temperatures of 500 °C.

It is noteworthy that this more highly oxidised iodine is consumed during CO₂ sorption after calcination, as the iodine spectra after CO₂ cycles for the sample calcined in nitrogen do no longer clearly show any sign of peaks around 636 and 624.5 eV, whereas the sample calcined in air shows a remainder of it, as evident by small peaks in this range (Figure 4.5.12b).

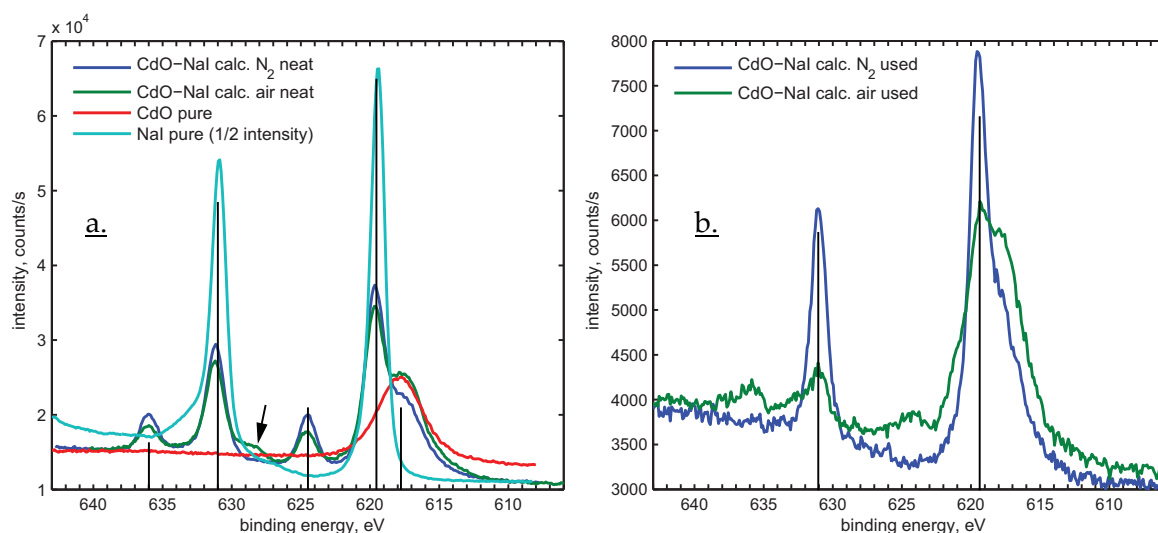


Figure 4.5.12: XP spectra for I 3d of neat mixed CdO-NaI samples, pure CdO and NaI (a) and CdO-NaI after 25 CO_2 sorption cycles (b).

Table 4.5.7: Literature values for I 3d binding energies taken from [10]. Averages were taken if multiple entries in the same order of magnitude were found in the database. Cd 3p shown for comparison.

compound	binding energy (eV)	remarks
NaI	618.55	average
I ₂	620.35	average
NaIO ₃	623.5	one entry
NaIO ₄	624	one entry
(Cd 3p 3/2)	(618.4)	Cd, element/metal, one entry

4.5.3.6 Sodium 1s

XP spectra for sodium 1s are given in Figure 4.5.13. They show that sodium (assumed to be Na^+) appears similar in all samples and is in good agreement with the NaI entry in the database (Table 4.5.8). Peak differences of less than 0.5 eV are considered to be due to sub-optimal charge compensation (as discussed previously), which are most evident for the neat CdO-NaI sample calcined in air (additional peak shoulder at 1069 eV, arrow in Figure 4.5.13a) and the used CdO-NaI sample calcined in air (shoulder at 1073 eV, arrow in Figure 4.5.13b).

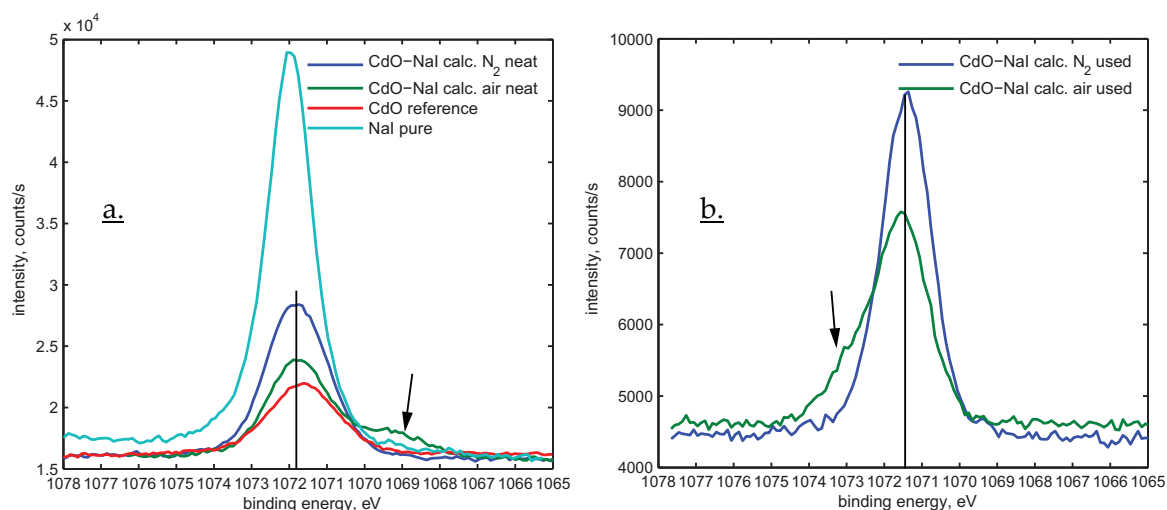


Figure 4.5.13: XP spectra for Na 1s of neat mixed CdO-NaI samples, pure CdO and NaI (a) and CdO-NaI after 25 CO₂ sorption cycles (b).

Table 4.5.8: Literature value for Na 1s binding energy [10].

compound	binding energy (eV)	remarks
NaI	1071.4	one entry

4.5.3.7 Summary of XPS results

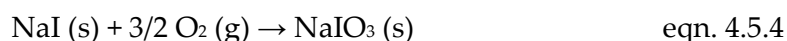
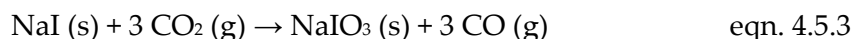
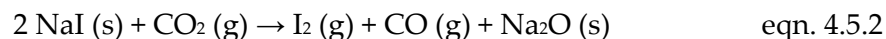
The XPS results indicated that iodine present in the mixed CdO-NaI sample after calcination consists of both iodide species (most likely unaltered sodium iodide as used in synthesis) and a highly oxidised species, potentially iodates. Elemental iodine was not evident, which is not surprising, as it would most likely evaporate during the calcination and CO₂ sorption experiments. This is also in agreement with the exit gas analysis (section 4.5.2), where an m/z of 127 (the g/mol molar mass of iodine) was observed. After 25 CO₂ sorption cycles, this highly oxidised iodine species disappeared, and the iodine loss of the sample that was calcined in air became evident as the peak intensity for iodine got weaker.

The iodine XPS results and the exit gas analysis both suggest that an oxidation of iodide took place during the initial calcination, according to eqn. 4.5.1.



As this was also the case for a sample that was never exposed to air at higher temperatures (the N_2 calcined CdO-NaI sample), it can be concluded that carbonate must play an

important role in the decay mechanism of the sorbents. It can be speculated that the oxygen within the CdCO₃ partially contributes to a formation of either iodine (eqn. 4.5.2) or iodate as a highly-oxidised iodine species upon calcination in both air and nitrogen (using CO₂ evolving from carbonate decomposition, eqn. 4.5.3, or oxygen, if air is present, eqn. 4.5.4).



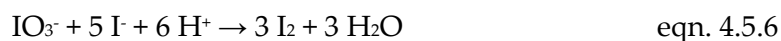
It must, however, be noted that the samples were exposed to atmospheric air during sample handling at room temperature. But given the fact that the samples calcined in air showed a much greater capacity decay and iodine loss than the sample calcined in N₂, it is assumed that exposure to air at room temperature only had a marginal effect on the sample decay.

Iodide has been studied as an ozone destructor [18], where it is considered to be oxidised to iodates [19] at ambient temperatures, according to eqn. 4.5.5.



Mechanistically, similar reactions (eqn. 4.5.1 to eqn. 4.5.4) could also be considered in the case of the CdO-NaI mixed material. No ozone is present here, but oxygen (during calcination in air) and CO₂, a compound which could potentially supply oxygen and decompose to CO. This reaction could likely be catalysed by the presence of cadmium at the high temperatures studied here, as the transition metal cadmium has some catalytic activity (it is stated that cadmium oxide is used as a catalyst in hydrogenation and dehydrogenation reactions [20]). Upon CO₂ sorption, the iodates disappeared, which is considered due to a reduction reaction involving iodide and iodates, forming volatile I₂, which was observed in the exit gas upon CO₂ sorption (section 4.5.2, Figure 4.5.8). For ambient ozone decomposition, the reaction given in eqn. 4.5.6 releases volatile I₂ in the presence of aqueous media (like water vapour or aerosols, to deliver protons) [19]. In this study, water vapour or acidic media were not used, so a different reaction must take place

in order to release iodine under the influence of cadmium compounds and carbon dioxide being present.



XPS spectra of Cd, O and C revealed the re-carbonation of the used NaI-doped samples in atmospheric conditions and the less facile recarbonation of the used air-calcined sample, which had lost a substantial amount of iodide promoter. Surprisingly, a reference CdO sample made from CdCO₃ showed a substantial amount of carbonate. As alkali halides were shown to promote the complete decomposition of cadmium carbonate [15], it is assumed that calcination of the pure CdCO₃ sample to CdO was not complete. XPS spectra for Na showed no significant changes among the samples. This is not surprising, as sodium is most prevalent as Na⁺ and different sodium compounds show only marginal differences in XPS [10]. These were hard to distinguish in the present study, as the samples used exhibited significant differential charging during XPS analyses, which was hard to overcome by charge neutralisation.

4.5.4 In-situ powder X-ray diffraction

Powder X-ray diffraction results of a CdO-NaI sample calcined in air are shown in Figure 4.5.14. It can be observed that the intensities of the pattern became stronger upon increasing the temperature from room temperature to 325 °C, indicating an increase in crystallinity (Figure 4.5.14a). The pattern was assigned to cadmium oxide. A second phase became apparent upon heating, which can be seen in Figure 4.5.14a at $Q < 2 \text{ \AA}^{-1}$ (two peaks). On a different scale and with the peaks assigned to CdO removed, it is evident that this phase is sodium iodide, as can be seen by comparison with a pure reference sample (Figure 4.5.14b).

Cadmium oxide is known to crystallise from an amorphous form upon heating in oxygen [20]. It is, however, noteworthy that the sample was calcined in air before the experiment, loaded to the diffractometer at room temperature and upon heating in nitrogen crystallised even further in nitrogen purge. This indicates that the crystallisation upon heating is either reversible (i. e., reverted by cooling down) or was not completed during the initial calcination in air. The sodium iodide peaks only became evident upon heating (Figure 4.5.14b). It thus appears that crystallinity was increased when the sample was

heated, both for the CdO and NaI phases. It is, however, speculative if this high crystallinity is actually required for the CO₂ uptake reaction performed in the diffractometer at this temperature (as reported in Chapter 3, sections 3.5.1 and 3.14.1), or if the elevated temperature is just a kinetic requirement for the sample to sorb CO₂.

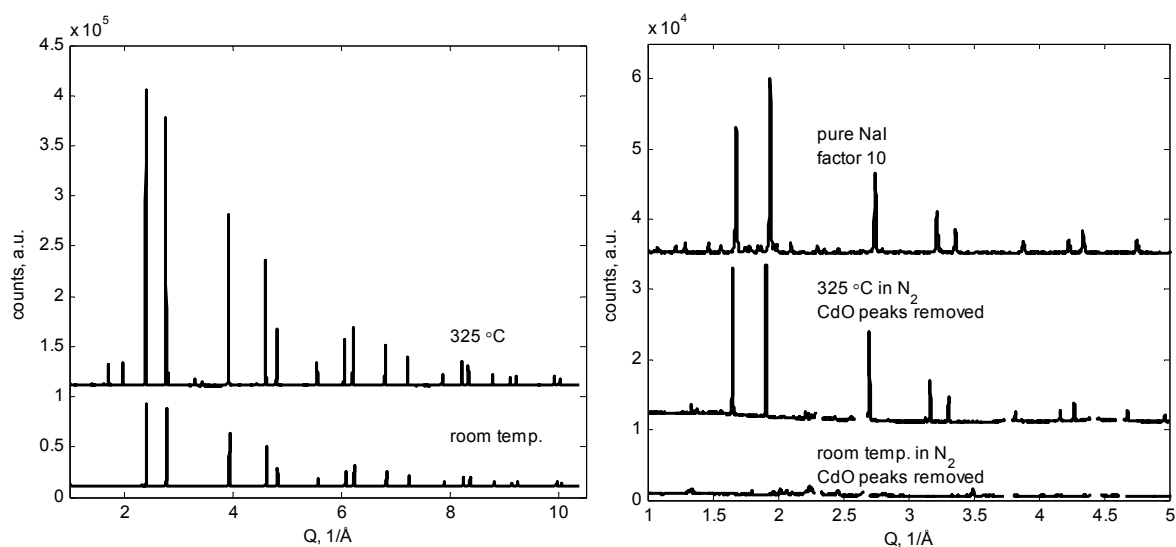


Figure 4.5.14: In-situ powder XRD patterns measured in N₂ purge of a CdO-NaI sample calcined in air. a. Full pattern at room temperature and 325 °C in N₂ purge, b. same dataset as a. but with CdO peaks removed. Intensities for pure NaI reference (lab instrument) multiplied with 10, other intensities to scale.

4.6 Conclusion

In this study, a cadmium oxide/sodium iodide based CO₂ sorbent was examined to gain details about the sorption capacity decay, which was observed in a previous study (Chapter 3, section 3.14.1). The change in morphology and crystallinity upon multiple-cycle CO₂ sorption was also analysed.

In-situ powder XRD revealed that the crystallinity of both cadmium oxide and sodium iodide in the sample significantly increased during heating of the sample in nitrogen flow to CO₂ sorption temperature. It can be speculated that high crystallinity of the CO₂ capture reactant (CdO) and its promoter (NaI) might be important for the CO₂ uptake reaction. It might, however, also be a simple kinetics consideration that higher temperatures than room temperature are required for CO₂ sorption with adequate reaction rates, with the increase in NaI and CdO crystallinity at higher temperatures being coincidental and not relevant for an improved carbonation behaviour of the material.

TEM revealed that the CdO-NaI mixed material consisted of crystalline and regularly-shaped spherical nanoparticles of approx. 250 nm diameter, which were fractured during multicyclic CO₂ sorption, possibly due to a mass density change during the reversible transformation of cadmium carbonate into oxide. These fractures could explain an initial rise in working capacities during the first cycles of some multicyclic CO₂ sorption experiments (Chapter 3, section 3.14.1) due to void formation and increased accessibility of the particles before the capacity decay took over. SEM also showed bigger nanoparticles than observed in TEM being present in the sample. Sodium iodide was shown to be interspersed irregularly throughout the sample, as seen in a SEM elemental map. Separation of iodine and sodium also suggested a reaction of the iodine and its re-deposition onto the sample into different spots than the sodium.

A CO₂ sorption and desorption experiment in a fixed bed equipped with a mass spectrometer as an exit gas analyser revealed the release of elemental iodine (m/z of 127) during initial calcination and CO₂ addition, whereas XPS confirmed the oxidation of iodide to a highly-oxidised iodate-like compound.

These results confirm that the loss of iodide promoter is related to both oxygen and carbon dioxide-induced oxidation of the iodide originating from the sodium iodide added during synthesis. During progressing CO₂ sorption cycles, it appeared that the iodate compounds were decomposed/reduced again, resulting in mostly iodide being observed in the cycled (used) samples.

Future research should be aimed at confirming CO formation and release to the exit gas by more sophisticated gas mass spectrometry techniques. This could help ascertain the exact mechanism of oxidation and release of the iodine, potentially leading to the design of fixation techniques in order to design a stable promoter for the CO₂ capture reaction that does not take part in a decay mechanism and is removed from the sample.

4.7 Acknowledgements

We thank Christin Patzschke for help with acquisition of SEM data and Anthony Auxilio for assistance with the AutoChem instrument. Monash Centre for Electron Microscopy is acknowledged for the use of the TEM and SEM facilities. The use of the Powder

Diffraction beamline at the Australian Synchrotron is acknowledged for obtaining in-situ XRD patterns. The authors also acknowledge funding provided by the Australian Government through its Cooperative Research Centre (CRC) program to support this CO2CRC research project. Financial support from the Faculty of Science, Monash University, is also gratefully acknowledged.

4.8 References for Chapter 4

- [1] A. A. Olajire, "CO₂ capture and separation technologies for end-of-pipe applications - A review," *Energy*, vol. 35, pp. 2610-2628, 2010.
 - [2] H. Yang, Z. Xu, M. Fan, R. Gupta, R. B. Slimane, A. E. Bland, and I. Wright, "Progress in carbon dioxide separation and capture: A review," *Journal of Environmental Sciences*, vol. 20, pp. 14-27, 2008.
 - [3] R. Singh, M. K. Ram Reddy, S. Wilson, K. Joshi, J. C. Diniz da Costa, and P. Webley, "High temperature materials for CO₂ capture," *Energy Procedia*, vol. 1, pp. 623-630, 2009.
 - [4] A. Doiwa and A. Tomanek, "Die Bildung von Cadmiumcarbonat und Cadmiumsulfid aus Cadmiumoxid," *Zeitschrift für anorganische und allgemeine Chemie*, vol. 334, pp. 12-14, 1964.
 - [5] A. Doiwa and H. Lommel, "¹⁴CO₂-Austausch an Cadmiumcarbonat," *Angewandte Chemie*, vol. 76, pp. 578-578, 1964.
 - [6] C. Vogt, G. P. Knowles, S. L. Y. Chang, and A. L. Chaffee, "Cadmium oxide/alkali metal halide mixtures - a potential high capacity sorbent for pre-combustion CO₂ capture," *Journal of Materials Chemistry A*, vol. 1, pp. 10962-10971, 2013.
 - [7] A. C. Larson and R. B. V. Dreele, "General Structure Analysis System (GSAS)," *Los Alamos National Laboratory Report* vol. LAUR 86-748, 1994.
 - [8] B. H. Toby, "EXPGUI, a graphical user interface for GSAS," *Journal of Applied Crystallography*, pp. 210-213, 2001.
 - [9] B. H. Toby, "CMPR - a powder diffraction toolkit," *Journal of Applied Crystallography*, vol. 38, pp. 1040-1041, 2005.
 - [10] (11/09/2013). *National Institute of Standards and Technology X-ray Photoelectron Spectroscopy Database, Version 4.1*. Available: <http://srdata.nist.gov/xps/>
 - [11] K.-H. Schulte-Schrepping and M. Piscator, "Cadmium and Cadmium Compounds," in *Ullmann's Encyclopedia of Industrial Chemistry: Wiley-VCH Verlag GmbH & Co. KGaA*, 2000.
 - [12] (07/09/2013). *National Institute of Standards and Technology Chemistry Webbook*. Available: <http://webbook.nist.gov>
 - [13] D. A. Skoog, F. J. Holler, and T. A. Nieman, *Principles of instrumental analysis*: Saunders College Publishing, 1998.
 - [14] L. F. J. Piper, P. H. Jefferson, T. D. Veal, C. F. McConville, J. Zuñiga-Pérez, and V. Muñoz-Sanjosé, "X-ray photoemission studies of the electronic structure of single-crystalline CdO(100)," *Superlattices and Microstructures*, vol. 42, pp. 197-200, 2007.
 - [15] A. Doiwa and R. Fischbach, "Zersetzung von Cadmiumcarbonat in Gegenwart von Alkalihalogeniden," *Angewandte Chemie*, vol. 74, p. 495, 1962.
 - [16] T. Kantia, L. Partanen, S. Aksela, and H. Aksela, "High resolution KLL Auger spectra of free sodium and magnesium atoms," *Journal of Electron Spectroscopy and Related Phenomena*, vol. 180, pp. 58-65, 2010.
 - [17] R. C. Weast, *CRC Handbook of Chemistry and Physics*. Cleveland, Ohio: The Chemical Rubber Co., 1968-1969.
 - [18] A. Alebic-Juretic, T. Cvitas, and L. Klasinc, "Ozone Destruction on Solid Particles," *Environmental Monitoring and Assessment*, vol. 44, pp. 241-247, 1997/02/01 1997.
-

- [19] M. A. Brown, J. T. Newberg, M. J. Krisch, B. S. Mun, and J. C. Hemminger, "Reactive Uptake of Ozone on Solid Potassium Iodide," *Journal of Physical Chemistry C*, vol. 112, pp. 5520-5525, 2008/04/01 2008.
- [20] A. F. Holleman, E. Wiberg, and N. Wiberg, *Inorganic Chemistry*. Berlin, New York: Walter de Gruyter, 1995.
-

Chapter 5 Improvement of Mg-Cs mixed sorbents

5.1 Chapter overview

The previous chapters described a novel high-capacity carbon dioxide sorbent based on cadmium oxide. As cadmium compounds are considered toxic, a requirement for appropriate occupational health and safety arrangements is likely if these sorbents are to be applied in an industrial process. Lower-capacity magnesium oxide/cesium carbonate mixed sorbents are therefore still promising candidates for pre-combustion carbon dioxide capture, due to their low toxicity, and thus, still worth studying.

This chapter presents a paper, which concerns the use of magnesium oxide/cesium carbonate composites synthesised by a solvothermal method. This method proved superior to a simple wet-mixing technique used in a previous study. A solvothermally synthesised Mg-Cs composite sorbent showed a higher working capacity. This appears to be a result of better interaction between cesium and magnesium-containing phases created by co-precipitation of the precursors in the solvothermal synthesis. The BET surface areas of these materials were also higher than those produced by wet mixing. TEM analysis showed there was good distribution of the cesium into the magnesium, with occasional clustering of cesium phases.

Declaration for Thesis Chapter

Improvements in the pre-combustion carbon dioxide sorption capacity of a magnesium oxide-cesium carbonate sorbent

Monash University

Declaration for Thesis Chapter 5.2-5.11

Declaration by candidate

In the case of Chapter 5.2-5.11, the nature and extent of my contribution to the work was the following:

Nature of contribution	Extent of contribution (%)
Proposed original idea; prepared and analysed samples; identified major issues; developed interpretations; fully drafted papers and conclusions	70 %

The following co-authors contributed to the work. If co-authors are students at Monash University, the extent of their contribution in percentage terms must be stated:

Name	Nature of contribution	Extent of contribution (%) for student co-authors only
Gregory P Knowles	Aided method development (TGA), input to results analysis, input to manuscript revision	N/A
Alan L Chaffee	Supervision, assisted interpretation of results, editorial assistance	N/A
Jamileh Taghavimoghaddam	Operating electron microscope, input to microscopy results discussion	N/A
Shery L Y Chang	Operating electron microscope, input to microscopy results discussion	N/A

The undersigned hereby certify that the above declaration correctly reflects the nature and extent of the candidate's and co-authors' contributions to this work*.

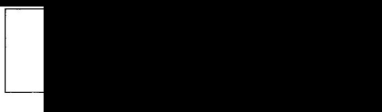
Candidate's
Signature



Date

26/9/13

Main
Supervisor's
Signature



Date

27/9/13

*Note: Where the responsible author is not the candidate's main supervisor, the main supervisor should consult with the responsible author to agree on the respective contributions of the authors.

Improvements in the pre-combustion carbon dioxide sorption capacity of a magnesium oxide-cesium carbonate sorbent

Christian Vogt^{#^}, Shery LY Chang⁺, Jamileh Taghavimoghaddam[^] and Alan L Chaffee^{#^*}

[#] Cooperative Research Centre for Greenhouse Gas Technologies (CO2CRC), [^]School of Chemistry, Monash University, VIC 3800 Australia

⁺ Monash Centre for Electron Microscopy, Monash University, VIC 3800 Australia

⁺ Current Address: Ernst Ruska-Centrum, Forschungszentrum Jülich GmbH, 52425 Jülich, Germany

* corresponding author: [REDACTED]

Phone: + [REDACTED] Fax: + [REDACTED]

5.2 Abstract

Cesium carbonate-doped magnesium oxide has been shown to be a prospective candidate for pre-combustion CO₂ capture at temperatures between 300 and 410 °C. Materials were synthesised by wet mixing commercially available materials as well as a solvothermal approach using a magnesium methoxide in methanol solution. The materials were activated by heat treatment at 600 to 610 °C in order to yield the active CO₂ sorbent. The sorbents showed working capacities of around 4 wt% in up to 25 partial pressure swing (12 min sorption, 24 min desorption) cycles. If the cesium carbonate was dissolved into the magnesium methoxide solution before solvothermal synthesis, multicyclic working capacities were increased to 5 wt%. BET surface area measurements of the activated materials showed that the solvothermal method led to materials with higher surface areas of ~ 13 m²/g, compared to 3.4 m²/g if made from commercial MgO. Transmission electron microscopy showed the morphology of the activated solvothermally mixed materials to consist of spheres of approx. 50 nm diameter, with crystallinity increasing during heat treatment. Powder X-ray diffraction results confirmed this result and also proposed a similar chemistry during CO₂ sorption of the solvothermally synthesised materials

compared to the ones made from commercial precursors. Elemental mapping using scanning transmission electron microscopy showed a uniform distribution of cesium and magnesium in the sample, with occasional clustering of cesium being visible in some particles. It is assumed that cesium carbonate addition into the solvothermal process created a better mixture of Cs and Mg in the particle than wet mixing onto dispersed particles. This led to the creation of a higher number of active sorption sites and thus, a higher capacity for CO₂ sorption.

5.3 Introduction

Carbon dioxide (CO₂), emitted from activities in the power generation industry, is considered to be a major contributor to anthropogenic climate change. In order to reduce these emissions, carbon dioxide capture has been proposed [1, 2]. While post-combustion capture focusses on the separation of dilute concentrations (up to 15 %) of CO₂ from a conventional power plant flue gas, the pre-combustion process involves separating CO₂ from a fuel gasification synthesis gas (syngas). After gasification, a water-gas shift reactor shifts the carbon monoxide by reacting it with water vapour to carbon dioxide and the valuable hydrogen fuel. A typical concentration of carbon dioxide in the shifted syngas is given as 38 % [3] and its temperature around 200 to 400 °C [4]. Separating the CO₂ in-situ at this temperature would be beneficial, as it could reduce the energy penalty arising from heating or cooling the syngas to required CO₂ separation temperatures. Furthermore, the in-situ removal of CO₂ would drive the shift reaction towards the product, and thus, towards the valuable hydrogen fuel side.

In the temperature range of 250 to 400 °C, a range of metal oxide based sorbents has been proposed to be suitable for CO₂ capture. These include layered double hydroxides [5, 6], lithium zirconates [7], magnesium-potassium double salts [6, 8], a magnesium-cesium composite [9, 10] and cadmium oxide/alkali halide mixtures [11]. Many of the aforementioned materials have been reported to have a low working capacity (< 10 %), whereas the lithium zirconates reach their best working capacity and kinetics for reversible CO₂ sorption at around 575 °C [12], and thus require the shifted syngas to be heated. Cadmium oxide-based materials have been shown to exhibit a high CO₂ sorption capacity of up to 26 % [11], but the toxicity of cadmium compounds could lead to

increased safety requirements in industrial applications compared to less toxic alkali and alkaline earth metal compounds. It is therefore still beneficial to further develop low-toxicity sorbents in order to increase their capacity.

The use of cesium carbonate/magnesium oxide composites was described previously [9], where the CO₂ sorption aspect was elaborated in detail with regard to temperature swing sorption. This means that sorption is carried out at lower temperature, whereas desorption is encouraged by raising the sorbent temperature. It is however beneficial to perform an isothermal pressure swing, by sorbing at high pressure and lowering the pressure for desorption, as a pressure change can be performed more quickly and easily than a uniform temperature change of a large sorbent bed [13, 14]. However, an assessment is required of whether the sorbent is actually capable of performing under these conditions. Furthermore, carbonation of MgO to MgCO₃ was found not to be the reaction mechanism of CO₂ uptake, but rather a formation of a previously unidentified mixed cesium-magnesium phase was assumed [10]. Under this assumption, the study also hypothesised that a better mixing of cesium and magnesium into each other might lead to higher sorption capacities, as this would lead to more interaction points between the cesium and magnesium bearing phases, encouraging mixed phase formation upon CO₂ uptake.

Utamapanya et al. have synthesised magnesium oxide nanoparticles using a solvothermal approach, beginning with magnesium metal dissolved in methanol, forming a magnesium methoxide solution. Toluene and water were added to the solution and the mixture aged overnight in order to partially hydrolyse the magnesium methoxide to hydroxide. The process was finished by treating the solution in an autoclave at 265 °C and subsequent pressure relief at this temperature. By this process, magnesium hydroxide-methoxide nanoparticles of high BET surface areas of up to 1104 m²/g were obtained. These could subsequently be calcined to magnesium oxide [15]. Montero et al. have used this approach to synthesise a magnesium oxide/cesium nitrate composite, which they tested for catalytic reactions for biodiesel synthesis [16, 17]. This group added cesium nitrate by wet mixing and evaporation as well as by direct addition of the nitrate to the autoclave. The success with this approach (improved catalytic activity) inspired the use of the solvothermal synthesis for the present study.

In this study, magnesium oxide/cesium carbonate composites were synthesised via both the classic wet mixing method (using commercial MgO) as well as the solvothermal approach, both using cesium carbonate as precursor. Both wet-mixing and direct addition of the cesium carbonate to the autoclave process were examined. The materials based on commercial MgO were studied in a single-cycle CO₂ sorption program using thermogravimetric analysis (TGA) for their ability to perform partial pressure swing sorption. The materials were also examined in a 25 cycle sorption/desorption TGA test, assessing their working capacity. Nitrogen adsorption at 77 K, powder X-ray diffraction (XRD) and transmission electron microscopy (TEM) were used to characterise the materials.

5.4 Experimental

5.4.1 Synthesis of Mg-Cs₂CO₃ via the wet mixing method

15 mol% Cs was loaded onto MgO using a wet mixing approach as described by Jahan [9]. In a typical synthesis, 0.7 g of Cs₂CO₃ was dissolved in approx. 120 mL deionised water in a beaker. Next, 1 g MgO was dispersed into the solution and the water evaporated by heating on a hotplate stirrer under vigorous stirring. As soon as the suspension became a thick paste, stirring was stopped and the beaker placed into an oven to dry at 120 °C for at least six hours. The as-synthesised powder sample was then removed from the beaker, ground using mortar and pestle and stored in a sealed vial for further use. The sample is referred to as 'Mg-Cs-wetmix'.

5.4.2 Synthesis of Mg-Cs₂CO₃ via solvothermal method

5.4.2.1 Magnesium methoxide-hydroxide nanoparticle synthesis ('nano-Mg')

Solvothermally synthesised magnesium hydroxide was prepared in a method similar to the one described by Utamapanya [15], which had also been used by Montero et al [16, 17]. In our method, 1.247 g magnesium turnings (Sigma-Aldrich, 98 %) were dissolved overnight in 51.25 mL methanol (Merck, >99.8 %) in a covered conical flask at room temperature while stirring using a magnetic stirrer. The top of the flask was purged with nitrogen in order to minimise atmospheric moisture to deposit in the solution. A clear solution of magnesium methoxide was expected to form, but a cloudy solution was

obtained. As this was considered to be due to Mg-methoxide prematurely hydrolysing and precipitating to form $\text{Mg}(\text{OH})_2$, the solution was centrifuged at 4500 rpm for five minutes in 45 mL tubes using a Hermle Z 200 A centrifuge. The clear Mg-methoxide solution was decanted off and the solids discarded. 28.75 g of the liquid was then mixed with 143.67 g toluene (Merck, >99.9 %) under vigorous stirring, while 1.3 mL of water was added dropwise using a syringe. The liquid was aged overnight in a covered flask while stirring lightly at room temperature.

After ageing, 45 mL of the liquid were transferred into an autoclave of 100 mL capacity, sealed and evacuated. Evacuation was restricted to 15 seconds in order to reduce solvent evaporation. Afterwards, the autoclave was pressurised with nitrogen to 0.6 MPa, sealed and heated in a fluidised sandbath to 265 °C (sample temperature measured inside the autoclave) in 80 minutes. After keeping the temperature constant for 20 min, the autoclave tap was opened and the liquids flash-evaporated. After allowing the autoclave to cool to room temperature, it was opened and a powdered sample was obtained. Samples from two autoclave reactions, which were heated in the sandbath simultaneously, were combined into one and the powder was dried at 120 °C overnight and stored in a sealed vial for further use. This sample was named 'nano-Mg'.

5.4.2.2 Synthesis of Mg- Cs_2CO_3 -nano using wet mixing technique ('nano-wetmix', 'nano-wetmix-lowCs')

1.189 g of the nano-Mg sample described in section 5.4.2.1 was dispersed in approx. 150 mL water and 0.594 g Cs_2CO_3 added to the slurry (this was calculated to result in a 15 mol% Cs to Mg ratio similar to the material described in section 5.4.1, assuming the nano-Mg sample consists solely of $\text{Mg}(\text{OH})_2$). The liquid was evaporated and the sample dried in an oven at 120 °C as described in section 5.4.1. This sample is referred to as 'nano-wetmix'.

A second preparation used 0.442 g nano-Mg and 0.151 g Cs_2CO_3 . Here, the presence of 100 % Mg-methoxide is assumed in the nano-Mg sample. This sample is referred to as 'nano-wetmix-lowCs' due to its lower Cs content than the nano-wetmix sample.

5.4.2.3 Synthesis of Mg-Cs₂CO₃-nano using direct addition ('nano-direct')

In this synthesis, Cs₂CO₃ was added directly into the autoclave process. Synthesis was commenced as for the nano-Mg sample (section 5.4.2.1), using 1.258 g Mg turnings and 51.5 mL methanol. In this case, the solids obtained after centrifugation were recovered and the volume of clear Mg-methoxide solution was measured using a measuring cylinder (37.5 mL). The methanol-soaked solids were calcined at 850 °C in air for three hours and the resulting powder (assumed to be solely MgO) was weighed (0.5171 g). This then allowed quantification of the remaining magnesium in the liquid and adjustment of the amount of Cs₂CO₃ to be added. The appropriate amount of Cs₂CO₃ to give a 15 mol% Cs to Mg ratio (1.119 g) was dissolved in 20 mL methanol and this liquid subsequently added to the mixture of Mg-methoxide solution (31.318 g) and toluene (155.28 g). 1.37 mL of water was then added and the ageing and autoclave process was continued as described in section 5.4.2.1. This sample is labelled 'nano-direct'.

5.4.3 Nitrogen physisorption

Nitrogen physisorption at 77 K was measured on a Micromeritics Tristar II 3020 instrument. Samples of 0.2 to 0.5 g were degassed at 120 °C to a vacuum of 0.05 bar using a Micromeritics VacPrep 061 degas station prior to analysis. BET surface areas were calculated at relative pressures between 0.05 and 0.35. Some samples were calcined in a muffle furnace at 600 °C for three hours in air in order to obtain nitrogen physisorption data for ex-situ activated materials.

5.4.4 Thermogravimetric analysis of carbon dioxide sorption

Carbon dioxide sorption analyses were performed using a Setaram TAG 24-16 symmetrical thermoanalyser fitted with programmable mass flow controllers (Bronkhorst model F-201DV-RAD-11-K). A total flow of 70 mL/min gas was always maintained, using either 50 % CO₂ in argon (sorption gas), or pure argon (desorption and pre-treatment gas). As per instrument design, 35 mL/min of gas flow into the sample furnace, whereas the other 35 mL/min flow through the reference side of the balance.

Experiments were designed according to Figure 5.4.1 using a pre-treatment step in argon designed to convert all magnesium compounds into magnesium oxide (610 °C for single cycle experiments, 510 °C for multiple cycles). Afterwards, the temperature was lowered

to the sorption temperature and the gas flow turned to sorption gas. An end step was performed at the same temperature as the pre-treatment to fully decarbonate the sample at the end of the run.

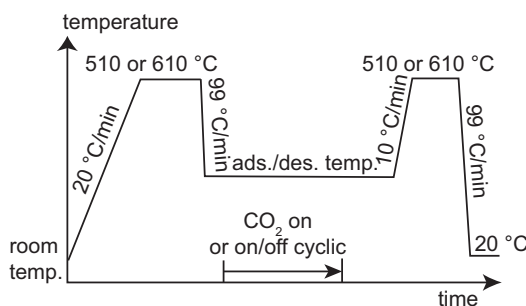


Figure 5.4.1: TGA program used for single-cycle (610 °C) or multi-cyclic (510 °C) sorption analysis

Sorption experiments were performed for the Mg-Cs-wetmix samples in a single cycle experiment at different temperatures, enabling sorption for two hours, followed by desorption in argon flow for one hour isothermally. A second set of experiments consisted of up to 25 cycles of isothermal sorption and desorption, cycling between sorption (12 min) to desorption gas (24 min) for the Mg-Cs-wetmix, nano-wetmix and nano-direct samples.

5.4.5 Powder X-ray diffraction

Powder X-ray diffraction experiments were performed on a Bruker D8 focus powder diffractometer using Cu K α radiation (1.5418 Å). Samples were mounted on a flat plastic sample holder for analysis and data was acquired at 0.5 ° 2 θ per minute speed at a resolution of 0.005 °. Powder Diffraction File entries 04-010-4039 (MgO), 04-010-8323 (Cs₂CO₃ (H₂O)₃), 00-022-1788 (Mg(OH)_{1.3}(OCH₃)_{0.7}) and 04-013-9511 (Mg(OH)₂) were used to identify and mark peaks in the patterns.

5.4.6 Transmission electron microscopy

Transmission electron microscopy (TEM) and selected area electron diffraction was performed on an aberration-corrected instrument, Titan (FEI Company), operated at 80kV. Bright-field TEM imaging was used to investigate the sample morphology and selected area electron diffraction was used to examine its crystallinity. Camera length was calibrated using a thin silicon TEM specimen.

For obtaining annular dark field images as well as elemental mapping for cesium, magnesium, oxygen and carbon, a JEOL 2100F instrument equipped with a Gatan CCD camera and a high angular annular dark field (ADF) detector (camera length 10 cm and 0.5 nm probe) to collect elemental mapping profiles. A 50 mm JEOL Si(Li) energy dispersive X-ray (EDX) detector was used for elemental mapping. EDX spectra obtained from the mapped images were checked to contain the elements being mapped and are given in the supplementary materials.

For the analysis of carbonated samples, 30 mg of each of the as-synthesised sample of both the nano-direct and nano-wet mix material was pre-treated in the thermoanalyser for 20 minutes at 610 °C in argon flow, subsequently cooled to 310 °C and exposed to 50 % CO₂ in Ar for 2 hours. Afterwards, it was cooled down to ambient temperature in the same atmosphere, removed from the thermoanalyser and stored in a sealed vial until TEM analysis.

5.5 Results

5.5.1 CO₂ sorption analysis

A full thermogram of the single-cycle sorption experiment of a Mg-Cs-wetmix sample is given in Figure 5.5.1a. It can be observed that the initial pre-treatment step caused a mass loss which is attributed to the removal of residual water and the decomposition of magnesium hydroxide, which originated from magnesium oxide during wet synthesis. In its activated state, the material then sorbed CO₂ once the gas flow was switched to sorption gas. Switching back to argon, the mass decreased, indicating an ability to perform pressure swing sorption by altering the partial pressure of CO₂ from 0.5 bar to 0 bar.

As the material is considered to consist of the active sorbent after the pre-treatment step, the mass was expressed as 100 % before the sorption gas was switched on and results plotted from there. Figure 5.5.1b shows the behaviour of this material at several sorption temperatures. The results show that a temperature of 247 °C gave a slow sorption of 2.9 wt% after two hours, and that desorption was not thermodynamically favoured, as most of the mass gain was retained during the argon purge. Higher temperatures led to faster CO₂ uptake, and desorption was more favoured. A maximum CO₂ uptake of

8.1 wt% was achieved at 313 °C after two hours of sorption. At temperatures of 354 to 391 °C, the material exhibited a fast uptake of CO₂ and was also capable of releasing the sorbed mass at isothermal conditions to a certain extent. This is indicated by the working capacities (Figure 5.5.1c) being highest around 380 °C. For this reason, subsequent temperatures for experiments of partial pressure swing were chosen in this temperature range.

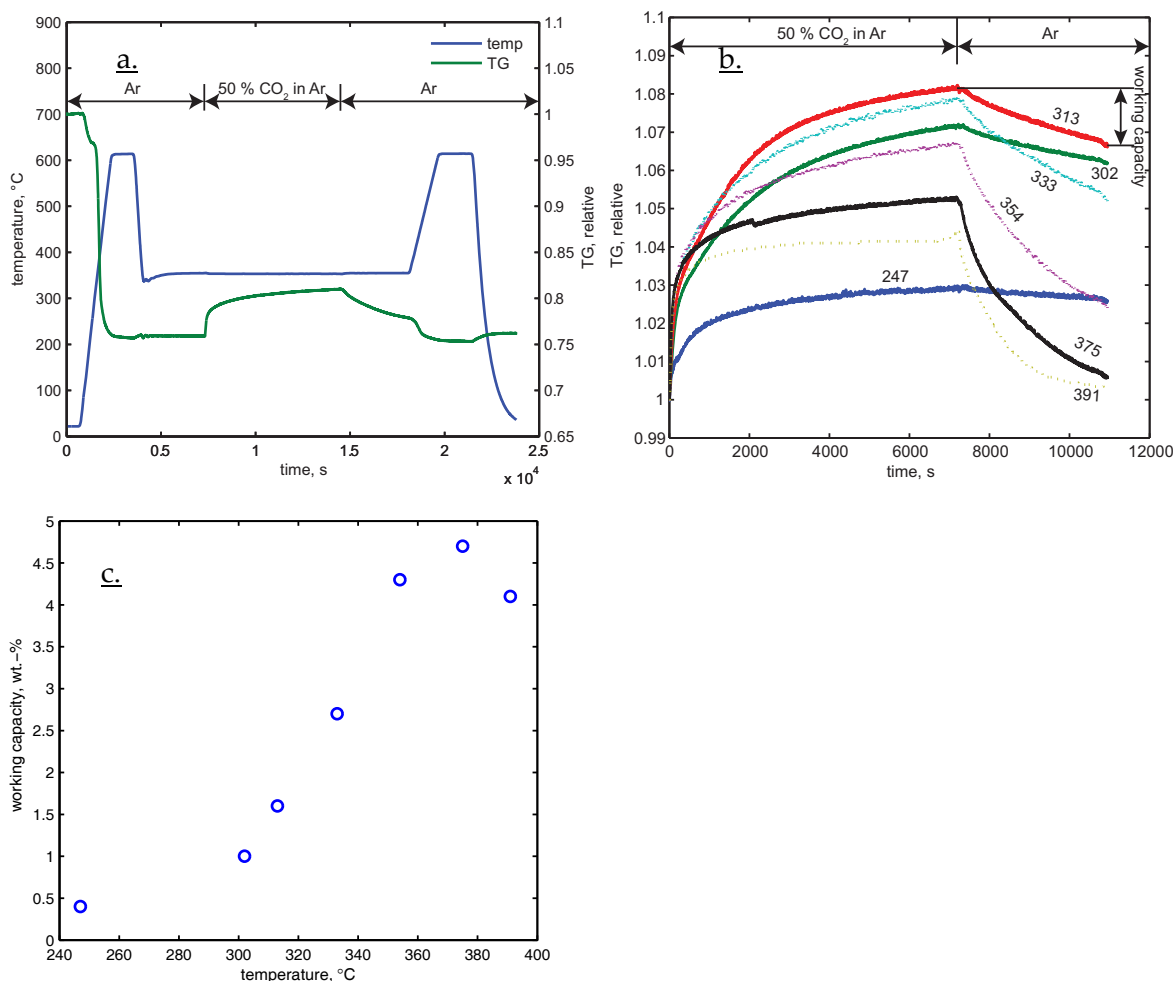


Figure 5.5.1: a. Full thermogram of a 2 hr sorption, 1 hr desorption run of a Mg-Cs-wetmix sample at 354 °C, b. 2 h Sorption and 1 h desorption excerpt from a. with 100 % mass set at the start of the sorption run for different temperatures, with working capacity indicated for the 313 °C experiment, c. working capacities derived from b.

It must be noted that Jahan obtained higher single cycle maximum sorption capacities of up to 12 wt% on this material [9]. This is assumed to be because her work involved a partial pressure of 0.9 bar CO₂ instead of the 0.5 bar used here.

It is necessary for an industrial application that the sorbents be fully regenerable over multiple cycles. In order to test this, a multiple cycle sorption TGA routine was applied and an example full thermogram (wet mix sample at 390 °C) given in Figure 5.5.2a. Here, the active material (i. e., 100 % mass) was yielded after the pre-treatment step, as for Figure 5.5.1, and the working capacity determined as the difference between the highest and lowest relative masses of each sorption cycle with 12 minutes of sorption (50 % CO₂) and 24 minutes of desorption (Ar). For the wet mix, nano-wet mix and nano-direct samples, these working capacities were plotted versus the cycle number in Figure 5.5.2 b, c and d. All full thermograms can be found in the supplementary materials, along with the excerpts showing 100 % mass at the start of the cycles.

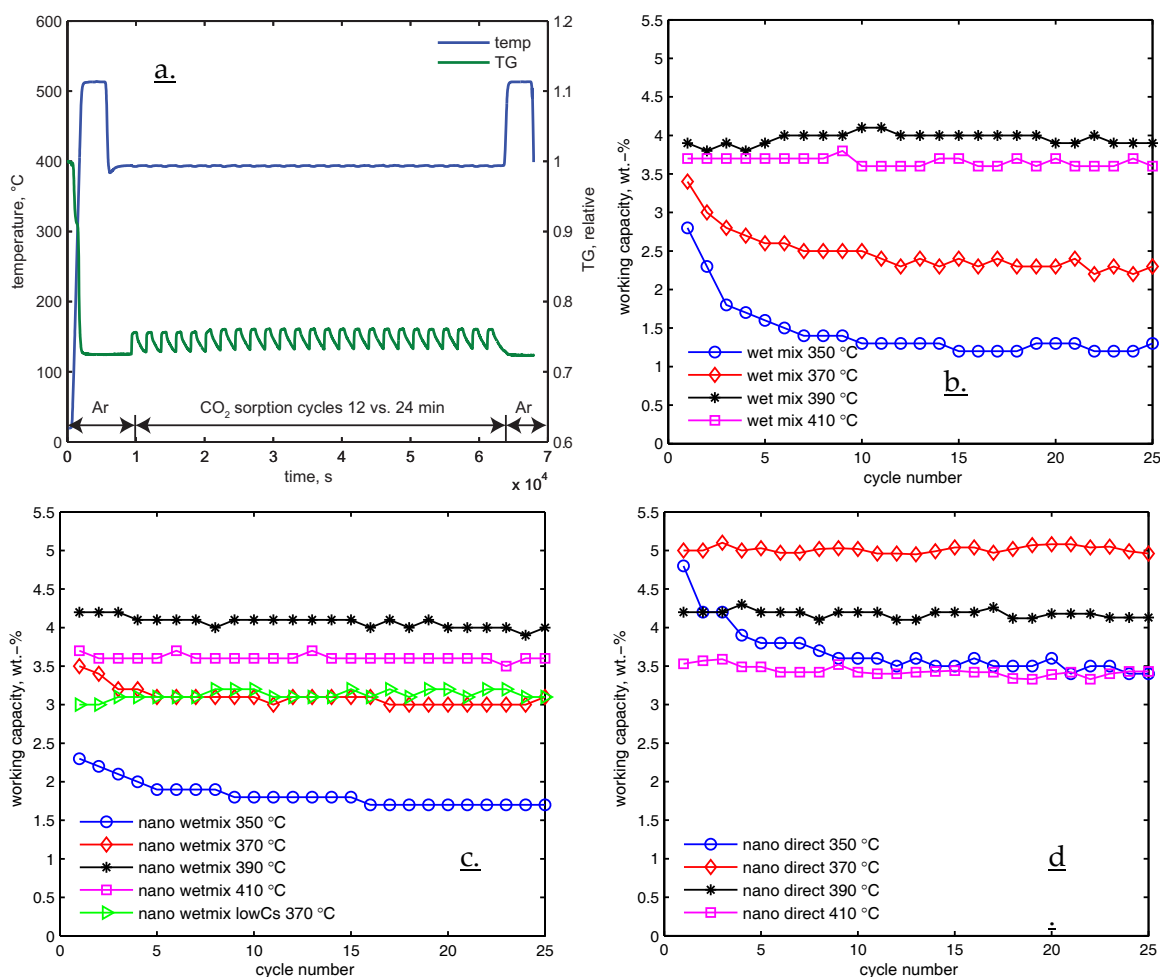


Figure 5.5.2. a. Full thermogram of a wet mix sample in 12 min sorption, 24 min desorption cycles at 390 °C, b. working capacities for wet mix samples at different temperatures over 25 cycles, c. and d. for nano-wetmix and nano-direct samples, respectively.

Figure 5.5.2b shows that the material is capable of a partial pressure swing by sorbing and desorbing CO₂ at isothermal conditions. It can be observed that the working capacities of the wet mix material were highest at 390 °C, reaching about 4 wt%, but are less both at higher and lower temperatures. Also noteworthy is a capacity loss at temperatures of 350 and 370 °C during the first (approx.) six cycles. This capacity loss eventually subsided, so that a constant working capacity was achieved with subsequent cycles. The full thermogram of the measurement at 350 °C (refer to supplementary material) also shows that the first cycle sorbed up to 5.5 wt%, but desorption was not complete, stopping at a mass percentage of 3% above the baseline. Subsequent sorption cycles showed an increasing amount of CO₂ retained. It is speculated that this CO₂ retention after several cycles is associated with annealing particles and an inclusion of CO₂ into deeper parts of the sample, so that the CO₂ was in turn harder to desorb isothermally. At higher temperatures, desorption took the relative mass closer back to the original tare point, which could mean that the higher temperature enables desorption of CO₂ trapped in inner layers of the material more easily, or, in other words, that a higher temperature makes CO₂ diffuse more easily into and out of the sample. Thus, the optimum pressure swing temperature, in terms of working capacity, is to be found at an intermediate point.

The nano-wetmix samples (Figure 5.5.2c), which were made from a nanoparticle magnesium hydroxide/methoxide substrate, showed similar working capacities to the samples made from commercially available MgO. Reducing the amount of cesium had a no effect on the working capacity. This result is in agreement with an observation made by Jahan, showing that the single cycle CO₂ sorption capacity is not very sensitive towards a variation in the cesium loading in a range of concentrations between 10 and 30 mol% Cs [9].

It was initially hypothesised that the wet mixing of the cesium carbonate onto a high surface area magnesium substrate after synthesis would lead to a better distribution and, in turn, to a higher working capacity than if commercial MgO was used. This was not the case. However, by directly adding the cesium carbonate to the autoclave in the solvothermal approach, the working capacity was increased, as the results in Figure 5.5.2d show.

It appears that the wet mixing approach had some constraints, as the working capacity results of the nano-wetmix samples were similar to the ones made from commercial MgO. It can be seen in Table 5.5.1 that the BET surface area of the nano-Mg is comparatively high (818 m²/g), but significantly reduced upon addition of cesium carbonate by wet mixing (32 m²/g) and further still on calcination (12.8 m²/g). A similar trend was observed for the samples made from commercial MgO, although their overall surface areas were lower, whereas the nano-direct sample had a similar surface area to the nano-wet mix sample after calcination. Thus, it appears that surface area is not the key indicator influencing the working capacities. This motivated a more detailed study of the powders by transmission electron microscopy and powder X-ray diffraction.

Table 5.5.1: BET surface areas from N₂ physisorption. Refer to supplementary materials for isotherms.

name	BET surface area, m ² /g
MgO, Sigma-Aldrich	122
wet mix	6.8
wet mix calcined 600 °C, 3 h	3.4
nano-Mg	818
nano-wet mix	32
nano-wet mix calcined 600 °C, 3 h	12.8
nano-wet mix-lowCs	52
nano-direct	84.3
nano-direct calcined 600 °C, 3 h	13.8

5.5.2 Morphology and crystallinity of the materials

The powder X-ray diffraction patterns for the nano-wetmix and nano-direct materials are provided in Figure 5.5.3, whereas a detailed analysis of the wet mixed materials made from commercial MgO has been published previously [10]. It can be observed that the nano-Mg material appeared to consist of small crystals, characterised by broad and flat peaks. The peaks in the pattern have been matched by Montero et al. to be of magnesium hydroxide methoxide [16], but this assumed the merging of three peaks to one at 58.8, 60.1 and 62.7 ° 2θ, and of two at 33.8 and 38.4 ° 2θ (refer to markers in Figure 5.5.3). This is the likely phase obtained in the methanol-based solvothermal synthesis. However, upon wet mixing, the material fully converted into magnesium hydroxide. The cesium carbonate phase was not observed in this pattern and thus had to be present as a mostly amorphous

phase. Upon calcination, $\text{Mg}(\text{OH})_2$ transformed into MgO and a hydrated cesium carbonate phase was observed. The hydration of the cesium phase presumably occurred due to its hygroscopic nature, taking up atmospheric moisture during sample handling during the transfer from the muffle furnace to the diffractometer. This phenomenon has been previously described for the wet-mix samples made from commercial MgO [10]. Furthermore, it was shown, using an in-situ powder XRD experiment, that avoiding atmospheric exposure preserves the dehydrated Cs_2CO_3 formed on calcination [10]. The nano-direct material obtained via solvothermal synthesis showed a similar behaviour upon calcination. Here, it appears that the magnesium hydroxide-methoxide and hydrated cesium carbonate phases were present in the as-synthesised material, which upon calcination converted to magnesium oxide and cesium carbonate. The hydration of cesium carbonate is assumed here to be due to atmospheric exposure after calcination as described for the nano-wet mix material. It appears, however, that the crystallinity of the hydrated cesium carbonate after calcination was higher in the nano-direct sample as compared to the nano-wetmix sample, given the peaks are of higher intensity relative to the MgO phase.

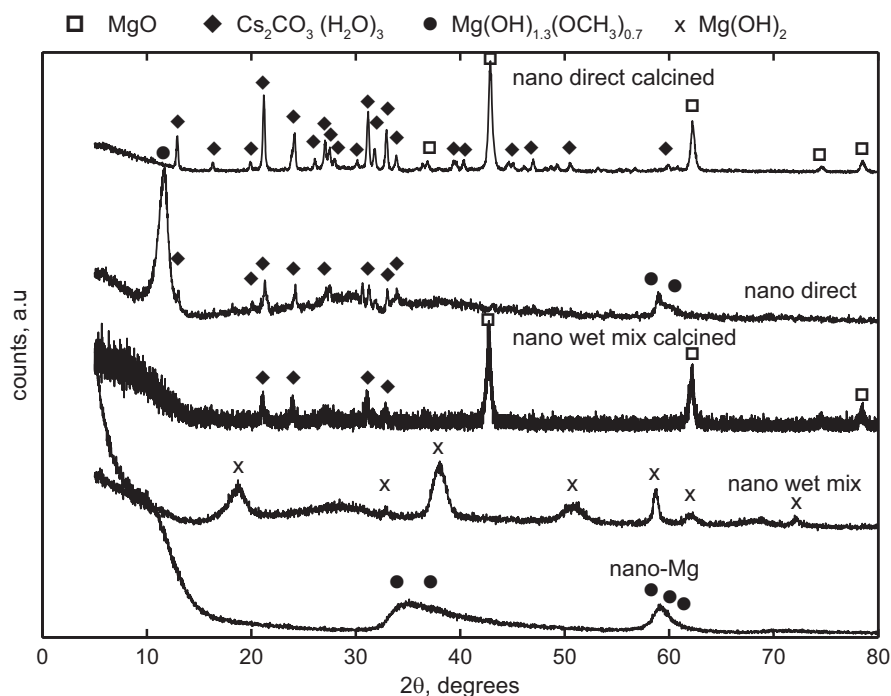


Figure 5.5.3: Powder X-ray diffraction patterns of the solvothermally synthesised Mg-Cs composite materials and the nano-Mg substrate. Peak markers are set according to Powder Diffraction File.

TEM images and selected area diffraction patterns are given in Figure 5.5.4 to Figure 5.5.10. For the nano-Mg sample, it is shown that it consisted of small crystallites, as evident from the electron diffraction pattern showing broad intense ring patterns (Figure 5.5.4b). The pattern was matched with MgO. This appears, at first, to contradict the XRD results in Figure 5.5.3. However, it should be noted that magnesium compounds tend to decompose to MgO in the electron microscope, as the electron beam supplies enough energy for this decomposition. This observation was also made in our earlier study [10]. The morphology of the particles as seen in the TEM image (Figure 5.5.4a) looks a little like flat chips. Scanning electron microscopy results published by Utamapanya et al. also showed this morphology [15].

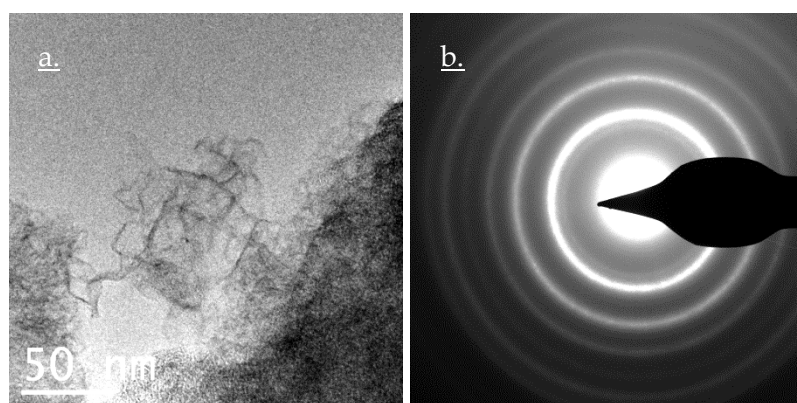


Figure 5.5.4: TEM image (a) and electron diffraction pattern (b) for the nano-Mg sample. Diffraction pattern matches MgO.

Upon wet mixing of the nano-Mg material with Cs_2CO_3 , the flake-like structure disappeared. It can be noted, in Figure 5.5.5a and b, that cesium addition led to the formation of larger, more bulky particles. It might be that the cesium compound had acted like a glue to stick the Mg-nano particles together as it dissolved and re-precipitated during the wet mixing synthesis. The electron diffraction pattern (Figure 5.5.5c) shows a weak signal of MgO, which is considered to be due to flat but large nanoparticles. High-resolution images (Figure 5.5.5d and e) show particles of approx. 50 nm width with a rough surface.

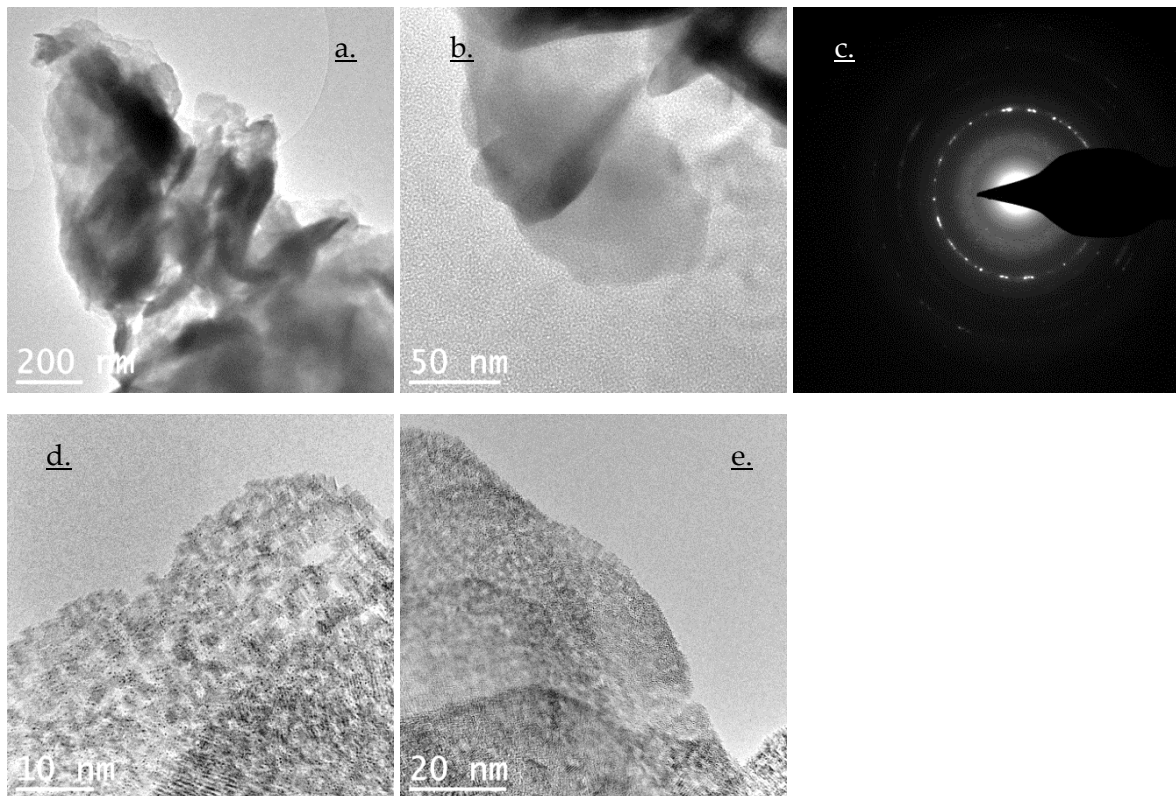


Figure 5.5.5: a, b, d ,e: TEM images of nano-wet mix as synthesised sample, c: electron diffraction pattern for b.

In contrast to the nano-wet mix sample, the nano-direct sample (in the as-synthesised state) showed bulky as well as wrinkled/chip-like particles, appearing like a mixture of the nano-Mg and the nano-wet mix samples (Figure 5.5.6a and c). High-resolution TEM showed a rough surface and few lattice fringes (Figure 5.5.6f) and the electron diffraction patterns consisted only of faint rings (Figure 5.5.6b and e), indicating polycrystalline particles. MgO was apparent in the diffraction patterns, but the ring diffraction pattern also indicates a small crystallite size. The appearance of both chipped and bulky particles here is somewhat surprising, as the direct mixing approach was intended to form a more homogeneous sample than the wet mix approach.

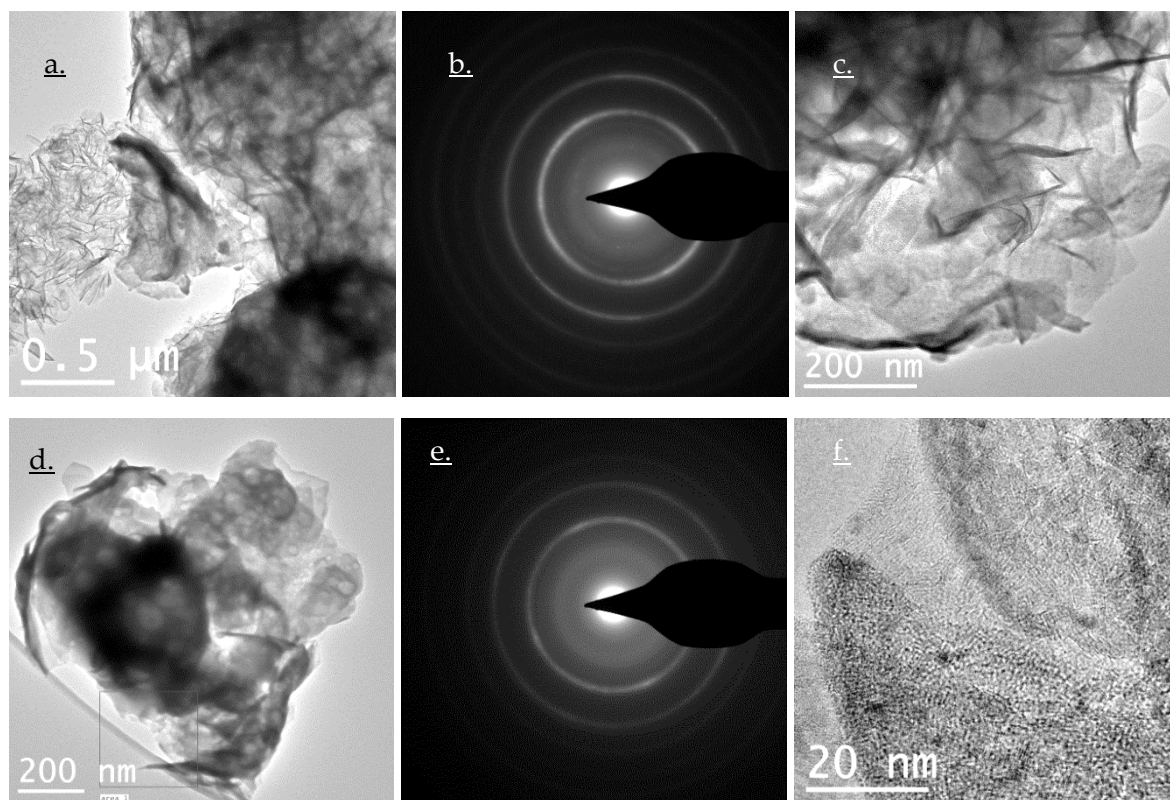


Figure 5.5.6: (a, c, d, f) TEM images of nano-direct sample, as synthesised; (b) electron diffraction image for (a), (e) for 'area1' marked in (d); (f) enlarged section of 'area1' in (d).

Upon calcination, the samples formed larger MgO crystals. This is evident from Figure 5.5.7c and d (nano-wet mix sample) and Figure 5.5.8a and b (nano-direct sample), if they are compared to their as-synthesised counterparts as described above. The morphology, consisting of irregular spheres (Figure 5.5.7a), was similar to the observations reported by Montero et al [16]. The nano-direct and nano-wet mix samples appeared similar in their morphology and crystallinity. It appears from electron diffraction images, giving spotted patterns (Figure 5.5.7b and Figure 5.5.8d and e), and high-resolution TEM images, showing regular lattices (Figure 5.5.7b and Figure 5.5.8c) that the crystallinity and crystallite size have increased during calcination, possibly due to annealing. Furthermore, the wrinkled/chipped appearance has disappeared during calcination, and more spherical particles have formed, being consistent with an annealing process.

Figure 5.5.9 and Figure 5.5.10 show the materials after CO₂ saturation, following calcination. Somewhat surprisingly, the morphology change compared to the calcined state was minimal. The material still consisted of polycrystalline almost-spherical particles.

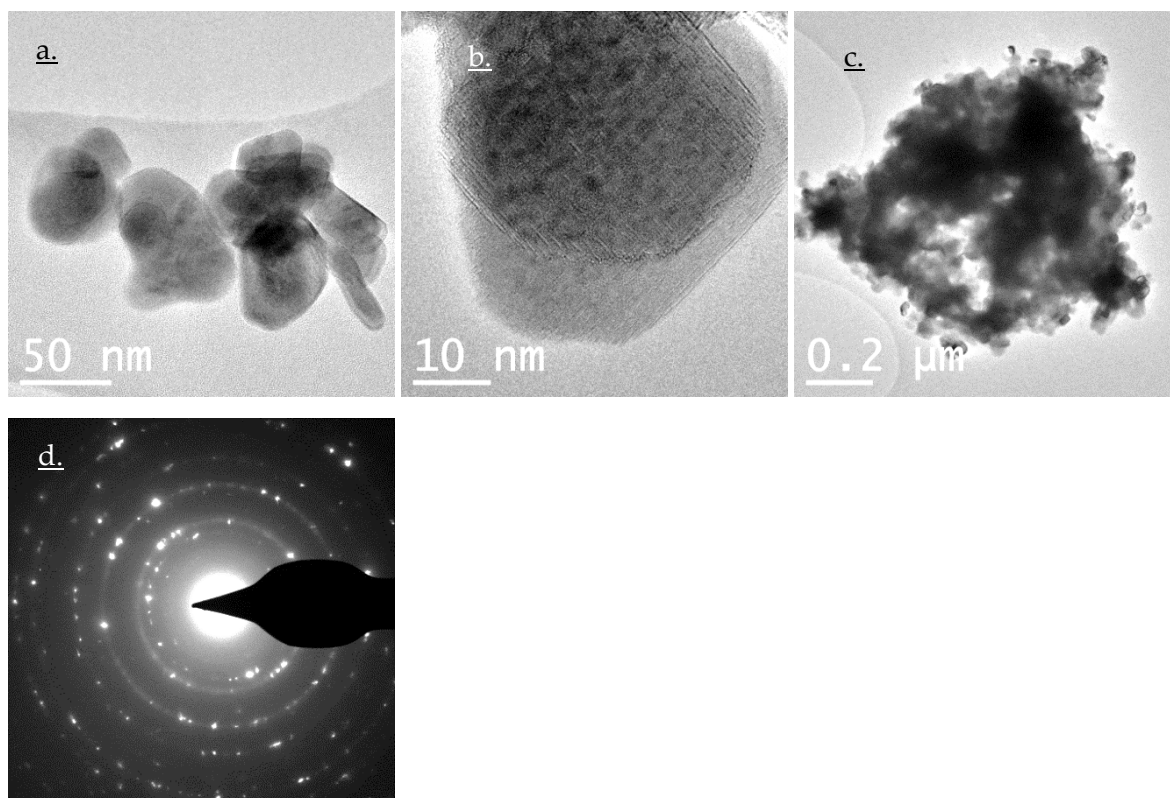


Figure 5.5.7: (a-c) TEM images of nano-wet mix sample after calcination (d) electron diffraction pattern of (c).

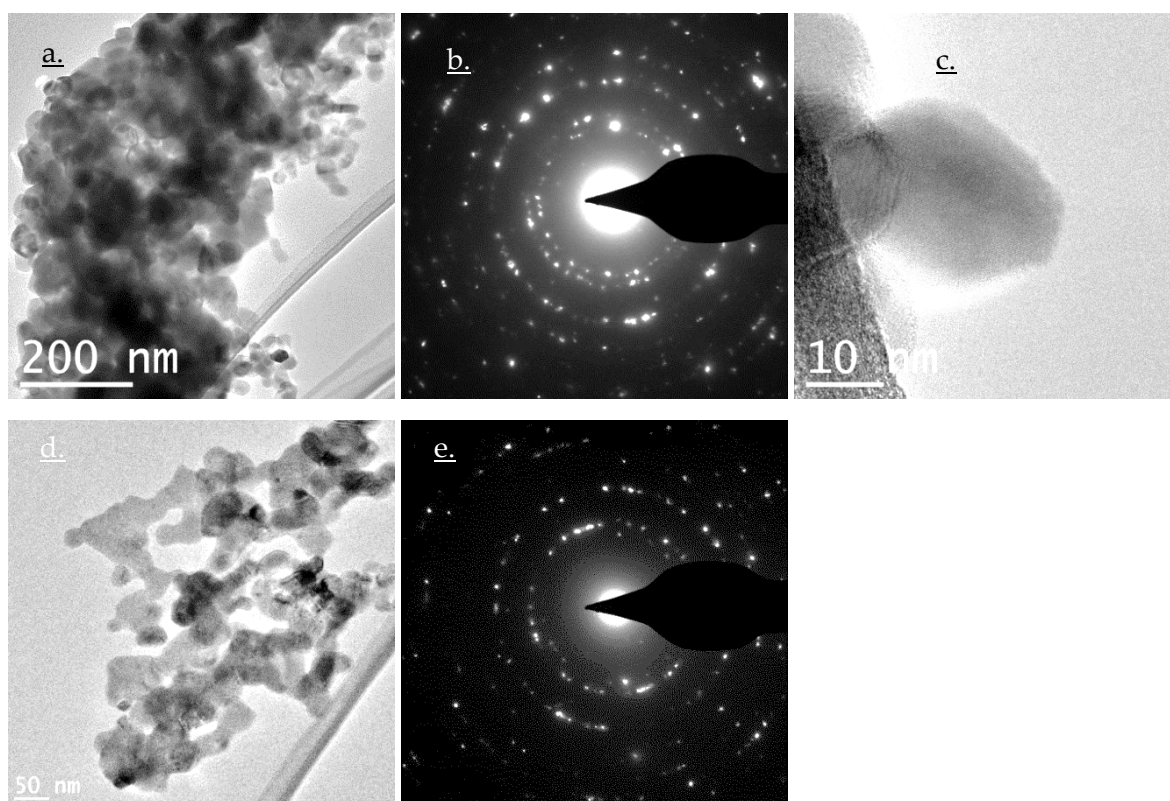


Figure 5.5.8: (a, c, d) TEM images of nano-direct sample after calcination, (b) electron diffraction for (a), (e) for (d) respectively.

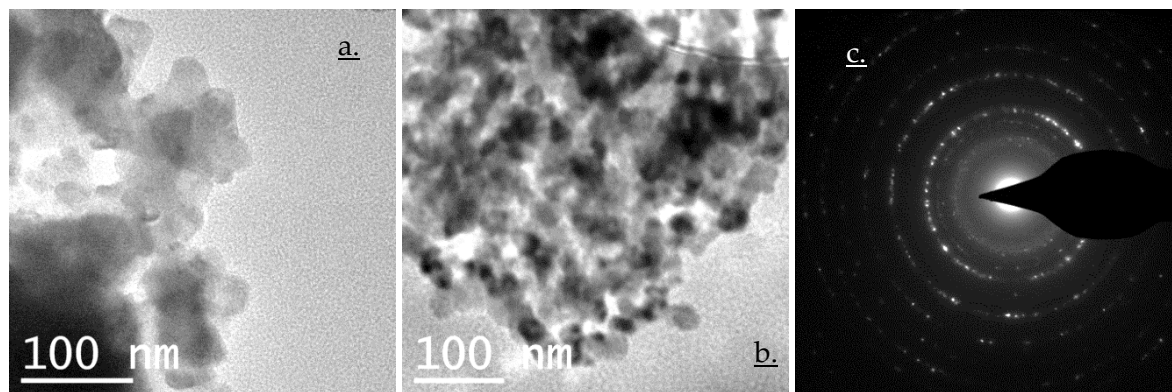


Figure 5.5.9: (a, b) TEM images of nano-wet mix sample after carbonation, (c) electron diffraction pattern of (b).

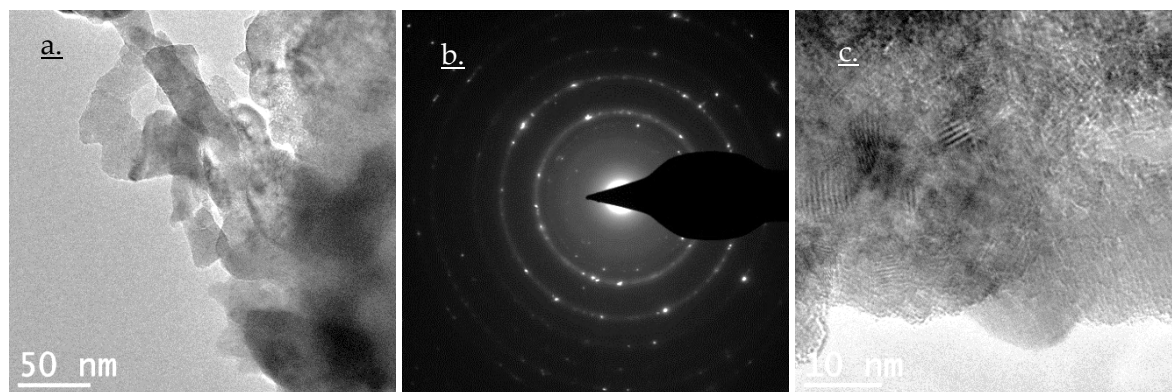


Figure 5.5.10: (a, c) TEM images of nano-direct sample after carbonation, (b) electron diffraction pattern of (a).

It is interesting to investigate the elemental distribution of the samples in order to assess how well cesium is distributed into the magnesium phase, as the interaction between cesium and magnesium phases is considered a key factor in carbon dioxide sorption. For this purpose, elemental mapping using scanning transmission electron microscopy has been performed on the as-synthesised and carbon dioxide saturated samples. Figure 5.5.11 shows the elemental maps of carbon, oxygen, magnesium and cesium for three specimens of the as synthesised nano-wetmix sample, along with an annular dark field and a bright field image. It can be observed that there is an even distribution of magnesium, cesium and oxygen, which is well in line with the intensities seen on the dark field images. Carbon is hard to interpret, as the TEM sample grid is made of carbon. It can however be observed that high intensities in the dark field images correspond to high concentrations of carbon.

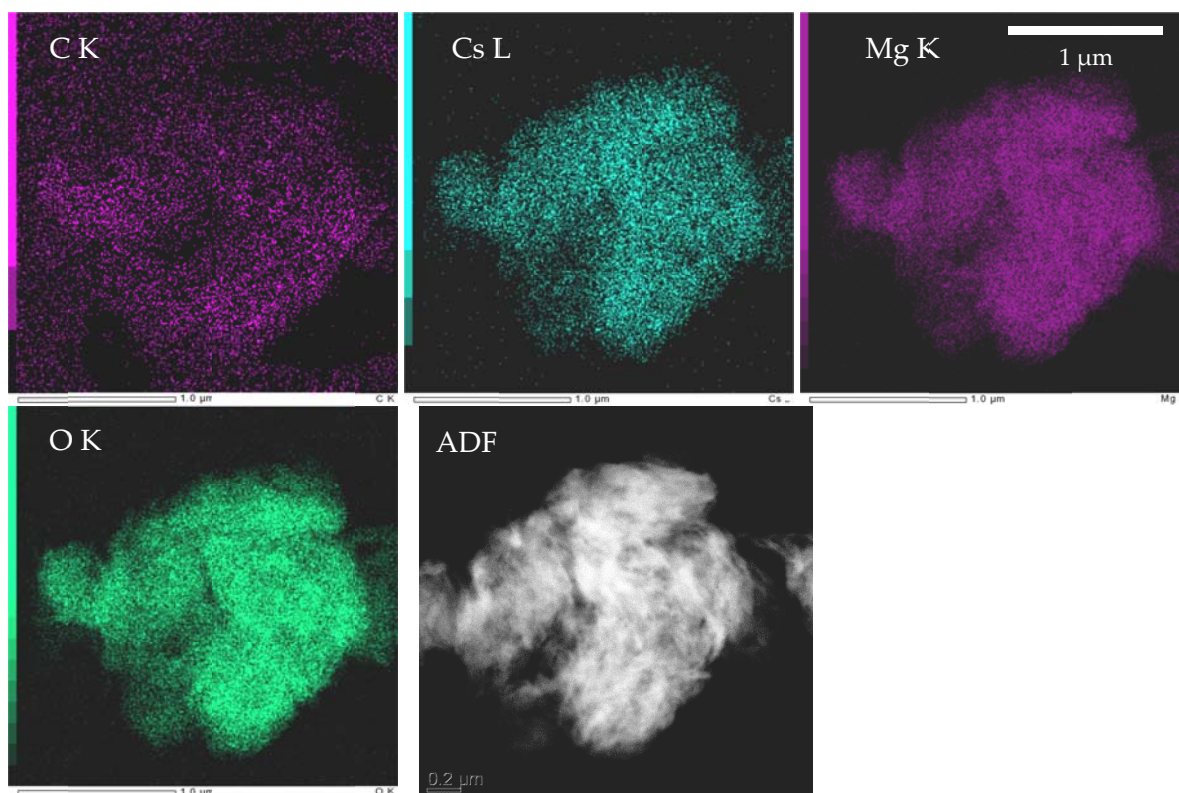


Figure 5.5.11: Elemental maps for carbon, cesium, magnesium and oxygen and scanning transmission electron microscopy dark field image of the nano-wet mix sample in the as-synthesised state. Refer to supplementary materials for duplicate specimens and EDX spectra.

A similar picture can be observed for the elemental maps of the nano-direct samples given in Figure 5.5.12. Here, clearly distinct clusters of cesium can be observed (as indicated). These regions were high in cesium, but low in magnesium. It also appears that magnesium-rich areas appear with thread-like morphology, whereas the cesium-rich area appears more like a sphere. These observations are in agreement with the TEM images provided in Figure 5.5.6, showing clusters of almost spherical particles (possibly cesium-rich) and also chip-like/wrinkled particles (possibly magnesium-rich). Other regions of the specimen exhibited a more uniform distribution of the elements shown. Additional maps can be found in the supplementary material.

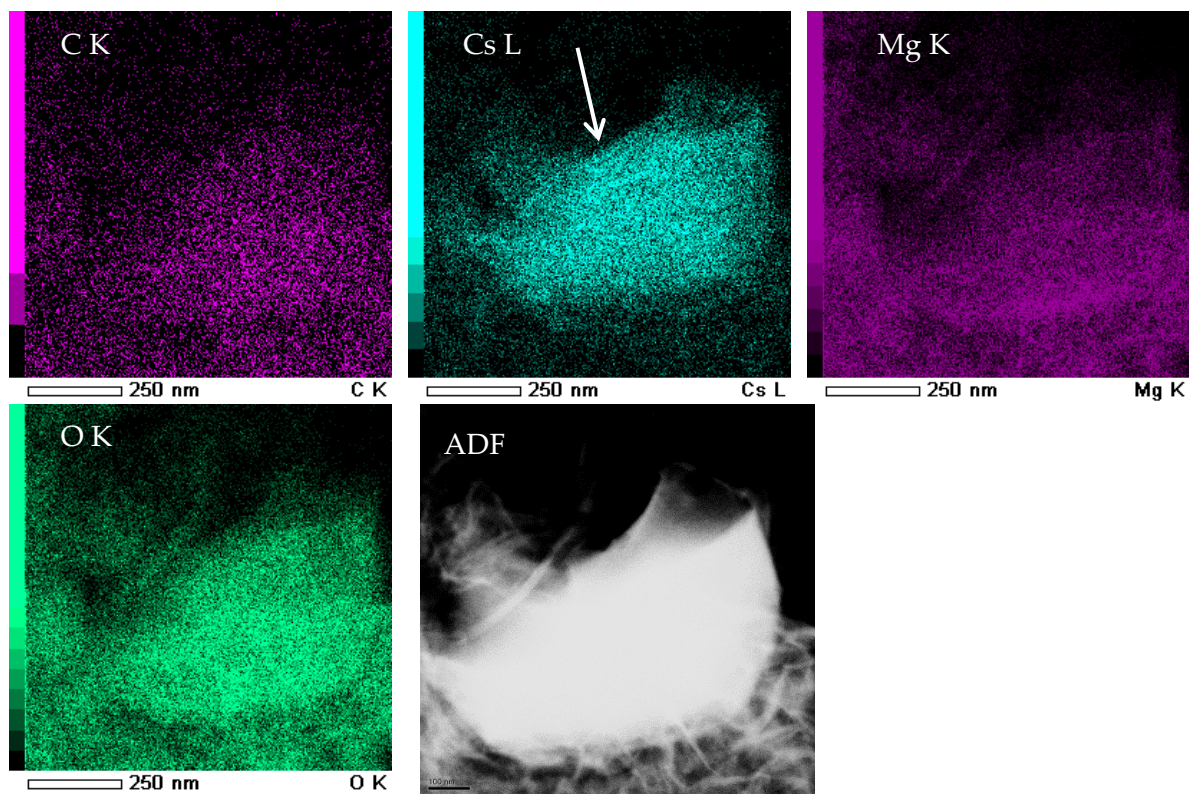


Figure 5.5.12: Elemental maps for carbon, cesium, magnesium and oxygen and scanning transmission electron microscopy dark field image of the nano-direct sample in as-synthesised state. White arrow indicates a cluster with increased Cs content, but low in Mg. Refer to supplementary materials for duplicate specimens and EDX spectra.

In the carbonated state, the nano-wet mix and nano-direct samples showed a similar appearance compared to their as-synthesised counterparts. Again, it can be seen that the cesium is comparatively well distributed over the magnesium (Figure 5.5.13 and Figure 5.5.14). The clustering effect of the cesium within the nano-direct sample was evident here, too, and also for the nano-wet mix specimen. It must be noted that the nano-wetmix sample after carbonation (Figure 5.5.13) was hard to capture in the annular dark field imaging mode. Two attempts to capture an ADF image showed a very oversaturated image like the one shown in Figure 5.5.13.

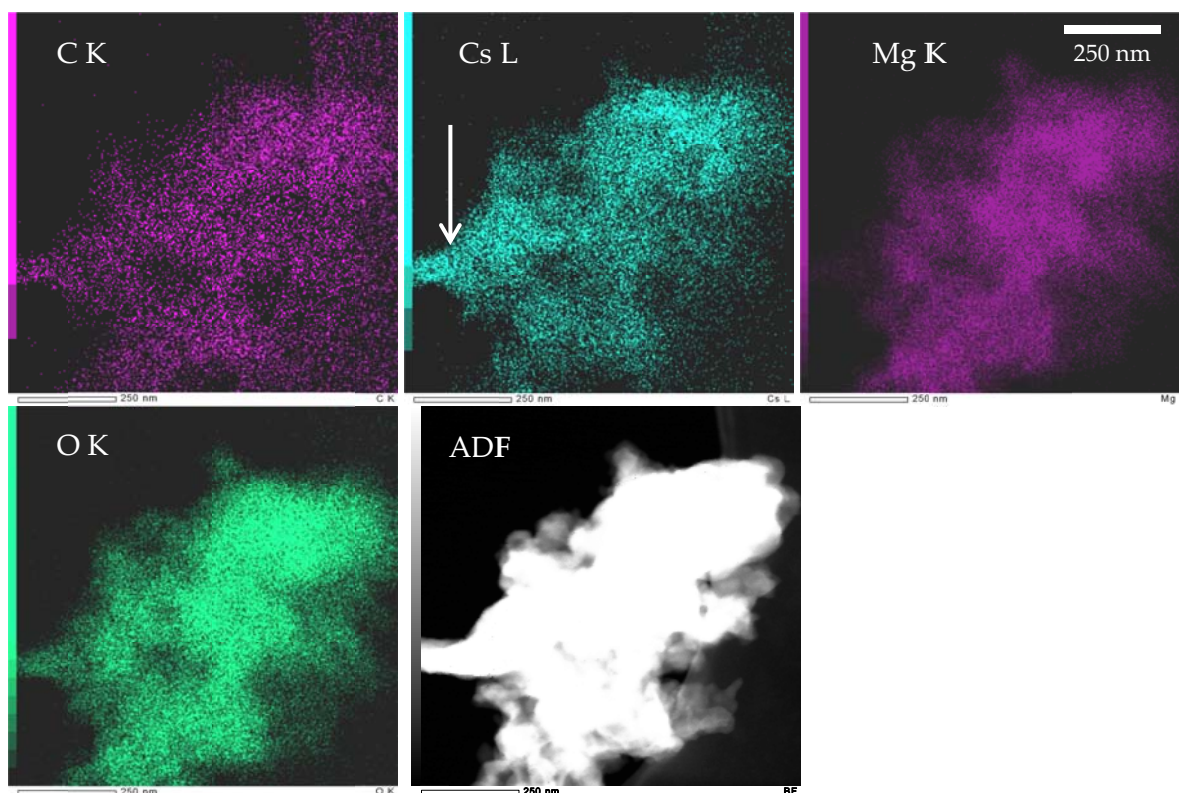


Figure 5.5.13: Elemental maps for carbon, cesium, magnesium and oxygen and scanning transmission electron microscopy dark field (mislabelled 'BF') image of the nano-wetmix sample after carbonation. White arrow indicates a cluster with increased Cs content, but low in Mg. Refer to supplementary materials for EDX spectrum.

The electron microscopy results generally showed that the particle size of the materials made by solvothermal methods (both nano-wet mix and nano-direct) led to a decrease in particle size compared to using commercial MgO as a starting material [10]. This, in turn, also led to an increased surface area as shown in Table 5.5.1. A good distribution of cesium and magnesium throughout the particles was achieved, although some segregation (spots of higher cesium than magnesium intensity in the elemental maps) seemed to occur. The occurrence of such segregation in the nano-direct samples, where the cesium and magnesium were both in liquid solution when mixed, is somewhat surprising. Occasionally, this segregation is also visible in the wet mixed sample (Figure 5.5.13).

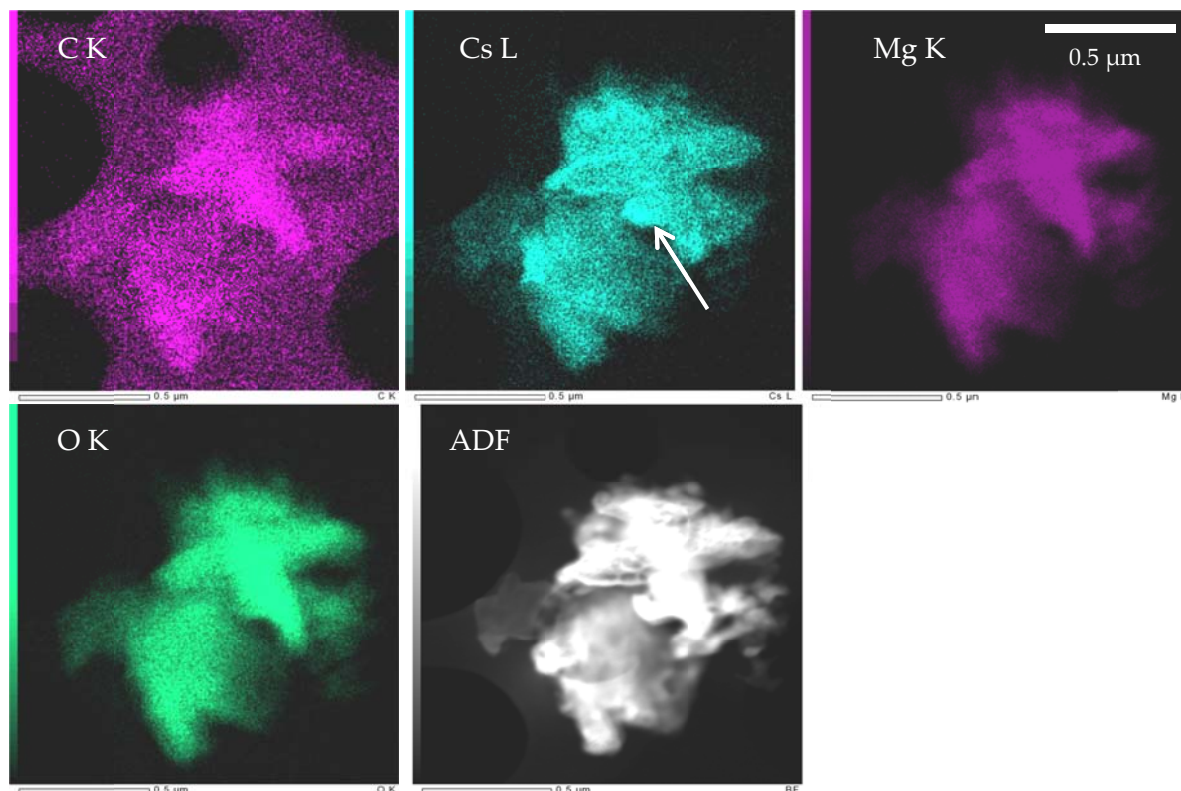


Figure 5.5.14: Elemental maps for carbon, cesium, magnesium and oxygen and scanning transmission electron microscopy dark field (mislabelled 'BF' at the bottom) images of the nano-direct sample after carbonation. White arrow indicates a cluster with increased Cs content, but low in Mg. Refer to supplementary materials for duplicate specimens and EDX spectra.

5.6 Conclusion

In this study, magnesium-cesium composites for pre-combustion CO₂ capture were synthesised via a solvothermal method, by (i) synthesising a magnesium hydroxide methoxide substrate and subsequent wet mixing with cesium carbonate as well as by (ii) directly mixing the cesium carbonate into the solvothermal synthesis of the magnesium substrate. These two materials were compared to a cesium carbonate-doped magnesium oxide, which had been described in earlier studies [9, 10]. The latter material was also synthesised and tested in TGA experiments to assess its performance in isothermal pressure swing CO₂ sorption in single cycles at different temperatures. It was shown that the material is able to sorb and desorb up to 4.7 wt% of CO₂ in this mode at temperatures of around 375 °C. Under more stringent multicyclic conditions, a stable working capacity of 4 wt% was achieved over 25 cycles at 390 °C. Synthesising the material in a similar manner, but using a nanoparticle magnesium substrate that was synthesised using a solvothermal method, gave a similar trend in working capacities. Using the direct mixing

approach, the working capacities were increased to 5 wt% and the optimal temperature was found to be lower, around 370 °C.

Powder XRD patterns of the solvothermally synthesised materials show that the material consists of magnesium oxide and hydrated cesium carbonate phases in its active (calcined, ex-situ) state. These results show that the chemistry of the solvothermal materials in their active states is the same as found in a previous study focussing on a material made from commercial MgO. Transmission electron microscopy indicated that the material crystallinity increases upon calcination and that particle sizes as low as about 50 nm are obtained for the Mg-Cs composites. This is smaller than the ones observed in the classic synthesis route using commercial MgO [10]. This is also reflected in the higher surface areas of the solvothermally synthesised materials. Elemental mapping revealed that a mostly uniform distribution of the cesium and the magnesium in the particles was achieved, with occasional clustering of cesium occurring.

It can be concluded that the solvothermal approach increased the working capacity if the cesium carbonate is added into the synthesis process as a solution, co-precipitating and hydrolysing with the magnesium methoxide precursor (nano-direct sample). It appears that an improved distribution of cesium was obtained in this case, leading to particles having cesium and magnesium interspersed into the core of the particles. In contrast to this, a wet mix of cesium carbonate solution onto dispersed magnesium precursor particles is assumed to lead to a different dispersion of cesium throughout the particles, particularly the core of the particles. Since the active sites for CO₂ sorption are considered to be a mixed metal oxide phase, this would be a less effective mixing strategy.

These differences in elemental distribution might potentially not be entirely visible in elemental mapping techniques, as here a 3D particle is projected onto a 2D surface (the picture). In this context, for wet mixed samples, the diffusion of the CO₂ through the cesium phase shell must be overcome, which is easier at a higher temperature of 390 °C. In the case of the direct-mix sample, more active sites could thus be considered to be available on the accessible surface, enabling better access of the CO₂ to active sites of the solid particles. This would explain both the lower temperature required for multicyclic

sorption (i. e., easier diffusion), as well as the higher working capacity achieved in the nano-direct sample (more active sites through better mixing of cesium and magnesium).

The results show that a better mixing of the cesium and magnesium phases lead to an improved Mg-Cs CO₂ sorbent. Future investigations should be directed at further increasing the BET surface area of the direct-mix sample, in order to preserve the initially high surface area of 84 m²/g, or to create even higher surface area materials when the sorbent is in its active (calcined or pre-treated) state.

5.7 Acknowledgements

The authors acknowledge Dr Yi Fei and Dr Marc Marshall for help with autoclave use and Greg Knowles for many helpful discussions. Monash Centre for Electron Microscopy is acknowledged for the use of the TEM facility. The authors acknowledge funding provided by the Australian Government through its Cooperative Research Centre (CRC) program to support this CO₂CRC research project. Financial support from the Faculty of Science, Monash University, is also gratefully acknowledged.

Supplementary material

Improvements in the pre-combustion carbon dioxide sorption capacity of a magnesium oxide-cesium carbonate sorbent

Christian Vogt^{#^}, Shery LY Chang⁺, Jamileh Taghavimoghaddam[^] and Alan L Chaffee^{#^*}

[#] Cooperative Research Centre for Greenhouse Gas Technologies (CO2CRC), [^]School of Chemistry, Monash University, VIC 3800 Australia

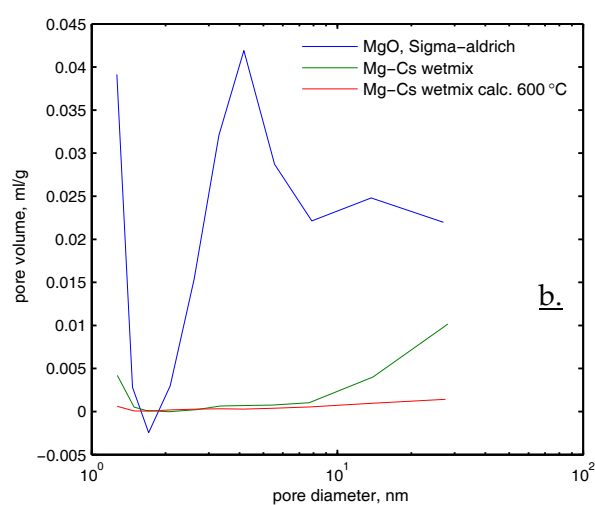
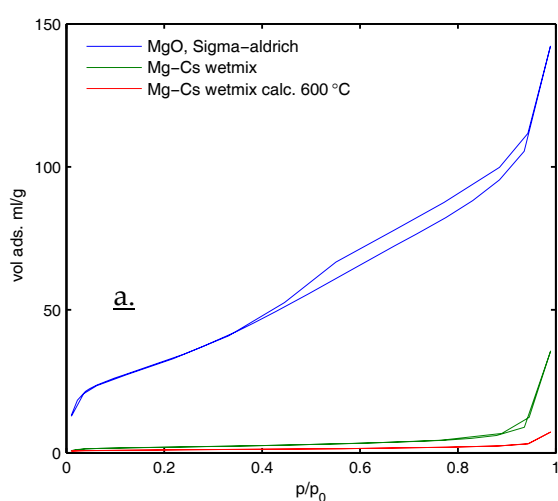
⁺ Monash Centre for Electron Microscopy, Monash University, VIC 3800 Australia

⁺ Current Address: Ernst Ruska-Centrum, Forschungszentrum Jülich GmbH, 52425 Jülich, Germany

* corresponding author: [REDACTED]

Phone: + [REDACTED] Fax: + [REDACTED]

5.8 Nitrogen physisorption isotherms and BJH pore volume distribution



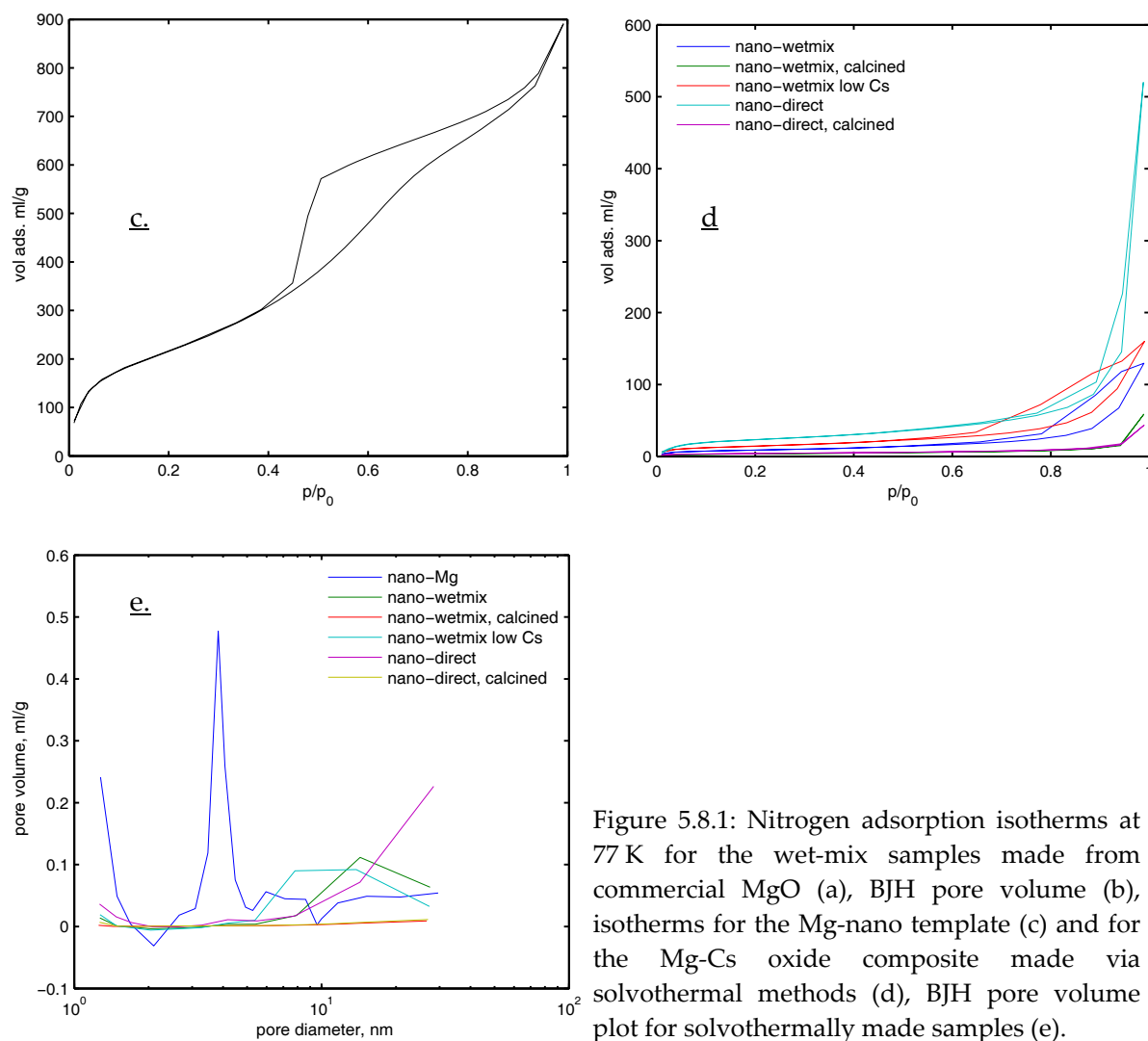
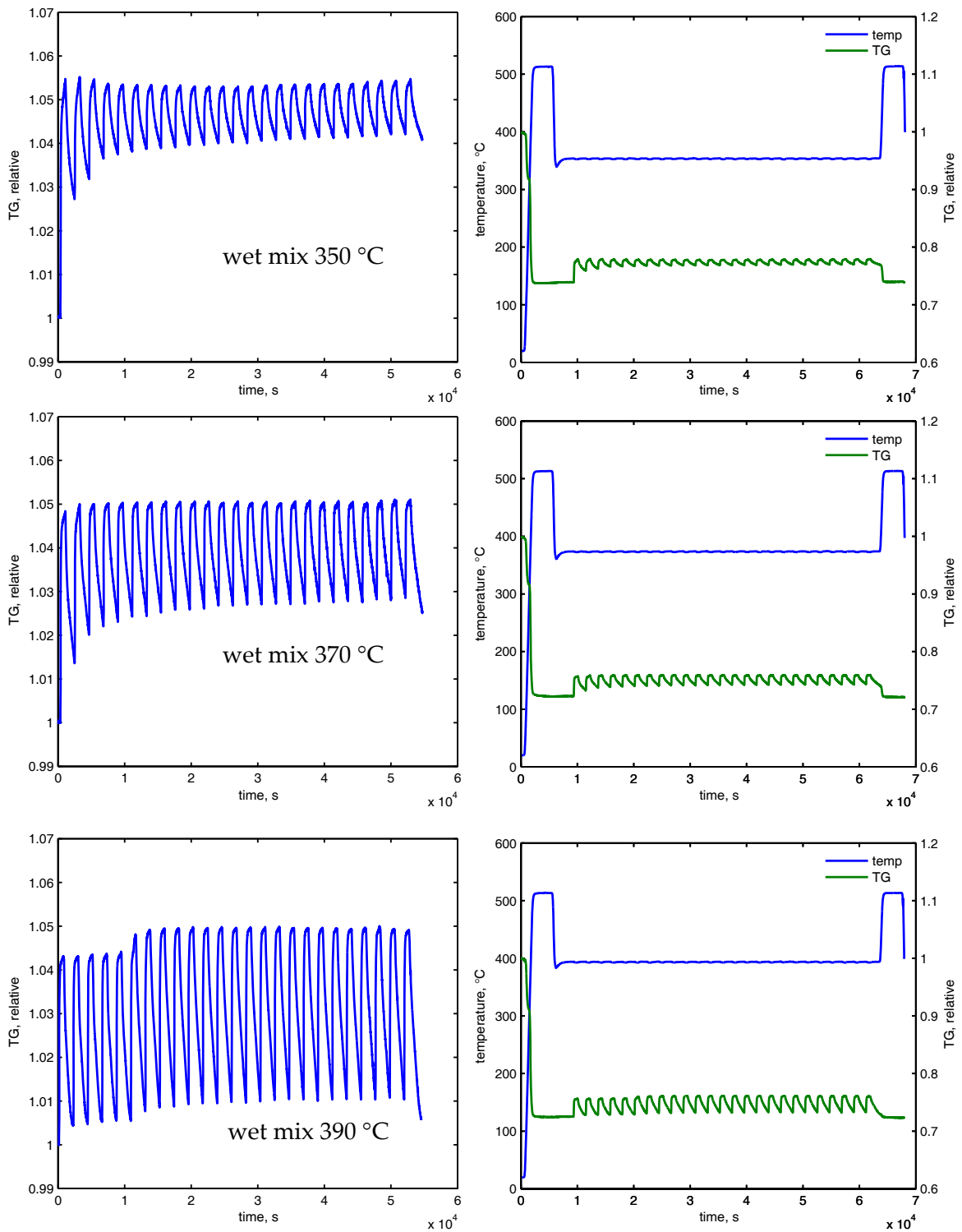
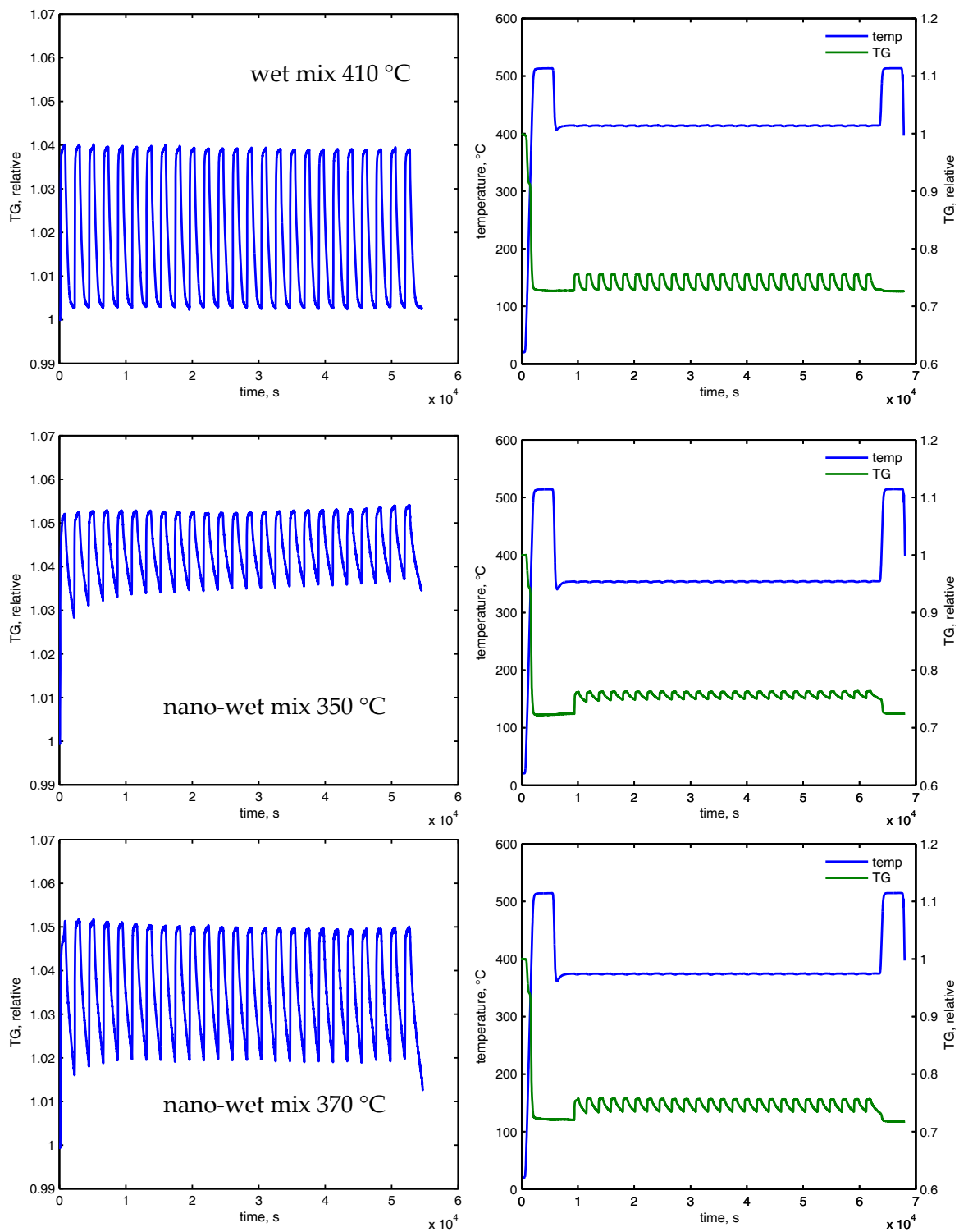
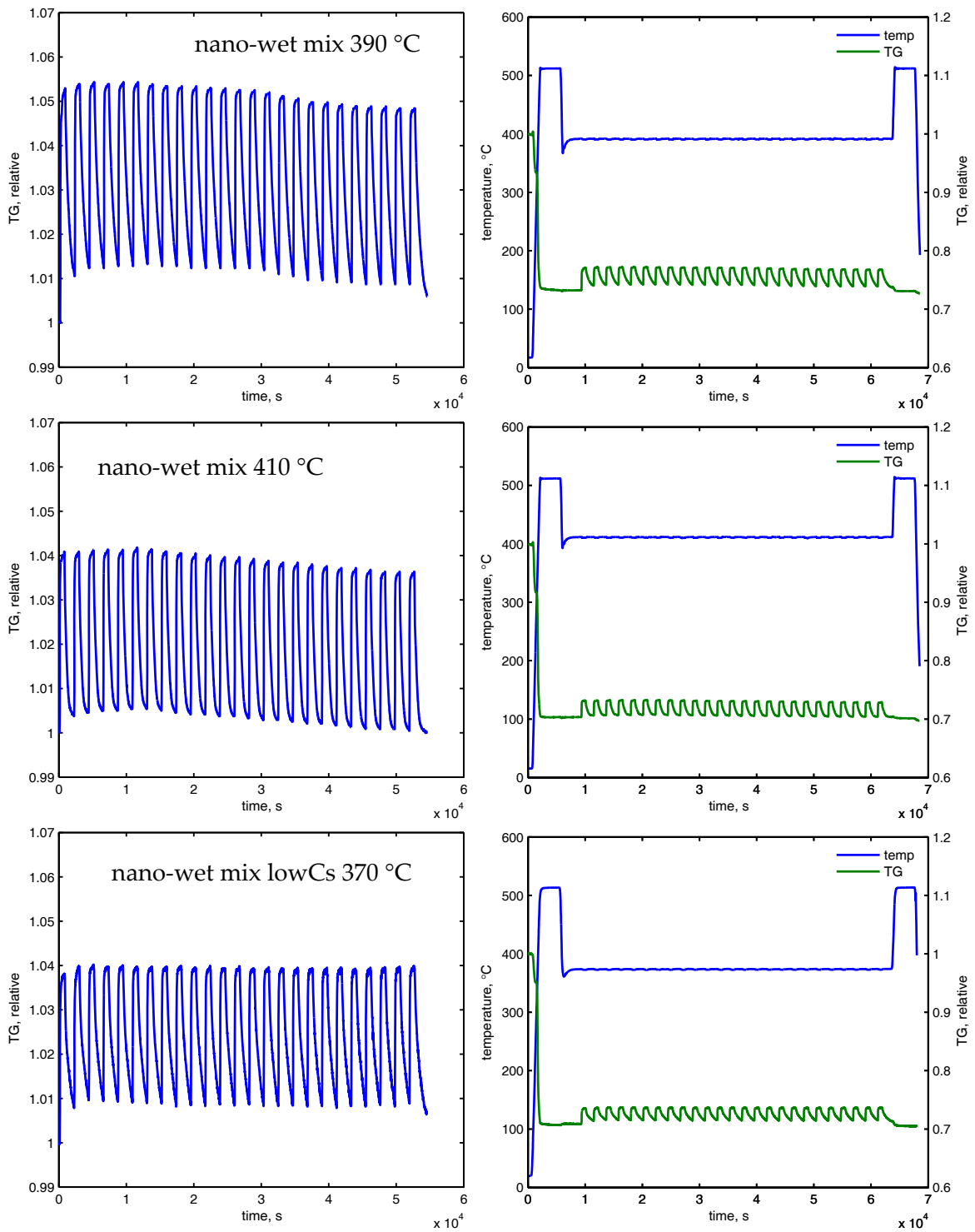


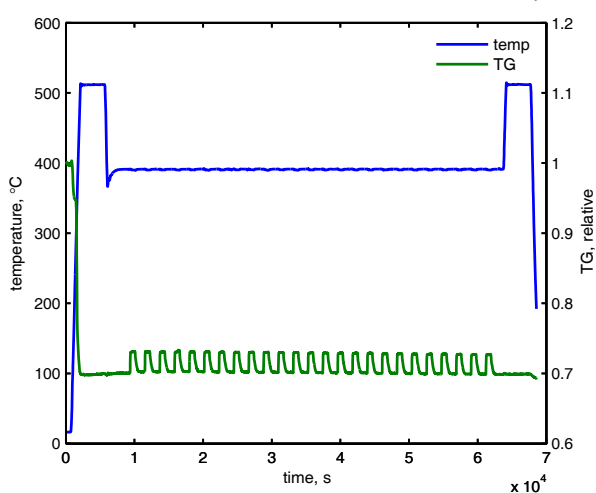
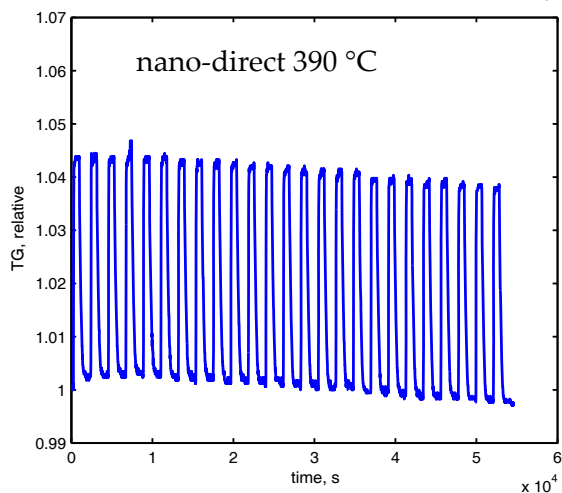
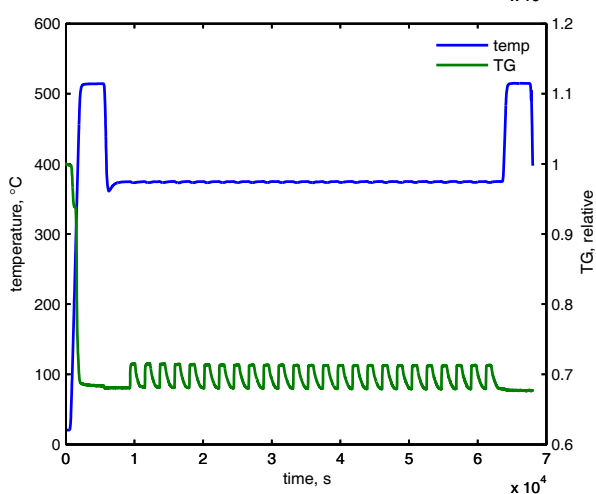
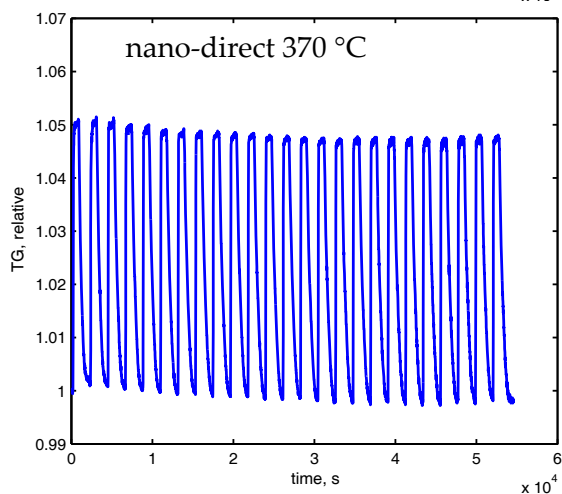
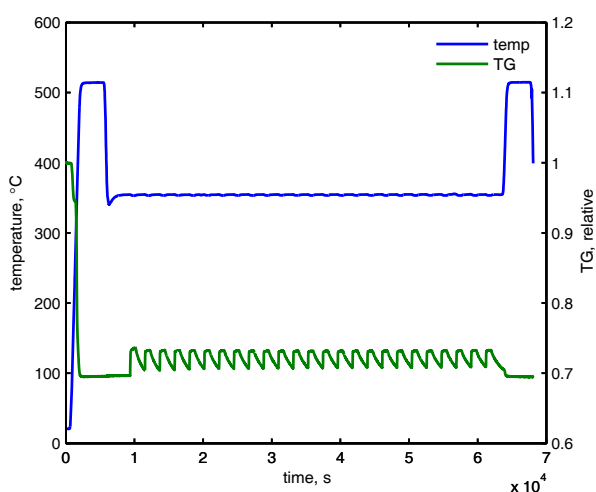
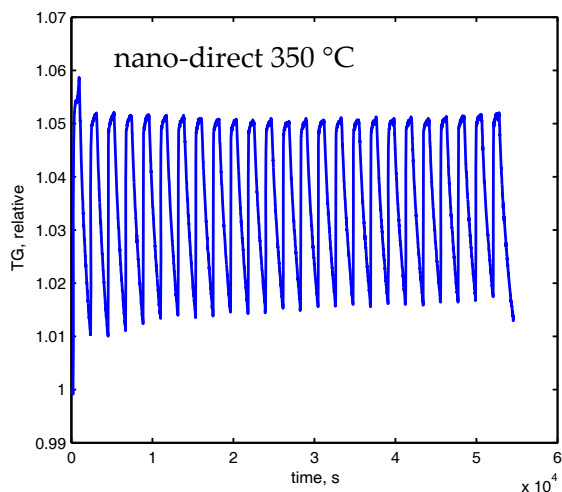
Figure 5.8.1: Nitrogen adsorption isotherms at 77 K for the wet-mix samples made from commercial MgO (a), BJH pore volume (b), isotherms for the Mg-nano template (c) and for the Mg-Cs oxide composite made via solvothermal methods (d), BJH pore volume plot for solvothermally made samples (e).

5.9 Detailed TGA plots









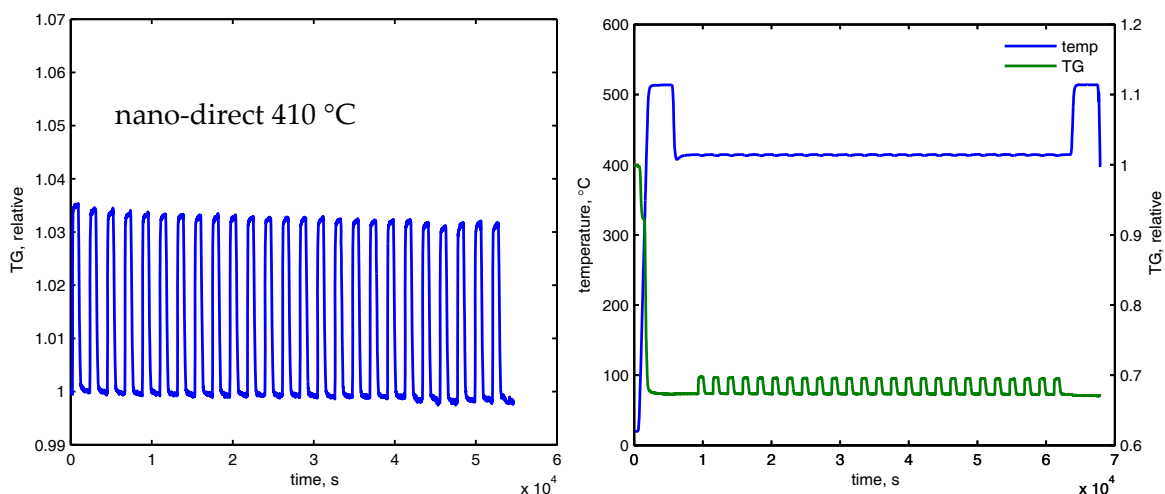
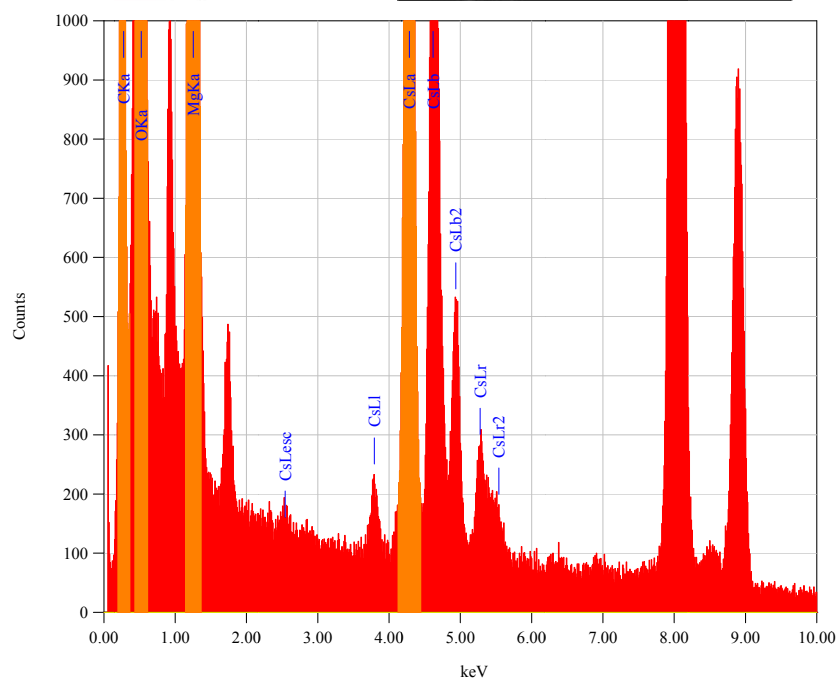
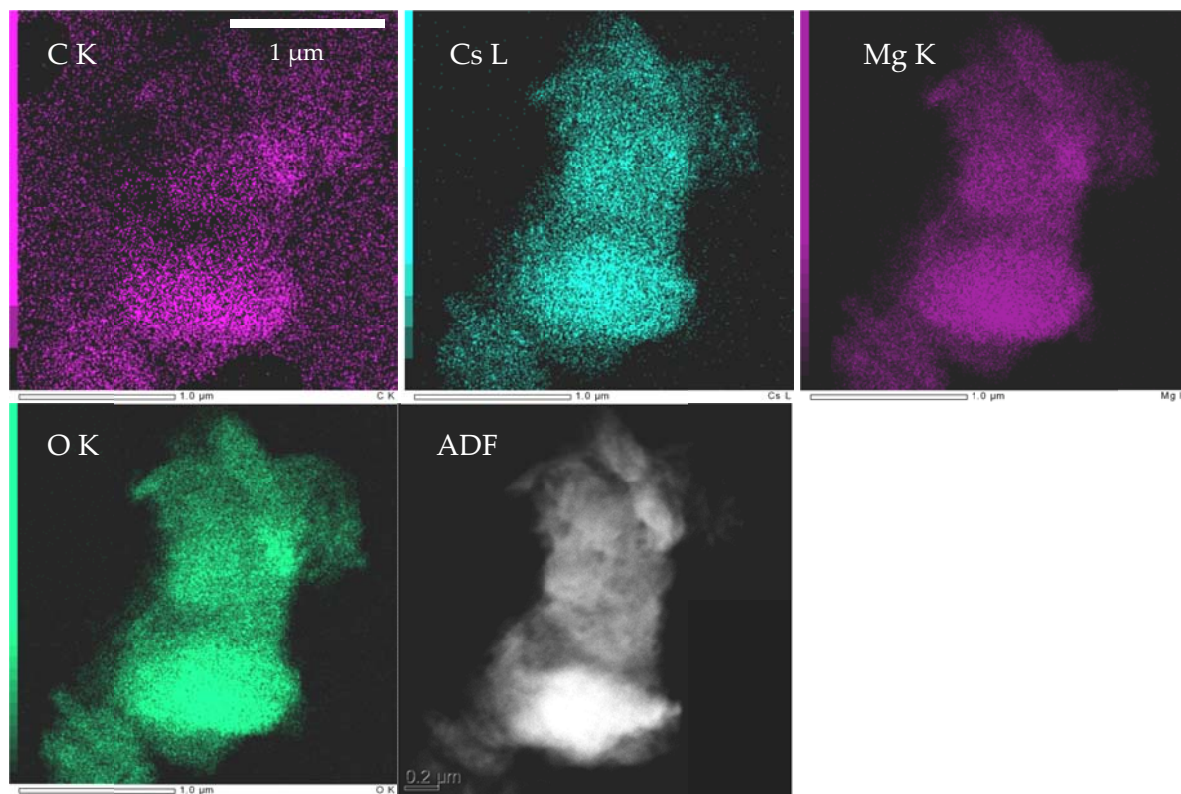


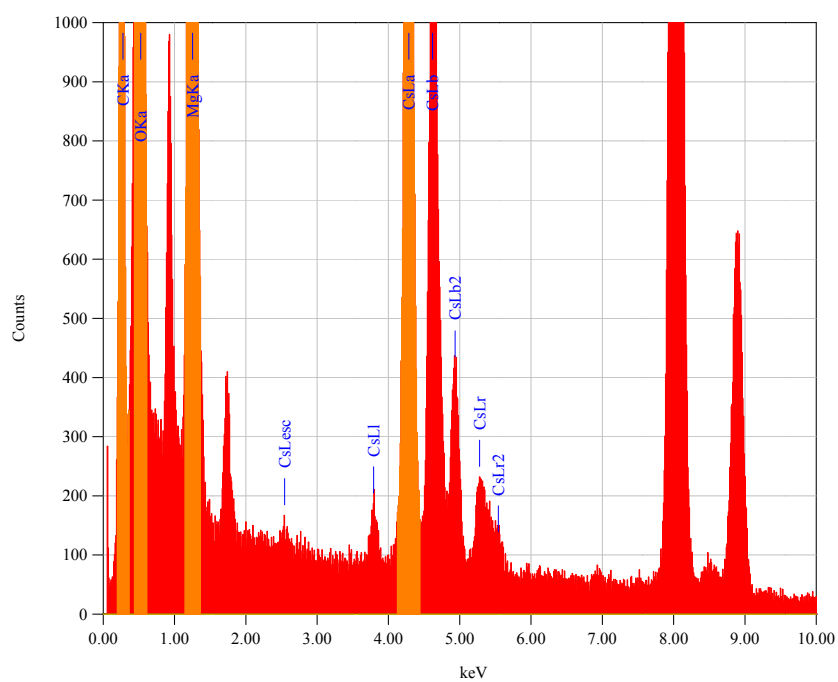
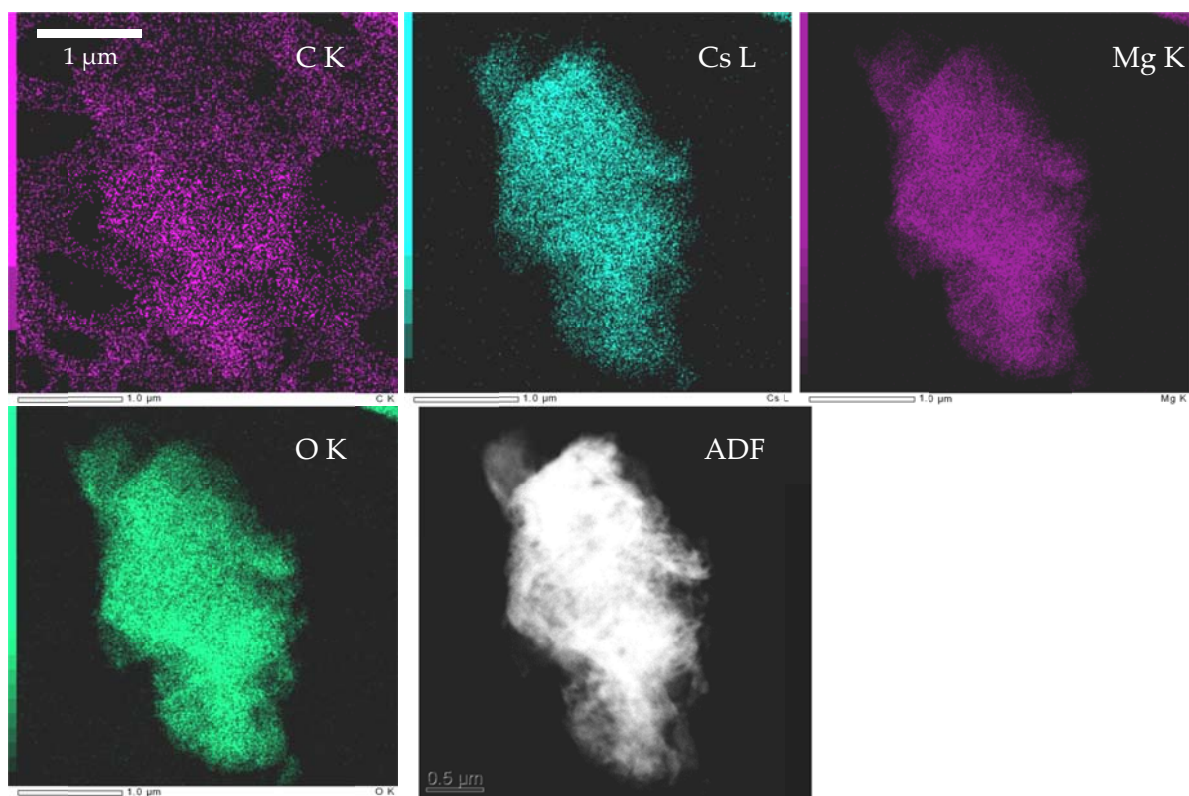
Figure 5.9.1: Thermograms (cycle plots, 100 % mass at start of cycles, left) and full plots (100 % mass at start of experiment, right) for the MgO-Cs₂CO₃ materials

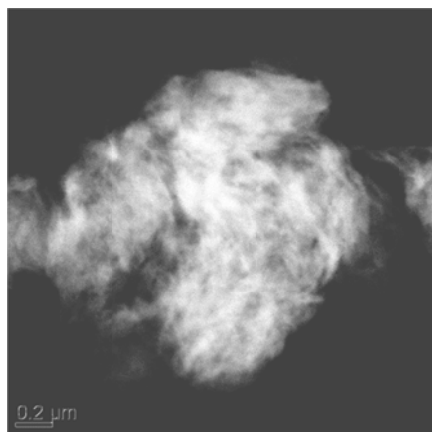
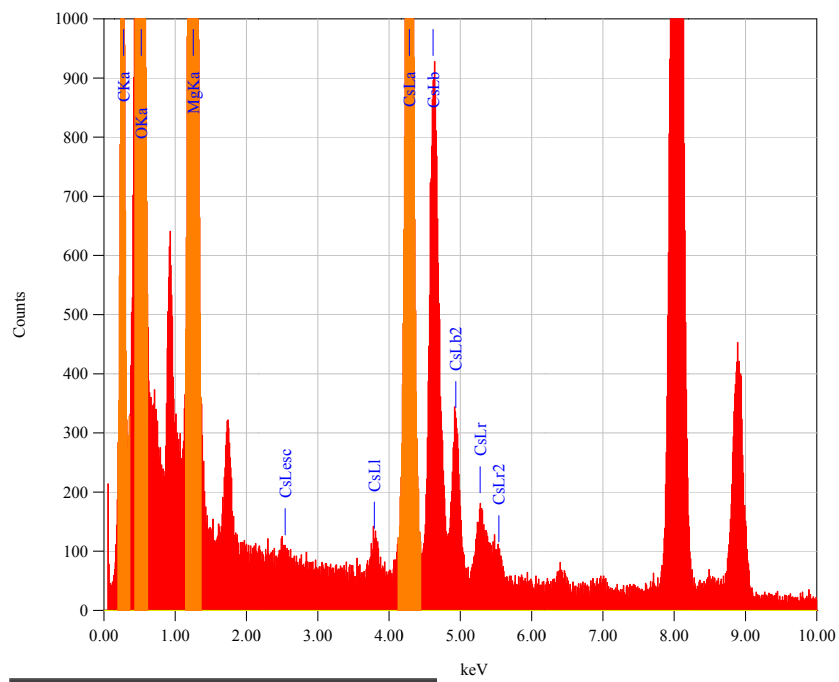
5.10 Energy dispersive X-ray spectra and additional elemental maps

The energy-dispersive X-ray (EDX) spectra confirmed the existence of the elements mapped in the samples (cesium, magnesium, carbon, oxygen) and are given here next to the dark-field images for recognition in the journal article. Additional elemental maps and their respective EDX spectra are shown in this section as well.

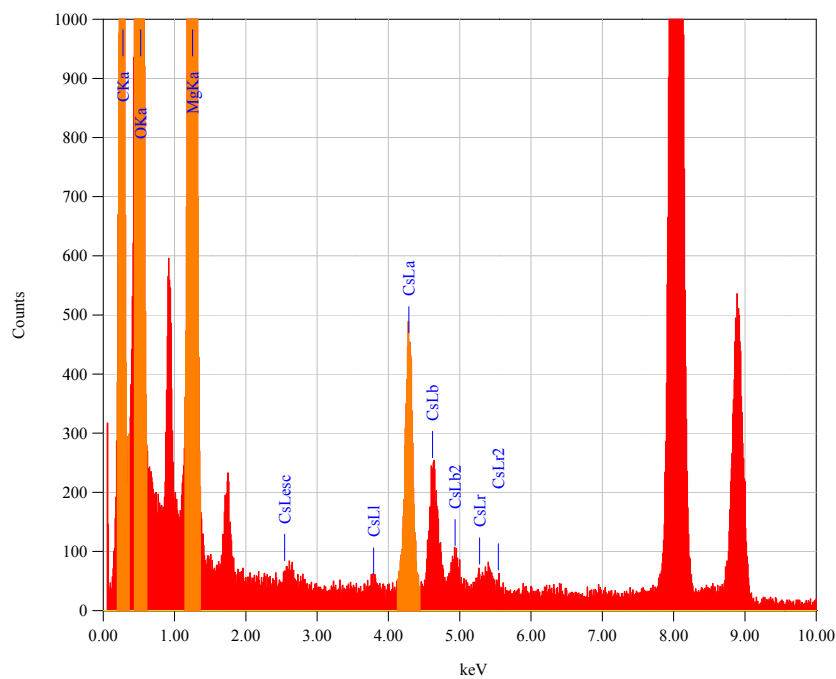
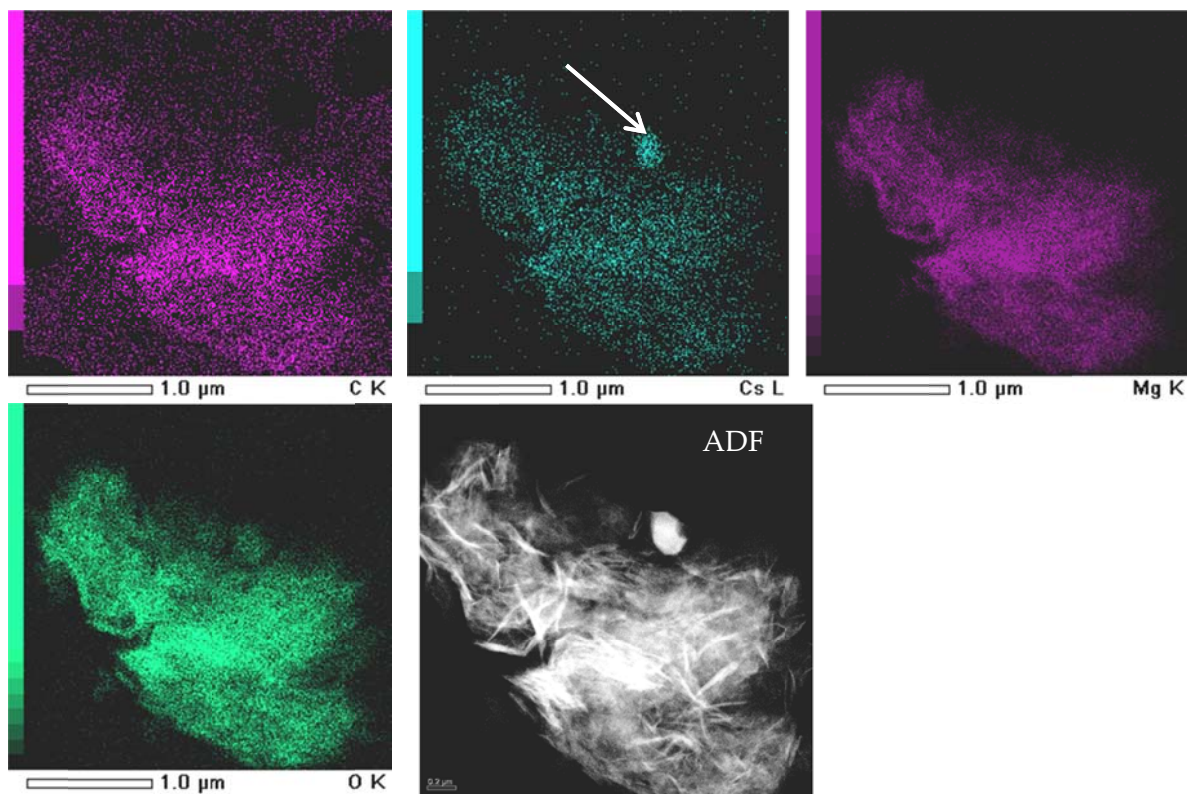
5.10.1 EDX spectra, dark field image and elemental maps of the nano-wet mix as synthesised sample.

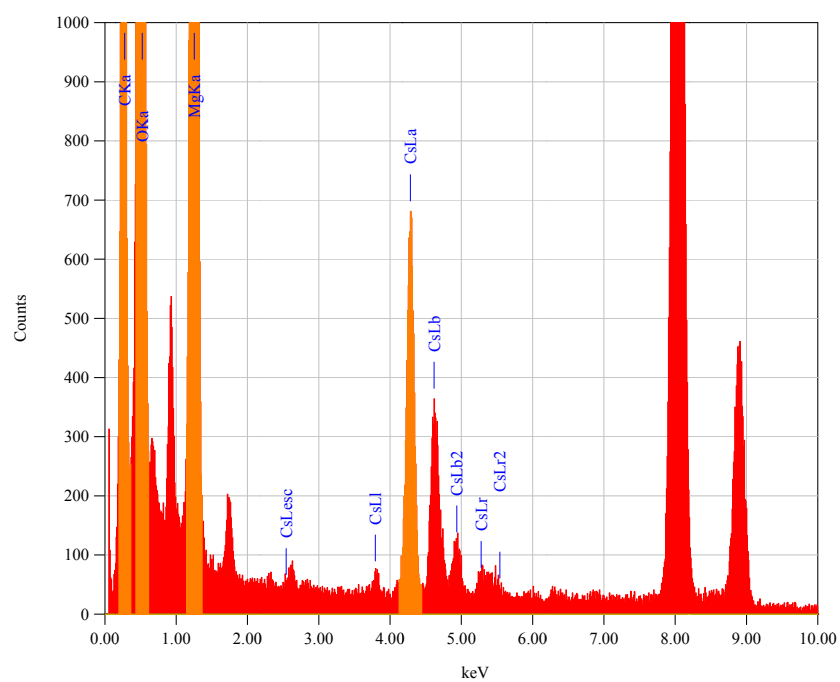
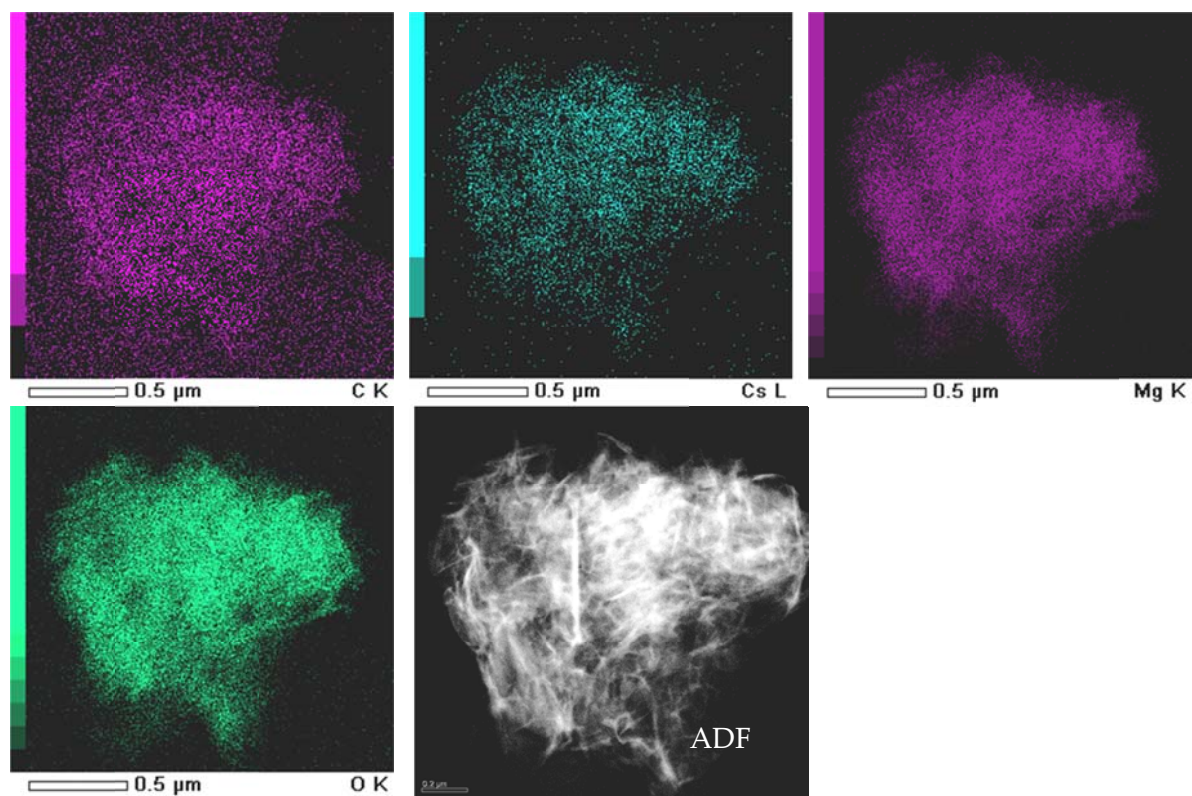


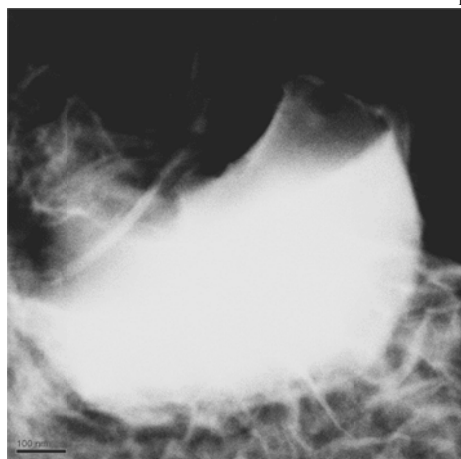
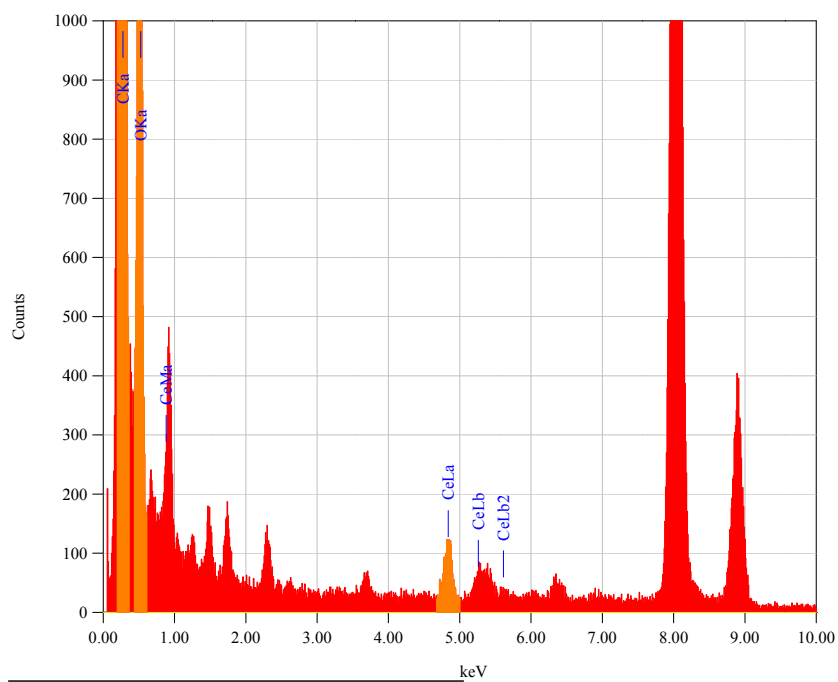




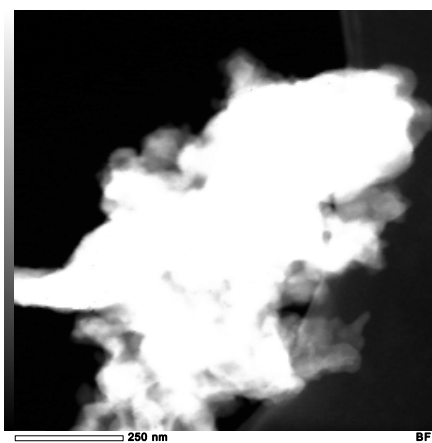
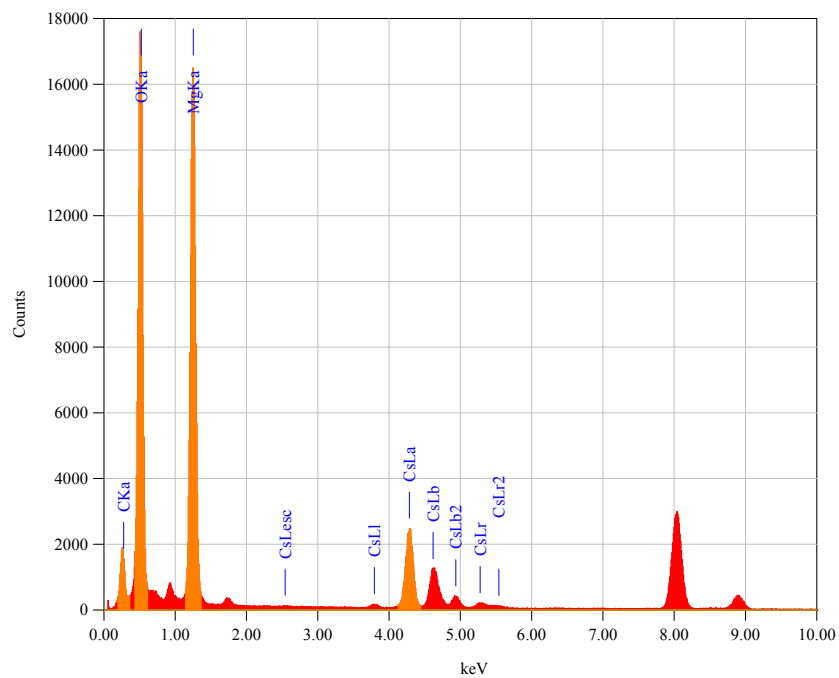
5.10.2 EDX spectra, dark field image and elemental maps of the nano-direct as synthesised sample



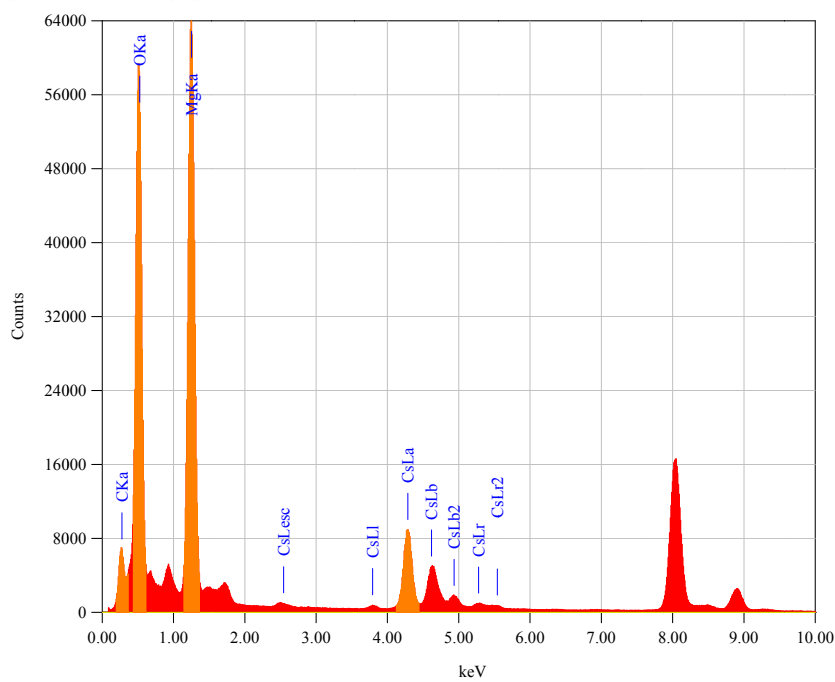
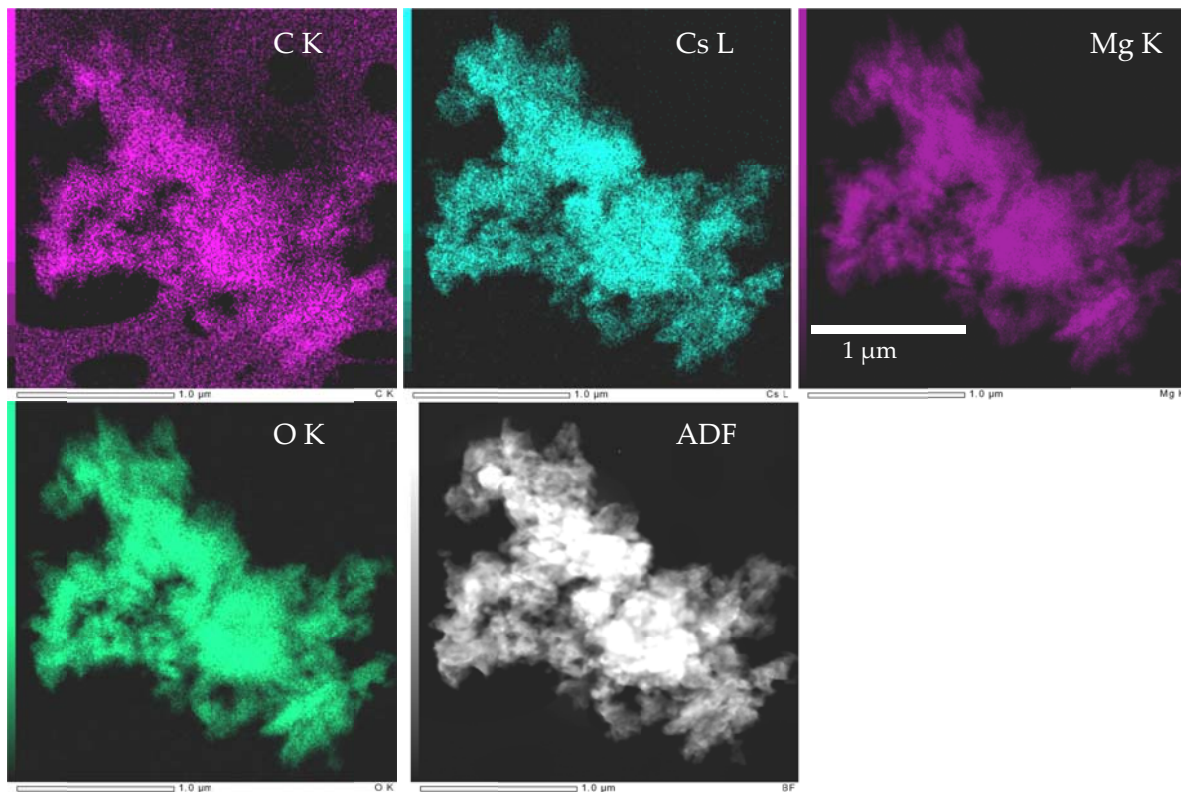


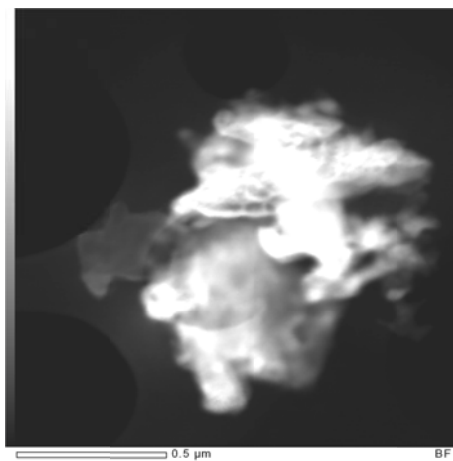
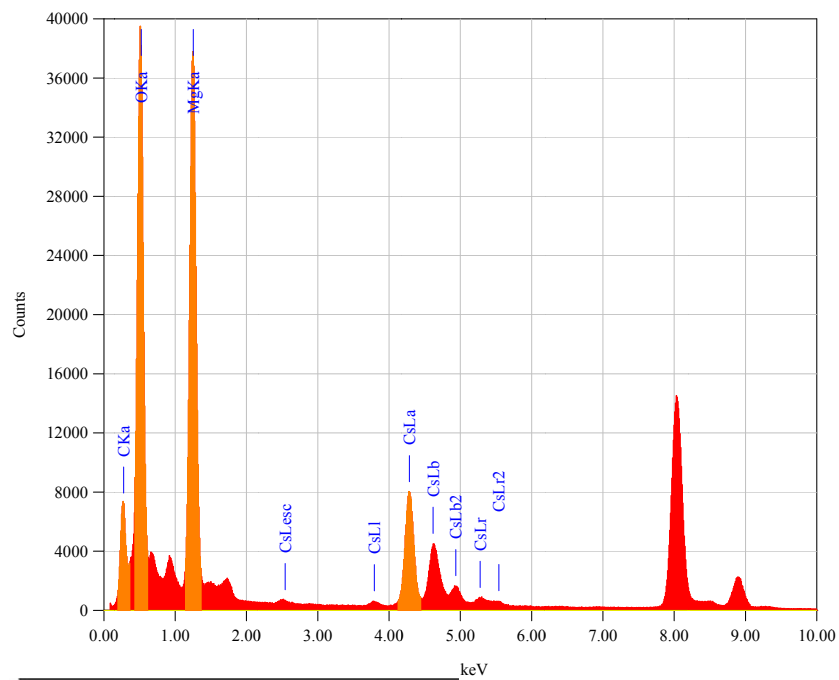


5.10.3 EDX spectrum and dark-field image of the elemental maps of the nano-wet mix carbonated sample.



5.10.4 EDX spectra, dark and bright-field images and elemental maps of the nano-direct carbonated sample.





5.11 References for Chapter 5

- [1] K. S. Lackner, A. H. A. Park, and B. G. Miller, "Eliminating CO₂ Emissions from Coal-Fired Power Plants," in *Generating Electricity in a Carbon-Constrained World*, Boston: Academic Press, 2010, pp. 127-173.
 - [2] P. Markewitz, W. Kuckshinrichs, W. Leitner, J. Linssen, P. Zapp, R. Bongartz, A. Schreiber, and T. E. Müller, "Worldwide innovations in the development of carbon capture technologies and the utilization of CO₂," *Energy & Environmental Science*, vol. 5, pp. 7281-7305, 2012.
 - [3] S. S. Hla, D. Park, G. J. Duffy, J. H. Edwards, D. G. Roberts, A. Ilyushechkin, L. D. Morpeth, and T. Nguyen, "Kinetics of high-temperature water-gas shift reaction over two iron-based commercial catalysts using simulated coal-derived syngases," *Chemical Engineering Journal*, vol. 146, pp. 148-154, 2009.
 - [4] P. Chiesa, S. Consonni, T. Kreutz, and R. Williams, "Co-production of hydrogen, electricity and CO₂ from coal with commercially ready technology. Part A: Performance and emissions," *International Journal of Hydrogen Energy*, vol. 30, pp. 747-767, 2005.
 - [5] H. T. J. Reijers, S. E. A. Valster-Schiermeier, P. D. Cobden, and R. W. van den Brink, "Hydrotalcite as CO₂ Sorbent for Sorption-Enhanced Steam Reforming of Methane," *Industrial & Engineering Chemistry Research*, vol. 45, pp. 2522-2530, 2005.
 - [6] R. Singh, M. K. Ram Reddy, S. Wilson, K. Joshi, J. C. Diniz da Costa, and P. Webley, "High temperature materials for CO₂ capture," *Energy Procedia*, vol. 1, pp. 623-630, 2009.
 - [7] K. Nakagawa and T. Ohashi, "A Novel Method of CO₂ Capture from High Temperature Gases," *Journal of The Electrochemical Society*, vol. 145, pp. 1344-1346, 1998.
 - [8] G. Xiao, R. Singh, A. Chaffee, and P. Webley, "Advanced adsorbents based on MgO and K₂CO₃ for capture of CO₂ at elevated temperatures," *International Journal of Greenhouse Gas Control*, vol. 5, pp. 634-639, 2011.
 - [9] M. Jahan, "Removal of Carbon Dioxide from Gas Streams with Metal Oxides at High Temperature," PhD thesis, School of Chemistry, Monash University, Victoria, Australia, 2011.
 - [10] M. Liu, C. Vogt, A. L. Chaffee, and S. L. Y. Chang, "Nanoscale Structural Investigation of Cs₂CO₃-Doped MgO Sorbent for CO₂ Capture at Moderate Temperature," *Journal of Physical Chemistry C*, vol. 117, pp. 17514-17520, 2013.
 - [11] C. Vogt, G. P. Knowles, S. L. Y. Chang, and A. L. Chaffee, "Cadmium oxide/alkali metal halide mixtures - a potential high capacity sorbent for pre-combustion CO₂ capture," *Journal of Materials Chemistry A*, vol. 1, pp. 10962-10971, 2013.
 - [12] E. Ochoa-Fernández, M. Rønning, X. Yu, T. Grande, and D. Chen, "Compositional Effects of Nanocrystalline Lithium Zirconate on Its CO₂ Capture Properties," *Industrial & Engineering Chemistry Research*, vol. 47, pp. 434-442, 2007.
 - [13] D. M. Ruthven, S. Farooq, and K. S. Knaebel, *Pressure swing adsorption*. New York: VCH Publishers, 1994.
 - [14] R. Yang, *Gas separation by adsorption processes*: Imperial College Press, 1997.
 - [15] S. Utamapanya, K. J. Klabunde, and J. R. Schlup, "Nanoscale metal oxide particles/clusters as chemical reagents. Synthesis and properties of ultrahigh
-

- surface area magnesium hydroxide and magnesium oxide," *Chemistry of Materials*, vol. 3, pp. 175-181, 1991.
- [16] J. Montero, K. Wilson, and A. Lee, "Cs Promoted Triglyceride Transesterification Over MgO Nanocatalysts," *Topics in Catalysis*, vol. 53, pp. 737-745, 2010.
- [17] J. M. Montero, P. Gai, K. Wilson, and A. F. Lee, "Structure-sensitive biodiesel synthesis over MgO nanocrystals," *Green Chemistry*, vol. 11, pp. 265-268, 2009.
-

Chapter 6 Effect of syngas constituents on the sorbents

6.1 Chapter overview

In previous chapters, laboratory testing of multicyclic carbon dioxide sorption via TGA was performed using a gas blend of carbon dioxide in an inert gas, and a pure inert gas for desorption, both also with the addition of water. In real syngas, however, there are other constituents that might have a different impact on the sorbent. Of particular concern is hydrogen, a strong reducing agent, which might react with the metal oxide sorbents to form their respective metallic element. Furthermore, hydrogen sulphide, a trace constituent in syngas, has been previously reported to be sorbed in competition with carbon dioxide, leading to inactivation of the sorbent for carbon dioxide.

The paper presented in this chapter shows screening test results using hydrogen and hydrogen sulphide for the two metal oxide systems described in the previous chapters, namely the CdO-NaI and the MgO-Cs₂CO₃ sorbents. It became evident that reduction due to hydrogen is not a concern at the optimal carbon dioxide sorption temperature. Furthermore, it was studied how hydrogen sulphide and carbon dioxide interact with the sample in competition during a multiple-cycle sorption TGA experiment. A working capacity reduction was observed, likely due to formation of a stable sulphide compound. In a moist mixed hydrogen/carbon dioxide environment, the MgO-Cs₂CO₃ sorbent proved stable in working capacity, whereas the CdO-NaI sorbent showed a capacity decrease, which is speculated to be due to reactions with hydrogen causing the removal or destruction of the halide promoter.

Declaration for Thesis Chapter

The effect of syngas constituents on CdO and MgO based sorbents for pre-combustion CO₂ capture
Monash University

Declaration for Thesis Chapter 6.2-6.8

Declaration by candidate

In the case of Chapter 6.2-6.8, the nature and extent of my contribution to the work was the following:

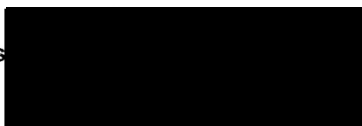
Nature of contribution	Extent of contribution (%)
Proposed original idea; prepared and analysed samples; identified major issues; developed interpretations; fully drafted papers and conclusions	80 %

The following co-authors contributed to the work. If co-authors are students at Monash University, the extent of their contribution in percentage terms must be stated:

Name	Nature of contribution	Extent of contribution (%) for student co-authors only
Gregory P Knowles	Aided method development (TGA), input to results analysis, input to manuscript revision	N/A
Alan L Chaffee	Supervision, assisted interpretation of results, editorial assistance	N/A

The undersigned hereby certify that the above declaration correctly reflects the nature and extent of the candidate's and co-authors' contributions to this work*.

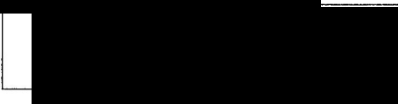
Candidate's
Signature



Date

26/9/13

Main
Supervisor's
Signature



Date

27/9/13

*Note: Where the responsible author is not the candidate's main supervisor, the main supervisor should consult with the responsible author to agree on the respective contributions of the authors.

The effect of syngas constituents on CdO and MgO-based sorbents for pre-combustion CO₂ capture

Christian Vogt, Gregory P Knowles and Alan L Chaffee *

Cooperative Research Centre for Greenhouse Gas Technologies (CO₂CRC), School of Chemistry, Monash University, VIC 3800, Australia

* corresponding author: [REDACTED]

Phone: +[REDACTED] Fax: +[REDACTED]

6.2 Abstract

Magnesium oxide/cesium carbonate composites as well as a cadmium oxide/sodium halide mixture have been previously described as potential candidates for pre-combustion carbon dioxide capture. Here, the effects of water and hydrogen alongside carbon dioxide were examined in simulated partial pressure swing experiments analysed by thermogravimetric means. It was shown that the magnesium-cesium sorbents are tolerant to hydrogen at a temperature of 370 °C and that their working capacities over 25 cycles are enhanced by the addition of water to the sorption gas stream. The cadmium-sodium iodide sorbent showed a stable working capacity for 23 sorption cycles at 285 °C, but tended to lose working capacity afterwards. At a temperature of 305 °C, a significant loss in capacity was observed during sorption cycling. As reduction in an inert gas/hydrogen mixture was not found to commence below 400 °C, a halide promoter disintegration mechanism is assumed to be the cause of the decay. The sorption of H₂S was also examined. Both cadmium and magnesium-based materials showed a significant uptake of H₂S, which was hard to desorb. It appears that H₂S sorption competes alongside carbon dioxide sorption causing a reduction in working capacities over multiple cycles. Powder X-ray diffraction showed that the cadmium-based sorbent forms CdS upon H₂S sorption, whereas the MgO phase of the magnesium-based sorbent is not changed. A new cesium phase was formed from cesium carbonate with H₂S, which is probably a previously unreported magnesium-cesium sulphide mixed phase.

6.3 Introduction

Anthropogenic greenhouse gas emission, especially of carbon dioxide from fossil fuel combustion, has been reported to be a contributor to climate change and associated global warming [1]. As fossil fuels are predicted to play an important role in the energy generation in the mid-term future, carbon dioxide capture and storage is considered a viable option to slow down climate change [2, 3]. Alongside the retrofitting of carbon dioxide capture systems to existing power plant processes (post-combustion capture), new power plant processes are under development that incorporate carbon dioxide capture in order to avoid its release to the atmosphere.

An example of such a process is the Integrated Gasification Combined Cycle (IGCC) process. Here, synthesis gas (syngas) is produced by gasifying coal in a low oxygen atmosphere containing steam at high temperatures. This syngas is made up of carbon monoxide and water, which is then shifted to hydrogen and carbon dioxide in a water gas shift (WGS) reactor located downstream of the gasifier [1]. Subsequent in-situ removal of the carbon dioxide from the WGS reactor to yield hydrogen fuel (pre-combustion capture) would be beneficial, as additional energy input to heat or cool the gas for carbon dioxide capture could then be avoided.

As the WGS reaction is typically conducted between 250 and 400 °C [4], recent studies have focussed on a magnesium-cesium composite [5] (Chapter 5) and a cadmium oxide-alkali halide mixture [6] that reversibly sorb carbon dioxide at temperatures around 370 °C and 300 °C, respectively. Both these sorbents have been shown to work well for selectively capturing carbon dioxide from mixtures with argon, achieving up to 5 wt% working capacity (Mg-Cs sorbent, Chapter 5) or up to 18 % (Cd sorbent, Chapter 3/section 3.14.1) in 12 minutes sorption/24 minutes desorption cycles. 1.2 vol% water addition to the gas stream showed a beneficial effect on multicyclic carbon dioxide sorption on the cadmium-based sorbent (Chapter 3, section 3.14.1), but had no effect on the magnesium-based sorbent [5]. It must, however, be noted that the latter was only checked during a single carbon dioxide sorption cycle.

It must, however, be noted that syngas contains hydrogen, which is a strong reducing agent. Conceivably, this might lead to difficulties in the use of metal oxide-based sorbents

in a syngas environment, as it might reduce the oxides into their respective metallic forms. Furthermore, trace impurities contained in syngas, like H_2S , are reported to react with metal oxide sorbents [7], which might then compete with carbon dioxide sorption.

The use of hydrotalcite materials for use in pre-combustion carbon dioxide capture has previously been reported. During fixed-bed studies, it was shown that the material can reversibly sorb and desorb both hydrogen sulphide and carbon dioxide in the presence of water and hydrogen at a pressure of 5 bar and a temperature of 400 °C [8, 9]. These materials, however, have also been shown to have comparatively low carbon dioxide sorption capacities (~ 4 wt%) in anhydrous conditions [10, 11]. Hydrotalcite sorbents [12] and calcium oxide-based sorbents [13, 14] have shown a retention of strongly bound sulphur compounds in the scope of post-combustion carbon dioxide capture from flue gases. It is hypothesised that H_2S also reacts with $\text{MgO-Cs}_2\text{CO}_3$ and CdO-NaI composites in a similar manner to carbon dioxide, forming either cadmium sulphide instead of carbonates, or, as observed in the $\text{MgO-Cs}_2\text{CO}_3$ sorbent, a mixed Mg-Cs phase while keeping the MgO phase mostly intact [15], similar to the one observed for carbonation.

This study is concerned with proposed CdO-NaI and $\text{MgO-Cs}_2\text{CO}_3$ composites towards the syngas constituents hydrogen, water, carbon dioxide and H_2S . Screening tests using thermogravimetric analysis (TGA) were used to examine the temperature range of the materials' tolerance towards hydrogen and H_2S . Multicyclic carbon dioxide sorption performance was studied using 50 % carbon dioxide in argon containing 0.2 % H_2S , which was also used in a previous study, representing a typical concentration in syngas [9]. TGA of multicyclic carbon dioxide sorption was also conducted in the presence of hydrogen, carbon dioxide (1:1 volume ratio) and 2.4 % water. This experiment aimed at mimicking the main components of syngas and testing the ability of the sorbents in this environment. Treatment of active sorbents with H_2S was also studied by powder X-ray diffraction (XRD) to further investigate any reactive chemistry.

6.4 Experimental section

6.4.1 Sorbent synthesis

The cadmium-based carbon dioxide sorbent was synthesised using a simple wet mixing approach described elsewhere [6]. Cadmium carbonate was dispersed in an aqueous solution of sodium iodide, so as to yield a mass fraction of 17.5 wt% NaI based on CdCO_3 . $\text{MgO-Cs}_2\text{CO}_3$ composites were made similarly by dispersing MgO into an aqueous solution of Cs_2CO_3 . Here, the cesium loading was adjusted to be 15 mol% Cs and 85 mol% MgO, which was determined to be the best-performing concentration in a previous study [5]. This sample is named 'Mg-Cs-wetmix'. A solvothermally synthesised $\text{MgO-Cs}_2\text{CO}_3$ composite was also analysed in this study. Its synthesis comprised the use of a solution of magnesium methoxide and cesium carbonate in methanol and toluene, which was hydrolysed with water and subsequently treated in an autoclave at 265 °C. At this temperature, the solvent vapour was vented to yield the precipitated powder sample (refer also Chapter 5). This sample is labelled 'Mg-nano-direct'.

After synthesis, all samples were dried in a nitrogen-purged oven at 120 °C overnight and stored in sealed vials for future use.

6.4.2 Thermogravimetric analysis (TGA)

A Setaram TAG 24-16 symmetrical thermoanalyser equipped with Bronkhorst model F-201DV-RAD-11-K programmable mass flow controllers was used. A sample mass of approx. 30 mg and total gas flow of 70 mL/min (35 mL/min on either sample and reference side of the balance) was used for the experiments.

In a screening test (which was similarly used for carbon dioxide tests [6]), the sample was heated up in pure argon flow to 610 °C and held at that temperature for 20 minutes. Afterwards, it was cooled to 125 °C and the gas flow was switched to either 50 % hydrogen in Ar, or to 1 % H_2S in Ar, while the temperature was ramped up to 610 °C (Figure 6.4.1a). The exposure to the reactive gases (H_2 , H_2S) over this temperature ramp was designed to indicate at which temperature the samples react with the hydrogen or H_2S , respectively. 1 % H_2S was chosen as a concentration significantly higher than in a

typical syngas in order to observe the effects on the sample in laboratory scale as well as possible.

In a second series of TGA experiments (Figure 6.4.1b), samples were exposed to 25 cycles of carbon dioxide sorption (12 minutes) and desorption (24 minutes) by switching the gas from pure Ar to a mixture of ‘contaminated’ carbon dioxide in argon (i. e., 50 % Ar, 0.2 % H₂S, 49.8 % CO₂). A pre-treatment step in pure Ar at 510 °C (Mg sorbents) or 380 °C (Cd sorbent) was performed both at the beginning and the end of the experiment to bring the material into its activated/initial state. The H₂S concentration of 0.2 % was chosen as a typical concentration of H₂S in a syngas, reported to be between 0.2 % and 1.3 %, depending on the type of gasifier, for unshifted syngas [16], and also used in a different experimental study [9].

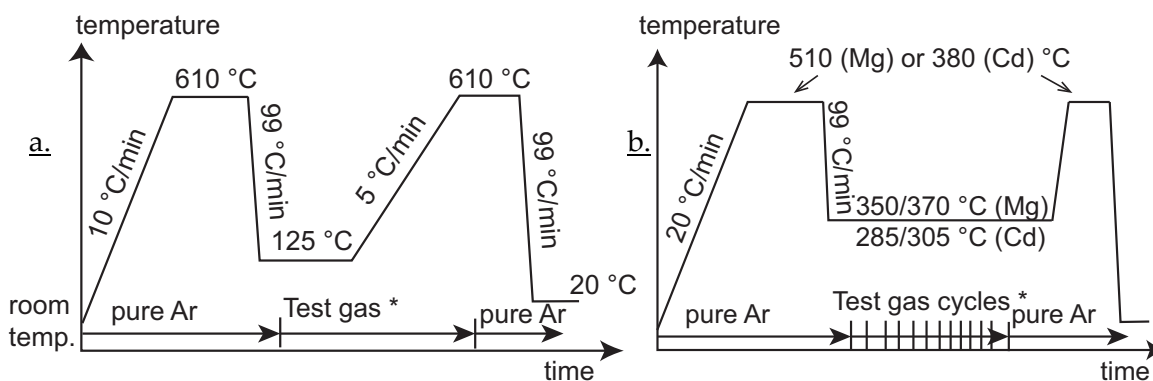


Figure 6.4.1: a. TGA screening test procedure, b. multicyclic procedure. * Test gas denotes 50 % H₂ in Ar or 1 % H₂S (Cd) or 0.2 % H₂S (Mg) in Ar for a.; and either 50 % Ar, 0.2 % H₂S, 49.8 % CO₂ or 48.8 % H₂, 48.8 % CO₂, 2.4 % water (sorption cycles), dry Ar (desorption cycles) for b.

A third set of TGA experiments, designed to mimic exposure of the samples to syngas, used 25 cycles of carbon dioxide sorption in a similar way. Here, a mixture of 48.8 % H₂, 48.8 % CO₂ and 2.4 % water was used for sorption. Water addition was achieved by bubbling carbon dioxide and hydrogen through wash bottles with distilled water, which were kept in a cooling bath at 10 °C. Desorption cycles were performed in pure dry argon, which meant reducing the partial pressure of the syngas constituents to zero, similar to a vacuum being drawn on the sample in a pressure swing process.

6.4.3 Analysis of samples exposed to H₂S

In order to examine the hydrogen sulphide uptake of the sorbents and their phase transformation, saturation of samples with H₂S was performed using the furnace and glass tubes of a Micromeritics VacPrep 061 instrument. Approx. 1 g of sample was placed into the tubes, then heated to 380 °C in nitrogen flow. After temperature equilibration (two hours), the gas flow was switched to a 2 % H₂S in Ar mixture. The samples were kept at this temperature for 2.5 hours and were then cooled to room temperature in H₂S/Ar flow. This procedure was selected to produce a sample of sufficient mass (1 g) for the powder XRD experiments, as the samples used in the TGA experiments were too small (between 20 and 30 mg).

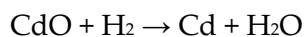
Subsequently, powder X-ray diffraction was performed on these samples using a Bruker D8 focus diffractometer with Cu K α radiation. Scans were obtained between 5 and 80 ° 2 θ at a step size of 0.02 ° and a speed of 0.5 °/min. Powder Diffraction File entries 04-001-3770 (CdO), 00-041-1049 (CdS) and 04-010-4039 (MgO) were used to index peaks in the patterns.

6.5 Results

6.5.1 Cadmium-based sorbent

The results of the screening test in 50 % hydrogen for the CdO-NaI sample are shown in Figure 6.5.1. The full thermogram with the mass normalised to 100 % at the start is shown in Figure 6.5.1a, whereas Figure 6.5.1b shows the second temperature ramp with the mass set to 100 % at the beginning of the ramp. At the beginning of the ramp, the sorbent is considered to be in its active state, as the initial decarbonation to cadmium oxide occurred in the pre-treatment step, as evident by a mass loss to 80 % of the initial mass (Figure 6.5.1b).

It is observed that the material is stable up to 400 °C in the presence of hydrogen (Figure 6.5.1b). Heating beyond this temperature causes the material to lose mass, which is considered to be due to the reduction of Cd²⁺ to Cd⁰ via reaction with hydrogen (eqn. 6.5.1). The initially dark red to brown powder (cadmium oxide) was subsequently found to have transformed into small metallic particles, supporting the suggestion that cadmium oxide is reduced by hydrogen to form metallic cadmium.



eqn. 6.5.1

The result of this screening test indicates that, at the ideal sorption temperature of around 300 °C (refer to [6]), the material does not appear to be affected by hydrogen.

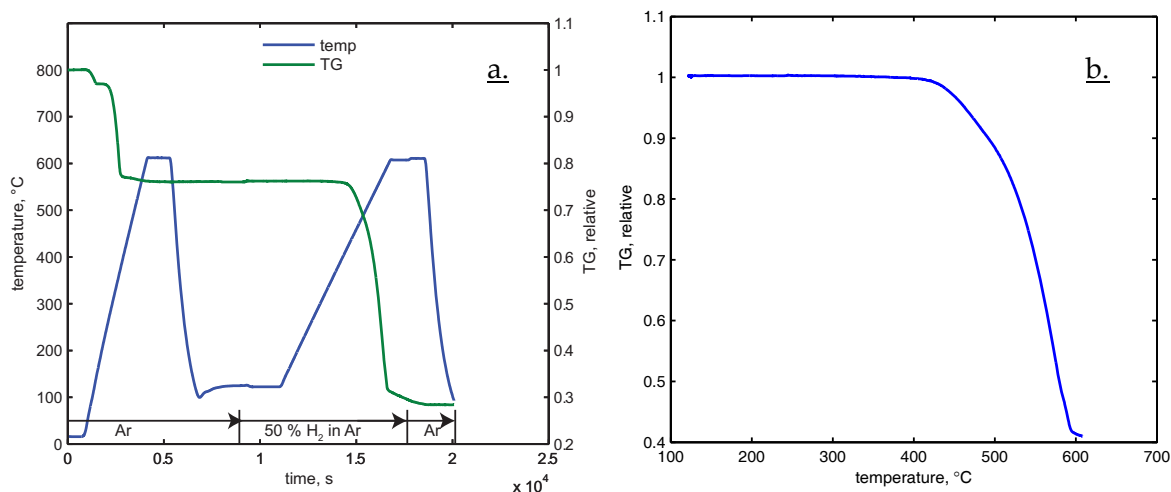


Figure 6.5.1: Hydrogen TGA screening test of a $\text{CdCO}_3\text{-NaI}$ sorbent sample. a. full thermogram, b. second temperature ramp of a. with hydrogen exposure vs. temperature.

A similar experiment was performed using hydrogen sulphide, with the results shown in Figure 6.5.2. It is evident from the mass increase with temperature that hydrogen sulphide was sorbed by the sample after H_2S had been added to the argon flow. The initial inflexion at 120 °C is an artefact of the gas changeover but, from about 300 °C, there is continuous mass increase observed up to about 500 °C (Figure 6.5.2b). After the H_2S has been removed from the argon flow, the mass does not fall significantly, indicating that the hydrogen sulphide is strongly bound to the sample and hard to desorb. The stoichiometric conversion of the sorbent would equate to a mass gain of 9.5 %, assuming the presence of the sodium iodide and only the reaction of the cadmium oxide to sulphide. This means that stoichiometric saturation was not achieved in the screening test (Figure 6.5.2). It must however be noted that the ramp test is not considered the appropriate design for a saturation experiment. Another artefact due to gas changeover took place upon switching back to pure argon flow, which was hard to avoid (experiment was repeated once). The sorption of H_2S might have an impact on the carbon dioxide sorption capabilities of the material in the presence of syngas, as H_2S (a trace constituent of syngas) sorption likely

competes with carbon dioxide sorption and, thus, might reduce the material's reversible carbon dioxide sorption capability. This was tested and the results are reported next.

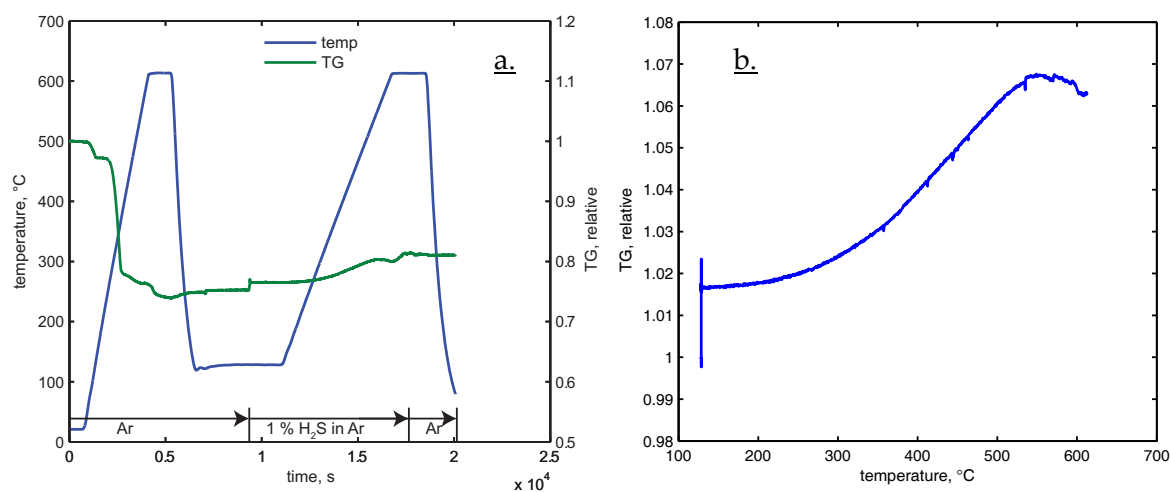


Figure 6.5.2: Hydrogen sulphide TGA screening test of a $\text{CdCO}_3\text{-NaI}$ sorbent sample. a. full thermogram, b. second temperature ramp of a. with hydrogen sulphide exposure plotted vs. temperature.

The results of a 25 cycle carbon dioxide sorption/desorption experiment, where the sorption gas stream contained 0.2 % H_2S alongside carbon dioxide, are shown in Figure 6.5.3. In addition, Table 6.5.1 and Table 6.5.2 summarise the working capacities using both CO_2/Ar (previous study, Chapter 3/section 3.14.1) and $\text{CO}_2/\text{H}_2\text{S}/\text{Ar}$ mixtures (this study). For the 285 °C case (Figure 6.5.3a), it can be observed that an initially large mass uptake is followed by a very small mass loss during desorption. This is because the desorption is not strongly favoured at this temperature and higher temperatures are required for full desorption, as shown in (Chapter 3/section 3.14.1 and 3.18).

There is also a constant downwards baseline drift over the cycles, possibly due to iodide promoter loss, as observed for experiments in pure carbon dioxide and argon mixtures (wet and dry, refer Chapter 3, section 3.18). In the final desorption step at 380 °C, an increased mass can be observed (comparing baselines before and after cycles as shown by arrows in Figure 6.5.3a). It appears that H_2S reacted with and reaction products were retained by the sample during the multiple cycles.

In a similar study undertaken with pure carbon dioxide (Chapter 3/sections 3.14.1 and 3.18), such mass retention was not observed; on the contrary, a mass loss being attributed

to halide loss was observed. It can also be seen that the working capacities are reduced over cycles and the overall working capacities in the 'contaminated' carbon dioxide are lower than in pure carbon dioxide (refer Chapter 3/sections 3.14.1 and 3.18 for the exact derivation of working capacities, Table 6.5.1, and working capacities in argon/carbon dioxide experiments (without H₂S) of previous projects (Chapter 5 and [6]) summarised in Table 6.5.2). At the higher temperature of 305 °C (Figure 6.5.3b), desorption is substantially improved, but the capacity decay over successive cycles is even worse than at the lower temperature. Also, at the higher temperature a mass retention at the end of the cycles is observed, which is assumed to be due to reaction with H₂S into a strongly bonded cadmium compound, which was also shown by the screening test in Figure 6.5.2. The decay in working capacity is much worse than if wet carbon dioxide in argon (without H₂S addition) is used (Chapter 3/sections 3.14.1 and 3.18).

Quantification of the incorporation of sulphur into the cadmium-based sorbent has been attempted; the data are shown in Table 6.5.3. If an exchange of O²⁻ with S²⁻ is assumed, in Figure 6.5.3b, the mass retention between the points I and VI would mean that 0.0469 mmol of CdO have changed into CdS. The working capacity in the first cycle (assumed to be only carbon dioxide to be sorbed and desorbed) was 2.565 mg, or 0.0583 mmol CO₂. This value reduced to 0.56 mg, or 0.0127 mmol, for the 25th cycle. The difference in working capacity between the 1st and 25th cycles is therefore 0.0456 mmol, which is quite close to the deactivated amount of CdO (0.0469 mmol) as stated above. It can thus be concluded that the retention of sulphide is very likely responsible for the deactivation of the active CdO sorbent, by forming a stable cadmium sulphide compound that can no longer sorb carbon dioxide.

A similar calculation for Figure 6.5.3a indicates a retention of 0.83 mg, equating to 0.0519 mmol CdO changing into CdS. The working capacities in the 1st and 25th cycle were 2.08 mg (0.0472 mmol) and 0.72 mg (0.0164 mmol), respectively. It appears here that the difference in working capacity (0.0308 mmol) was less than the amount of CdO deactivated by sulphide formation. This difference calculation however, is probably not appropriate in this case, as the baseline (dash-dotted arrows in Figure 6.5.3a) was not reached at the end of each cycle. This indicates carbon dioxide retention, as the

temperature was not high enough to desorb all carbon dioxide during the short cycle time. If a hypothetical desorption down to the baseline (dash-dotted arrows in Figure 6.5.3a, left baseline for 1st cycle, right for 25th cycle) was assumed, the difference in hypothetical working capacity (0.0687 mmol between 1st and 25th cycle) would be in the order of magnitude of the degenerated sorbent (0.0519 mmol as stated above).

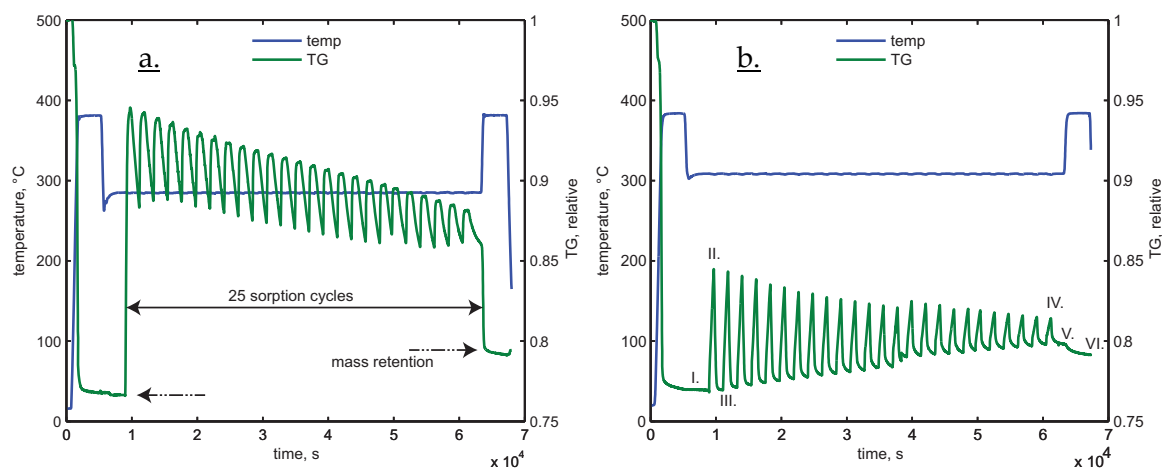


Figure 6.5.3: Isothermal multiple sorption cycles (12 min sorption in 50 % Ar/49.8 % CO₂/0.2 % H₂S, 24 minutes desorption in pure Ar) of a CdCO₃-NaI sample. a. 285 °C, b. 305 °C. Pre-treatment and after-treatment in pure Ar at 380 °C.

In a third set of experiments, the sorbent was exposed to a mixture of hydrogen, carbon dioxide and water for sorption cycles, whereas desorption was performed in pure dry argon. The results are shown in Figure 6.5.4. It can be observed that the material exhibits a comparatively stable working capacity at a temperature of 285 °C. There is, however, a continuous mass loss over the cycles, which is more severe than for the same samples in a similar wet carbon dioxide/argon sorption experiment with 1.2 % water addition, but without hydrogen. However, at 305 °C, an even more severe loss in working capacities and overall mass loss is observed. Using wet carbon dioxide in argon at these temperatures was formerly considered to be the preferred operating condition for this adsorbent, since working capacities were almost completely stable and the overall mass loss was low (Chapter 3/sections 3.14.1 and). It thus appears that hydrogen has a negative effect on these samples.

Table 6.5.1: Working capacities (wt%) for sorbent samples in H₂ and H₂S multicyclic experiments.

Sample	1st cycle	25th cycle	Comments
Cd H ₂ S 285 °C	8.2 %	3.1 %	
Cd H ₂ S 305 °C	9.8 %	2.0 %	
Cd H ₂ 285 °C	10.1 %	12.4 %	
Cd H ₂ 305 °C	20.4 %	0.8 %	
Mg-Cs-wetmix H ₂ S 350 °C	2.5 %	1.3 %	
Mg-Cs-wetmix H ₂ S 370 °C	2.9 %	1.0 %	
Mg-Cs-wetmix H ₂ 370 °C *	4.0 %	3.4 %	
Mg-Cs-wetmix 370 °C wet CO ₂ *	4.0 %	3.0 %	wet gas (1.2 % water) Ar and CO ₂ flow, no H ₂ /H ₂ S.
Mg-nano-direct H ₂ S 350 °C	3.3 %	0 %	0.5 % after 8th cycle, then 0 %
Mg-nano-direct H ₂ S 370 °C	3.9 %	0 %	0.5 % after 7th cycle, then 0 %
Mg-nano-direct H ₂ 370 °C	5.6 %	6.7 %	

* capacity reduction to 3 % in 4th cycle, then stable.

Table 6.5.2: Working capacities of a previous project in dry and wet (1.2 % water) gas cycles containing 50 % CO₂/Ar and pure Ar (no H₂S). Refer section 3.14.1 and 3.18 for Cd and Chapter 5 for Mg samples. Cd sample name of sections 3.14.1 and 3.18 given in comments.

Sample	1st cycle	25th cycle	Comments
Cd wet gas 285 °C	18 %	19 %	285-Ar380-s-w
Cd wet gas 305 °C	24 %	23 %	305-Ar380-s-w
Cd dry gas 285 °C	10 %	10 %	285-Ar380-s-d
Cd dry gas 305 °C	24 %	13 %	305-Ar380-s-d
Mg-nano-direct dry gas 350 °C	4.9 %	3.4 %	
Mg-nano-direct dry gas 370 °C	5.0 %	5.0 %	
Mg-Cs-wetmix dry gas 350 °C	2.8 %	1.3 %	
Mg-Cs-wetmix dry gas 370 °C	3.4 %	2.4 %	

Table 6.5.3: Assessment of degradation of CdO sample due to assumed S²⁻ retention of the experiment in Figure 6.5.3b.

Numeral	Absolute mass, mg	
I.	-7.835	I.-VI.: 0.75 mg (S ²⁻ retention, replacing O ²⁻)
II.	-5.275	III.-II.: 2.565 mg (CO ₂ captured 1 st cycle)
III.	-7.840	V.-IV.: 0.56 mg (CO ₂ captured 25 th cycle)
IV.	-6.315	
V.	-6.875	
VI.	-7.085	total sample mass (TG relative = 1): 34.0 mg

In contrast to the screening test (Figure 6.5.1), which showed that hydrogen has a reducing effect on the samples only at temperatures above 400 °C, it is speculated that hydrogen reacts with the halide promoter (NaI), and that this effect is more pronounced at 305 °C than at 285 °C. Reduction of the sample does not seem to occur, because the weight loss is not great enough and the sample still appeared as a dark red powder characteristic of cadmium oxide after completion of the experiment.

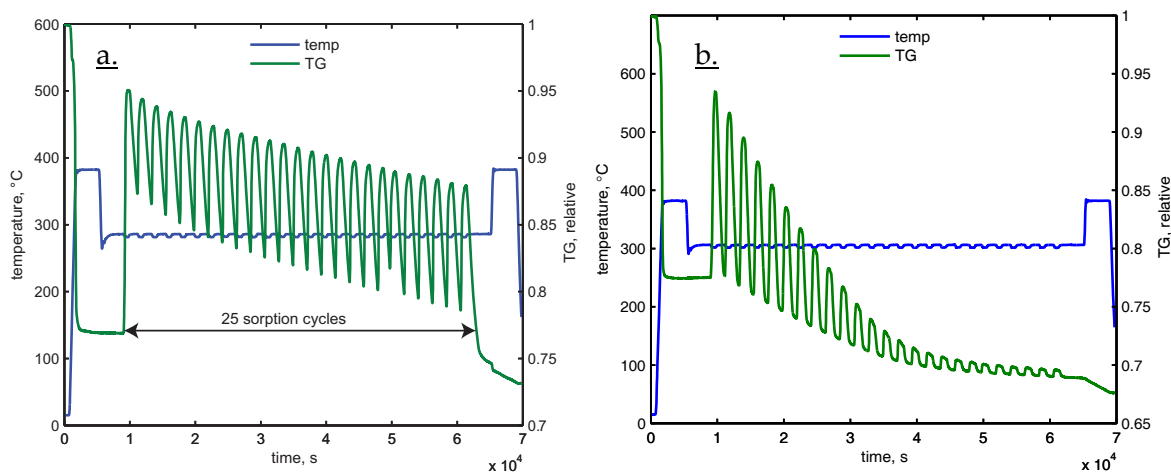


Figure 6.5.4: Isothermal 25-cycles TGA experiment using Cd-NaI sorbent in 48.8 % H₂, 48.8 % CO₂ and 2.4 % water (12 minutes sorption) and pure dry Ar (24 minutes desorption). a. 285 °C, b. 305 °C.

6.5.2 Magnesium-based sorbent

Analogous screening test results for the Mg-Cs-wetmix material, using 50 vol% hydrogen, are shown in Figure 6.5.5. In contrast to the CdCO₃-NaI sorbent (Figure 6.5.1), there was only a slight observable mass loss after hydrogen exposure (Figure 6.5.5a), indicating that this material showed no significant reaction to hydrogen gas. Mass changes of only up to 1 % are evident (Figure 6.5.5b), but measurement uncertainties (buoyancy artefacts) due to the change from 100 % argon to a lower-density 50 % hydrogen/argon mixture (glitch at the beginning of temperature ramp) have reduced the accuracy of the mass measurement in this range. Limited ability to precisely adjust the flow through the furnace also result in uncertainties in the mass measurement, if such small mass changes are the only ones being observed.

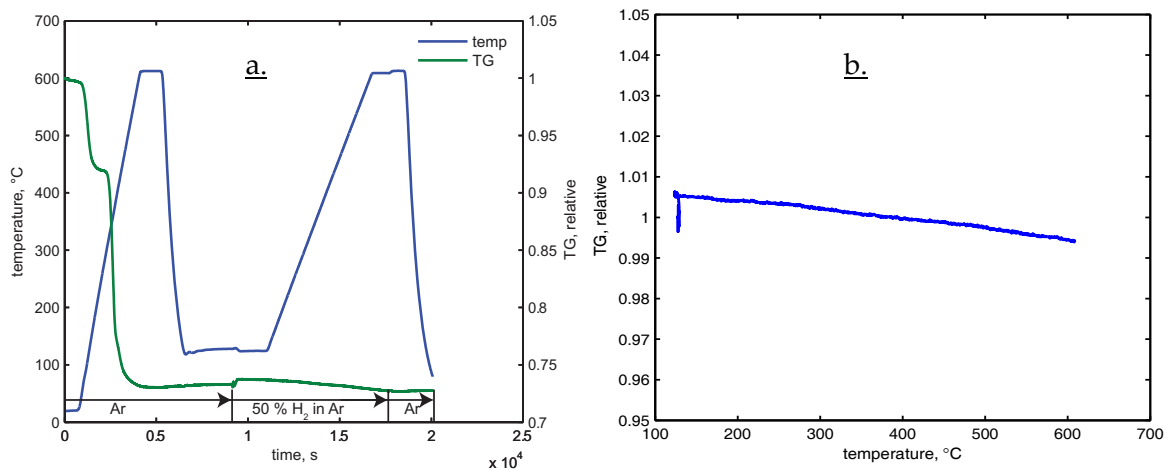


Figure 6.5.5: Hydrogen TGA screening test of a Mg-Cs-wetmix sorbent sample. a. full thermogram, b. second temperature ramp with hydrogen exposure vs. temperature.

Exposure of the material to H_2S , however, leads to a significant mass uptake (Figure 6.5.6), which is not reduced after the H_2S is removed from the Ar stream at 610 °C. This indicates a high retention of H_2S in the sample, similar to the result obtained for the cadmium-based material (Figure 6.5.2), and that it is difficult to desorb.

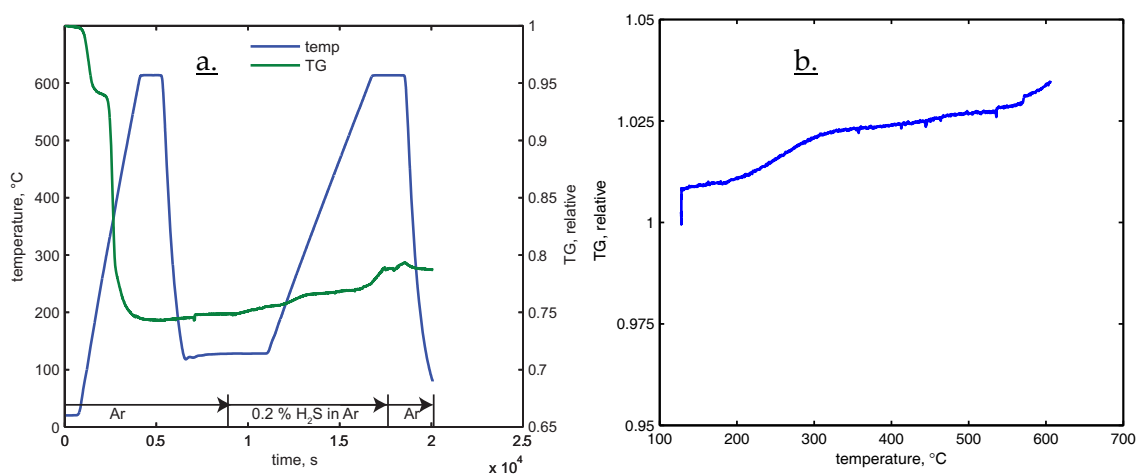


Figure 6.5.6: H_2S TGA screening test of a Mg-Cs-wetmix sorbent sample. a. full thermogram, b. second temperature ramp with hydrogen sulphide exposure vs. temperature.

The results of a multicyclic carbon dioxide sorption experiment with H_2S addition for the magnesium-based sorbents are shown in Figure 6.5.7 and the results of a previous study (multicyclic sorption in uncontaminated carbon dioxide, Chapter 5) are given in Table 6.5.2 for comparison. These results show that the material, which is stable in sorption

experiments in a pure carbon dioxide/argon mixture (Chapter 5), exhibits a capacity decay if H₂S is present (also indicated in Table 6.5.1). Also here, it becomes evident that a substantial amount of mass is retained during the sorption cycles. It appears that H₂S competes with carbon dioxide uptake in a similar way as described for the cadmium-based samples (Figure 6.5.3), with regard to the mass retention. For the Mg-nano-direct sample (Figure 6.5.7c and d), the capacity decay happens even quicker than for the Mg-Cs-wetmix samples. Here, after seven to eight cycles in H₂S-contaminated carbon dioxide, no more cyclability could be observed. Also here, a high mass retention, presumably of H₂S, was observed. As the solvothermal method is assumed to give a sample with a higher dispersion of cesium into the magnesium (Chapter 5), giving a higher carbon dioxide working capacity than the Mg-Cs-wetmix sample, the same might apply for the H₂S retention and sample degradation, which evidently happens faster for the solvothermally synthesised sorbent.

Quantitative assessment of the degradation of the Mg-Cs-wetmix sorbent (Figure 6.5.7b, in a similar way as shown in Table 6.5.3 and section 6.5.1 for the cadmium sample), revealed a mass retention (mass difference before and after cycles) of 0.54 mg, which equates to 0.034 mmol of O²⁻ replaced by S²⁻. The first and 25th sorption cycle showed a working capacity of 0.7 mg (0.0159 mmol) and 0.24 mg (0.0055 mmol), respectively. The decrease in absolute working capacity (0.0104 mmol) is therefore significantly less than the amount of sulphide formed of 0.034 mmol (as indicated by mass retention after cycles, compared to before). Thus, it can be speculated that, for the magnesia sorbents, the sulphides likely compete with the carbon dioxide sorption, but also probably adsorb at additional active sites. It can be noted that for all experiments shown in Figure 6.5.7, desorption did not bring the mass back down to the baseline.

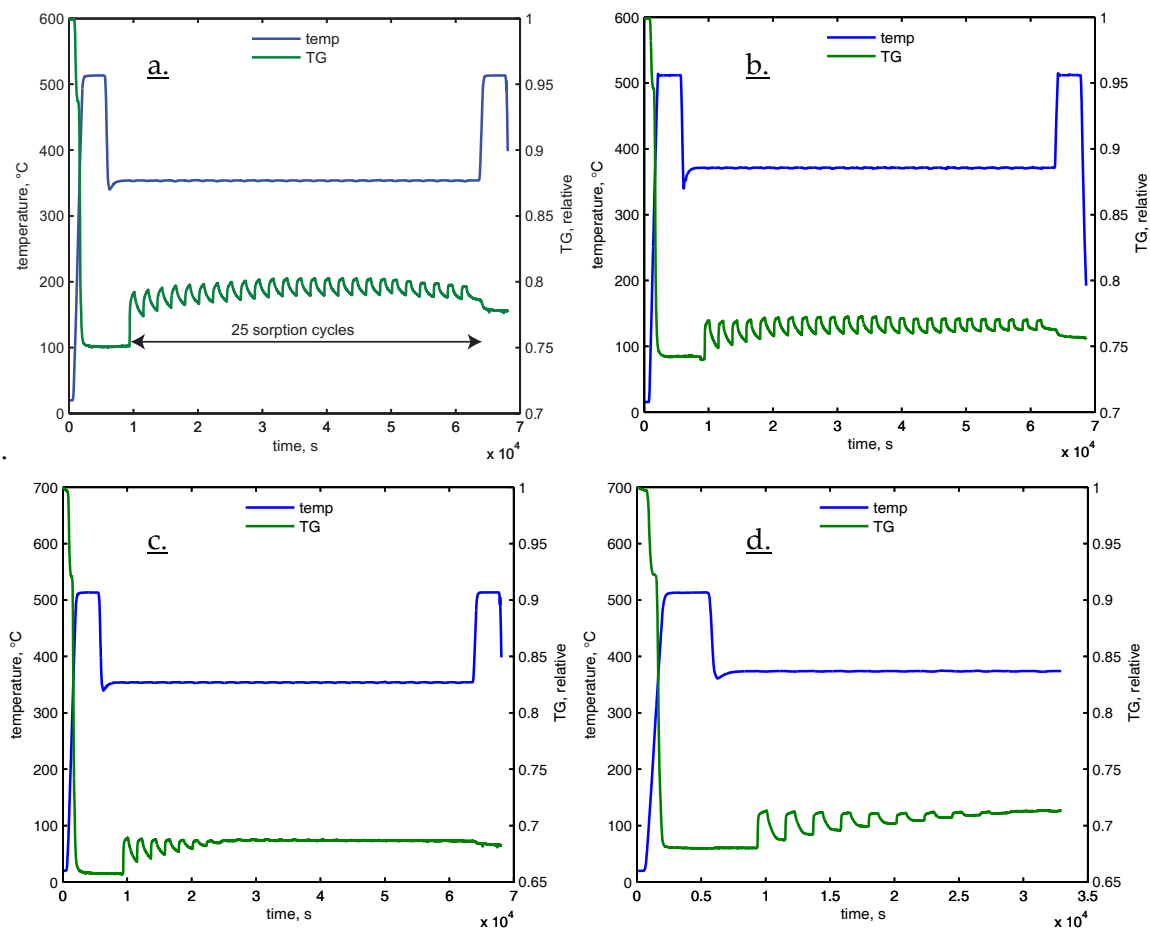


Figure 6.5.7: Isothermal multiple sorption cycles (12 min sorption 50 % Ar/49.8 % CO₂/0.2 % H₂S, 24 minutes desorption pure Ar) of a Mg-Cs-wetmix (a, b) and a Mg-nano-direct sample (c, d). a+c. 350 °C, b+d. 370 °C. Pre-treatment and after-treatment in pure Ar at 510 °C. Experiment d. was stopped as no more cyclic capacity was observed.

The magnesium-based materials exhibit a good stability if a mixture of wet carbon dioxide and hydrogen is used in sorption experiments (Figure 6.5.8). In this case, 25 cycles were successfully completed without a significant loss in its stable working capacity after the 4th cycle (also refer Table 6.5.1). From the screening test in Figure 6.5.5 and the results in Figure 6.5.8, it appears that the Mg-Cs composite is not very susceptible to any reaction with the hydrogen gas, in contrast to the cadmium-based sorbent (Figure 6.5.4).

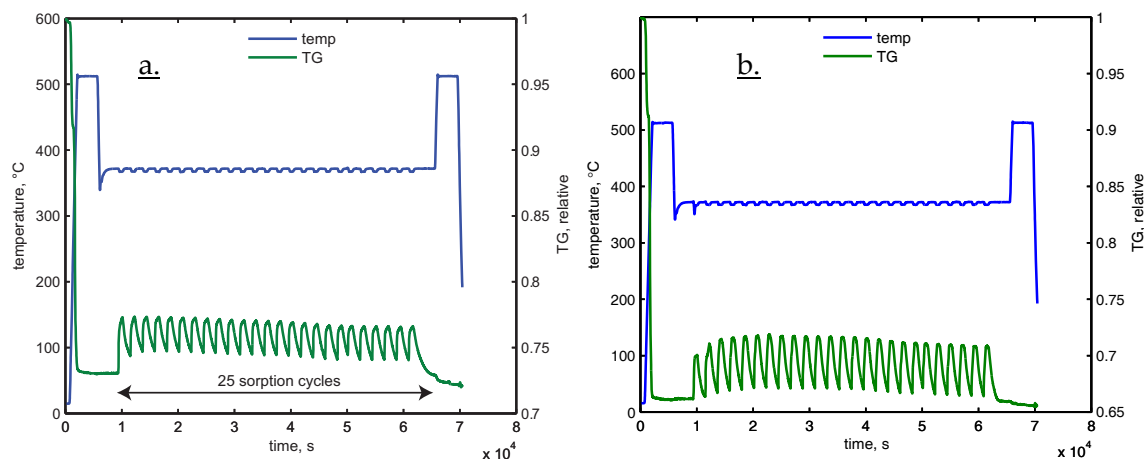


Figure 6.5.8: Isothermal (370 °C) 25-cycles TGA experiment using Mg-Cs sorbent in 48.8 % H₂, 48.8 % CO₂ and 2.4 % water (12 minutes sorption) and pure dry Ar (24 minutes desorption). a. Mg-Cs-wetmix, b. Mg-nano-direct.

From Table 6.5.1 it also becomes evident that the working capacities for the Mg-Cs-wetmix and Mg-nano-direct samples are substantially higher than in a previous study, which only involved dry gas (Chapter 5). For the Mg-Cs-wetmix sample, a value of 2.3 wt% was reported in dry gas in the last few cycles of a 25 cycle experiment at 370 °C (Chapter 5), whereas here, we observe 3.4 % for the same sample. The Mg-nano-direct sample gives a similar picture (5 wt% (Chapter 5) vs. 6.7 wt% reported here). In order to test if hydrogen or water has this influence, a 25 cycle experiment was performed using wet carbon dioxide (1.2 % water) and 50 % argon as sorption gas (without hydrogen or H₂S) and pure wet argon for desorption. The working capacities are also shown in Table 6.5.1. It is evident that water addition has a beneficial effect on the multicycle sorption of the magnesium-based materials; thus it is now apparent that this is the cause of increased working capacities in the hydrogen cycle experiments (Figure 6.5.8) compared to dry gas experiments. This result presents an apparent inconsistency with accounts by Jahan [5], who had found no significant effect of water addition to the sorption gas for Mg-Cs composites. It must, however, be noted that that study only involved one cycle of carbon dioxide sorption in wet gas, in comparison to the multiple cycles studied here. As there was some increase in working capacity during the first cycles in wet gas (Figure 6.5.8b and Table 6.5.1), potentially due to expansion of nanoparticles during initial sorption and the creation of voids causing higher accessibility of the particles to the gas, the single-cycle result might not show the full development of working capacity in wet gas.

6.5.3 Powder X-ray diffraction

The results of the powder XRD of samples treated in H_2S are given in Figure 6.5.9. It can be observed that the CdO-NaI sorbent (which is obtained upon initial calcination as the active sorbent) is partially converted to cadmium sulphide. As cadmium sulphide has a high decomposition temperature (sublimation in N_2 reported at 980°C [17]), its formation appears to explain the high impact on the carbon dioxide working capacity. Cadmium carbonate appears to easily decompose in a partial pressure swing (as shown in Chapter 3/section 3.14.1). This is not the case for the sulphide, so sulphide formation causes a mass increase of the sample and blocks the active sites for reversible carbon dioxide sorption, causing a capacity decay as observed in Figure 6.5.3.

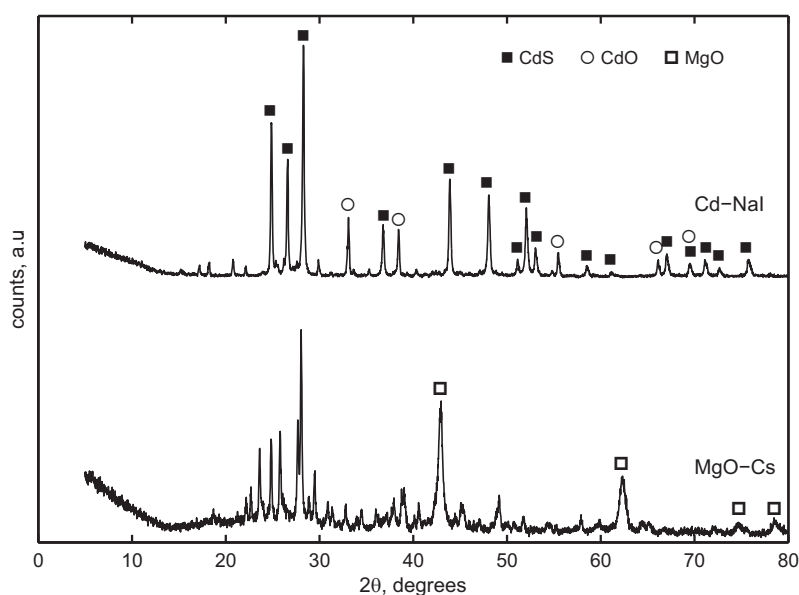


Figure 6.5.9: Powder XRD patterns ($\text{Cu K}\alpha$ radiation) of a MgO-Cs wetmix and a $\text{CdCO}_3\text{-NaI}$ sample conditioned in 2 % H_2S at 380°C for two hours.

The XRD pattern obtained for the Mg-Cs -wetmix sample shows magnesium oxide, but no evidence of magnesium sulphide and so, its formation was not evident during exposure of the sample to H_2S . The original material contained MgO and a hydrated Cs_2CO_3 phase if analysed by ex-situ powder XRD after heat treatment (refer [15] and Chapter 5). After H_2S treatment, MgO is still visible in the pattern. Evidently, a transformation of the Cs_2CO_3 phase has occurred, as the pattern no longer matches this compound (especially peaks between 20 and $40^\circ 2\theta$). The peaks in this range were thoroughly checked against a series

of cesium and magnesium sulphides, hydrogen sulphides and sulphates (also hydrated) contained in Powder Diffraction File, but a match could not be found. The result suggests that a new cesium-magnesium mixed sulphide phase has formed. Thus, it may be that a mixed metal oxide/sulphide phase has formed, somewhat analogous to the mixed metal oxide/carbonate phases that are formed during carbon dioxide sorption/desorption cycling of this material [15]. A competition between the sulphide and carbon dioxide uptake would, under these circumstances, also explain the carbon dioxide sorption capacity loss & mass retention, which was observed for H₂S-contaminated carbon dioxide used in a multicyclic TGA experiment (Figure 6.5.7).

6.6 Conclusion

In the present study, a CdCO₃-NaI and two MgO-Cs₂CO₃ mixed sorbents proposed for pre-combustion carbon dioxide capture have been analysed for their reversible carbon dioxide sorption in contaminated gas streams and under simulated syngas conditions.

The cadmium-based sorbent was found to reduce to metallic cadmium only at temperatures above 400 °C in a screening test involving hydrogen. Multiple sorption cycles at 305 °C involving wet hydrogen and carbon dioxide however showed a significant capacity decay compared to a sorption experiment involving only pure carbon dioxide and inert gas (Ar). In this case, reduction to cadmium metal was not visibly observed. It appears that the hydrogen (possibly in conjunction with the carbon dioxide) has a detrimental effect on the halide promoter and thus, causes a loss in multicyclic capacity stability. This might also be the case in the 285 °C case, where working capacities are comparatively stable, but a continuous mass loss is observed, possibly due to the reaction of the gas mixture with the promoter.

A magnesium-cesium mixed oxide sorbent, on the other hand, showed no significant reaction to hydrogen, both in the screening test and also in a multicyclic carbon dioxide sorption TGA test using simulated syngas. The sorption capacity was stable over 25 cycles. It appears that the magnesium composite is not prone to reduction by the hydrogen, in contrast to the cadmium-based sorbent.

Exposure of the cadmium-based sorbent to H₂S led to a mass increase in a TGA screening experiment. If carbon dioxide is contaminated with H₂S in a multicyclic sorption test, a capacity decay was also observed. Furthermore, a retention of mass at the end of the experiment is evident. It appears that the reaction with H₂S competes with the reaction with carbon dioxide, leading to the formation of cadmium sulphide, as evident in powder XRD. As the sulphide is hard to decompose, it remains there under the cycling conditions deactivates the material for further carbon dioxide sorption.

The magnesium-cesium mixed sorbents showed good suitability for sorption experiments in a hydrogen-containing environment, exhibiting a stable working capacity over 25 cycles. Exposure of the sorbent to H₂S in a screening test showed sorption of H₂S, which was hard to desorb, similar to the case for the cadmium sorbent. In a multicyclic experiment, H₂S addition led to a decrease in working capacity and a retention of mass even after the final desorption step. Formation of known cesium or magnesium sulphates or sulphides could not be observed in powder XRD. It appears likely that the Mg-Cs composite forms a previously unreported sulphide phase during H₂S exposure.

The results show that carbon dioxide capture from syngas is feasible using the Mg-Cs composite sorbents (both wet mixed and direct/solvothermal) described here. For the cadmium-based sorbent, it was shown that reduction to cadmium metal is not a concern in the optimal carbon dioxide sorption temperature range, however, a capacity decrease was observed in hydrogen-containing atmospheres, likely due to a deactivation reaction with the halide promoter. Thus, investigations directed at understanding this phenomenon are necessary if this material is to be pursued further.

Hydrogen sulphide is a concern for both carbon dioxide sorbent materials studied here. It appears that hydrogen sulphide sorption competes with carbon dioxide sorption, creating strong bonds that deactivate the materials for further carbon dioxide sorption. If these sorbents are to be used in a pre-combustion carbon dioxide capture environment, it must be ensured that the syngas upstream the carbon dioxide capture reactor is made H₂S free. However, further research should be directed to investigating H₂S sorption behaviour in the presence water. This might make the H₂S sorption more reversible, as a previous study has shown for hydrotalcite materials [8, 9].

Given that H₂S is only a trace contaminant in syngas, it is believed that ways of regenerating sorbents could also be an option. It is therefore also considered worth investigating if a sulphide-saturated sorbent can be reformed into its active state, possibly using water or air, assuming that the carbon dioxide sorption promoter is not harmed during such a regeneration.

6.7 Acknowledgements

The authors acknowledge funding provided by the Australian Government through its Cooperative Research Centre (CRC) program to support this CO₂CRC research project. Financial support from the Faculty of Science, Monash University, is also acknowledged.

6.8 References for Chapter 6

- [1] H. Yang, Z. Xu, M. Fan, R. Gupta, R. B. Slimane, A. E. Bland, and I. Wright, "Progress in carbon dioxide separation and capture: A review," *Journal of Environmental Sciences*, vol. 20, pp. 14-27, 2008.
 - [2] K. S. Lackner, A. H. A. Park, and B. G. Miller, "Eliminating CO₂ Emissions from Coal-Fired Power Plants," in *Generating Electricity in a Carbon-Constrained World*, Boston: Academic Press, 2010, pp. 127-173.
 - [3] M. Mikkelsen, M. Jørgensen, and F. C. Krebs, "The teraton challenge. A review of fixation and transformation of carbon dioxide," *Energy & Environmental Science*, vol. 3, pp. 43-81, 2010.
 - [4] P. Chiesa, S. Consonni, T. Kreutz, and R. Williams, "Co-production of hydrogen, electricity and CO₂ from coal with commercially ready technology. Part A: Performance and emissions," *International Journal of Hydrogen Energy*, vol. 30, pp. 747-767, 2005.
 - [5] M. Jahan, "Removal of Carbon Dioxide from Gas Streams with Metal Oxides at High Temperature," PhD thesis, School of Chemistry, Monash University, Victoria, Australia, 2011.
 - [6] C. Vogt, G. P. Knowles, S. L. Y. Chang, and A. L. Chaffee, "Cadmium oxide/alkali metal halide mixtures - a potential high capacity sorbent for pre-combustion CO₂ capture," *Journal of Materials Chemistry A*, vol. 1, pp. 10962-10971, 2013.
 - [7] R. Singh, M. K. Ram Reddy, S. Wilson, K. Joshi, J. C. Diniz da Costa, and P. Webley, "High temperature materials for CO₂ capture," *Energy Procedia*, vol. 1, pp. 623-630, 2009.
 - [8] E. van Dijk, S. Walspurger, P. Cobden, and R. van den Brink, "Testing of hydrotalcite based sorbents for CO₂ and H₂S capture for use in sorption enhanced water gas shift," *Energy Procedia*, vol. 4, pp. 1110-1117, 2011.
 - [9] H. A. J. van Dijk, S. Walspurger, P. D. Cobden, R. W. van den Brink, and F. G. de Vos, "Testing of hydrotalcite-based sorbents for CO₂ and H₂S capture for use in sorption enhanced water gas shift," *International Journal of Greenhouse Gas Control*, vol. 5, pp. 505-511, 2011.
-

- [10] C. T. Yavuz, B. D. Shinall, A. V. Iretskii, M. G. White, T. Golden, M. Atilhan, P. C. Ford, and G. D. Stucky, "Markedly Improved CO₂ Capture Efficiency and Stability of Gallium Substituted Hydrotalcites at Elevated Temperatures," *Chemistry of Materials*, vol. 21, pp. 3473-3475, 2009.
- [11] M. Maroño, Y. Torreiro, and L. Gutierrez, "Influence of steam partial pressures in the CO₂ capture capacity of K-doped hydrotalcite-based sorbents for their application to SEWGS processes," *International Journal of Greenhouse Gas Control*, vol. 14, pp. 183-192, 2013.
- [12] M. K. R. Reddy, Z. P. Xu, G. Q. Lu, and J. C. Diniz da Costa, "Effect of SO_x Adsorption on Layered Double Hydroxides for CO₂ Capture," *Industrial & Engineering Chemistry Research*, vol. 47, pp. 7357-7360, 2008.
- [13] H. Lu and P. G. Smirniotis, "Calcium Oxide Doped Sorbents for CO₂ Uptake in the Presence of SO₂ at High Temperatures," *Industrial & Engineering Chemistry Research*, vol. 48, pp. 5454-5459, 2009.
- [14] M. Guo, L. Zhang, Z. Yang, and Q. Tang, "Removal of CO₂ by CaO/MgO and CaO/Ca₉Al₆O₁₈ in the Presence of SO₂," *Energy & Fuels*, vol. 25, pp. 5514-5520, 2011/11/17 2011.
- [15] M. Liu, C. Vogt, A. L. Chaffee, and S. L. Y. Chang, "Nanoscale Structural Investigation of Cs₂CO₃-Doped MgO Sorbent for CO₂ Capture at Moderate Temperature," *Journal of Physical Chemistry C*, vol. 117, pp. 17514-17520, 2013.
- [16] F. N. Cayan, M. Zhi, S. R. Pakalapati, I. Celik, N. Wu, and R. Gemmen, "Effects of coal syngas impurities on anodes of solid oxide fuel cells," *Journal of Power Sources*, vol. 185, pp. 595-602, 2008.
- [17] R. C. Weast, *CRC Handbook of Chemistry and Physics*. Cleveland, Ohio: The Chemical Rubber Co., 1968-1969.
-

Chapter 7 Concluding remarks

7.1 Cadmium based sorbents: summary

In this work, several metal oxides were screened for their suitability for pre-combustion carbon dioxide capture. Based on a literature review, metal carbonates that decompose to oxides at temperatures between 250 and 400 °C were investigated via TGA for their ability to gain mass by re-forming their respective carbonates by exposure to carbon dioxide. It was found that a cadmium carbonate/sodium iodide mixture reversibly decomposes to oxide and re-forms carbonate upon carbon dioxide exposure at temperatures between 250 and 320 °C. This material was found to be a suitable candidate for carbon dioxide capture and thus, studied in detail. Powder XRD and FTIR spectroscopy confirmed the reversible formation of cadmium carbonate in a sorbent made with sodium iodide. It was also demonstrated that sodium bromide, lithium iodide, lithium bromide and potassium iodide can be used as alternative dopants, but the carbonation rates and working capacities were found to be lower in these cases. A cadmium oxide sample with no halide addition showed no carbonation upon exposure to carbon dioxide, whereas a sample made with sodium iodide addition carbonated almost stoichiometrically (26 % mass gain after two hours of exposure to 50 vol% carbon dioxide in argon). Additional sorption tests via TGA showed that the material is capable of reversibly sorbing and desorbing carbon dioxide at isothermal conditions using a partial pressure swing (i. e., using 50 vol% carbon dioxide for 12 minutes of sorption, and 24 minutes of desorption in inert gas purge), reaching working capacities of up to 24 wt% at a temperature of 305 °C. Water addition to the gas stream had a beneficial effect, as it increased the working capacities and improved the multicyclic stability. This experiment proved the material's potential for pressure swing sorption at isothermal conditions.

The cadmium oxide/sodium iodide mixed sorbent was, however, found to exhibit a significant working capacity reduction over up to 25 sorption and desorption cycles. It was shown that there was a gradual mass decrease over the multiple cycles and that the capacity reduction was most evident if the samples were initially decarbonated in air instead of inert gas (nitrogen or argon). Elemental analyses helped determine that this

mass loss is associated with the loss of iodine. It was concluded that the loss of iodide means a loss of sorption promoter, causing the material to become less efficient over multiple sorption cycles.

Pelletised samples were investigated in multiple sorption cycles as well and showed a reduced working capacity, presumably due to the limitation of gas diffusion in and out of a compact pellet in comparison to a powder. Pellets made in the carbonate state became mechanically unstable (i. e., crumbled into powder) after 25 carbon dioxide sorption cycles. A pellet made in the oxide state maintained its integrity well, but showed virtually no working capacity. The addition of a porous spacer (SBA-15 silica) aided gas accessibility and led to better performance of a pellet made in the oxide state, however, this also slightly reduced the mechanical integrity.

Further investigations of the capacity decay associated with iodine loss were performed using gas-phase mass spectrometry, XPS, TEM and SEM. The exit gas of a fixed-bed sorption experiment indicated that iodine in its elemental form is released from the sample upon initial heating from room temperature in inert gas purge and subsequent carbon dioxide exposure. For a cadmium oxide sample made from a mixture of cadmium carbonate and sodium iodide by calcination, it was shown via XPS that two iodine species existed on the surface. These were iodide, as evident from a comparison with a pure sodium iodide sample, and also a highly-oxidised iodine species, identified to be iodate. From these studies, it was concluded that the decay mechanism of the cadmium oxide/sodium iodide mixed sorbent is related to an oxidation reaction. The reduced (-I) form of iodide, brought into the sample during synthesis with sodium iodide, is thus considered to be oxidised to both iodide (0), as evident from the exit gas analysis, and iodates (e. g. probably +V for IO_3^-), as evident by surface analysis via XPS. It appears that carbon dioxide is inducing the iodine loss mechanism, as iodine is lost from the sample even without exposure to air at high temperature. Given the more significant iodine loss for a sample calcined in air, it is concluded that air (most likely the oxygen contained in it) plays an important role as well.

Electron microscopy methods (SEM and TEM) revealed the structural morphology of the cadmium oxide/sodium iodide sample. It was shown via TEM that the powder consisted

of regular spherical and crystalline cadmium oxide nanoparticles of approx. 250 nm width. Sodium iodide was occasionally found as discrete nanoparticles next to areas of high cadmium content. The morphology of the cadmium oxide nanoparticles was severely altered after 25 carbon dioxide sorption cycles performed via TGA. The particles appeared fractured and less regular, presumably due to the formation of intra-particle voids/cracks during conversion from oxide to carbonate and vice versa. An SEM image showed that larger particles in the micrometre range are also present in the sample. Elemental maps in this micrometre scale revealed a segregation of sodium and iodide, indicating a reaction and re-deposition of iodine, which could be due to oxidation reactions and the surface re-deposition of iodine species, according to the mechanism discussed above.

Sorption experiments in the presence of hydrogen showed that reduction of the cadmium carbonate to cadmium metal is not of a concern at the temperature used for carbon dioxide capture. It has, however, a detrimental effect on the sodium iodide promoter. Hydrogen sulphide was shown to compete with carbon dioxide sorption, forming very stable cadmium sulphide as confirmed by powder XRD, reducing carbon dioxide sorption capability.

In conclusion, a novel high-capacity cadmium oxide-based carbon dioxide sorbent has been developed. The reaction mechanism, a carbonation of cadmium oxide to cadmium carbonate was proven. The material showed reversible carbonation and decarbonation, but was subject to a capacity loss over multiple cycles due to oxidation of the halide promoter, or, in the presence of hydrogen, due to promoter inactivation by hydrogen. Deactivation of the promoter by hydrogen was also observed, reducing the working capacity over multiple sorption cycles.

As cadmium is a toxic element, a risk assessment is advocated before the use of cadmium-based sorbents in an industrial process. The mechanism of carbonation might, however, lead to a series of novel carbon dioxide sorbents based on metal oxide carbonation, once the mechanism of carbonation promotion is fully unravelled. It is assumed that the materials studied here will prove to be an example of a novel promoted carbonation mechanism, which can potentially be applied to other less toxic metal oxides in the future and induce them to form carbonates suitable for carbon dioxide capture.

7.2 Magnesium-based sorbents: summary

A magnesium oxide/cesium carbonate composite was described in a previous project as a carbon dioxide sorbent and was studied in detail in the scope of pressure swing sorption in this work. Using a wet-mixing technique as reported in previous work, a magnesium oxide/cesium carbonate composite was synthesised by dispersing magnesium oxide into a solution of cesium carbonate and subsequently evaporating the water by heating. This material exhibited a working capacity of 4 wt% in 12 minutes carbon dioxide sorption vs. 24 minutes desorption (inert gas purge) cycles at 390 °C. Powder XRD results showed that this material uses a mixed metal oxide mechanism to sorb carbon dioxide. This mechanism does not involve the formation of magnesium carbonate from magnesium oxide at temperatures around 370 °C, but rather a previously unreported phase, possibly involving cesium carbonate and magnesium, was observed upon carbonation.

In order to improve the interaction of the cesium and magnesium phases in the sorbent, a solvothermal method was employed to synthesise the magnesium/cesium metal oxide composite. Synthesising magnesium hydroxide-methoxide nanoparticles and subsequently wet-mixing them with cesium carbonate led to a material with no significant increase in carbon dioxide sorption working capacity compared to the wet-mixed sample described above. If the cesium carbonate was added directly into the solvothermal synthesis, leading to a co-precipitation of the cesium and magnesium phases, the cyclic working capacity could be increased to 5 wt%, now exhibiting its optimum performance at 370 °C. The increase in working capacity for the solvothermally synthesised material is considered to be due to better mixing between the two metal compound phases in the solvothermal synthesis and also due to a higher BET surface area than in the sorbent made from magnesium oxide.

TEM elemental mapping, however, showed a good distribution of magnesium and cesium throughout all samples, with occasional clustering of cesium-bearing phases. TEM images also showed that the solvothermally made nanoparticles are slightly smaller than the ones obtained from magnesium oxide during wet-mixing. Powder XRD confirmed that the chemistry of the solvothermally synthesised samples is similar to the wet-mixed ones.

It was shown that the material's working capacity for carbon dioxide sorption is stable in a hydrogen-containing environment and that water addition had a beneficial effect on the sorption capacity. Hydrogen sulphide addition to the gas, however, competed with carbon dioxide sorption, forming a strongly-bound compound that had a decreased carbon dioxide sorption ability. Similar to carbon dioxide sorption, hydrogen sulphide reacted in a way to form a new phase as confirmed by XRD, but did not lead to the transformation of magnesium oxide to sulphide.

The solvothermal method showed that magnesium oxide/cesium carbonate composite sorbents can be improved by improving the interaction between cesium and magnesium-containing phases. A further improved carbon dioxide sorption working capacity may result if ways can be found to further increase and preserve the surface area of the sorbent nanoparticles, by ensuring good cesium and magnesium phase interaction.

7.3 Suggestions for future work

With regard to the cadmium oxide/sodium iodide sorbents, it was shown that a working capacity loss is evident in multicyclic carbon dioxide sorption; this is even worse if hydrogen is present. In order to make this sorbent industrially viable, the carbonation mechanism promoted by the halide and the decay mechanism must be fully studied and addressed. The following points should be considered and addressed:

- It has not yet been fully determined how the alkali halide exactly decomposes during the carbonation and decarbonation of the cadmium oxide. A more sophisticated residual gas analysis in a fixed bed sorption process, like that described in Chapter 6, might be of help. It would be necessary to use helium instead of nitrogen as carrier gas; and to incorporate a method to separate carbon dioxide and carbon monoxide (for example, via gas chromatography), in order to obtain more detailed information about the exit gas composition. As speculated in Chapter 6, carbon dioxide might provide oxygen to facilitate the oxidation of the iodide promoter, yielding carbon monoxide. To confirm or refute this speculation, the appearance of traces of carbon monoxide must be investigated.
-

- Obtaining details about the exact promotion mechanism of the alkali halide is advocated. This could be studied by in-situ electron microscopy techniques, using carbon dioxide sorption and imaging or diffraction at the same time. A constraint might be the usually high vacuum requirement for electron microscopy techniques.
- Future research should be directed at finding ways of fixing the promoter in the oxide sample, so it is unable to evaporate from the sorbent, making the sorbent more stable and avoiding mass losses during multiple carbon dioxide sorption cycles. Alternatively, ways should be investigated to regenerate decayed sorbents in a facile process, for example by recovering and re-supplying lost elements like iodine. Also, in terms of sorbent decay by hydrogen and hydrogen sulphide, regeneration methods might be worth investigating, for example oxidising the sulphide-containing samples in oxygen, but without destroying the promoter.
- An improvement in the mechanical stability of pelletised samples should be sought by using suitable binding agents.
- Once the exact mechanism is known, future studies should be focussed on synthesising promoted metal oxide systems, which use less toxic metals than cadmium, but which work via the same mechanism and lead to a similarly high (i. e., stoichiometric) capacity.

With regard to the magnesium oxide/cesium carbonate sorbents, research should be mainly directed at a further improvement in nanoparticle or high surface area synthesis. This, it is assumed, would lead to further improvement in the interaction between cesium and magnesium compound phases, which, in turn, it is anticipated would lead to higher carbon dioxide sorption capacity.

In general, once reproducible synthesis of stable high-capacity materials can be shown, pelletisation and carbon dioxide sorption experiments are recommended, since this would be necessary at pilot plant scale. Here, special focus must be given to the tolerance of the sorbents to real syngas, that is, a mixture of carbon dioxide, carbon monoxide, water (higher concentration than studied here), hydrogen sulphide, carbonyl sulphide, ammonia and methane.

Chapter 8 Experimental details

8.1 Introduction

The experimental details are given in each thesis chapter in the style of journal publications. This chapter aims to provide more detailed descriptions of the experimental techniques, about what they are capable of and why they have been chosen for this study.

8.2 Chemicals

Table 8.2.1 provides a list of chemicals and gases and their purity (if given by the manufacturer) used in this thesis.

Table 8.2.1: Specifications of chemicals used in this thesis.

Chemical name	Formula	Purity, supplier
Argon	Ar	high purity, BOC #
Cadmium carbonate	CdCO ₃	99+ %, Alfa Aesar
Calcium carbonate	CaCO ₃	GR grade, Merck
Carbon dioxide	CO ₂	food grade, BOC #
Cesium carbonate	Cs ₂ CO ₃	99.9 %, Sigma Aldrich
Ethanol	CH ₃ CH ₂ OH	absolute, for analysis, Merck
Hydrochloric acid	HCl	32 %, analytical reagent grade, Merck
Hydrogen	H ₂	Industrial, BOC
Hydrogen sulphide (2 % in argon mixture)	H ₂ S	Air Liquide, 2.01 mol% certified
Lanthanum carbonate	La ₂ (CO ₃) ₃	99.9 %, Alfa Aesar
Lithium bromide	LiBr	> 99 %, Alfa Aesar
Lithium iodide	LiI	98 % for synthesis, Merck
Magnesium acetate, tetrahydrate	Mg(CH ₃ COO) ₂ · 4 H ₂ O	98 %, Unilab
Magnesium nitrate, hexahydrate	Mg(NO ₃) ₂ · 6 H ₂ O	ACS reagent grade, Merck
Magnesium oxide	MgO	99+ %, Sigma Aldrich

Magnesium turnings	Mg	98 %, Sigma-Aldrich
Methanol	CH ₃ OH	99.8 % for analysis, Merck
Nitrogen	N ₂	liquid nitrogen or liquid evaporated to gas, School of Chemistry supply, BOC
Poly(ethylene glycol)-block-poly(propylene glycol)-block-poly(ethylene glycol)	Pluronic P123	Sigma-Aldrich
Potassium bromide	KBr	IR grade, Sigma Aldrich, or 98.5 %, Univar
Potassium iodide	KI	99.5 %, BDH
Sodium bromide	NaBr	> 99 %, Sigma-Aldrich
Sodium carbonate	Na ₂ CO ₃	> 99 %, BDH
Sodium iodide	NaI	99 %, Alfa Aesar
Sucrose	C ₁₂ H ₂₂ O ₁₁	AnalaR, Merck
Sulphuric acid	H ₂ SO ₄	98 % AR grade, Merck
Tetraethylorthosilicate	C ₈ H ₂₀ O ₄ Si	98 %, reagent grade, Sigma-Aldrich
Toluene	C ₆ H ₅ CH ₃	99.9 % for analysis, Merck
Zinc oxide	ZnO	99.9 %, Alfa Aesar

used after in-line purification by a zeolite 13X-based water trap

8.3 Synthesis

For wet-mixing synthesis of mixed sorbents, standard laboratory glassware was used. All glassware was washed with 5 % acid (either hydrochloric or sulphuric) at room temperature and then rinsed with distilled water before and after each synthesis run. The acid washing ensured that all metal oxide residues were removed from the glassware surface. The wet-mixing synthesis was performed using a beaker and a magnetic hotplate stirrer.

For solvothermal synthesis, stainless steel autoclaves were used (Figure 8.3.1), which were heated in a fluidised sand bath equipped with electric heating.

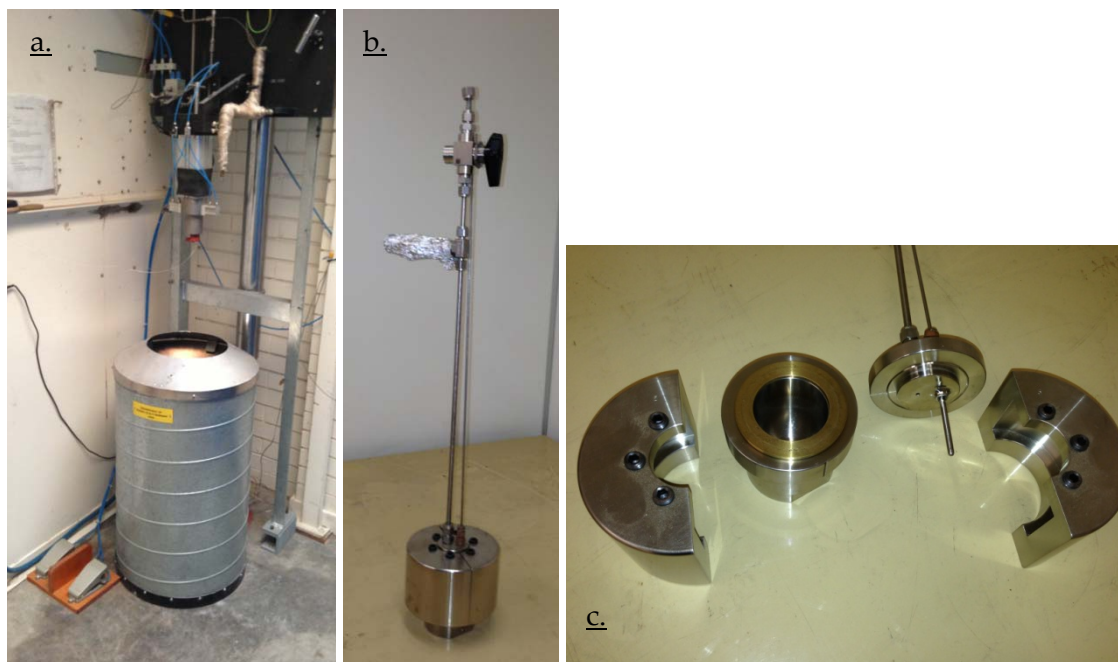


Figure 8.3.1: a. sand bath, b. closed autoclave, c. opened autoclave.

8.4 Thermogravimetric analysis

As metal oxides gain weight due to the change in molar mass as soon as they sorb carbon dioxide or any other gas, thermogravimetric analysis (TGA) was considered a suitable way of analysing their sorption behaviour. Furthermore, the technique allows immediate determination of possible mass losses due to decomposition of samples. TGA mainly uses an enclosed balance, which measures masses of specimens in-situ while heating and purging the sample with gas. The sample mass and temperature are continuously logged while the experiment is running, so that temperature and mass plots versus time are obtained.

Thermogravimetric analysis was performed on a Setaram TAG 24-16 symmetrical thermoanalyser (Figure 8.4.1). Gas supplies for argon and carbon dioxide were fed through a zeolite 13X filled water trap for moisture removal. A custom-built gas supply box enabled manual control of the different gas feeds. Gas flow was controlled by Bronkhorst model F-201DV-RAD-11-K mass flow controllers, which are built into the gas supply box.

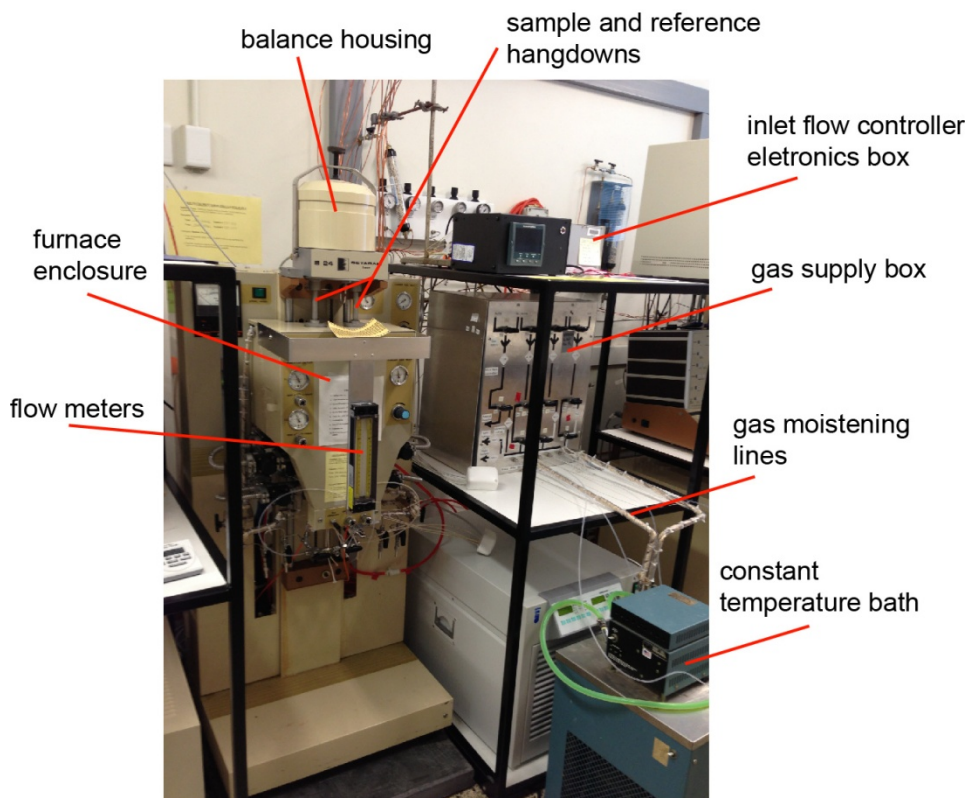


Figure 8.4.1: Setaram TAG 24-16 thermoanalyser and auxiliaries.

The gas supply box has outlets at the front, through which the gas can be looped in order to moisten it. For this purpose, a constant-temperature water bath was set up in front of the unit. This water bath was set to 10 °C for the cooling of wash bottles with sinter heads, which were filled with distilled water. A volume percentage of 2.4 % of water is achieved in the gas stream according to the steam tables [1], if gas is bubbled through the water at this temperature. As the gas lines of the thermoanalyser are not heated, the moisture achieved with 10 °C of water posed an upper limit in order to prevent condensation of water in the gas supply lines before the gas enters the instrument.

A schematic of the gas flow through the thermoanalyser is shown in Figure 8.4.2. In all experiments, the balance housing must be purged with an inert gas (in this study, argon) in order to prevent sample gas from diffusing into the balance electronics.

The default configuration with top-to-bottom flow (Figure 8.4.2a) was used for the majority of experiments. Here, the balance housing purge flow (35 mL/min) mixes with the sample gas (35 mL/min). For example, a 50 % carbon dioxide in argon mixture is

created by using 35 mL/min argon in the balance housing and 35 mL/min of pure carbon dioxide as the sample gas flow. In the bottom-to-top flow, a total flow of 70 mL/min was always used. It must, however, be noted that the total flow over the sample is then 35 mL/min, as the flow is split over the sample and reference crucibles. The flow meters and metering valves at the outlet of the instrument were used to ensure a balanced flow over both crucibles. For the use of wet gas, a water content of 1.2 vol% was reached in this configuration, as only the sample gas is bubbled through water at 10 °C before being split in two halves and entering the two instrument furnaces as shown in Figure 8.4.2a. Before the gas flows past the sample and reference crucibles, it gets diluted by the dry balance housing flow, halving the water content of 2.4 vol% of the sample gas flow.

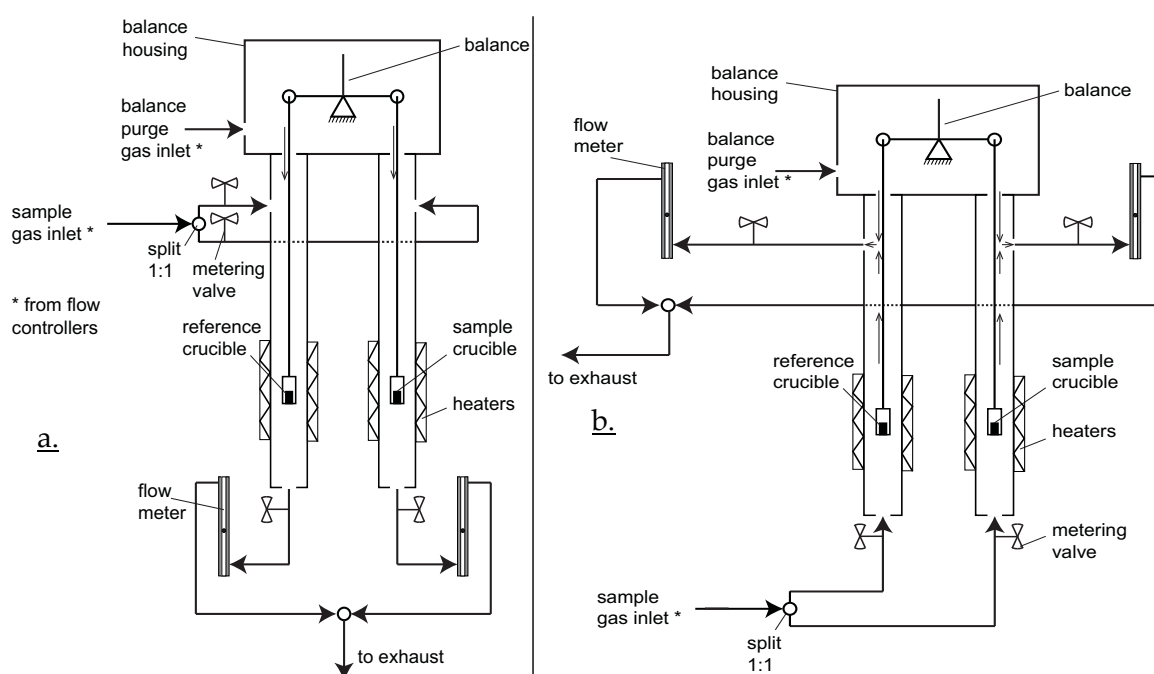


Figure 8.4.2: Schematic of the TAG 16-24 thermoanalyser. a. Top-to-bottom gas flow, b. Bottom-to-top gas flow

For the sorption studies in Chapter 6 using a moistened hydrogen/carbon dioxide mixture, the bottom-to-top configuration (Figure 8.4.2b) was used. With this assembly, a higher water content up to 2.4 vol% (actually flowing across the sample) can be achieved. This is closer to the value contained in real syngas. In this configuration, the balance housing flow and the sample gas flow entering the instrument were both set to 70 mL/min each. This then resulted in a total flow of 140 mL/min, but the sample gas flow was still 35 mL/min,

as the balance housing flow was not directed past the sample in this configuration. Ensuring that the sample is purged with 35 mL/min as in other experiments was considered essential in order to ensure comparability of results.

The upgrade of the thermoanalyser for use of the bottom-to-top flow (Figure 8.4.2b), as well as to use specialty gases, was performed during the course of this thesis.

8.5 Powder X-ray diffraction

8.5.1 Basic principles

Powder X-ray diffraction (XRD) is a technique to characterise crystalline solids that also allows identification of different crystal phases using a database. The basic principle is that X-rays, a form of high-energy electromagnetic radiation, are reflected by atoms in a crystal lattice, similarly to how visible light is reflected by a mirror. X-rays, however, are able to penetrate deep into the material, so they are able to pass several layers of atoms in the lattice. If the X-rays interact with an atom, they are reflected by the electron shell, and exit the sample in the same angle to the surface normal as they entered the sample (Figure 8.5.1). Before the X-rays are reflected by atoms in different layers, the distances travelled by different X-ray photons are different until they hit an atom. For instance, the wave hitting the atom N in Figure 8.5.1 travels the sections [PN] before and [NQ] after reflection in addition to the distance travelled by a photon hitting the atom M. The reflected beams can then be out of phase in a way that they extinguish each other (destructive interference, shown in Figure 8.5.1), or in a way that they are in phase and add up their intensities (constructive interference). If the distance [PN] + [NQ] is equal to a multiple of the wavelength, the waves are in phase and a high-intensity reflection is observed. This is dependent on the incident angle θ . As, by geometry, [PN] = [NQ] = $d \cdot \sin \theta$, this can be summarised as eqn. 8.5.1, which is known as the Bragg equation [2], wherein λ is the wavelength and n is an integer.

$$2d \cdot \sin \theta = n\lambda \quad \text{eqn. 8.5.1}$$

In a powder diffractometer using the Bragg-Brentano configuration, a sample is irradiated with X-rays while the sample is tilted over an angle θ and a detector measures the reflected intensity at an angle of 2θ . If constructive interference occurs, a high intensity of

reflected X-rays is detected, so that a plot of reflection intensity over the angle 2θ will show peaks at the positions of constructive interference. As this diffraction pattern is wavelength-dependent, the concept of the wavelength-independent value of Q has been introduced according to eqn. 8.5.2. This is a handy way of plotting and comparing XRD patterns that have been obtained on different instruments that use different wavelengths. For the calculation of XRD patterns from different wavelengths into Q , the free software package CMPR was used [3].

$$Q = \frac{4\pi \sin \frac{2\theta}{2}}{\lambda} \quad \text{eqn. 8.5.2}$$

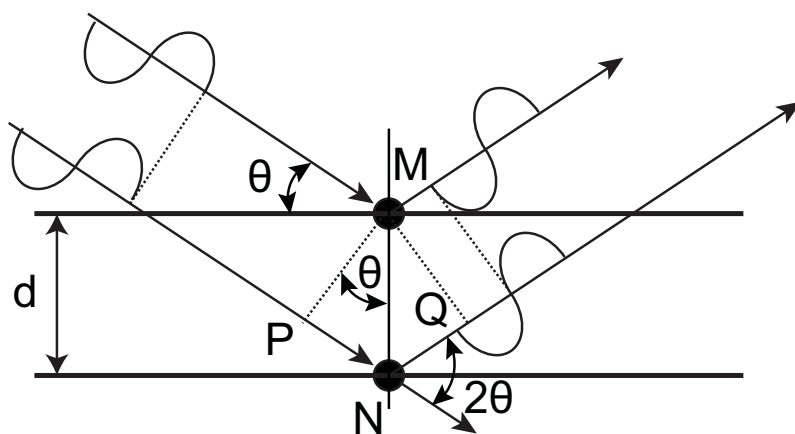


Figure 8.5.1: Illustration of an X-ray beam being reflected by two atom layers in a crystal lattice.

At the School of Chemistry, a Bruker D8 focus Bragg-Brentano powder X-ray diffractometer was available for this study, as shown in Figure 8.5.2. This instrument allowed the acquisition of patterns at ambient temperature using approx. 1 g of sample. Smaller samples (ones which did not fill up the sample holder completely) were also able to be analysed, but gave worse signal-to-noise ratios in the patterns. The instrument uses an X-ray source with a copper anode, giving Cu $K\alpha$ radiation of a wavelength of 1.54059 Å ($K\alpha_1$) and 1.54443 Å ($K\alpha_2$) in the intensity ratios $K\alpha_1/K\alpha_2 = 2:1$.

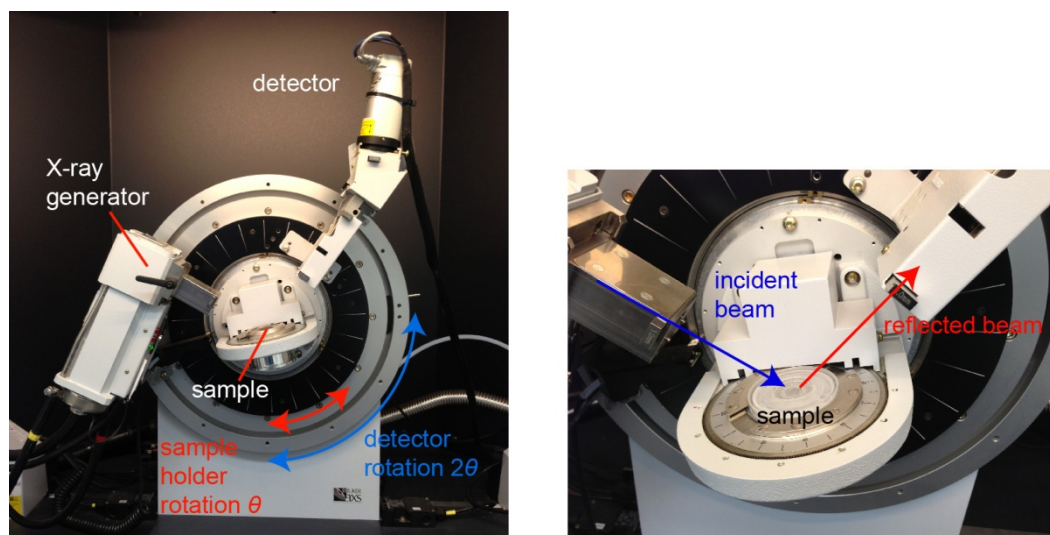


Figure 8.5.2: Bruker D8 focus powder diffractometer.

In-situ powder X-ray diffraction studies were performed at the Australian Synchrotron using the Powder Diffraction beamline. A schematic of the diffractometer is given in Figure 8.5.3. X-rays from the synchrotron are channelled into the diffractometer and target the sample, which is contained in a quartz capillary. The sample capillary can be heated using a hot air blower and purged with a gas while the diffraction pattern is obtained.

The detector, as shown in Figure 8.5.3, is capable of measuring the full range of angles 2θ at once, without scanning over the angles. However, the detector consists of several modules, which are joint together to form the arc-like assembly. Gaps between these modules cause missing data in a diffraction pattern. In order to obtain the full range of angles 2θ without gaps, two scans were performed for each run, where the detector was slightly tilted for the second scan. This way, the gaps in the pattern occurred at two different angles 2θ in each of the two scans. For data analysis, the two patterns needed to be merged in order to eliminate these gaps. This data post-processing was performed via the software 'Datapro', which was provided by the Australian Synchrotron. Here, the first scan result is loaded into the software and the gaps are filled with the data from the second scan. The complete file written by the Datapro software is then saved and used for subsequent data analysis and interpretation.

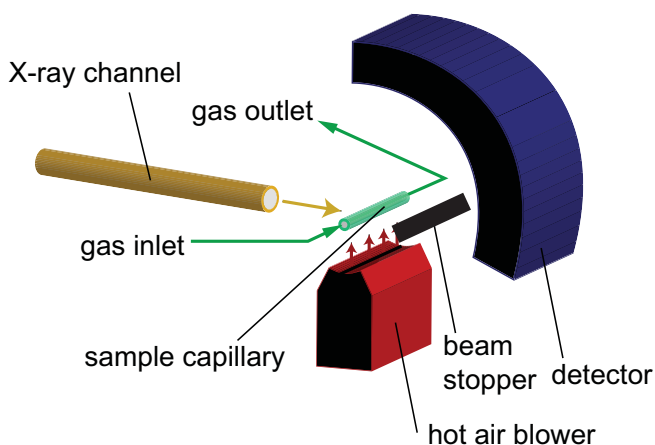


Figure 8.5.3: Schematic of the diffractometer at the Powder Diffraction beamline of the Australian Synchrotron.

In general terms, XRD provided a way of identifying phase changes in metal oxide samples originating from carbonation due to carbon dioxide exposure or, as shown in Chapter 6, due to hydrogen sulphide exposure. It was assumed that the metal oxide samples in this study are crystalline to a certain extent (which proved true), which is a requirement to obtain a reasonable diffraction pattern.

8.5.2 Pattern refinement

Powder XRD pattern refinement is a mode of obtaining data about the unit cell of a crystalline powder. It uses the whole measured pattern and fits peak data into it, using known possible unit cell parameters (size, atom positions) as starting values. A background correction is applied and peaks are subsequently fitted using Gaussian and Lorentzian functions, the combination of which is also called a Pseudo-Voigt function [4]. By varying parameters that are set as refinable variables, like unit cell dimensions, atom positions, wavelength, zero offset, or Gaussian/Lorentzian parameters, the peaks are fit into the pattern to give the lowest-possible deviation between calculated and measured data. Refined variables can then be obtained after the calculation is complete. The Rietveld method refines the unit cell size and also the atomic coordinates, whereas a Le Bail fit only refines unit cell parameters, ignoring the atomic positions in the unit cell.

Le Bail refinement was used in this study to obtain information on the cadmium oxide unit cell size, which was thought to be influenced by sodium iodide doping. For this purpose,

the unit cell parameters were refined using the XRD patterns obtained from the laboratory instrument, with the given (fixed) wavelength of Cu K α radiation.

For data obtained from the Australian Synchrotron, a standard sample (lanthanum hexaboride, LaB₆, NIST standard reference material 660b) was first measured on the synchrotron diffractometer at room temperature. As the unit cell size of the standard is known, but the wavelength of the synchrotron radiation is variable and subject to setpoint tolerances, the standard material provides a way of obtaining a wavelength and zero offset closest to the true value. Using the measured XRD pattern of the standard, a Rietveld or Le Bail fit was used to refine the wavelength and zero offset values, with the unit cell parameters set to fixed values as per standard reference material certificate. The obtained wavelength and zero offset were then used as fixed values to refine the unit cell size of cadmium oxide in the cadmium oxide/alkali halide sorbent using the Le Bail method.

Refinements were performed using the free DOS software package GSAS [5], with its graphical user interface extension EXPGUI [6]. The latter allows the control of the GSAS software using a Windows interface to enter all required data, and then forwards these parameters to GSAS for the actual refinement, omitting the need for manual typing of lengthy DOS commands.

8.6 Electron microscopy

Transmission electron microscopy (TEM) was used to analyse the changes in nanoparticle morphology of a cadmium oxide/sodium iodide carbon dioxide sorbent over multiple sorption and desorption cycles, as well as to obtain images of the magnesium oxide/cesium carbonate sorbents. Elemental mapping using energy-dispersive X-ray spectroscopy (EDX) was used to investigate the distribution of cesium and magnesium throughout these samples.

Scanning electron microscopy was used to determine the morphology of a cadmium oxide/sodium iodide sample on a lower magnification (micrometres) scale. EDX was used here to determine the distribution of sodium and iodine throughout the sample.

The differences between TEM and SEM can be described by an analogy to the difference between a slide film and a paper photograph. In TEM, similar to a slide film, the beam

(light) passes through the specimen (the slide), projecting the image onto a surface. In SEM, similar to a paper photograph, the beam (light) hits the specimen (the photograph), is reflected and the reflection is detected or observed. Details of the techniques are given in the following two subsections.

8.6.1 TEM

The transmission electron microscope possesses a similar setup as a light microscope, in a way that a radiation source emits light through a set of condenser lenses, which focus them onto the specimen. Radiation passing through the specimen is then passed through a second set of lenses onto a screen or detector. Using an electron beam, magnetic lenses are used instead of optical lenses as found in an optical microscope.

In addition to images, a series of affiliated techniques are available in TEM:

- As the electrons interact with the specimen, an electron diffraction pattern can be obtained. This is similar to X-ray diffraction, in a way that the electron beam hits the sample, the passing electrons are shielded off by a beam stopper, and the diffracted electrons provide a diffraction pattern, which is projected onto the viewing area (i. e., the screen or the image detector). A silicon calibration sample was used to obtain a diffraction pattern of known d -spacings. These were calibrated by calculation of a factor (\AA^{-1} per pixel in the image file of the diffraction pattern) via the use of picture editing software. Diffraction pattern files obtained from samples could then be indexed using the Powder Diffraction File database, via the calibration factor.
 - Similar to an X-ray tube, the electron beam can produce X-ray photons being emitted from the specimen. These photons have characteristic wavelengths with respect to the elements in the specimen. This provides an elemental composition of the specimen, showing relative amounts of different elements to each other.
 - The instrument can be switched to a scanning TEM (STEM) mode. Here, the electron beam is narrowed in a way that it only hits approx. a square nanometre of the specimen, and can then be scanned along it. During the scan, a bright-field and annular dark field image can be obtained. The bright-field image is constructed from the electrons that pass the specimen during scanning. The annular dark-field
-

image is produced from scattered electrons that hit a detector, which does not sit in the electron beam pathway, but rather is arranged in a circular fashion around it (Figure 8.6.1).

- EDX in STEM mode can be used to create element maps. This is performed by using the EDX detector while scanning the specimen, so that the intensities of characteristic X-rays generated at each spot of the specimen are arranged into an image, which has increasing colour intensity with increasing X-ray intensity obtained.

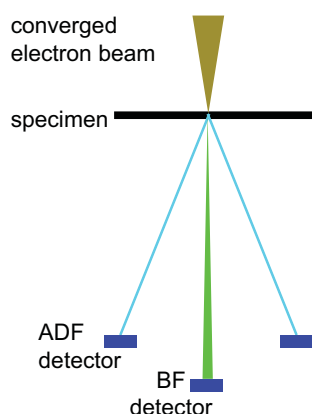


Figure 8.6.1: Location of the bright field (BF) and annular dark field (ADF) detectors in STEM [7].

In this thesis, a JEOL 2100F transmission microscope (Figure 8.6.2) was used for imaging and mapping. Some images were obtained on an aberration-corrected instrument, Titan (FEI). Both instruments are located at the Monash Centre for Electron Microscopy. Gatan Digital Micrograph software was used for data post-processing using image Fast Fourier transformation (FFT) and the measurement of lattice distances.

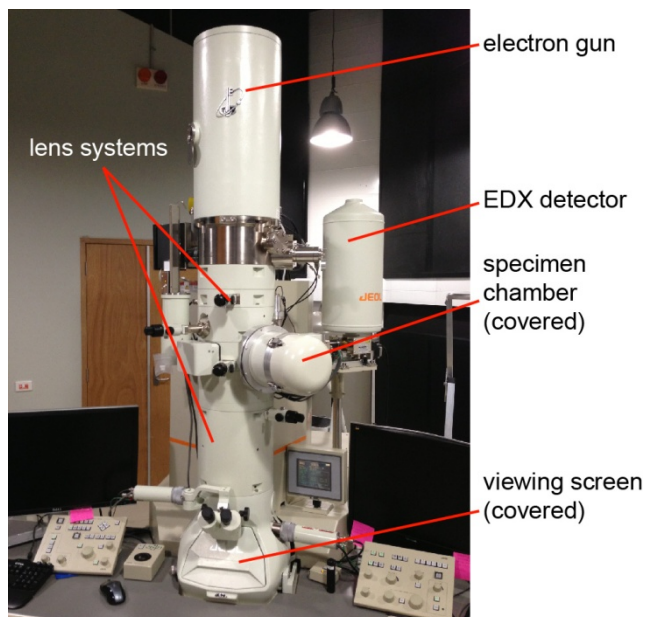


Figure 8.6.2: JEOL 2100F transmission electron microscope.

8.6.2 SEM

In SEM, the specimen is scanned in lines using an electron beam and the information about the intensity measured by an electron detector located above the sample. The sample is normally coated with a conductive material (here, platinum was used) and mounted on a conductive plate, so that charge build-up is prevented during irradiation with the electron beam. In this study, secondary electron scans were performed, which means that the electrons measured by the detector are electrons of up to 50 eV [8], which are emitted from the sample itself as a result of the irradiation with the electron beam. For elemental mapping, EDX was used, which works in a similar fashion to STEM as described above. The instrument used in this thesis was a JEOL JSM 7100 F (Figure 8.6.3).

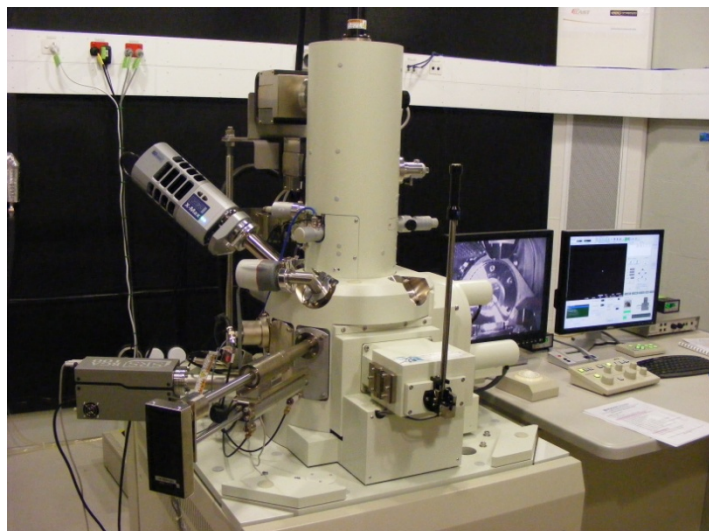


Figure 8.6.3: JEOL 7001 F scanning electron microscope.

8.7 Fourier-transform infrared spectroscopy

Fourier-transform infrared (FTIR) spectroscopy is an instrumental method, in which a sample is irradiated with infrared radiation and the passing (transmission) intensity at different wavelengths is detected. The principle relies on the vibration (stretching and bending) of molecules, which is excited at different wavelengths of non-ionising infrared radiation, causing absorption of the infrared beam [9]. In modern instruments, a Michelson interferometer is used, which creates an infrared beam with certain wavelengths intensified by constructive interference of two beams. Scanning these wavelengths over time gives a raw signal, from which the transmittance spectrum is calculated via a Fourier transformation, hence the name.

FTIR spectroscopy was used to confirm the carbonate formation during carbon dioxide exposure in a cadmium oxide/sodium iodide sorbent sample. A Perkin-Elmer Spectrum RXI instrument was used in this thesis and samples were dispersed in IR-grade potassium bromide and pressed to a pellet for analysis.

FTIR was able to confirm carbonate formation. However, in the course of this work, the technique proved inferior to powder XRD, as powder XRD was also able to identify the phase of cadmium carbonate and oxide, not only the carbonate anion.

8.8 Inductively coupled plasma mass spectrometry

Inductively coupled plasma mass spectrometry (ICP-MS) involves the ionisation of a liquid by an argon plasma. The plasma is generated in a plasma torch, which energises an argon flow by high alternating currents flowing through a coil. A liquid sample is injected into the plasma torch using a peristaltic pump and nebuliser. The compounds to be analysed are broken up into atoms and subsequently ionised by the hot plasma. By subsequent injection into a mass spectrometer (refer section 8.11), elemental compositions can then be obtained after a calibration using standard liquids of known concentrations was performed.

ICP-MS was used to determine the content of cadmium and iodine in the cadmium oxide/sodium iodide sample. For sample preparation, powder samples were dissolved in hydrochloric acid at room temperature and diluted to a (expected) measurable range in the μg element per kg liquid range. More sophisticated sample digestion procedures were not considered as cadmium oxide and carbonate are easily soluble in acids, whereas the halide promoter already dissolves in water.

A GBC Optimass 9500 instrument with time of flight mass spectrometer was used in this thesis. Sodium was initially intended to be measured by this method as well; but results were not satisfactory due to a high sodium background noise produced by the instrument. The background noise was assumed to be due to sodium being eroded from the quartz glass components of which the plasma torch is made. For this reason, the sodium content was measured by atomic absorption spectrometry (section 8.9).

8.9 Atomic absorption spectrometry

Atomic absorption spectrometry (AAS) is a spectrometric technique, which involves the atomisation of a liquid sample by injection into an acetylene flame. An element-specific hollow cathode lamp gives light of a certain wavelength, which is absorbable by the atoms of the element that is to be measured. During irradiation of the acetylene flame, containing the atomised sample, with the hollow cathode lamp rays, the change in transmission of the light through the flame is measured on the opposite side of the flame. The more of the element that is atomised in the flame, the less light transmission is observed by the

detector. Quantification of the element can be performed, after the instrument is calibrated using solutions of known concentrations.

In this thesis, a GBC XplorAA model instrument was used. Samples were diluted to expected values in the mg sodium per kg liquid range, as AAS is a less sensitive technique than ICP-MS.

8.10 Fixed-bed sorption study

Fixed-bed carbon dioxide sorption was performed on a Micromeritics AutoChem II 2950 instrument (Figure 8.10.1). This instrument is capable of purging a heated powder sample with a variety of gases and can be programmed for temperature ramps/isotherms and automatic gas flow switching. A portion of the exit gas stream is fed to a mass spectrometer (refer section 8.11) for analysis. The instrument is designed to do catalytic studies and thus, its capabilities go beyond this study.



Figure 8.10.1: Left: AutoChem instrument. Right: Furnace opened with quartz sample tube.

8.11 Mass spectrometry

Mass spectrometers were used in the scope of fixed-bed residual gas analysis (section 8.10) and ICP-MS (section 8.8). Their purpose is to distinguish different masses of ionised atoms or molecules to perform composition analyses.

The ICP-MS instrument includes a time-of-flight mass spectrometer. Here, the ions created by the plasma torch are accelerated by an electric field pulse of 10^3 to 10^4 V [9]. This electric field provides a set amount of kinetic energy, resulting in a mass-dependent speed of the

ions. The accelerated ions pass through a drift tube of set length, at the end of which a detector is attached. By the time required for the ions to reach the detector, the different masses can be discriminated.

The MKS Cirrus 2 model mass spectrometer used in the fixed-bed studies is a quadrupole mass spectrometer. In this setup, ionised molecules or atoms are injected into the centre between two opposite positive electrode rods, with two negative electrode rods sitting perpendicular to them. By applying both static and oscillating electric fields of varying intensities to the ion path, only ions of certain mass are guided onto a stable trajectory and reach the detector on the end of the electrode assembly, whereas other ions move in unstable trajectories and hit one of the electrodes. Scanning over different electric field intensities allows ions of different mass to pass through to the detector.

In mass spectrometry, it must be noted that ions reaching the detector are of a particular mass-to-charge (m/z) ratio. For example, hypothetically, an I_2^{2+} ion passes at the same m/z as an I_1^{1+} ion. This is one reason why compounds give several m/z in a mass spectrum, as ionisation does not create singly-charged ($1+$) ions only. Molecules also can fracture on or after ionisation, creating ionised fragments, which are also detected in the mass spectrometer.

8.12 Nitrogen adsorption

Nitrogen adsorption at liquid nitrogen temperature (77 K) is a common method to obtain adsorption isotherms, which can be used to calculate a pore size distribution and specific surface area of a powder sample. The samples are prepared by degassing in a vacuum at elevated temperatures to remove all previously adsorbed species (like atmospheric gases, moisture) from the surface of the sample.

The gas sorption analyser consists of a manifold of known volume, which can be filled with gas or evacuated. Pressure measurement is implemented at the manifold as well.

The measurement principle is as follows:

1. Sample tubes are attached to the manifold, evacuated and kept at 77 K in a liquid nitrogen bath.
-

2. Gas is dosed into the manifold to a certain pressure, with the sample tube connection blocked by a closed valve, and the manifold pressure is recorded.
3. The gas is expanded into the sample by opening the sample valve. Expansion into both the manifold and the headspace above the sample lowers the pressure. Assuming the headspace volume of the sample is known, a certain pressure is to be expected.
4. Due to adsorption of part of the gas, removing gas molecules from the gaseous phase, the pressure is lowered further. The difference between expected pressure and measured pressure is the basis of calculation of the amount of gas adsorbed at the specific pressure.
5. The gas dosing is repeated several times between vacuum and atmospheric pressure.

In order to obtain a value for the headspace volume above the sample, a helium calibration is used before analysis. The principle is the same as described above with regard to dosing the manifold, measuring the pressure and expanding into the sample chamber and measuring the pressure again. As helium is assumed not to adsorb on the sample, the expanded pressure can be used for calculating the headspace volume.

At the start of this project, a Coulter Omnisorp 360CX gas sorption analyser was used. After a recent laboratory upgrade, nitrogen adsorption experiments were delegated to a new instrument, a Micromeritics Tristar II 3020. The measurement principles of both of these instruments are the same (as outlined above) and the dosing and measurement is fully automated.

For sample preparation (outgassing), the Omnisorp 360CX instrument provided a built-in degas station, whereas for analysis on the Tristar II 3020, a Micromeritics VacPrep 061 degassing station was used.

The specific surface area of the material was calculated using the Brunauer-Emmett-Teller (BET) model [10] using isotherm points between 0.05 and 0.35 relative pressures, whereas the pore size distribution in the mesopore area was calculated via the Barrett-Joyner-Halenda (BJH) model [11] using the desorption isotherm. These models are available in the

instrument control software for data post-processing, however, for ease of routine analyses, they were transferred into a custom MATLAB code.

8.13 X-ray-photoelectron spectroscopy

The principle of X-ray photoelectron spectroscopy (XPS) is the removal of core electrons out of an atom using soft X-radiation that exceeds the binding energy of the respective electron (Figure 8.13.1a). A simple energy balance can be written for this process (eqn. 8.13.1) [12].

$$E_B = h\nu - E_K - W \quad \text{eqn. 8.13.1}$$

Here, the incident energy of the radiation $h\nu$ (Planck constant times frequency) is equal to the sum of the binding energy of the core shell electron E_B being overcome, the kinetic energy of the ejected electron once ejected E_K , and an instrument-specific work function term W . By measuring the kinetic energies of the ejected electrons using a detector, the binding energies of the core shell electrons can be calculated.

Auger electrons (Figure 8.13.1b) are obtained by electrons of outer shells moving into the vacancy caused by the X-ray. The energy released by the electron moving between these shells (red arrow) then ejects the Auger electron (blue arrow). In contrast to the photoelectrons, these Auger electrons have a constant kinetic energy, irrespective of the incident energy of the X-rays being used. Auger electrons are usually unwanted during XPS, however, they are the focus of study within a different discipline, Auger electron spectroscopy.

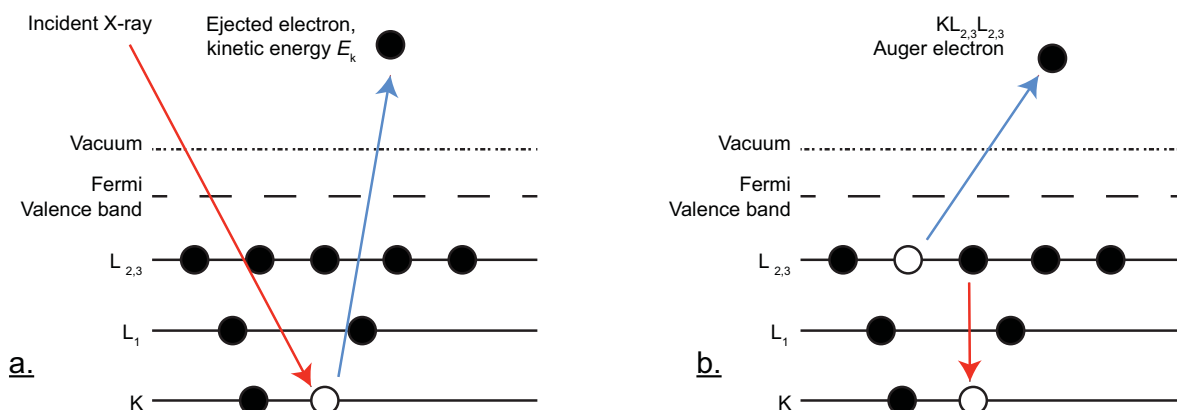


Figure 8.13.1: a. Removal of a 1s photoelectron during XPS, b. Auger electron ejection as a result of an electron vacancy in the K shell [12].

In different chemical compounds, atoms have different electron characteristics, which result in different binding energies for electrons in the core shells. Thus, XPS can be used to gain knowledge of the nature of atoms in a compound. It must, however, be noted that the electrons ejected from atoms in XPS are unable to escape the matrix (and, hence be detected) from a depth of more than two to five nanometres [9]. Thus, XPS is a surface analysis technique. However, the chemical analysis by XPS can provide insights about possible reactions of the material examined.

XPS was performed at CSIRO Materials Science and Engineering and a Kratos AXIS Ultra DLD spectrometer was used. The incident X-rays had an energy of 1486.7 eV.

8.14 References for Chapter 8

- [1] R. C. Weast, *CRC Handbook of Chemistry and Physics*. Cleveland, Ohio: The Chemical Rubber Co., 1968-1969.
 - [2] R. E. Dinnebier and S. J. Billinge, "Powder diffraction: theory and practice," Royal Society of Chemistry, 2008, pp. 1-19.
 - [3] B. H. Toby, "CMPR - a powder diffraction toolkit," *Journal of Applied Crystallography*, vol. 38, pp. 1040-1041, 2005.
 - [4] G. Will, *Powder Diffraction: The Rietveld method and the two-stage method*: Springer, 2006.
 - [5] A. C. Larson and R. B. V. Dreele, "General Structure Analysis System (GSAS)," *Los Alamos National Laboratory Report* vol. LAUR 86-748, 1994.
 - [6] B. H. Toby, "EXPGUI, a graphical user interface for GSAS," *Journal of Applied Crystallography*, pp. 210-213, 2001.
 - [7] P. Nellist, "The Principles of STEM Imaging," in *Scanning Transmission Electron Microscopy*, S. J. Pennycook and P. D. Nellist, Eds.: Springer New York, 2011, pp. 91-115.
 - [8] S. Amelinckx, D. van Dyck, J. van Landuyt, and G. van Tendeloo, *Electron microscopy: Principles and Fundamentals*: Wiley-VCH, 1997.
 - [9] D. A. Skoog, F. J. Holler, and T. A. Nieman, *Principles of instrumental analysis*: Saunders College Publishing, 1998.
 - [10] S. Brunauer, P. H. Emmett, and E. Teller, "Adsorption of Gases in Multimolecular Layers," *Journal of the American Chemical Society*, vol. 60, pp. 309-319, 1938.
 - [11] E. P. Barrett, L. G. Joyner, and P. P. Halenda, "The Determination of Pore Volume and Area Distributions in Porous Substances. I. Computations from Nitrogen Isotherms," *Journal of the American Chemical Society*, vol. 73, pp. 373-380, 1951.
 - [12] J. F. Watts and J. Wolstenholme, *Electron Spectroscopy: Some Basic Concepts*: John Wiley & Sons, Ltd, 2005.
-

Appendix 1: Additional Journal Paper

'Nanoscale Structural Investigation of Cs₂CO₃-Doped MgO Sorbent for CO₂ Capture at Moderate Temperature'

The following paper resulted mainly from a third year project completed by M. Liu. It is given on the following pages and presents previous work that later led to Chapter 5 of this thesis.

Copyright 2013, The American Chemical Society. Reproduced with permission.

Full citation: <http://dx.doi.org/10.1021/jp4024316>

M. Liu, C. Vogt, A. L. Chaffee, and S. L. Y. Chang, "Nanoscale Structural Investigation of Cs₂CO₃-Doped MgO Sorbent for CO₂ Capture at Moderate Temperature," *Journal of Physical Chemistry C*, vol. 117, pp. 17514-17520, 2013.

Declaration for Thesis Chapter

Nanoscale Structural Investigation of Cs₂CO₃-Doped MgO Sorbent for CO₂ Capture at Moderate Temperature

Monash University

Declaration for Thesis Appendix

Declaration by candidate

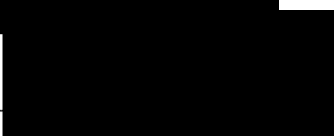
In the case of the paper shown in the Appendix, the nature and extent of my contribution to the work was the following:

Nature of contribution	Extent of contribution (%)
Performing in-situ and ex-situ powder XRD experiments, performing TGA experiments, assisted laboratory/synthesis work, editorial & results discussion assistance	20 %

The following co-authors contributed to the work. If co-authors are students at Monash University, the extent of their contribution in percentage terms must be stated:

Name	Nature of contribution	Extent of contribution (%) for student co-authors only
Alan L Chaffee	Supervision, assisted interpretation of results, editorial assistance	N/A
Maoyuan Liu (1 st author)	Prepared and analysed samples; identified major issues; developed interpretations; fully drafted papers and conclusions	N/A
Shery L Y Chang	Operating electron microscope, input to microscopy results discussion, supervision of 1 st author	N/A

The undersigned hereby certify that the above declaration correctly reflects the nature and extent of the candidate's and co-authors' contributions to this work*.

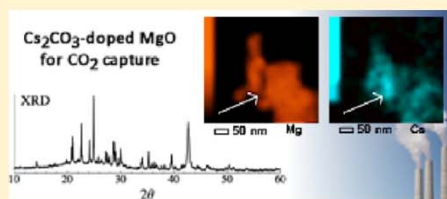
Candidate's Signature		Date	26/9/13
Main Supervisor's Signature		Date	27/9/13

*Note: Where the responsible author is not the candidate's main supervisor, the main supervisor should consult with the responsible author to agree on the respective contributions of the authors.

Nanoscale Structural Investigation of Cs₂CO₃-Doped MgO Sorbent for CO₂ Capture at Moderate Temperature

Maoyuan Liu,^{†,||} Christian Vogt,^{†,‡} Alan L. Chaffee,^{*,†,‡} and Shery L. Y. Chang^{*,§,⊥}[†]School of Chemistry, [‡]Cooperative Research Centre for Greenhouse Gas Technologies (CO2CRC), and [§]Monash Centre for Electron Microscopy, Monash University, Victoria 3800, Australia

ABSTRACT: MgO sorbents doped with alkali-metal carbonates have been shown to exhibit improved sorption capacities at both low and moderate operating temperatures, compared to pure MgO sorbents. However, the mechanism of how alkali-metal carbonates enhance the CO₂ sorption is not well understood. Using in situ X-ray diffraction, TEM, and thermogravimetric analysis, we have shown that the cesium dopants in the Cs₂CO₃-doped MgO nanoparticle system do not simply act as a promoter in sorption of CO₂, but rather as a reagent alongside MgO. A new mixed magnesium–cesium carbonate phase has been found to be responsible for the improved sorption capacity of the doped-MgO-based sorbents. On the basis of our findings, it is suggested that a higher sorption capacity may be achieved if cesium is uniformly dispersed throughout the MgO particles.



INTRODUCTION

CO₂ generated from power plants has been recognized as one of the major contributors to the global CO₂ emissions. As the large-scale carbon-emission-free energy sources are still many years to come,¹ it is therefore attractive to remove CO₂ from the flue gas (for postcombustion) and/or syn-gas (for precombustion) streams in the power plants. Several material systems can be used to capture CO₂, including liquid-phase solvents,^{2–4} membranes,^{5,6} and molecular sieves.^{7,8} However, many of these systems are considered costly and often require significant additional energy.⁹ Consequently, regenerable solid sorbents based on chemical sorption process have been developed for a range of temperatures and pressures.^{10–12} In particular, sorbents containing alkali metal or alkaline-earth metal operating at low temperature (50–150 °C) and moderate temperature (300–500 °C) find applications in post- and precombustion capture, respectively.^{13,14}

Due to their low cost, abundance, and low toxicity, alkaline earth metal oxides such as MgO have been shown to be good candidates for carbon dioxide capture materials. CO₂ is captured through chemisorption of MgO to form MgCO₃ (MgO + CO₂ ⇌ MgCO₃). However, MgO has a very low sorption capacity of 0.13 mmol/g at moderate temperatures under a dry environment.¹⁵ Therefore, improvements have been made by adding “promoters” to increase sorption capacities at low and moderate operating temperatures. Alkali-metal carbonates, for example, have been used as promoters to enhance the sorption capacities and to tune the sorption temperatures.^{12,16–22} Although alkali-metal carbonates on their own can absorb CO₂ through the reaction M₂CO₃ + H₂O + CO₂ ⇌ 2MHCO₃, the reaction only happens at low temperatures and in the presence of water.^{23–25}

A systematic study of alkali-metal carbonate double salts [(Z₂CO₃)_x(MgCO₃)_y, where Z = Li, Na, K, and Cs] supported on MgO under dry and humid conditions reported a broad

range of sorption capacities (~0.1–11.9 mmol/g) at 350–400 °C, depending on the synthesis conditions.¹⁶ The highest capacity in this study was observed for Na double salt at 11.9 mmol/g and 375 °C with a Z/Mg ratio of 0.36. On the other hand, recent reports have suggested a trend of increase in sorption capacities with the increase of atomic radii of alkali metals.^{18,19} For example, for the alkali-metal-doped CaO at both 50 and 450 °C under dry conditions, Reddy et al. reported that sorption capacity follows the order of Li < Na < K < Rb < Cs.¹⁸ Similarly, for sodium, potassium, and cesium carbonates doped on MgO, the capacities were found to be Na < K < Cs, at 200–450 °C.¹⁹

Although most of the studies on MgO promoted with alkali-metal carbonates assumed that the reaction mechanism is based on the carbonation of MgO, with the carbonates as passive promoters, recent reports have indicated that a mixed cation carbonate phase [Z₂Mg(CO₃)₂] is the product after CO₂ sorption.^{17,20,21} A recent study by Lee et al. on K₂CO₃-promoted MgO has measured about 4 mmol/g capacity at lower temperatures (50–100 °C) in the presence of water.¹⁷ Double salt carbonates of K₂Mg(CO₃)₂ and K₂Mg(CO₃)₂·4(H₂O) were found in the sorbents after CO₂ sorption. Zhang et al. also observed double salt Na–Mg carbonates formation on Na₂CO₃-promoted MgO sorbents at 300–470 °C under dry conditions with an sorption capacity of 3.4 mmol/g.²⁰ However, the experimentally observed sorption capacities, as pointed out by the authors, are much smaller than the theoretically predicted values. This is also the case for many examples in the literature.¹⁶

Despite the successful development of alkali-metal carbonate promoted MgO sorbents for pre- and postcombustion CO₂

Received: March 10, 2013

Revised: July 18, 2013

Published: July 25, 2013

capture applications, there exists a broad deviation of reported sorption capacities and performances. This deviation reflects that the nanoscopic structures of promoted MgO sorbents are not well understood. In order to improve the sorption performances of the alkali-metal carbonate promoted MgO sorbents, it is therefore important to have a detailed understanding of the structures of sorbents during the sorption process. Here, we report a nanoscale structural characterization on Cs_2CO_3 -doped MgO sorbents, at different stages of the CO_2 sorption process. This material has been shown to be a good sorbent for postcombustion applications, with optimum sorption at 380 °C and regeneration at 550 °C under dry conditions (total pressure 1 atm).¹⁹ Characterization in a controlled environment was conducted using in situ powder X-ray diffraction (PXRD) to investigate the structural transformations in the CO_2 sorption process. In addition, thermogravimetric analysis (TGA), laboratory-based PXRD, and transmission electron microscopy (TEM) have also been applied to investigate the sorption capacity and the structural, morphological, and compositional distribution changes of the doped sorbents during the process. A detailed understanding of the structural changes of the sorbents will provide valuable insights into the directions of optimizing sorbents for CO_2 capture at suitable operating conditions.

METHODS

Synthesis of Materials. Cesium carbonate doped magnesium oxide sorbents were synthesized by the wet impregnation method. MgO (99.9% Sigma Aldrich) and cesium carbonate (99.9% Sigma Aldrich) were used to produce sorbents with a cesium loading of 15 mol %. This loading has been previously found as the optimum loading.¹⁹ Powdered MgO was added with rigorous stirring to an aqueous solution of cesium carbonate, which forms a suspension. Water was then evaporated via heating and continued stirring using a magnetic hot-plate stirrer. The solid was dried in a N_2 -purged oven at 120 °C for 2 h. To avoid extensive exposure to air and moisture, the materials were always stored in a desiccator after synthesis and treatments.

To investigate the effects of the treatment process used in thermogravimetric analysis (see later section), a portion of the synthesized material was calcined in air at 600 °C for 5 h. This allowed us to perform ex situ analysis in TEM.

Thermogravimetric Analysis. The CO_2 sorption capacity of this sorbent was determined by TGA using a Setaram TAG 24 symmetrical thermoanalyzer. The gas flow was controlled by programmable mass flow controllers and the total volumetric flow rate was maintained at 70 mL/min at atmospheric pressure.

Approximately 20 mg of the sample was used for this analysis. At the start of the experiment, the gas flow was pure argon (~1 bar) and the instrument was allowed to equilibrate at room temperature for 20 min. Pretreatment of the sorbent was commenced by heating to 600 °C (from room temperature) over a 30-min period. This temperature was maintained for 20 min and then allowed to cool and equilibrate at the specified carbon sorption temperature (300 or 235 °C) over 45 min. The pretreatment step was carried out in order to decompose hydroxides formed during the wet synthesis (as both Cs_2CO_3 and MgO are mixed in aqueous solution) to form oxide and to desorb atmospheric contaminants, without exposing the sample to the atmosphere before sorption analysis. In addition, the pretreatment temperature ranging

from 450 to 650 °C was found to achieve optimum sorption capacity.¹⁹ All samples in this study were pretreated in the thermoanalyser and not exposed to atmospheric contaminants before the actual sorption study. This ensures that the all sorption studies started from the same structure. Next, the gas was switched to a mixture of CO_2 and argon, each at 0.5 bar partial pressure, while a constant temperature was maintained. Afterwards, the sorbent was allowed to absorb CO_2 at this condition for 2.25 h and then allowed to cool to room temperature over 30 min. This gas mixture was maintained over the cooling period to prevent pressure-swing-induced decarbonation. At the end of the experiment, the carbonated sorbents were collected and stored in a desiccator. The temperature and pressure programming for the case of carbonation at 300 °C is illustrated in Figure 1.

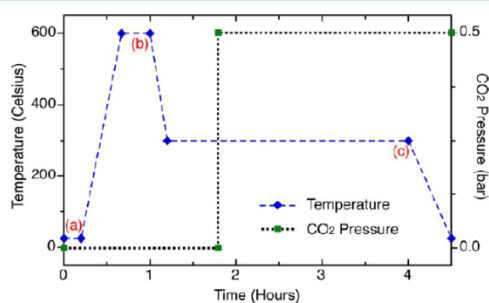


Figure 1. TGA program of CO_2 chemisorption of as-synthesized Cs_2CO_3 -doped MgO at 300 °C. The temperature programming is given by the blue dashed line, and the partial pressure of CO_2 is given by the black dotted line. Samples at the three stages in this program, labeled as (a) as-synthesized, (b) pretreated at 600 °C, and (c) carbonated at 300 °C, were characterized.

Characterization Methods. PXRD patterns were measured both in situ and ex situ to identify the structures of materials. Ex situ PXRD analysis was performed for the carbonated sorbent on a Bruker D8 focus powder diffractometer using $\text{Cu K}\alpha$ radiation. In situ PXRD analysis was performed on the powder diffraction beamline at the Australian Synchrotron. A lanthanum hexaboride standard was used for calibration. The wavelength and zero offset were determined by a Rietveld refinement to be 0.793 049 2 Å and $-0.002\ 990\ 7^\circ$ 2θ , respectively. For in situ characterization, the as-synthesized sorbent was initially heated under pure N_2 (~1 bar) at a rate of 10 K/min, with measurements taken at 120, 200, 300, 350, 400, 450, 500, and 650 °C. The sorbent was then allowed to cool to room temperature under N_2 . Subsequently, the gas was switched to CO_2 (1 bar). The temperature was then ramped up at a rate of 10 K/min and the measurement was carried out at 300 °C. The in situ PXRD data were converted to the copper $\text{K}\alpha$ emission line for direct comparison with ex situ data. The structures of the materials have been identified and rigorously checked with the known crystal structures from the ICSD and PDF databases.²⁶

Transmission electron microscopy and energy disperse X-ray spectroscopy (EDX) were carried out on the neat MgO (Sigma Aldrich), the as-synthesized sorbent, the pretreated sorbent, and the carbonated sorbent (the samples at the stages labeled in Figure 1) using a JEOL 2100F TEM. Size distribution and morphology of nanoparticles were examined using the bright-field TEM (BFTEM), and the crystallinity of nanoparticles was

examined using high-resolution TEM and selected-area diffraction (SAD). Elemental distributions were measured using EDX under scanning TEM (STEM) mode with a 1 nm size probe to generate elemental maps.

RESULTS AND DISCUSSIONS

CO₂ Sorption Capacities and Cycling Stability. The sorption capacity of Cs₂CO₃-doped MgO, measured from TG CO₂ sorption analysis at 235 and 300 °C, is shown in Figure 2.

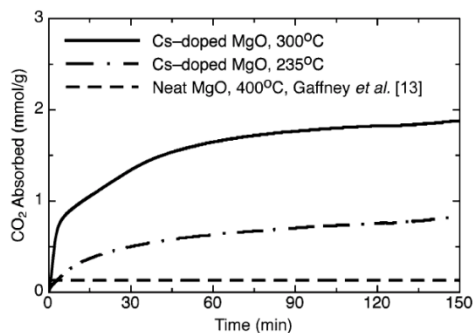


Figure 2. CO₂ sorption yields of Cs₂CO₃-doped MgO and neat MgO.

The sorption capacities of the doped sorbents are found to be 1.9 mmol of CO₂ per gram of sorbent at 300 °C and 0.8 mmol/g at 235 °C. These capacities are significantly higher compared with the low capacity of 0.13 mmol/g for the undoped MgO under similar conditions.¹⁵ The approximately 14-fold improvement in the maximum sorption capacity when doping with Cs₂CO₃ demonstrates that the dopants clearly play a critical role in increasing the CO₂ sorption yield of MgO at low pressures (~0.5 bar) and moderate temperatures (~300 °C).

The regenerability of Cs₂CO₃-doped MgO is presented in Figure 3, showing the pressure swing sorption/desorption cycles. The test was carried out using (~0.5 bar) CO₂ and Ar

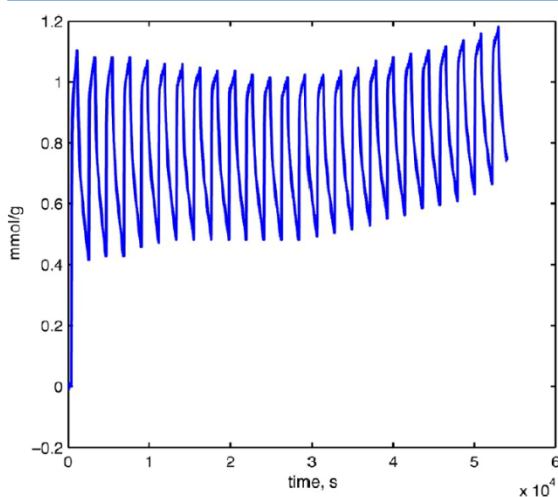


Figure 3. Multiple sorption/desorption cycles of Cs₂CO₃-doped MgO using pressure swing.

mixture for 12 min and switching to pure Ar for 24 min. The cycles were repeated 25 times at constant temperature of 370 °C. As shown in Figure 3, there is a continuous baseline drift; however, the sorption capacity is stable throughout the cycles and did not show any apparent loss of capacity. This result demonstrates the good regenerability of the Cs₂CO₃-doped MgO.

Structure of Sorbents before and after CO₂ Sorption.

The structures of the sorbents were measured using in situ and ex situ PXRD, as presented in Figure 4. The condition of the in situ experiment was set to be close to the TG experiments, so the structure changes of the sorbents can be identified in a controlled environment. The PXRD patterns of the commercial MgO and Cs₂CO₃ (not shown here) were also measured to serve as references. The as-synthesized Cs₂CO₃-doped MgO sorbent (Figure 4a) was found to be composed of Mg(OH)₂ ($2\theta = 18^\circ, 37^\circ$)²⁷ and Cs₂CO₃·(H₂O)₃ (peaks predominantly at $2\theta < 35^\circ$).²⁸ As both MgO and Cs₂CO₃ are hygroscopic and the impregnation method uses water as the solvent, both compounds are therefore hydrated.

Upon pretreatment at the temperatures between 120 and 350 °C, it was found that the diffraction peaks related to Cs₂CO₃·(H₂O)₃ disappeared while a partial conversion from Mg(OH)₂ into MgO (Figure 4b)²⁹ occurred. Upon further heating to 400 °C a monoclinic Cs₂CO₃ phase ($20^\circ < 2\theta < 40^\circ$, Figure 4f)³⁰ was formed, and Mg(OH)₂ was completely converted into MgO. The sorbent remained as a mixture of the monoclinic Cs₂CO₃ phase and MgO upon further heating to 650 °C (Figure 4f–i). It was observed that peaks shift slightly toward lower angles with increasing temperature, due to the thermal expansion of the solids. Although the pretreatment temperature in our TG analysis is 600 °C, the in situ PXRD measurements simulating the pretreated conditions were carried out up to 650 °C. Since the structure of the sorbent does not change between 400 and 650 °C, the starting structures of the sorbents are therefore determined to be monoclinic Cs₂CO₃ and MgO.

An ex situ PXRD was also carried out on the sorbent sample after a pretreatment step in TGA, to compare the structure measured in a controlled environment with that exposed to the atmosphere during specimen storage and ex situ measurement. Figure 4j shows the PXRD pattern for a sorbent sample that has been pretreated at 600 °C in TGA and then allowed to cool to room temperature. It can be seen that the monoclinic Cs₂CO₃ phase spontaneously converted back to Cs₂CO₃·(H₂O)₃, whereas the MgO phase did not reabsorb moisture to become Mg(OH)₂. This result demonstrates the hygroscopic nature of Cs₂CO₃, which readily absorbs moisture from the atmosphere.

The in situ and ex situ PXRD patterns of the sorbents upon chemisorption of CO₂ are presented in patterns k and l of Figure 4, respectively. It can be seen that the Cs₂CO₃ phase is completely converted upon CO₂ sorption, as the monoclinic Cs₂CO₃ reflections in Figure 4f–i are not present in Figure 4k. In order to identify the reflections in the region $2\theta \leq 35^\circ$ in Figure 4k,l, these patterns have been exhaustively compared with all known compounds containing Cs, Mg, O, H, and/or C, as shown in Figure 5. Firstly, it was found that MgCO₃ was not present in the carbonated product³¹ and the intensity of the MgO peak remains prominent. As MgO is expected to be carbonated into MgCO₃ upon chemisorption of CO₂, the lack of MgCO₃ strongly suggests that the carbonation of MgO is not the reaction route for Cs₂CO₃-doped MgO. Secondly, it was found that there are no documented crystal structures that

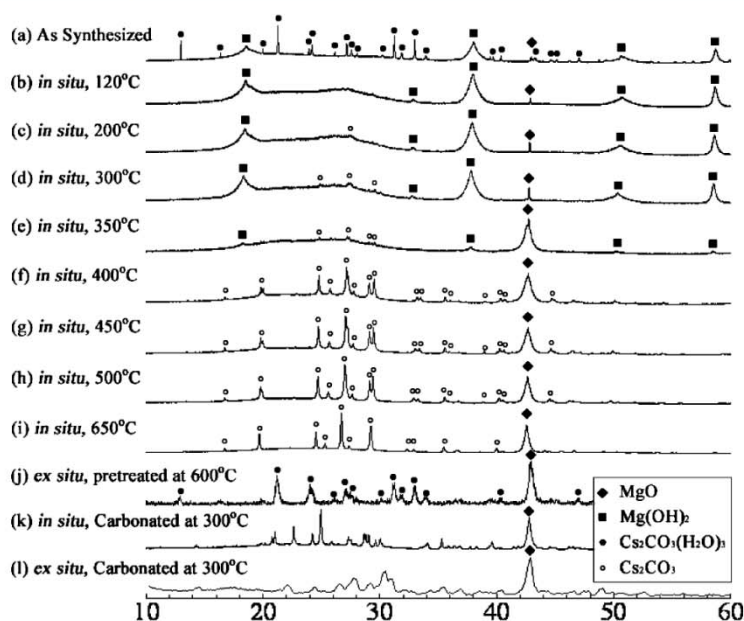


Figure 4. PXRD patterns of Cs_2CO_3 -doped MgO (a) as-synthesized, (b–i) pretreated from 120 to 650 °C in N_2 , and (k) after CO_2 sorption. Patterns a–i and k were taken in situ using synchrotron radiation and patterns j and l ex situ under typical laboratory conditions.

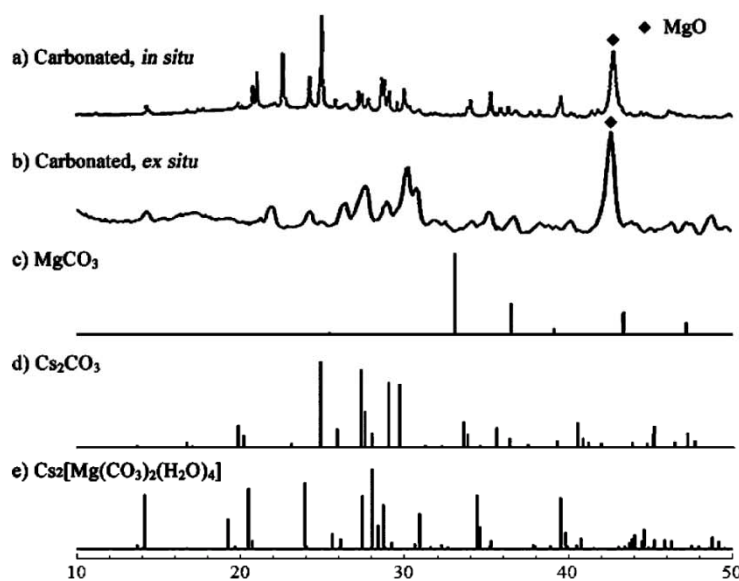


Figure 5. Comparison of in situ and ex situ XRD patterns with simulated patterns of MgCO_3 , Cs_2CO_3 , and $\text{Cs}_2[\text{Mg}(\text{CO}_3)_2(\text{H}_2\text{O})_4]$.^{30–32}

can match this measured pattern. As the mixed alkali metal and magnesium carbonates have been found in the carbonated product for the MgO doped with sodium and potassium carbonates, we have therefore also compared our experimental XRD pattern with the one known mixed Cs–Mg carbonate structure, $\text{Cs}_2[\text{Mg}(\text{CO}_3)_2(\text{H}_2\text{O})_4]$ (Figure 5d), reported by Zheng and Adam.³² However, its XRD pattern does not match our measured pattern. It should also be noted that a similar study on the Cs-doped MgO attributes the structure of the Cs phase in a low-angle region ($2\theta < 35^\circ$) to the mixed-cation

phase $\text{Cs}_2\text{Mg}(\text{CO}_3)_2$.³³ However, we find that this reported pattern actually matches with the known structure of $\text{Cs}_2\text{CO}_3 \cdot (\text{H}_2\text{O})_3$ ²⁸ instead.

There are significant differences between the PXRD patterns of the carbonated sorbent measured in situ (Figure 5a) and ex situ (Figure 5b). As the Cs_2CO_3 phase is highly hygroscopic and is present only as $\text{Cs}_2\text{CO}_3 \cdot (\text{H}_2\text{O})_3$ when exposed to atmospheric moisture, a likely analogue is that the phase observed in the in situ pattern may become hydrated to give the observed ex situ pattern. To the best of our knowledge, these

cesium-containing phases after CO₂ sorption (Figure 5a,b) have not been reported before. This strongly suggests that the structure we have observed here is a new phase.

Morphology of Sorbents. In order to understand the possible morphological changes of the sorbents during a sorption process, TEM imaging and average particle size analysis based on the XRD results have been conducted.

The morphology of the sorbents at different stages of the CO₂ sorption (stages labeled in Figure 1), has been examined using TEM. Figure 6 shows the bright-field TEM images of the

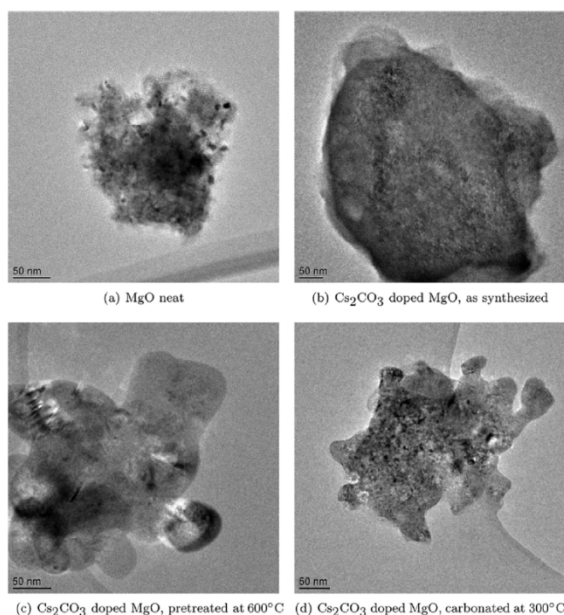


Figure 6. TEM images of (a) neat MgO (as received) and (b) as-synthesized, (c) pretreated, and (d) carbonated Cs₂CO₃-doped MgO.

neat MgO and as-synthesized, pretreated, and carbonated Cs₂CO₃-doped MgO. It can be seen that the morphology of the doped sorbents differ significantly from the neat MgO. The doped sorbents appear to be aggregates of nanoparticles, and the aggregates tend to have an overall diameter in the range of 100–500 nm.

The detailed morphological changes through the different stages can be seen in the corresponding HRTEM images shown in Figure 7. Figure 7a shows that neat MgO consists of aggregates of randomly oriented small nanoparticles of around 10 nm. Upon doping via the impregnation method, the surface of the particle is visually more uniform and smooth, as seen in Figure 7b. As the high-energy electron radiation used in a TEM is known to decompose Mg(OH)₂ to MgO,³⁴ the electron diffraction shows reflections corresponding to MgO spacings instead of Mg(OH)₂ spacings, as confirmed by X-ray diffraction. The pretreated sorbent given in Figure 7c shows a similarly smooth surface, and it consists of larger crystalline nanoparticles, as the corresponding electron diffraction pattern appears as spots instead of rings. These larger nanoparticles are likely formed as the result of annealing at a high temperature during the pretreatment process prior to CO₂ sorption. After CO₂ sorption, the surfaces of the carbonated nanoparticles become distinctly regular and crystalline. An example of such

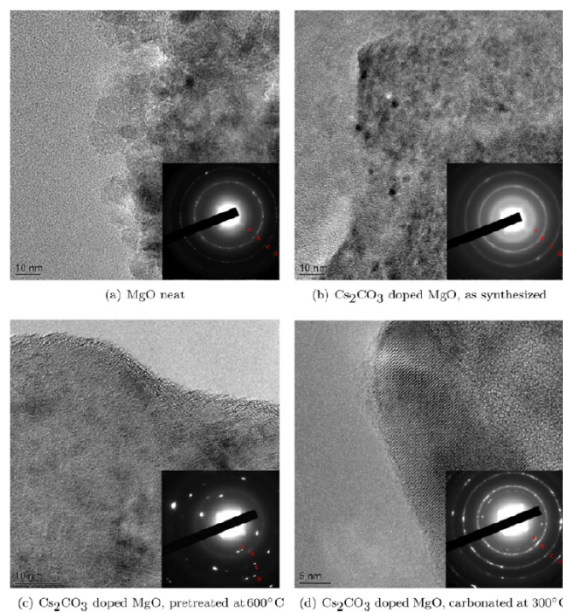


Figure 7. High-resolution TEM images and their corresponding selected-area electron diffraction patterns (inset) of the (a) neat MgO and (b) as-synthesized, (c) pretreated, and (d) carbonated Cs₂CO₃-doped MgO. The reflections labeled in the diffraction patterns correspond to the spacings of MgO.

morphology is given in Figure 7d. This finding is consistent with the observations of CO₂ sorption in alkaline-metal oxides.^{35,36} The electron diffraction pattern for the carbonated sorbent consists of spots and rings, indicating a greater variation in the distribution of the size of particles in the carbonated sorbent compared to the pretreated sorbent.

To estimate the average size of the sorbent particles, we have used the Scherrer equation to calculate the average sizes of particles measured from the widths of Bragg reflections in the XRD patterns. The full width at half-maximum (fwhm) of peaks is obtained by fitting the specified peaks to a pseudo-Voigt distribution. Table 1 shows the average size of the

Table 1. Average Particle Size of Cs₂CO₃-Doped MgO Sorbents before and after CO₂ Sorption

temp	MgO (nm)	Cs ₂ CO ₃ (nm)	carbonated Cs (nm)
pretreatment, 400 °C	11.4	8.3	
pretreatment, 450 °C	12.9	10.3	
pretreatment, 500 °C	14.9	10.8	
pretreatment, 650 °C	19.6	11.1	
carbonated, 300 °C	21.1		8.9

Cs₂CO₃ and MgO particles in the sorbent as well as the carbonated product. It can be seen that the sizes of both MgO and Cs₂CO₃ particles increase with increasing pretreatment temperatures. This is consistent with the observations that the sizes of particles grow upon annealing. Upon CO₂ sorption, there is also a slight increase in the MgO crystal size and the formation of much smaller particles of the carbonated Cs–Mg phase. This trend of size increment is in agreement with our TEM observations.

Composition Distribution of Dopants before and after CO₂ Sorption. In order to understand the distribution of the dopants (Cs₂CO₃) and the matrix (MgO) before and after CO₂ sorption, EDX mapping using a 1 nm STEM probe has been employed to obtain the composition distribution at the nanoscale. Figure 8 shows the annular dark field (ADF)

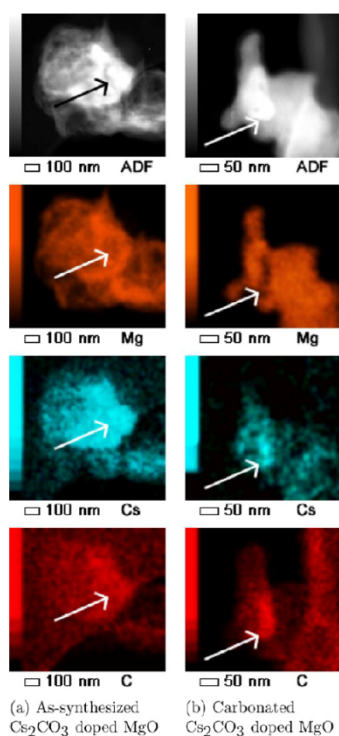


Figure 8. Composition distribution of Cs, Mg, and C in the as-synthesized (a) and carbonated (b) sorbents. Arrows highlight regions that are rich in Cs and C but poor in Mg.

images and the Cs, C, and Mg composition maps before (a) and after (b) CO₂ sorption. The ADF intensity reveals the average atomic number density (mass thickness) of the specimen, whereas an EDX map reveals the atomic density distribution of a given element. If Cs₂CO₃ dopants were evenly distributed across the MgO matrix, the Cs, C, and Mg intensity distribution in the EDX maps would be expected to be in accord with the ADF intensity.

It can be seen in both part a and b of Figure 8 that there are regions showing relatively high intensity in Cs and C, relatively low intensity in Mg, and at the same time relatively high intensity in ADF images, as indicated by arrows. This means that the indicated areas are rich in Cs and C and poor in Mg. The comparison between the EDX map and ADF intensity of the same region suggests that there is inhomogeneous distribution of cesium in the sorbents, both before and after CO₂ sorption. It should also be noted that as the sorbents are supported on amorphous carbon coated TEM grids, the C densities shown in Figure 8 represent both C from the dopants in the sorbents and also from the amorphous carbon film on the TEM grid. The presence of a Cs-rich region in Figure 8a suggests that the inhomogeneity occurs even in the as-synthesized sample. As the nominal amount of dopants is

relatively low (15 mol %) in this case, it is expected that the clustering effect could be more significant if a higher loading of dopant was used.

Possible Phase of the Carbonated Product. The in situ XRD results establish that at the activated state of the sorbent, the structure of the dopant is monoclinic Cs₂CO₃ and the matrix MgO (Figure 4f–i). Since Cs₂CO₃ cannot independently sorb additional CO₂ under dry environments and all of Cs₂CO₃ is converted during carbonation, it follows that Cs₂CO₃ is not simply acting as a catalyst. On the contrary, Cs₂CO₃ must be a reagent in CO₂ sorption. In addition, the absence of MgCO₃ in the carbonated product suggests that MgO follows a different reaction route in CO₂ sorption from the expected reaction (MgO + CO₂ ⇌ MgCO₃). The elemental analysis of the carbonated product based on EDX shows that only Mg, Cs, C, and O are present in the sample. All of this evidence led to the conclusion that the product is highly likely to be a Cs–Mg mixed carbonate phase.

A recent report on a similar study of CO₂ sorption properties of K₂CO₃-doped MgO also found a K–Mg mixed carbonate phase upon sorption of CO₂ and steam.¹⁷ It was found that the activated state of the sorbent was a mixture of K₂CO₃ and MgO, which then formed K₂Mg(CO₃)₂ and K₂Mg(CO₃)₂·4(H₂O) upon sorption of CO₂ and steam at 50–100 °C under atmospheric pressure. The similarities between their and our findings provide an indication that the product upon CO₂ sorption is of an alkali-metal–Mg mixed carbonate phase. In the present study, CO₂ sorption takes place under dry, inert environments (dry CO₂ in Ar or N₂); thus, a likely chemical formula for the product is Cs_xMg_y(CO₃)_{x/2+y}. This product may then become hydrated upon exposure to atmospheric moisture.

As it is difficult to experimentally determine the stoichiometry in the final mixed phase product, we have attempted to estimate the possible stoichiometry by calculating the theoretical yields using various atomic ratios between Mg and Cs and then comparing this with our TGA data. Our calculations suggest that the product could be Cs₂Mg₂(CO₃)₃, Cs₂Mg₃(CO₃)₄, or Cs₂Mg₄(CO₃)₅. It is also probable that the experimentally observed carbonated product is a mixture of these plausible mixed magnesium–cesium carbonate phases. We also anticipate that the formation of the magnesium–cesium carbonate phases could be sensitive to the temperature, partial pressure of CO₂, and the presence of moisture, and these factors could lead to different phases under different sorption conditions.

CONCLUSIONS

Using a simple impregnation synthesis method, Cs₂CO₃ has been doped on MgO, with a maximum CO₂ sorption capacity of greater than 1.9 mmol/g at a sorption temperature of 300 °C. Through characterization by PXRD, TEM, and EDX, it was found that both Cs₂CO₃ dopants and MgO matrix participate in the CO₂ sorption process. The results suggest that CO₂ chemisorption of Cs₂CO₃-doped MgO forms a mixed Mg–Cs carbonate phase with undetermined stoichiometry, and the activation energy of this reaction route is lower than the carbonation of MgO at moderate temperatures. The formation of this mixed phase is the reason why Cs₂CO₃-doped MgO shows an improved CO₂ sorption capacity compared to pure MgO sorbent.

It is speculated that in order to maximize the CO₂ sorption capacity, the Cs-loading should be increased so that a greater

portion of sorbent can form a mixed Mg–Cs carbonate phase. Efforts to optimize the sorption capacity might thus be directed to homogeneous distribution of Cs_2CO_3 on MgO, so as to prevent segregation and clustering. New methods may achieve higher yields by increasing the density of Cs or even developing a method to dope Cs throughout the volume of MgO while nanoporosity is maintained.

AUTHOR INFORMATION

Corresponding Author

*E-mail: [REDACTED] (A.L.C.); [REDACTED] (S.L.Y.C.).

Present Addresses

^{||}School of Chemistry, University of Melbourne, Victoria 3010, Australia.

[†]Ernst Ruska-Centre for Microscopy and Spectroscopy with Electrons, Peter Grueberg Institute, Forschungszentrum Juelich, Germany.

Notes

The authors declare no competing financial interest.

ACKNOWLEDGMENTS

The authors acknowledge the support provided by the Australian Government through its CRC Program for this CO2CRC research project. The authors acknowledge the use of the Powder Diffraction beamline at the Australian Synchrotron and the Centre for Electron Microscopy (MCEM) at Monash University.

REFERENCES

- (1) Lund, H.; Mathiesen, B. V. *Energy* **2009**, *34*, 524–531.
- (2) Rochelle, G. T. *Science* **2009**, *325*, 1652–1654.
- (3) Hagewiesche, D. P.; Ashour, S. S.; Al-Ghawas, H. A.; Sandall, O. C. *Chem. Eng. Sci.* **1995**, *50*, 1071–1079.
- (4) Wilson, M.; Tontiwachwuthikul, P.; Chakma, A. R.; Veawab, A.; Aroonwilas, A.; Gelowitz, D.; Barrie, J.; Mariz, C. *Energy* **2004**, *29*, 1259–1267.
- (5) Li, J.-R.; Ma, Y.; McCarthy, M.; Sculley, J.; Yu, J.; Jeong, H.-K.; Balbuena, P.; Zhou, H.-C. *Coord. Chem. Rev.* **2011**, *255*, 1791–1823.
- (6) Mavroudi, M.; Kaldis, S.; Sakellariopoulos, G. *Fuel* **2003**, *82*, 2153–2159.
- (7) D'Allesandro, D.; Smit, B.; Long, J. *Angew. Chem., Int. Ed.* **2010**, *49*, 6058–6082.
- (8) Siriwardane, R. V.; Shen, M. S.; Fisher, E. P.; Poston, J. A. *Energy Fuels* **2001**, *15*, 279–284.
- (9) Aaron, D.; Tsouris, C. *Sep. Sci. Technol.* **2005**, *40*, 321.
- (10) Singh, R.; al., E. *Energy Procedia* **2009**, *1*, 623–630.
- (11) Alvarez, D.; Abanades, J. *Ind. Eng. Chem. Res.* **2005**, *44*, 5608–5615.
- (12) Hassanzadeh, A.; Abbasian, J. *Fuel* **2010**, *89*, 1287–1297.
- (13) Wang, M.; Lawala, A.; Stephenson, P.; Sidders, J.; Ramshaw, C.; Yeung, H. *Chem. Eng. Res. Des.* **2011**, *89*, 1609–1624.
- (14) Figueroa, J. D.; Fout, T.; Plasynski, S.; Mcllvried, H.; Srivastava, R. D. *Int. J. Greenhouse Gas Control* **2008**, *2*, 9–20.
- (15) Gaffney, T.; Golden, T.; Mayorga, S.; Brzozowski, J.; Taylor, F. US005917136A—Carbon dioxide pressure swing adsorption process using modified alumina adsorbents. US patent 5,917,136, 1999.
- (16) Mayorga, S. G.; Weigel, S. J.; Gaffney, T. R.; Brzozowski, J. US006280503B1—Carbon Dioxide Adsorbents Containing Magnesium Oxide Suitable for Use at High Temperatures. US patent 6,280,503, 2001.
- (17) Lee, S. C.; Chae, H. J.; Lee, S. J.; Choi, B. Y.; Yi, C. K.; Lee, J. B.; Ryu, C. K.; Kim, J. C. *Environ. Sci. Technol.* **2008**, *42*, 2736–2741.
- (18) Reddy, E. P.; Smirniotis, P. G. *J. Phys. Chem. B* **2004**, *108*, 7794–7800.
- (19) Jahan, M. Ph.D. thesis, Monash University, Victoria, Australia, 2011.
- (20) Zhang, K.; Li, X. S.; Duan, Y.; King, D. L.; Singh, P.; Li, L. *Int. J. Greenhouse Gas Control* **2013**, *12*, 351–358.
- (21) Xiao, G.; Singh, R.; Chaffee, A. L.; Webley, P. *Int. J. Greenhouse Gas Control* **2011**, *5*, 634–639.
- (22) Lee, S. C.; Choi, B. Y.; Lee, T. J.; Ryu, C. K.; Ahn, Y. S.; Kim, J. C. *Catal. Today* **2006**, *111*, 385–390.
- (23) Hayashi, H.; Taniuchi, J.; Furuyashiki, N.; Sugiyama, S.; Hirano, S.; Shigemoto, S.; Nonaka, T. *Ind. Eng. Chem. Res.* **1998**, *37*, 185.
- (24) Liang, Y.; Harrison, D.; Gupta, R. P.; Green, D. A.; McMichael, W. J. *Energy Fuels* **2004**, *18*, 569–575.
- (25) Duan, Y.; Zhang, B.; Sorescu, D. C.; Johnson, J. K. *J. Solid State Chem.* **2011**, *184*, 304–311.
- (26) ICDD. *PDF-4+ (Database)*; Kabekodu, S., Ed.; International Centre for Diffraction Data: Newtown Square, PA, 2011.
- (27) Catti, M.; Ferraris, G.; Hull, S.; Pavese, A. *Phys. Chem. Miner.* **1995**, *22*, 200–206.
- (28) Cirpus, V.; Wittrock, J.; Adam, A. Z. *Anorg. Allg. Chem.* **2001**, *627*, 533–538.
- (29) Sasaki, S.; Fujino, K.; Takeuchi, Y. *Jpn. Acad.* **1997**, *55*, 43–48.
- (30) Ehrhardt, H.; Schweer, H.; Seidel, H. Z. *Anorg. Allg. Chem.* **1980**, *462*, 185–198.
- (31) Ross, N.; Reeder, R. *Am. Mineral.* **1997**, *82*, 682–688.
- (32) Zheng, Y. Q.; Adam, A. *Chem. Res. Chin. Univ.* **1999**, *15*, 211–217.
- (33) Montero, J. M.; Wilson, K.; Lee, A. F. *Top. Catal.* **2010**, *53*, 737–745.
- (34) Goodman, J. F. *Proc. R. Soc. A* **1958**, *247*, 346–352.
- (35) Bhatia, S. K.; Perlmutter, D. D. *AIChE J.* **1980**, *26*, 379–386.
- (36) Bhatia, S. K.; Perlmutter, D. D. *AIChE J.* **1981**, *27*, 247–254.

Appendix 2: About the author

Education

PhD Candidate *March 2010-October 2013*

School of Chemistry, Monash University, Clayton, VIC, Australia

- Research project 'High-temperature carbon dioxide capture using metal oxides'
- Financial support by the Cooperative Research Centre for Greenhouse Gas Technologies (CO2CRC) and Monash University's Faculty of Science Dean's International Postgraduate Research scholarships

Diplom-Ingenieur (Dipl.-Ing.), Chemical Engineering *October 2000-April 2007*

University of Dortmund, Germany

- Two electives 'Energy Process Engineering' and 'Engineering Thermodynamics'
- Final thesis supervised by Prof Karl Strauß, University of Dortmund, in collaboration with Prof Günter Scheffknecht, University of Stuttgart, Germany, *September 2006-April 2007*
- Undergraduate thesis supervised by Prof Karl Strauß, in collaboration with Prof Alan L Chaffee, Monash University, Clayton, *March 2005-July 2005*

Employment

Chemistry Laboratory Demonstrator *March 2011-May 2013*

School of Chemistry, Monash University, Clayton, VIC, Australia

- Assisting & supervising students attending the laboratory classes 'Chemistry – Principles and Practice' (2nd year engineering course) and 'Chemistry for Engineering' (1st year engineering course), marking of weekly student laboratory reports
-

Research Assistant *July 2008-December 2009*

Chair for Energy Systems and Energy Process Engineering, Ruhr-University of Bochum, Germany

- Research on the combustion behaviour of secondary fuels in industrially and publicly funded projects
- Manual and automated operation of laboratory and pilot plant scale combustion research facilities in a team of other research staff and technicians
- Managing, operation and upgrading of the Fuel Laboratory of the workgroup
- University teaching duties: Tutorials, consultation hours for the students, outlining tasks for exam papers, exam supervision, exam marking
- Occupational Health and Safety Consultant within the workgroup

Research Assistant *November 2007-June 2008*

Institute of Process Engineering and Power Plant Technology, University of Stuttgart, Germany

- Design of laboratory equipment for a European Union funded research project about mercury behaviour on denitrification catalyst (SCR) systems for power plants
- Continuous operation of large pilot plant facilities (grate fired combustor, pulverised coal fired combustor) in a team of researchers and technicians in two- or three-shift rosters
- Work on pilot plant facility upgrading, repairs and decommissioning
- Trained operator of cranes to lift machinery parts and containers in the pilot plant hall

Student Research Assistant *June 2003-March 2005*

Department of Energy Process Engineering and Fluid Mechanics, University of Dortmund, Germany

- Design of lecture presentations and handouts using LaTeX, Corel Draw and Mathcad
 - Assisting postgraduate and postdoctoral staff with analytical laboratory work and results analysis on the kinetics of inorganics removal from brown coal and straw as secondary fuel
-

Journal publications

M. Liu, C. Vogt, A. L. Chaffee, and S. L. Y. Chang, "Nanoscale Structural Investigation of Cs₂CO₃-Doped MgO Sorbent for CO₂ Capture at Moderate Temperature," *Journal of Physical Chemistry C*, vol. 117, pp. 17514-17520, 2013.

C. Vogt, G. P. Knowles, S. L. Y. Chang, and A. L. Chaffee, "Cadmium oxide/alkali metal halide mixtures - a potential high capacity sorbent for pre-combustion CO₂ capture," *Journal of Materials Chemistry A*, vol. 1, pp. 10962-10971, 2013.

C. Vogt, T. Wild, C. Bergins, K. Strauß, J. Hulston, and A. L. Chaffee, "Mechanical/thermal dewatering of lignite. Part 4: Physico-chemical properties and pore structure during an acid treatment within the MTE process," *Fuel*, vol. 93, pp. 433-442, 2012.

Conference attendance

Christian Vogt, Maoyuan Liu, Shery L. Y. Chang, Alan L. Chaffee: Cesium-doped MgO sorbents for pre-combustion CO₂ capture. Poster, CO₂CRC Research Symposium 2012, Adelaide, 27/11/2012 – 29/11/2012.

Christian Vogt, Gregory P Knowles, Alan L Chaffee, Shery LY Chang: Cadmium oxide based sorbents for pre-combustion CO₂ capture - sorbent stability. Presentation, CO₂CRC Research Symposium 2012, Adelaide, 27/11/2012 – 29/11/2012.

Christian Vogt, Shery L. Y. Chang, Gregory P Knowles, Alan L Chaffee: The CO₂ capture potential of cadmium oxide/alkali halide mixtures. Poster, Challenges in Inorganics and Materials Chemistry (ISACS8), Toronto, Ontario, Canada, 19-22 July, 2012.

Christian Vogt, Gregory P Knowles, Alan L Chaffee: Cadmium-based metal oxide sorbents for pre-combustion carbon dioxide capture. Poster, CO₂CRC Research Symposium 2011, Adelaide, 29/11/2011 – 01/12/2011.
